Ebb and Flow:

Preserving Regulated Rivers Through

Strategic Dam Operations

by

Quentin Brent Travis

A Dissertation Presented in Partial Fulfillment
of the Requirements for the Degree
Doctor of Philosophy

Approved November 2010 by the
Graduate Supervisory Committee:

Larry Mays, Chair
Mark Schmeeckle
Sandra Houston

ARIZONA STATE UNIVERSITY

December 2010

ABSTRACT

Fluctuating flow releases on regulated rivers destabilize downstream riverbanks, causing unintended, unnatural, and uncontrolled geomorphologic changes. These flow releases, usually a result of upstream hydroelectric dam operations, create manmade tidal effects that cause significant environmental damage; harm fish, vegetation, mammal, and avian habitats; and destroy riverbank camping and boating areas.

This work focuses on rivers regulated by hydroelectric dams and have banks formed by sediment processes. For these systems, bank failures can be reduced, but not eliminated, by modifying flow release schedules. Unfortunately, comprehensive mitigation can only be accomplished with expensive rebuilding floods which release trapped sediment back into the river.

The contribution of this research is to optimize weekly hydroelectric dam releases to minimize the cost of annually mitigating downstream bank failures. Physical process modeling of dynamic seepage effects is achieved through a new analytical unsaturated porewater response model that allows arbitrary periodic stage loading by Fourier series. This model is incorporated into a derived bank failure risk model that utilizes stochastic parameters identified through a meta-analysis of more than 150 documented slope failures. The risk model is then expanded to the river reach level by a Monte Carlos simulation and nonlinear regression of measured attenuation effects. Finally, the comprehensive risk model is subjected to a simulated annealing (SA) optimization scheme that accounts for physical, environmental, mechanical, operations, and flow constraints.

The complete risk model is used to optimize the weekly flow release schedule of the Glen Canyon Dam, which regulates flow in the Colorado River within the Grand Canyon. A solution was obtained that reduces downstream failure risk, allows annual rebuilding floods, and predicts a hydroelectric revenue increase of more than 2%.

DEDICATION

Any genuine contributions of this work are dedicated to three beloved family members who left too soon:

Bruce Kent – my Uncle, a gifted engineer and my inspiration;

Connie Peterson – my Grandmother, a bemused intellectual and my greatest asset;

Rusty Limauro – my Mother, a poet, scholar, volunteer, and still my guiding light.

ACKNOWLEDGMENTS

Extraordinary people carried me through this effort. My committee – Larry Mays, Sandra Houston, and Mark Schmeeckle – were insightful when opportune, critical when necessary, and endlessly supportive. I am privileged to work with the incredible staff at WEST Consultants, Inc., and thank Jeff Bradley, Brian Wahlin, Chuck Davis, and Riley Rasbury for their financial, technical, and psychological support. Dan Rothman helped me navigate the process that he made look so easy and I found so perilous. Of course, my greatest ally is my family: Dad – you showed me that it could be done; Chris – you are, have been, and will always be Mom to me; Barry and Rita – you are my role models and parents in all ways that matter; kids – Micah, Summer, Sky, Sammy, Soleil, Cali, Declan, and Kingston – you have taught me everything worth learning; and Lori – my wife, friend, partner, co-conspirator, and love – with you everything is possible; without you nothing would matter.

TABLE OF CONTENTS

LIST OF TABLES

LIST OF FIGURES

CHAPTER 1. INTRODUCTION

> Only rivers appear inviolable. They travel without plan, twisting like tendrils, as indirect as idle thoughts. Bordered by corridors of green, they seem immune from encroachment – until you look closer and see a length of river that has been "channelized" for the convenience of barges, its bends ironed out like wrinkles. Then you see the sudden widening of a reservoir, the broad end blunted by the abrupt slash of a concrete dam, and all arguments of utility lose their force. A river dammed or straightened is a travesty, a violation, an outrage. If you want to see people enraged, strangle the rivers they love.
>
> – from *The Bird in the Waterfall*
> by Glenn Wolff

> There is something deeply satisfying about directing the flow of water.
>
> – David Lynch

Background

The first large dam in recorded history was built in 2,700 BCE near present day Cairo. It stood 40 feet tall and more than 300 feet wide, carefully constructed from ungrouted rock and sand. The dam, later named Sadd-el-Kafara (Dam of the Pagans), was built for the sole purpose of protecting the early Egyptians from flooding from the Nile River.

Historical evidence indicates that the Sadd-el-Kafara construction was an ambitious, noble, well planned, and well executed public works project (Mays, 2010). Unfortunately, it was also doomed to failure. Just after the dam had reached its design height, but before the floodways had been formed, intense storms began. As the Nile River rose so did the seepage pressures on the dam. When the river stage reached its crest, Sadd-el-Kafara collapsed. The resulting catastrophe was so devastating that it would be eight centuries before the Egyptians again attempted to construct another large dam.

Sadd Al-Kafara is not only the first large scale dam in recorded history but also the first dam failure in recorded history. More than that, it was also the first attempt to completely regulate a riparian system (Drower, 1954), and the first recorded massive slope failure to occur as a result.

Dam building technology has much improved since the Sadd Al-Kafara disaster, and it is extremely rare (but not unheard of) for a new dam to fail. River regulation technology, however, remains imperfect, and massive slope collapses are still common; only now it is the downstream riverbanks that fail, rather than the dams themselves.

The problems are worldwide. There are currently more than 800,000 dams in operation, generating enough hydroelectricity to supply nearly one-fifth of the world's energy, but adversely affecting more than half of the world's large water systems as a result (Jacquot, 2009). These adverse effects include ecological damage, environmental changes, and water quality reduction (Goodwin et al., 2000). Moreover, regulating the river through controlled flows can cause tremendous geomorphologic effects, often expressed through numerous streambank failures. These failures can cause unchecked lateral bank migration, thalweg reorienting and even avulsions, resulting in an unintended, unnatural, and uncontrolled restructuring of the entire riparian area.

The adverse geomorphologic consequences of river regulation have been well documented at the Glen Canyon Dam, located on the Colorado River within the Grand Canyon. A number of large downstream bank failures have been recorded since dam operations began. In general, these failures occur at eddy

sandbars, which are formed by fine sands transported into eddies adjacent to the riverbanks. These sandbars are popular camping areas for hikers, campers, boaters, and other visitors to the canyon. Thus their destruction is not only damaging environmentally and aesthetically, but also constitutes a potential risk to public safety. Minimizing the risk of these failures in the Canyon has led to significant changes to the hydroelectric dam operations (Budhu and Gobin, 1994). These operational changes have reduced sandbar failures at the cost of significantly reduced revenue.

Sandbars are a particular type of riverbank, but unlike riverbanks, sandbars can form over just a few hours and are made up almost entirely of sandy sediment conveyed by the river. Sandbars are typically formed in dynamic river systems, such as the Grand Canyon, where bank formation occurs from sediment deposit, often at angles just below the angle of repose (Budhu, 1993). Because the banks are formed near failure, their stability is particularly sensitive to loading conditions, including the river stage fluctuations and the resulting porewater pressure and matric suction pressure changes, often rapidly changing as the bank approaches failure (Iverson et al., 1997). Since slope stability prediction techniques are strictly dependent on estimating these forces, much of the existing theory becomes suspect. Thus, one of the critical challenges of modeling sandbar failures is to identify and apply an appropriate slope stability model.

Problem Statement

It is evident that hydroelectric dams are a crucial component of the world's energy grid, yet it is also evident that significant energy loss occurs from

failed attempts to regulate dam operations in order to prevent downstream bank collapse. This challenge may be summarized in the following problem statement:

How can hydroelectric dam operations be optimized to minimize the cost of successfully mitigating downstream bank failures?

Answering this question requires a firm understanding of the problem parameters not only from a general, theory based perspective, but also from a site specific perspective.

Glen Canyon Dam constitutes a nearly ideal application of a theory of bank failure from dam operations. The river stages are closely monitored, the slope failures widely documented, and the soil parameters have been repeatedly measured. Moreover, optimizing the Glen Canyon Dam operations would constitute an appreciable contribution to the public good, maximizing profit from hydroelectric power generation while simultaneously helping to preserve one of the world's greatest natural resources. For these reasons, the Glen Canyon Dam is used throughout the paper to explore site specific problem elements and to test the accuracy and applicability of the developed theory.

Contributions and Organization

Quantifying slope failure risk

Adjusting dam operations to mitigate adverse consequences requires a model of downstream riverbank reactions to dam flow release schedules. Some models are available in the literature: Simon et al. (2000), used field recorded

porewater pressures to explain several bank failures, applying two-dimensional limit equilibrium (2DLE) analysis with an assumed a wedge shaped failure surface. Darby and Thorne (1996) successfully predicted a number of failures utilizing a wedge type 2DLE. Rinaldi et al. (2002) explained several downstream riverbank failures utilizing 2DLE (Spencer's method) applied to an irregular failure surface. Budhu and Gobin investigated a number of sandbar failures on the Colorado River in the Grand Canyon, utilizing a number of approaches including 2DLE and finite element modeling (1994, 1995a, 1995b).

A critical limitation of these 2DLE approaches is that they are deterministic, whereas slope failure risk appears to be inherently stochastic, as evidenced by numerous failure studies (Duncan and Wright, 2005). Error propagation techniques can be used to estimate risk; however, these require particular and unverified assumptions of safety distributions and uncertainties that can vary widely between analysts.

This challenge was addressed herein by directly researching documented slope failures and their associated analyses. The resulting database was then interpreted statistically to develop a global risk model of slope stability. This research constitutes the first contribution of this dissertation:

Contribution 1: Determining the inherent statistical distribution of and the key parameters influencing slope stability risk by meta-analysis.

This work resulted in several publications (Travis et al. 2010b,c), and is the subject of Chapters 2 and 3.

Determining the role of matric suction

A further complication of slope failure modeling is representing matric suction. Matric suction affects slope stability in several ways, increasing apparent cohesion and causing nonlinear and dynamic soil weight distribution because of variations in saturation. These aspects do not appear to have heretofore been rigorously considered in terms of slope stability analysis. Indeed, most slope analyses assume fully saturated / dry conditions.

The fully saturated / dry assumption model does not consider unsaturated conditions and in particular does not account for unsaturated flow, matric suction, or the dependence of unit soil weight on the degree of saturation. Instead, unit soil weight is typically represented as fully saturated below the phreatic surface and as some constant value (the "dry" value) above the phreatic surface. It is an assumption often made in practice (e.g. USACE, 2003; USDA, 1994), and in the literature (e.g. Simon et al., 2002; Zhang et al., 2005).

An alternative approach to the dry / saturated model is to assume a constant soil unit weight throughout the subsurface (e.g. Duncan and Wright, 2005) but this requires either the conservative assumption of saturated unit weight or some lesser value, a "moist" unit weight, which must be estimated by the engineer. Truly unsaturated conditions, including the soil suction and moist unit weight that vary above the phreatic surface, are typically disregarded for slope stability analysis.

Recent efforts to extend the problem of slope stability to include unsaturated conditions has considered slope instability from storm water infiltration (Iverson, 2000; Cho and Lee, 2002) and bank instability resulting from rising porewater pressures (Simon et al., 2000; Rinaldi et al., 2004). The results of these and other similar studies have led to a general consensus that unsaturated conditions, with its associated matric suction, tend to increase slope stability due to an increase in apparent cohesion (Jakob and Hungr, 2005). In practice then, disregarding unsaturated soil modeling and matric suction is seen as inherently conservative for purposes of slope stability analysis. However, this perspective, even if correct, is purely design based, and does not help to predict the actual conditions leading to failure. Thus, if matric suction is a significant factor, then in must be included within a bank stability model as accurately as reasonably obtainable. Quantifying the role of matric suction in slope stability modeling constitutes the second contribution of this research.

Contribution 2: Quantifying both the conservative and nonconservative aspects of matric suction for slope stability modeling.

This contribution was achieved by modeling the effects of matric suction on infinite slope stability. The resulting research is described in another publication (Travis et al. 2010a), and is the subject of Chapter 4.

Seepage effects

Unlike bank stability and matric suction modeling, wherein the core equation assumptions are still debated, seepage modeling is an established application of the basic laws of saturated groundwater flow. Indeed, from the well accepted observation of Henry Darcy in 1856 that groundwater flow is proportional to hydraulic head (Darcy, 1856), the complete governing equations of dynamic seepage flow can be immediately derived (see Mays and Todd, 2005). Therefore, while groundwater flow remains a highly active area of research, current efforts on the subject are focused on particular applications, analytical solutions, or finite difference / element algorithms, rather than further examination of the governing equations (e.g. Boutt, 2010; Haitjema et al., 2010; Hill et al., 2010; Rojas et al., 2010; Siade et al., 2010; Younes and Ackerer, 2010; others).

The research herein considers the governing flow equations along with the model elements developed in Chapters 2 through 4, and combines them to develop a finite difference model of bank failures due to seepage forces. Derivation and application of this model was presented in conference (Travis and Schmeeckle, 2007) and is described in Chapter 5. Unfortunately, despite its success, the model was subsequently found to be too computationally expensive to meet the objective of this research.

It is not clear if the developed finite difference model constitutes a new contribution to the literature, since the number of finite element and difference models developed for slope stability analysis is immense, and the particular

procedures are often closely guarded within third party software. Capitalizing on key findings of the finite difference model, however, led to what is believed to be a new contribution to the field: an analytical model of saturated flow in a deep streambank, derived by the generalization of the groundwater response equation. Utilizing a Fourier series solution to the two dimensional unsteady saturated flow differential equations, the derived model allows any form of periodic river stage conditions, such as those expected downstream from the hydroelectric dam. The derivation and application of this model is the subject of Chapter 6.

Contribution 3: Deriving an analytical solution to seepage flows within a deep riverbank, driven by arbitrary periodic river stage functions.

Riparian scale generalization of 2DLE models

Dam operations affect entire riparian systems, not just individual banks. Responsible risk analysis must take a global, rather than individual, approach to the stochastic aspect of failures. Unfortunately, while three dimensional modeling of slope failures has become feasible in recent years, it remains far too computationally expensive to apply over even moderately sized downstream areas. Interestingly, it is risk analysis that allows the two dimensional model to be generalized to three dimensions. This is accomplished by applying a Monte Carlo simulation.

A Monte Carlo simulation allows stochastic interpretation of a model by repeatedly executing it while randomly varying the input parameters within their

respective statistical distributions. A 2D slope stability model can therefore be generalized to a 3D model by allowing the input parameters to vary according to their position along the river. A design of experiments (DOE) approach can even be utilized to guide the simulation and statistically analyze the results. The overall algorithm of this approach constitutes the fourth contribution of this research:

Contribution 4: Developing an algorithm to generalize two-dimensional slope failure models to larger scales by means of a Monte Carlo simulation.

This method was applied to the Glen Canyon dam by generating more than 3,000 separate risk calculations. The predictions were verified by field observations. A reduced ANOVA model was then utilized to relate downstream slope stability risk to key dam operation parameters.

Simple non-linear equations were then developed to model the downstream responses (attenuation) to fluctuating dam operations. In this way, a comprehensive model of bank failure risk was developed for the entirety of the Colorado River within the Grand Canyon.

Optimizing dam operations

The overarching objective of this research is to optimize dam operations given the developed model. Given the size, environmental impact, public safety risk, cost, and potentially high profits from hydroelectric power generation, dams have been and remain a critical area of optimization research. Carriaga and Mays

(1995a,b) optimized seasonal dam operations to minimize downstream sediment releases. Dam operations have been optimized for hydropower generation and irrigation supply by dynamic programming (Tilmant et al., 2002), for general water use by stochastic fuzzy dynamic programming (Abolpour and Javan, 2007), and for groundwater control by nonlinear programming (Naveh & Shamir, 2004). Optimization efforts have also considered watershed scale effects, with optimization schemes developed to minimize location costs of detention reservoirs (Mays and Bedient, 1982) and retention reservoirs (Travis and Mays, 2008). Nicklow and Mays (2001, 2002) optimized seasonal dam operations for entire watershed networks.

The current solution to mitigating ongoing sandbar bank failures in the Grand Canyon is to periodically flood the canyon by releasing high flows through the Glen Canyon Dam, flushing built up sediment downstream to rebuild the lost sandbars. These controlled floods are not currently set to a particular schedule. Three controlled floods have been conducted, one in 1996, one in 2004, and one in 2008. The controlled flood usually lasts about seven days.

The controlled flood technique has been successful, not only in rebuilding numerous sandbars, but also by providing vital research on sandbar renewal and long term stability. Several key studies on the 1996 controlled flood revealed the following:

1. Of all the sediment that was transported into the canyon during the flood, the vast majority went almost exclusively toward rebuilding the sandbars. (Hazel et al., 1999)

2. Kearsley et al. (1999) estimated that 84 high elevation sandbars had been formed by the building flood, but about 44% of these failed over the following six months, leaving a total of 262 high elevation sandbars of sufficient size to be used a campsites.
3. The 1996 flood cost approximately 2.5 million dollars, or about 3% of the overall 1996 Glen Canyon Dam revenue. In addition, approximately 1.5 million dollars was spent on physical and biological research (Harpman, 1999).

Of particular importance here are the results of Kearsley et al. (1999) study. If taken as representative, the results of the 1996 flood suggest that each controlled flood will build about 47 new sandbars, constituting about 20% of the total stable sandbars after the flood. More frequent controlled floods would be expected to build more sandbars, assuming sufficient sediment was available for transport.

The general optimization problem is thus to minimize the cost of mitigating downstream slope failures throughout an entire river reach by controlled flooding, subject to the constraints specific to physical limitations, water balance targets, and environmental concerns. The presentation of the optimization problem, the corresponding constraints, and solution algorithm together constitute the last new contribution of this research:

Contribution 5: Optimization of hydroelectric dam operations to mitigate downstream bank failures at minimum cost.

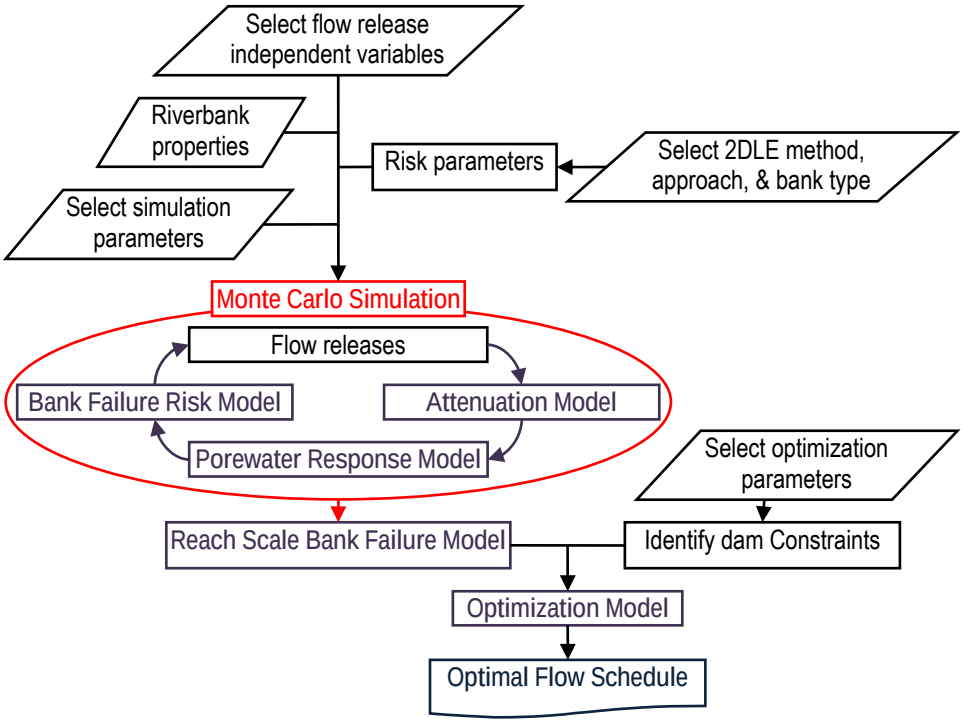

Figure 1. Comprehensive model schematic

The comprehensive model is shown in Figure 1. After developing the bank failure risk, attenuation, and porewater response models, selected parameters and gathered data can be routed through the Monte Carlo simulation to obtain and reach scale bank failure model. This model, coupled with selected parameters and appropriate constraints, is routed through the optimization model to finally obtain the optimal flow schedule.

CHAPTER 2. SLOPE FAILURE LITERATURE

> It is a capital mistake to theorize before one has data. Insensibly one begins to twist facts to suit theories, instead of theories to suit facts.
>
> – Sherlock Holmes,
> in *A Scandal in Bohemia*,
> by Sir Arthur Conan Doyle

Introduction

Since the early part of the twentieth century, two dimensional limit equilibrium (2DLE) analyses have been the engineering community's primary means of slope stability calculation. However, the input parameters to 2DLE, namely soil strength and anisotropy, slope geometry, porewater pressures, failure surface geometry, applicable correction factors, and loading conditions are all inherently uncertain, and thus statistical consideration is necessary for an accurate model. Despite the moderate success of the statistical approach and its corollary, risk analysis (e.g. Christian et al., 1994; Duncan and Wright, 2005), acceptance by the general engineering community has been slow, likely because the applicable statistical information is not readily available or reliably estimable.

Perhaps the greatest challenge with obtaining statistical information on slope stability is that the computed safety factor (SF) cannot be directly equated to measurable slope characteristics. From a strictly deterministic standpoint, a slope will fail if $SF < 1$, and be unconditionally stable for $SF > 1$. Thus, the SF can be verified (deterministically) only for a failed slope where $SF = 1$.

It is to be expected, however, that real slope failures will occur at SF slightly lower or higher than 1. From a statistical perspective, then, it is generally assumed that the safety form a statistical distribution with a mean value = 1. The

exact parameters of this distribution are unknown; indeed, even the form of the distribution itself is not known. Literature on slope stability risk analysis typically assumes a normal (e.g. Christian et al., 1994) or log normal (e.g. Lee & Kim, 2000) distribution. Unfortunately, the reality is that there are an infinite number of potential distributions and thus model uncertainty is introduced at the most fundamental level.

Complicating the search for a descriptive SF distribution is that there are many choices an analysis must make prior to calculating the SF, each introducing uncertainty and/or bias. Specifically, an analyst must choose a calculation *method* (e.g. infinite slope, simplified Bishop, Spencer's, etc.), a porewater pressure analytical *approach* (effective versus total stress) and a failure surface *model* (planar, circular, or irregular). Moreover, the analyst most choose basic modeling parameters (e.g. specific failure geometry location, number of slices, etc.). Finally, an analyst may choose to apply *correction factors* for slopes with particular soil types and/or loading conditions. Given these numerous individual decisions, it is inevitable that different analysts will calculate different safety factors, even if all other model inputs are the same.

Beyond analyst differences, there are also fundamental uncertainties and biases in the 2DLE analysis that arise from its application to a real slope, including three dimensional effects, constitutive effects, complicated porewater loading, and soil strength distribution. The uncertainty of the latter is a direct consequence of heterogeneity and differences between the actual and sampled soils (sample disturbance, strength anisotropy, vane strength bias in clay soils),

temporal changes (strain rate, consolidation, creep), slope integrity (cracking), and strain softening (peak versus mean versus reduced versus residual strength).

Finally, there may be fundamental differences between *slope type*. The 2DLE approach is typically applied to both natural slopes (landslides) and engineered slopes (cut or fill). The engineered slopes may be further divided into unmonitored field applications, test slopes (monitored slopes brought to failure), and experimental slopes (highly monitored slopes brought to failure under tightly controlled conditions).

In response to the need in slope stability risk analysis for statistical information and clear answers regarding the effect of different model techniques and assumptions, a meta-analysis was conducted on a database of 157 slope failures and the corresponding 301 SF calculations. A meta-analysis, typically applied as a statistical analysis of multiple, published analyses, is a well established approach to marketing research (Bijmolt and Pieters, 2001), but rarely used in civil engineering research (notable exceptions include Horman and Kenley, 2005, and Schueler, 2009). The latter observed disregard is unfortunate, since meta-analysis seems eminently applicable to a field where there are often many equations competing to describe the same process (e.g. sediment transport, unsaturated soil permeability description, hydrology models, etc.)

The meta-analysis here is divided into two papers. This paper describes the compiled database, reporting the minimum SF for each slope analyzed in each reference, and the corresponding slope location, soil description, Atterberg limits,

applied correction(s), and slope angle. In addition, the database also reports the following factor information:

- Analytical method: infinite slope, simplified Bishop, etc.
- Slip surface geometry: planar, circular, or irregular
- Slope type: test fill, test cut, fill, cut, or landslide

Some of the specific details of this information may be unfamiliar to the reader (indeed, one of the interesting results is that many of the applied correction factors and techniques were quite specific to a particular region.) For detailed information on these elements, the reader is referred to Chapter 3.

Chapter 3 analyzes the potential effect that each of the identified factors has on SF calculation. Based on theory and the literature, predictions are made with regard to the effect of each of the recorded factors on SF calculation, and specific hypothesis tests are utilized to test these predictions. The results are used to establish an overall statistical description of slope stability.

Compilation

The compiled slope failure database may be found in Table 1. Since many safety factors were often reported in a study, only the minimum justifiable safety factor per a given analytical method and porewater stress approach was considered here. The justifiable requirement was introduced because arbitrary assumptions were occasionally introduced by analysts for sake of discussion; however, these instances were quite rare. The average slope angles, soil types, and Atterberg limits (the liquid limit LL, plastic limit PL, and plasticity index PI)

shown in Table 1 were either reported directly by the analysts or estimated from the published figures and tables.

Several abbreviations were used in Table 1: "OMS" refers to the Ordinary Method of Slices, "COE" refers to the Army Corps of Engineers Modified Swedish 2DLE method, "Bishop" refers to the Simplified Bishop method; "Janbu" refers to Janbu's 2DLE method, and "irreg" refers to an irregular (e.g. non-planar and non-circular) slip surface.

Analysts are selective and sometimes in error when including SF calculations cited from other studies, so only primary references were allowed in the database. The only exception to this policy was when a reference included calculations from an earlier work written by them or one of the co-analysts and this referenced work could not be obtained by the authors (e.g. a conference paper, private industry report, etc.).

Any available published paper that independently calculated a safety factor for a real failed slope based on measured or modeled parameters was included in the database. These included peer reviewed articles, conference papers, textbooks, and online articles. The only qualifying paper not included within the database was Lade (1993) wherein a safety factor over 2.5 was calculated for a failed submarine berm. This very high SF was rejected as an outlier.

Slope failures from earthquakes were considered a separate issue and not included in this database, but the general results appear to be consistent with the relevant literature (e.g. Teoman et al. 2004). Likewise, only slope failures on the

planet earth were considered, although the overall database appears to be consistent with slope failures on other planets (e.g. Neuffer & Schultz 2006).

Slope Name	Reference	Slope Type	Soil	Analytical Method	Pore-water Approach	Failure Surface	Min SF	Correction	Slope Angle (deg)	LL (%)	PL (%)	PI (%)	Notes
Alani-Paty	Baum & Fleming (1991)	Landslide	Weathered basalt clasts in a clayey silt / silty clay matrix.	Janbu	Effective	Irreg	0.99	residual	9	97	48	49	1, 2
	Baum & Reid (1995)			Janbu	Effective	Irreg	0.82	residual friction					
Antoniny	Wolski et al. (1989)	Test Fill	Peat underlain by weak calcareous soil underlain by sand	Bishop	Effective	Circle	0.7	Consolidation, creep, anisotropy	24	197	107	90	3, 4
				Janbu	Total	Irreg	0.85						
Ås	Flaate & Preber (1974)	Fill	Fill over silty clay	$\phi = 0$	Total	Circle	0.8	-	27	42	22	20	5
Aulieva	Ferkh & Fell (1994)	Fill	Fill over dry crust over silty clay	Bishop	Effective	Circle	1.28	Min. foundation strength	24	48	25	23	5
	Flaate & Preber (1974)			Janbu	Total	Irreg	0.92	-					
Bangkok-Siracha Hwy 1	Eide & Holmberg (1972)	Test Fill	Uniform sand on soft Bangkok clay	$\phi = 0$	Total	Circle	1.5	Cracked fill	27	150	65	85	5
Bangkok-Siracha Hwy 2		Test Fill	Uniform sand on soft Bangkok clay	$\phi = 0$	Total	Circle	1.5	Cracked fill	27	150	65	85	5
Bangkok-Siracha Hwy A		Test Fill	Uniform sand on soft Bangkok clay	$\phi = 0$	Total	Circle	1.46	Cracked fill	27	150	5	85	5
	Ferkh & Fell (1994)			Bishop	Effective	Circle	1.01	Min. foundation strength; cracked fill.					
Bangkok-Siracha Hwy B	Eide & Holmberg (1972)	Test Fill	Uniform sand on soft Bangkok clay	$\phi = 0$	Total	Circle	1.61	Cracked fill	27	150	65	85	5
	Ferkh & Fell (1994)			Bishop	Effective	Circle	1.36	Min. foundation strength; cracked fill.					
Bangkok-Siracha Hwy C	Eide & Holmberg (1972)	Test Fill	Uniform sand on soft Bangkok clay	$\phi = 0$	Total	Circle	1.33	Cracked fill	27	150	65	85	5
Bradwell	Duncan & Wright (2005)	Cut	London clay	COE	Total	Circle	1.8	-	-	-	-	-	-
				Janbu			1.63						6

Slope Name	Reference	Slope Type	Soil	Analytical Method	Pore-water App-roach	Fail-ure Sur-face	Min SF	Correc-tion	Slope Angle (deg)	LL (%)	PL (%)	PI (%)	Notes
				$\phi = 0$			1.76						-
Breckenridge 1963	Eden & Mitchell (1973)	Landslide	Champlain Sea sensitive marine clays	Bishop	Effective	Circle	1.05	-	24	-	-	20	7
Carsington Dam I	Chen et al. (1992)	Fill	Yellow clay & dam core material.	Sarma	Effective	Irreg	1.04	Weakened strength	18	-	-	-	8
					Total		1.1						
	Skempton and Coats (1985)			Wedge	Effective	Irreg	1.02	Critical State; Progressive failure					
Carsington Dam II		Fill	Dark grey mudstone over yellow clay.	Wedge	Effective	Irreg	1.35	Critical State; Progressive failure	14	79	34	45	3
Caudalosa tailings dam	Garga & de la Torre (2002)	Fill	Silty sand tailings over lacustrine clay	Morgenstern Price	Effective	Irreg	0.98	-	11	62	27	35	4, 11
Chung-Nam Province	Yoo & Jung (2006)	Fill	Complete decomposed granite	Bishop	Effective	Circle	0.97	-	44	-	-	-	4
Combs reservoir	Otoko (1987)	Fill	Firm brown or yellow-brown sandy silty clay.	Bishop	Effective	Circle	0.95	-	-	36	16	20	-
Contra Costa County	Adib (2000)	Fill	Fat clay with sand & gravel	Spencer	Effective	Irreg	1.07	Residual; Mesri & Abdel Gaffar (1993)	27	55	21	34	-
Cubzac	Pilot et al. (1982)	Test Fill	Clean gravel over an overconsolidated clayey silty crust over organic silty clay.	Bishop	Effective	Circle	1.24	-	41	105	40	65	2
				$\phi = 0$	Total		1.44	Vane test strength					
	Talesnick & Baker (1984)			Spencer	Total	Irreg	1.14	Minimum strength					4
Cuyahoga AA	Wu et al. (1975)	Fill	Gray clay & shale fragment fill over silty clay	Morgenstern Price	Effective	Irreg	1	High pore pressure	27	40	20	20	13

Slope Name	Reference	Slope Type	Soil	Analytical Method	Pore-water App-roach	Fail-ure Sur-face	Min SF	Correc-tion	Slope Angle (deg)	LL (%)	PL (%)	PI (%)	Notes
Cuyahoga BB		Fill	Gray clay & shale fragment fill over silty clay	Morgenstern Price	Total	Irreg	1.04	Reduced preconsolidation pressure	27	40	20	20	13
Daikoku-cho	Hanzawa et al. (2000)	Fill	Marine clay	$\phi = 0$	Total	Circle	0.91	Strain rate; SHANSEP	-	-	-	50	14
Desert View Drive	Day (1996)	Fill	Fill	Janbu	Total	Circle	1.15	-	30	-	-	-	2
Drammen River	Kjærnsli & Simons (1962)	Fill	Sandy rock over fine & medium sand over silty clay	Bishop	Effective	Circle	1.01	-	-	35	18	17	15, 16
				$\phi = 0$	Total		0.47						
Durham City	Attewell & Farmer (1976)	Fill	Sand-gravel-silt-laminated clay	Bishop	Effective	Circle	1.08	residual	8	-	-	-	-
				Infinite		Planar	0.957						
				Janbu		Circle	1.07						
				OMS			1.07						
Edmonton	Ferkh & Fell (1994)	Fill	-	Bishop	Effective	Circle	1.54	Lower quartile foundation strength	-	-	-	45	5
Fair Haven		Fill	Varved silts & silty clay	Bishop	Effective	Circle	0.96	Min. foundation strength	-	-	-	17	5
	Haupt and Olson (1972)			$\phi = 0$	Total	Circle	1	-	11	35	21	14	17
Falkenstein	Flaate & Preber (1974)	Fill	Fill over soft silty quick clay	$\phi = 0$	Total	Circle	0.89	-	11	22	14	8	5
Fore River	Azzouz et al. (1981)	Test Fill	Fill over soft, silty, slightly organic clay	Bishop	Effective	Circle	0.8	SHANSEP	-	-	-	34	12
Gatineau rue Le Coteau	Lefebvre (1981)	Landslide	Soft Canadian clay	Bishop	Effective	Circle	0.99	Water filled cracks; reconsolidated strength	31	78	28	50	-
Goodwin Creek I	Simon et al. (2000)	Landslide	Brown clayey-silt over gray, blocky silt over sand & gravel.	OMS	Effective	Planar	1	-	51	-	-	-	18

Slope Name	Reference	Slope Type	Soil	Analytical Method	Pore-water App-roach	Fail-ure Sur-face	Min SF	Correc-tion	Slope Angle (deg)	LL (%)	PL (%)	PI (%)	Notes
Goodwin Creek II		Landslide	Brown clayey-silt over gray, blocky silt over sand & gravel.	OMS	Effective	Planar	1	-	51	-	-	-	18
Goodwin Creek III		Landslide	Brown clayey-silt over gray, blocky silt over sand & gravel.	OMS	Effective	Planar	1	-	51	-	-	-	18
Grand Canyon 172L	Budhu & Gobin (1995a)	Landslide	Fine to medium sand with a small amount of silt & clay	COE	Effective	Irreg	1.72	Worst case pore pressure	26	-	-	-	-
				Janbu			1.6						2
				Lowe Karafiath			1.7						
				Spencer			1.75						
Green Creek 1955	Eden & Mitchell (1973)	Landslide	Champlain Sea sensitive marine clays	Bishop	Effective	Circle	1.05	-	19	-	-	20	-
Green Creek 1971		Landslide	Champlain Sea sensitive marine clays	Bishop	Effective	Circle	0.96	-	25	-	-	20	-
Grohovo	Benac et al. (2005)	Landslide	Clayey silt cover over Flysch bedrock	Bishop	Effective	Circle	1.109	-	21	-	-	-	-
				Spencer		Irreg	1.078						
Hasamiishi	Kawamura & Ogawa (1997)	Cut	Tertiary mudstone	OMS	Effective	Circle	1.25	Residual	40	82	48	34	-
Headrace	Lydon & Long (2001)	Fill	Sandy slightly gravelly clay	COE	Effective	Circle	1.5	Rapid drawdown	27	31	21	10	19
Hill Hall	Otoko (1987)	Fill	London clay	Bishop	Effective	Circle	1.2	-	29	59	23	36	-
	Sainak (1999)			Bishop	Effective	Circle	1.16	-					
				Wedge		Irreg	1.02						
Hull, Leamy Creek	Lefebvre (1981)	Landslide	Soft Canadian clay	Bishop	Effective	Circle	1.64	Water filled cracks; reconsolidated strength	17	78	28	50	-
Iverson I	Iverson et al. (1997)	Experiment	60% poorly sorted sand, 40% fine gravel by weight	Janbu	Effective	Irreg	1.11	-	31	-	-	-	-
Iverson II		Experiment	60% poorly sorted sand, 40% fine gravel by weight	Janbu	Effective	Irreg	1.28	-	31	-	-	-	-

Slope Name	Reference	Slope Type	Soil	Analytical Method	Pore-water App-roach	Fail-ure Sur-face	Min SF	Correc-tion	Slope Angle (deg)	LL (%)	PL (%)	PI (%)	Notes
Jackfield	Skempton (1964)	Landslide	Weathered, fissured clay	Bishop	Effective	Circle	1.11	-	10	44	22	22	-
James Bay	Duncan & Wright (2005)	Fill	Soft & sensitive clay	COE	Total	Irreg	1.17	-	3	-	-	-	20
						Circle	1.45						
				Spencer		Irreg	1.17						
James Bay Test	Dascal & Tournier (1975)	Test Fill	Lacustrine clay overlying glacial till & bedrock	Bishop	Total	Circle	1.1	Bjerrum (1972); time effect	14	33	19	14	21, 22
				$\varphi = 0$			1.03						
	Ferkh & Fell (1994)			Bishop	Effective	Circle	0.9	Min. foundation strength				20	5
Jarlsberg	Ferkh & Fell (1994)	Fill	Fill over soft silty quick clay	Bishop	Effective	Circle	1.3	Min. foundation strength	27	45	20	25	5
	Flaate & Preber (1974)			$\phi = 0$	Total	Circle	1.1	-					
Juban I	Zhang et al. (2005)	Fill	Clay, silt, & sand	Bishop	Total	Circle	0.991	-	12	42	20	22	-
Juban II		Fill	Clay, silt, & sand	Bishop	Total	Circle	0.983	-	17	50	21	29	-
Kameda	Hanzawa et al. (2000)	Fill	Peat & sandy clay	$\varphi = 0$	Total	Circle	0.98	Strain rate; recompression.	-	-	-	-	14
Kensal Green	Skempton (1964)	Cut	London clay	Bishop	Effective	Circle	0.6	Residual	27	83	30	53	23
Kettleman Hills	Byrne et al. (1992)	Fill	Landfill liner system	Janbu	Total	Irreg	0.81	Residual	2	-	-	-	2
	Seed et al. (1990)			Wedge	Total	Irreg	1.1	Residual					24
Kewaunee A	Edil & Vallejo (1977)	Landslide	Sand over silt & clay	Bishop	Effective	Circle	1.81	Drained	58	23	17	6	1, 4, 25
Kewaunee B		Landslide	Sand over silt & clay	Bishop	Effective	Circle	1.06	Drained	45	28	21	7	1, 4, 25
Kewaunee C		Landslide	Silty sand over silt & clay	Bishop	Effective	Circle	1.02	Undrained	45	19	10	9	1, 4, 25
Khor Al-Zubair	Hanzawa et al. (2000)	Fill	Highly aged clay	$\phi = 0$	Total	Circle	0.71	Strain rate; SHANSEP	-	-	-	33	14

Slope Name	Reference	Slope Type	Soil	Analytical Method	Pore-water App-roach	Fail-ure Sur-face	Min SF	Correc-tion	Slope Angle (deg)	LL (%)	PL (%)	PI (%)	Notes
King's Lynn	Ferkh & Fell (1994)	Test Fill	Weakly cementing sandstone over alluvial clayey silts & sands over fen peat over soft silty & organic clays.	Morgenstern Price	Effective	Irreg	1.04	Min. foundation strength	34	60	30	30	5
	Wilkes (1972)			Janbu	Total	Irreg	1	Skempton & Hutchinson (1969)					26
				Spencer			1.49	Reduced strength					
Koyama	Kawamura & Ogawa (1997)	Cut	Tertiary mudstone	OMS	Effective	Circle	0.83	Residual	-	-	-	-	-
Lachute 1	Lefebvre (1981)	Cut	Soft Canadian clay	Bishop	Effective	Circle	1.23	Water filled cracks; reconsolidated strength	23	55	24	32	-
Lachute 2		Cut	Soft Canadian clay	Bishop	Effective	Circle	1.11	Water filled cracks; reconsolidated strength	25	60	22	39	-
Lanester	Bjerrum (1972)	Test Fill	Compacted sandy clayey gravel over soft, organic sandy clay & silt.	Bishop	Effective	Circle	1.38	Vane test strength	34	115	45	70	-
	Ferkh & Fell (1994)			Bishop	Effective	Circle	0.97	Min. foundation strength; cracked fill.					5
	Pilot (1972)			Bishop	Total	Circle	1.35	Vane test strength					9, 26, 28
	Pilot et al. (1982)			Bishop	Effective	Circle	1.13	-					9
				$\phi = 0$	Total		1.27	Vane test strength					
	Talesnick & Baker (1984)			Spencer	Total	Irreg	0.99	-					4
Linkou 1	Chen (1988)	Landslide	Gravel deposits	Bishop	Total	Circle	0.995	Saturated, crack	27	-	-	-	-
Linkou 2		Landslide	Gravel & lateritic soil	Bishop	Total	Circle	0.953	Partially saturated, crack	27	50	30	20	-
Lodalen	Sevaldson (1956)	Cut	Soft marine clay with thin silt layers	Bishop	Effective	Circle	1	-	27	34	20	14	1, 29
				OMS			0.79						
				$\phi = 0$	Total		0.93						
Maine	Ferkh & Fell (1994)	Fill	-	Bishop	Effective	Circle	1.61	Lower quartile foundation strength; cracked fill.	-	-	-	32	5

Slope Name	Reference	Slope Type	Soil	Analytical Method	Pore-water App-roach	Fail-ure Sur-face	Min SF	Correc-tion	Slope Angle (deg)	LL (%)	PL (%)	PI (%)	Notes
Massa E Cozzlle	Casagli et al. (2006)	Landslide	silty sand	Morgenstern Price	Effective	Irreg	0.83	Residual strength	-	-	-	-	10
Matagami	Bjerrum (1972)	Fill	Fill over plastic lacustrine clay.	Bishop	Effective	Circle	1.53	Vane test strength	-	85	38	47	-
	Ferkh & Fell (1994)			Bishop	Effective	Circle	1.12	Min. foundation strength					5
Merriespruit tailings dam	Fourie et al. (2001)	Fill	Tailings (fine sand & silt)	Bishop	Effective	Circle	1.24	Min. strength values	-	-	-	-	30
Minazuki	Kawamura & Ogawa (1997)	Cut	Tertiary mudstone	OMS	Effective	Circle	0.94	Residual	34	75	42	33	-
Morton Road	Burns (1999)	Landslide	Clays & silts over sands & gravels	Bishop	Effective	Circle	1.24	Undrained; reduced strength.	7	58	21	38	-
Muar	Ferkh & Fell (1994)	Test Fill	-	Bishop	Effective	Circle	0.8	Min. foundation strength; cracked fill.	-	-	-	50	5
Narbonne		Test Fill	Gravelly & clayey compacted fill over soft clayey silt deposit	Bishop	Effective	Circle	0.84	Min. foundation strength; cracked fill.	39	-	-	32	5
	Pilot (1972)			Bishop	Total	Circle	0.96	Vane test strength		35	21	14	
	Pilot et al. (1982)			Bishop	Effective	Circle	1.05	-					9
				$\phi = 0$	Total		0.83	Vane test strength					
	Talesnick & Baker (1984)			Spencer	Total	Irreg	0.8	-				32	4
Nawalapitiya	Seneviratne & Ilmudeen (1994)	Landslide	Sandy silty clay	Bishop	Effective	Circle	0.97	Undrained	35	-	-	-	31
NBR Development	Dascal et al. (1972)	Test Fill	Lacustrine clay overlying glacial till	Bishop	Total	Circle	1.2	Bjerrum (1972)	27	70	30	40	-
				$\phi = 0$			1.1						
Nesset	Flaate & Preber (1974)	Fill	Sand & gravel over silty clay	$\phi = 0$	Total	Circle	0.88	-	27	44	22	22	5
New Liskeard	Azzouz et al. (1981)	Test Fill	Gravelly sand over silty clay over varved clay.	Bishop	Effective	Circle	0.94	SHANSEP	27	50	16	34	12
	Bjerrum (1972)			Bishop	Effective	Circle	1.05	Vane test strength		58	25	33	

Slope Name	Reference	Slope Type	Soil	Analytical Method	Pore-water App-roach	Fail-ure Sur-face	Min SF	Correc-tion	Slope Angle (deg)	LL (%)	PL (%)	PI (%)	Notes
	Ferkh & Fell (1994)			Bishop	Effective	Circle	0.83	Min. foundation strength					5
	Lacasse et al. (1977)			Bishop	Effective	Circle	1.05	-		50	16	34	9
					Total		0.99	Bjerrum (1972)					
	Lo & Stermac (1965)			OMS	Effective	Circle	1.03	Crack, no fill strength, 0 cohesion.	26				9, 31
					Total		0.74						
Nice	Seed et al. (1988)	Fill	Fill over clayey silt	Bishop	Effective	Circle	1.35	-	18	-	-	-	32
Nigoriike	Kawamura & Ogawa (1997)	Cut	Tertiary mudstone	OMS	Effective	Circle	0.94	Residual	45	-	-	-	-
Nonburi	Brand & Krasaesin (1970)	Fill	Compacted lateritic fill over weathered clay.	$\phi = 0$	Total	Circle	1.2	-	45	-	-	-	23
Nong Ngoo Hao	Balasubramaniam et al. (1979)	Test Fill	Dense sand fill over weathered clay over soft Bangkok clay	Bishop	Effective	Circle	1.01	-	27	120	42	78	1, 33
							0.73						
				OMS	Total		0.77						
North Ridge Dam	Rivard & Lu (1978)	Fill	Glacial clay fill over highly plastic clay	Bishop	Effective	Circle	0.96	Normally consolidated strength	13	72	21	51	34
				Janbu		Irreg	1.15						2, 34
NTU Slip 3	Rahardjo et al. (2001)	Landslide	Sandy silty clay	Bishop	Effective	Circle	1.05	-	29	48	24	24	-
Oceanside Manor	Arellano & Stark (2000)	Landslide	Claystone & sandstone	Janbu	Effective	Irreg	0.92	residual and fully softened	9	89	45	57	35
Orleans	Eden & Mitchell (1973)	Landslide	Champlain Sea sensitive marine clays	Bishop	Effective	Circle	0.95	-	35	-	-	20	-
Ottawa Test	Mitchell & Williams (1981)	Landslide	Champlain Sea clay	Bishop	Effective	Circle	0.98	-	-	66	25	41	-
Pacifica 1	Merifield (1992)	Fill	Artificial slope	Infinite	Total	Planar	1.2	-	-	-	-	-	10
Pacifica 2		Fill	Artificial slope	Infinite	Total	Planar	1.1	-	-	-	-	-	10

Slope Name	Reference	Slope Type	Soil	Analytical Method	Pore-water App-roach	Fail-ure Sur-face	Min SF	Correc-tion	Slope Angle (deg)	LL (%)	PL (%)	PI (%)	Notes
Pacifica 3		Fill	Artificial slope	Infinite	Total	Planar	1	-	-	-	-	-	10
Pacifica 4		Fill	Artificial slope	Infinite	Total	Planar	1	-	-	-	-	-	10
Pacifica 5		Fill	Artificial slope	Infinite	Total	Planar	1	-	-	-	-	-	10
Pacifica 6		Fill	Artificial slope	Infinite	Total	Planar	1	-	-	-	-	-	10
Pacifica 7		Fill	Artificial slope	Infinite	Total	Planar	0.9	-	-	-	-	-	10
Pacifica 8		Fill	Artificial slope	Infinite	Total	Planar	0.7	-	-	-	-	-	10
Pilarcitos Dam	Duncan et al. (1990)	Fill	Sandy clay	COE	Effective	Circle	0.82	Rapid drawdown	22	45	23	22	-
				Lowe Karafiath			1.05						
	Wong et al. (1982)			Bishop	Total		1.46	Rapid drawdown					
					Effective		1.15						
				COE			0.85						
				Lowe Karafiath			1.13						
				Morgenstern Price			1.17						
Pornic	Pilot (1972)	Fill	Embankment on soft blue & brown clay	Bishop	Total	Circle	1.17	Vane test strength	69	80	35	45	-
Port Washington A	Edil & Vallejo (1977)	Landslide	Brown silty clay with thin fine sand layer.	Bishop	Effective	Circle	0.6	Drained	31	31	18	13	1, 4, 25
Port Washington B		Landslide	Brown silty clay with thin fine sand layer.	Bishop	Effective	Circle	0.6	Drained	30	32	19	13	1, 4, 25
Port Washington C		Landslide	Brown silty clay with thin fine sand layer.	Bishop	Effective	Circle	0.97	Drained	45	32	19	13	1, 4, 25
Portsmouth Test	Azzouz et al. (1981)	Test Fill	Granular fill over soft, very sensitive Marine illitic clay	Bishop	Effective	Circle	0.91	Bjerrum (1972)	9	-	-	16	12
	Bowders & Lee (1990)			Bishop	Effective	Circle	0.994	-					4
				COE		Irreg	1.196						
				Janbu			1.075						2, 4
				Lowe Karafiath			1.148						4
				OMS		Circle	0.916						
				Spencer		Irreg	1.02						

Slope Name	Reference	Slope Type	Soil	Analytical Method	Pore-water App-roach	Fail-ure Sur-face	Min SF	Correc-tion	Slope Angle (deg)	LL (%)	PL (%)	PI (%)	Notes
	Ferkh & Fell (1994)			Bishop	Effective	Circle	0.73	Min. foundation strength					5
	Ladd (1972)			Bishop	Effective	Circle	0.82	SHANSEP	14	35	20		
				$\phi = 0$	Total		0.7						
Presterod	Ferkh & Fell (1994)	Fill	-	Bishop	Effective	Circle	0.84	Min. foundation strength	-	-	-	17	5
Presterød bakke	Flaate & Preber (1974)	Fill	Granular fill over clayey silt	$\phi = 0$	Total	Circle	0.83	-	34	36	19	17	5
Red River	Rivard & Lu (1978)	Fill	Compacted highly plastic clay over plastic clay	Bishop	Effective	Circle	1.27	Normally consolidated strength	14	82	26	56	36
				Janbu		Irreg	1.36						2, 36
Rio de Janeiro	Ferkh & Fell (1994)	Test Fill	-	Bishop	Effective	Circle	0.85	Min. foundation strength; cracked fill.	27	120	60	60	5
	Ramalho-Ortigão et al (1984)			Bishop	Total	Circle	0.959	Reduced strength; fully fissured					
					Effective		0.6						
River Thames	Ferkh & Fell (1994)	Test Fill	-	Morgenstern Price	Effective	Irreg	1.03	Min. foundation strength	-	-	-	25	5
Rockcliffe 1967	Eden & Mitchell (1973)	Landslide	Champlain Sea sensitive marine clays	Bishop	Effective	Circle	1.02	-	27	-	-	20	-
Rockcliffe 1969		Landslide	Champlain Sea sensitive marine clays	Bishop	Effective	Circle	0.99	-	24	-	-	20	-
Rosemère	Lefebvre (1981)	Cut	Soft Canadian clay	Bishop	Effective	Circle	1.05	Water filled cracks; reconsolidated strength	24	61	28	33	-
RS-736 1	Bressaani & Ridley (1997)	Cut	Sandy silt on silty clay on swelling grey clay.	Bishop	Effective	Circle	1.03	Critical State	-	45	22	23	21

Slope Name	Reference	Slope Type	Soil	Analytical Method	Pore-water App-roach	Fail-ure Sur-face	Min SF	Correc-tion	Slope Angle (deg)	LL (%)	PL (%)	PI (%)	Notes
RS-736 2		Cut	Sandy silt on silty clay on swelling grey clay.	Bishop	Effective	Circle	1.02	Critical State	-	45	22	23	21
Saint Aidans	Hughes & Clarke (2001)	Cut	Silty clay sand & gravel over mudstone & siltstone.	Janbu	Effective	Irreg	0.82	Cracking, residual shear strength	45	-	-	-	37
Saint Alban	Bowders & Lee (1990)	Test Fill	Uniform medium to coarse sand fill over weathered clay over top soil over a soft silty marine clay.	Bishop	Effective	Circle	1.021	-	37	44	21	23	4
				COE		Irreg	1.156						
				Janbu			1.023						2, 4
				Lowe Karafiath			1.134						4
				OMS		Circle	0.971						
				Spencer		Irreg	1.007						
	Ferkh & Fell (1994)			Bishop	Effective	Circle	0.96	Min. foundation strength; cracked fill.					5
	La Rochelle et al. (1974)			Bishop	Effective	Circle	0.89	Residual Undrained Strength					9, 38
	Pilot et al. (1982)			Bishop	Effective	Circle	1.04	CIU triaxial test					
				$\phi = 0$	Total		1.2	Vane test strength					
	Talesnick & Baker (1984)			Spencer	Total	Irreg	1.03	-					4
Saint-André	Ferkh & Fell (1994)	Fill	Fill over clay, peaty clay, peat, & organic mud.	Bishop	Effective	Circle	1.48	Min. foundation strength; cracked fill.	20	102	55	47	5
	Pilot (1972)			Bishop	Total	Circle	1.38	Vane test strength					1, 5

Slope Name	Reference	Slope Type	Soil	Analytical Method	Pore-water App-roach	Fail-ure Sur-face	Min SF	Correc-tion	Slope Angle (deg)	LL (%)	PL (%)	PI (%)	Notes
Saint-Hilaire Test 34°	LaFleur et al. (1988)	Test Cut	Champlain Sea clay	Bishop	Total	Circle	1.23	Min strength; Bjerrum (1973)	34	62	24	38	1
Saint-Hilaire Test 45°		Test Cut	Champlain Sea clay	Bishop	Total	Circle	1.15	Min strength; Bjerrum (1973)	45	62	24	38	1
San Francisco Bay	Duncan & Wright (2005)	Cut	San Francisco Bay mud	Spencer	Effective	Irreg	1.17	-	41	90	45	45	-
					Total		1.17						
Santiago	Stark & Eid (1992)	Landslide	Claystone & sandstone	Spencer	Effective	Irreg	1	Remolded	8	89	44	45	39
Saskatchewan Bypass	Otoko (1987)	Fill	Highly plastic clay fill	Bishop	Effective	Circle	1.17	-	23	80	42	38	-
Saugus	Azzouz et al. (1981)	Test Fill	Fill over partially consolidated Boston Blue Clay	Bishop	Effective	Circle	0.82	SHANSEP	-	-	-	21	12
Scottsdale	Ferkh & Fell (1994)	Fill	-	Bishop	Effective	Circle	1.79	Min. foundation strength	34	150	45	105	5
	Parry (1968)			Bishop	Effective	Circle	0.93	Critical state					
					Total		1.6						
Scrapsgate	Bjerrum (1972)	Fill	Dike on plastic, organic clay.	Bishop	Effective	Circle	1.52	Vane test strength	-	150	65	85	-
	Ferkh & Fell (1994)			Bishop	Effective	Circle	1.14	Median foundation strength; cracked fill.					5
Selset	Ho et al. (1997)	Cut	Boulder clay	Morgenstern Price	Effective	Irreg	1.02	-	28	26	13	13	40
	Skempton (1964)			Bishop	Effective	Circle	0.69	Residual					
Seven Sisters	Moore (1970)	Fill	Medium to highly plastic clay over plastic clay	Bishop	Effective	Circle	1	-	22	97	30	67	-
	Rivard & Lu (1978)			Bishop	Effective	Circle	0.97	Normally consolidated strength					
				Janbu		Irreg	1.04						2
Shellmouth	Rivard & Kohuska (1965)	Test Fill	Well graded sand & gravel mixture over alluvial clay with dividing sand layer	Bishop	Effective	Circle	0.88	-	30	46	16	30	1, 25, 41
	Rivard & Lu			Bishop	Effective	Circle	1.08	0 clay					36

Slope Name	Reference	Slope Type	Soil	Analytical Method	Pore-water App-roach	Fail-ure Sur-face	Min SF	Correc-tion	Slope Angle (deg)	LL (%)	PL (%)	PI (%)	Notes
	(1978)			Janbu		Irreg	1.02	cohesion					2, 36
Siburua August 12	Wolfskille & Lambe (1967)	Fill	Shaley clay	Bishop	Total	Circle	0.8	-	22	45	24	21	28, 42
					Effective		0.97						
				Morgenstern Price	Total	Irreg	0.96						
					Effective		1						
				OMS	Total	Circle	0.8						
					Effective		0.83						
Siburua July 15		Fill	Shaley clay	Bishop	Total	Circle	0.88	-	22	45	24	21	28, 42
					Effective		1.02						
				Morgenstern Price	Total	Irreg	1.01						
					Effective		1.05						
				OMS	Total	Circle	0.88						
					Effective		0.88						
Siburua October 5	Otoko (1987)	Fill	Compacted shaley clay	Bishop	Effective	Circle	0.99	-	22	45	24	21	-
							0.99						
	Wolfskill & Lambe (1967)			Bishop	Total	Circle	1.02	-					28, 42
					Effective		1.05						
				Morgenstern Price	Total	Irreg	1.07						
					Effective		1.03						
				OMS	Total	Circle	1.02						
					Effective		0.9						
Sieve River	Rinaldi et al. (2004)	Landslide	Silty fine sand over sand with cobbles over silty sand.	Morgenstern Price	Effective	Irreg	0.978	-	65	-	-	-	25
Skjeggerφd	Ferkh & Fell (1994)	Fill	Fill over dry crust over clay	Morgenstern Price	Effective	Irreg	1.06	Min. foundation strength	15	29	18	11	5
	Flaate & Preber (1974)			$\phi = 0$	Total	Circle	0.73	-					
Snake Pass	Leadbeater (1985)	Landslide	Shale & shaley clay	OMS	Effective	Circle	0.94	Residual strength	-	82	20	62	9, 25
South Nation 1	Eden & Mitchell (1973)	Landslide	Champlain Sea sensitive marine clays	Bishop	Effective	Circle	1.02	-	29	-	-	20	-

Slope Name	Reference	Slope Type	Soil	Analytical Method	Pore-water App-roach	Fail-ure Sur-face	Min SF	Correc-tion	Slope Angle (deg)	LL (%)	PL (%)	PI (%)	Notes
South Nation 2		Landslide	Champlain Sea sensitive marine clays	Bishop	Effective	Circle	1.02	-	20	-	-	20	-
South of France	Pilot (1972)	Fill	Slightly muddy loose sand over muddy-shelly-clay.	Bishop	Total	Circle	1.3	Vane test strength	9	65	30	35	-
Spady 1997	Burns (1999)	Landslide	Silty loam	Bishop	Effective	Circle	1.131	-	19	39	27	12	43
Springfield Dam	Huang & Yamasaki (1993)	Fill	-	Bishop	Total	Circle	0.97	-	-	-	-	-	42
				Sarma	Effective		0.77	Undrained					
St. Léon	Lefebvre (1981)	Landslide	Soft Canadian clay	Bishop	Effective	Circle	0.98	Water filled cracks; reconsolidated strength	32	53	26	27	-
St. Vallier de Bellechasse 1		Landslide	Soft Canadian clay	Bishop	Effective	Circle	1.07	Water filled cracks; reconsolidated strength	31	60	23	37	-
St. Vallier de Bellechasse 2		Landslide	Soft Canadian clay	Bishop	Effective	Circle	1	Water filled cracks; reconsolidated strength	-	58	21	37	-
Sundaram I	Sundaram & Bell (1972)	Experiment	Clean dry uniform quartz sand	Bishop	Effective	Circle	1.02	-	90	-	-	-	-
				Log Spiral			1.01						
				OMS			1.09						
				$\phi = 0$			1.07						
Sundaram II		Experiment	Clean dry uniform quartz sand	Bishop	Effective	Circle	1.01	-	63	-	-	-	-
				Log Spiral			1						
				OMS			1.07						
				$\phi = 0$			1.02						
Sundaram III		Experiment	Clean dry uniform quartz sand	Bishop	Effective	Circle	1.02	-	45	-	-	-	-
				Log Spiral			1						
				OMS			1.05						
				$\phi = 0$			1.04						
Sunnyside Hill	Clark et al. (1971)	Landslide	Silts, sands, & clays	Bishop	Effective	Circle	0.96	-	27	-	-	-	-
				Morgenstern Price		Irreg	0.98						
				OMS		Circle	0.9						

Slope Name	Reference	Slope Type	Soil	Analytical Method	Pore-water App-roach	Fail-ure Sur-face	Min SF	Correc-tion	Slope Angle (deg)	LL (%)	PL (%)	PI (%)	Notes
Thames	Marsland & Powell (1977)	Test Fill	Sandy gravel fill over soft silty clay & clay-silt	Bishop	Total	Circle	0.95	Undrained	-	-	-	37	44
Tianshenq iao	Chen & Shao (1988)	Landslide	Road fill over Quaternary alluvium & talus over Tertiary bedrock	Chen Morgenste rn	Total	Irreg	0.863 1	-	34	-	-	-	-
Tjernsmyr	Flaate & Preber (1974)	Fill	Granular fill over peat over soft silty clay	φ = 0	Total	Circle	0.87	-	27	26	18	8	5
Tohari 2	Tohari et al. (2007)	Experiment	River Sand	Bishop	Effective	Circle	1.047	Toe tension crack	45	-	-	-	-
				Janbu			1						
				OMS			0.999						
				Spencer			1.075						
Tohari 3		Experiment	River Sand	Bishop	Effective	Circle	1.103	Toe tension crack	45	-	-	-	-
				Janbu			1.08						
				OMS			1.082						
				Spencer			1.097						
Tohari 4		Experiment	Residual Granite Soil	Bishop	Effective	Circle	0.965	-	32	-	-	-	-
				Janbu			1.019						
				OMS			1.013						
				Spencer			0.966						
Ugai	Ugai (1988)	Experiment	Wet Tyoura sand	OMS	Total	Circle	0.781	-	49	-	-	-	45
Ullensaker	Kenney & Drury (1973)	Landslide	Retrogressi ve quick clay	Bishop	Effective	Circle	0.9	-	22	42	25	17	21, 46
Usuno	Kawamura & Ogawa (1997)	Cut	Tertiary mudstone	OMS	Effective	Circle	0.91	Residual	30	-	-	-	-
Uzzano	Casagli et al. (2006)	Landslide	gravelly, clayey, sand with silt	Morgenste rn Price	Effective	Irreg	0.966	-	24	-	-	-	-
Waco Dam	Bowders & Lee (1990)	Fill	-	Bishop	Effective	Circle	1.07	-	27	-	-	-	4
				COE		Irreg	1.114						
				Janbu			1.043						2, 4
				Lowe Karafiath			1.11						4
				OMS		Circle	0.986						
				Spencer		Irreg	1.03						

Slope Name	Reference	Slope Type	Soil	Analytical Method	Pore-water App-roach	Fail-ure Sur-face	Min SF	Correc-tion	Slope Angle (deg)	LL (%)	PL (%)	PI (%)	Notes
Waghad Dam 1907	Nagarkar et al. (1981)	Fill	Highly plastic expansive black clay	Bishop	Effective	Circle	0.83	-	26	70	35	35	27, 42
				$\phi = 0$			0.72						
Waghad Dam 1919		Fill	Highly plastic expansive black clay	Bishop	Effective	Circle	0.99	-	26	70	35	35	27, 42
				$\phi = 0$			0.61						
Waghad Dam 1976		Fill	Highly plastic expansive black clay	Bishop	Effective	Circle	0.99	-	26	70	35	35	27, 42
				$\phi = 0$			0.89						
Walter Bouldin Dam	Duncan et al. (1990)	Fill	Clay, silt, & sand	COE	Effective	Circle	0.93	Rapid drawdown	22	47	30	17	-
				Lowe Karafiath			1.09						
	Wong et al. (1982)			Bishop	Effective	Circle	0.98	Rapid drawdown					
					Total		1.27						
				COE	Effective		0.99						
				Lowe Karafiath			1.14						
Welland	Kwan (1971)	Test Cut	Lacustrine clays, clay tills, & non-plastic tills.	Bishop	Effective	Circle	0.9	-	90	40	20	20	1
				OMS			1.07						
					Total		1.16						
Yamaska	Lefebvre (1981)	Landslide	Soft Canadian clay	Bishop	Effective	Circle	1.04	Water filled cracks; reconsolida ted strength	28	53	26	27	-

Table 1. Slope failure database

Notes

1. Atterberg limits averaged over slip surface.
2. Not specified if Janbu SF was corrected or uncorrected.
3. Reported Atterberg limits are specific to foundation soil only.
4. Slope angle was approximated from report figure.
5. Soil strength determined from uncorrected vane testing.
6. Janbu SF is corrected.
7. A lower SF was reported but appeared to be back analyzed.
8. Non-uniform mobilized shear strength calculated by finite element analysis.
9. Atterberg limits averaged over depth.
10. Safety factor estimated from figure.
11. Atterberg limits are specific to clay only. A pseudo-static seismic analysis was included but not reported here.
12. Bishop's method indicated indirectly from citation.
13. Soil strength determined from the simple shear test.
14. Author reports using OMS but considers only cohesion and thus the = 0 method was actually used.

15. Soil strength was determined from a combination of lab and uncorrected vane tests.
16. PI estimated from figure.
17. Soil strength back calculated but confirmed by lab analysis.
18. Soil strength determined by borehole shear testing. Slope stability analysis is OMS modified for planar failure (infinite failure radius).
19. Rapid drawdown analysis per Duncan et al. (1990).
20. The force equilibrium method described is equivalent to COE.
21. Median Atterberg limits reported here.
22. Author also suggests correcting for progressive failure.
23. Slope includes a retaining wall.
24. Failure took place completely within the fill & liner system.
25. Soil strength was determined by tri-axial testing.
26. Foundation soil strength determined by vane testing.
27. Soil strength determined by direct shear test.
28. Embankment strength determined by unspecified laboratory testing.
29. Soil strength determined by a combination of both laboratory and vane testing.
30. Slope angle not reported.
31. Soil strength determined by consolidated undrained tri-axial tests.
32. Progressive failure believed to have occurred.
33. Unjustified $\varphi = 0$ results not reported here.
34. Atterberg limits reported did not include the contribution from a thin sand layer.
35. Safety factor averaged over 44 cross sections.
36. The intact soil strength was used in the analysis.
37. Safety factor reported here from the lower phreatic surface calculations (per author's recommendations).
38. A wide range of assumptions is explored by the authors. The minimum SF reported here is the lower bound author recommended value.
39. Soil strength determined from a ring shear test.
40. Min SF calculated using peak strength values.
41. A 2nd SF was reported but method used was not clear and so is not included here.
42. Slope failure occurred completely within the embankment material.
43. Soil strength determined by unspecified laboratory testing.
44. Plasticity index is averaged over failure depth.
45. Small scale slope model.
46. The safety factor was given as 1 +/- 0.10.

Analysis

Descriptive Statistics

The meta-analysis database consists of 301 safety factor (SF) calculations of 157 different slope failures as reported in 83 publications spanning more than 5 decades. One complexity inherent to the database was the tendency for analysts to consider more than one slope in a publication or utilize more than one method of analysis for a particular slope. Some publications even included multiple

analyses of multiple slopes with multiple methods. Here, all SF calculations are assumed to be independent. The justification for and implications of this assumption may be found in Chapter 3.

Certain slopes proved quite popular in the literature, particularly the Lanester test fill failure (six publications) and the Bradwell cut slope failure (five publications). The overall SF database had a range of $0.47 \le SF \le 1.81$, a mean of 1.05, a median of 1.02, and a standard deviation of 0.22. The average values seem reasonably close to 1, and the standard deviation is consistent with other studies of individual slopes, including Mostyn and Small (1987) and Wu et al. (1975).

Distribution Fit

Historically, SF distributions have been assumed as either normal (e.g. Christian et al., 1994) or log normal (e.g. Duncan and Wright, 2005). These assumptions are seen to bookend Box-Cox transformations from $\lambda = 0$ (log normal distribution) to $\lambda = 1$ (normal distribution), where λ is the Box-Cox transformation variable. Therefore, the SF database was investigated by the Box-Cox analysis at 95% confidence. The results indicate that the log-normal fit was the most applicable ($-0.34 \le \lambda \le 0.63$, recommended value for $\lambda = 0.0$). Other standard distributions were also considered (Weibull, gamma, etc.), but none were convincingly better. For this reason, and since the log normal distribution is widely known and applied to risk analysis, the log normal distribution was used here.

For the transformed database, the mean SF was 1.03 (corresponding to a log transformed value of 0.0135) and the standard deviation was 0.087. Figure 2 shows the normality plot. While the overall fit is reasonable, strong curvature is also evident, suggesting that modeling the database as a simple distribution is not sufficient; the contributions from individual slope factors need to also be considered. In response, Chapter 3 explores and models the effects of the individual slope factors, largely resolving the curvature seen in Figure 2.

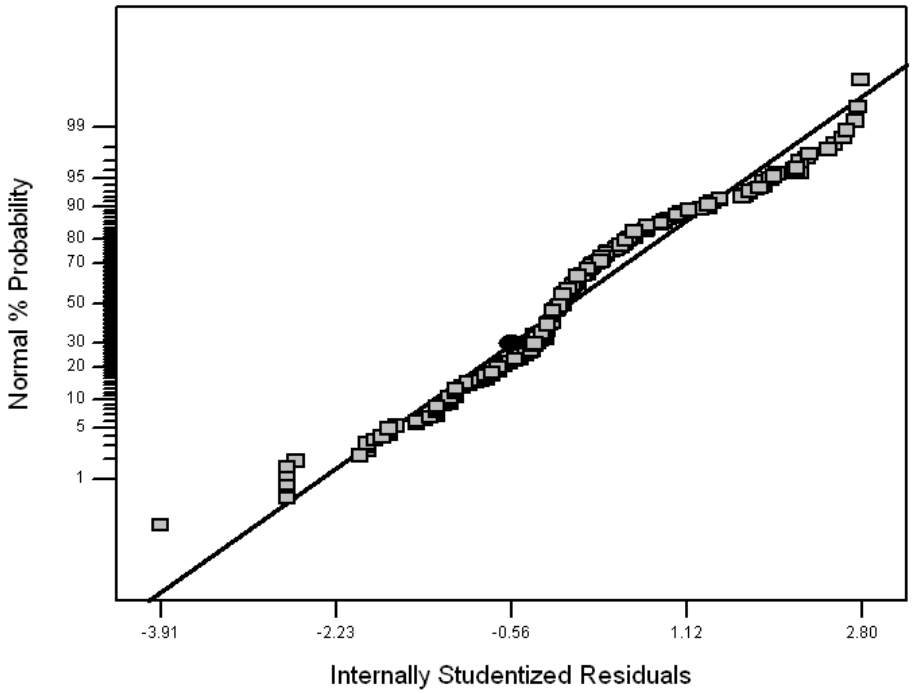

Figure 2. Normality plot of log SF

Trends

The potential that the predicted mean SF and SF variability may have changed over time was investigated. Indeed, the objectives of responsible engineering science must include improved accuracy and reduced scatter over time. Ideally then, one would hope that the published safety factor predictions for

failed slopes would tend to converge to 1 with declining deviation over last the five decades.

Figure 3 shows reported SF values versus reference publication date. The data exhibits considerable scatter. Little change is seen over time, both in terms of mean SF and variance (e.g. no evidence of heteroskedasticity). These observations were initially tested by regressing SF values onto publication date.

Both raw and log transformed data were considered. The results were as follows:

- Overall, both the linear and log models were statistically significant ($R^2 = 0.02,\ F = 7.0,\ p < 0.01;\ R^2 = 0.03,\ F = 8.0,\ p < 0.005$).
- Contrary to what would be ideal, SF prediction was not found to improve over time. The linear model indicated that average SF increased from 0.98 in 1956 to 1.11 in 2007. Similarly, the log transformed model indicated that mean SF predictions increased from 0.96 in 1956 to 1.09 in 2007.
- Variability change over time was investigated by White's test for heteroskedasticity (White, 1980); the results were not significant for either the linear or the log model ($\chi^2 = 0.57,\ p = 0.75;\ \chi^2 = 0.48,\ p = 0.79$).

Unfortunately, resulting conclusions from the regression approach are potential invalid, since highly significant lack of fit metrics were measured for both the linear and log-transformed models ($F = 2.7, p < 0.0005;\ F = 2.8,\ p < 0.0005$). Attempts were made to reduce lack of fit by adding polynomial

terms, but this proved unsuccessful. Regression analysis was therefore judged inconclusive.

With lack of fit making analysis by regression problematic, analysis by subsetting was considered. Specifically, the database was divided as evenly as possible into two sub-databases made up of the 155 SF calculations published before 1984 and the 146 published in 1984 and later (see Figure 4). Mean value differences were evaluated with the two-factor T-test and variance differences were evaluated with the F-test.

No significant differences were found between subset mean values for either the linear or log transformed data ($T = 1.44$, $p = 0.15$; $T = 1.56$, $p = 0.12$). Likewise, no differences were found between the subset variances of either the linear or log transformed data ($F = 1.1$, $p = 0.56$; $F = 0.90$, $p = 0.51$). Unlike regression, subsetting indicated that neither SF prediction nor variance have significantly changed over time.

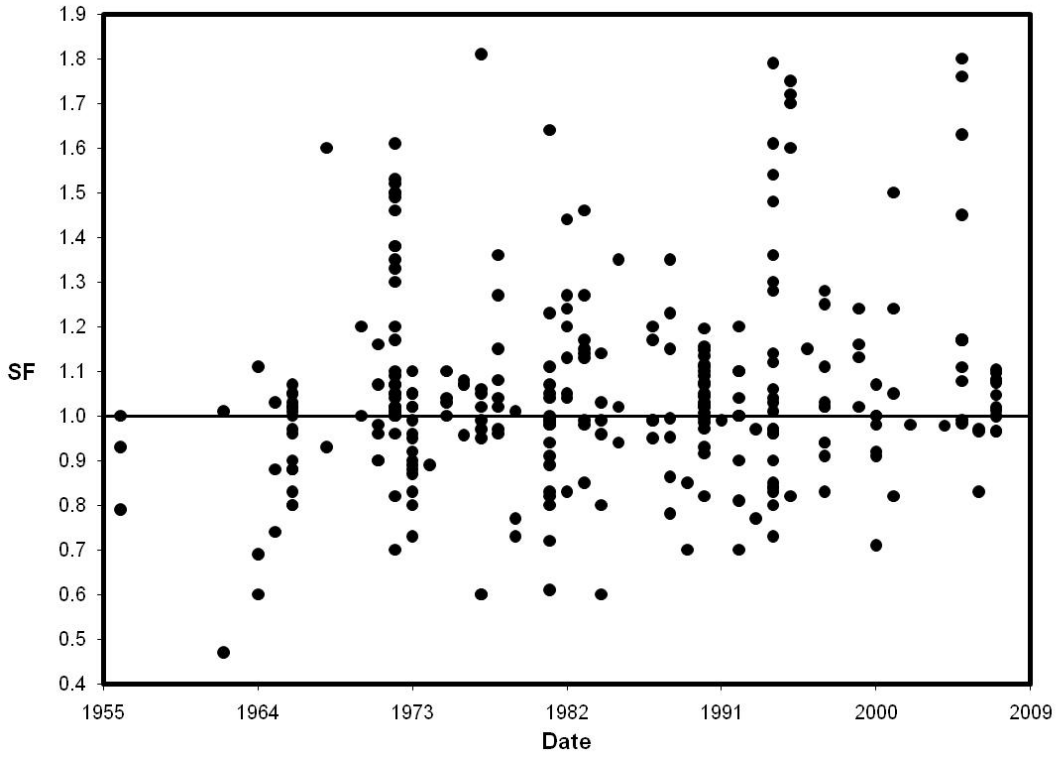

Figure 3. Minimum SF (over all methods) vs. reference publication year

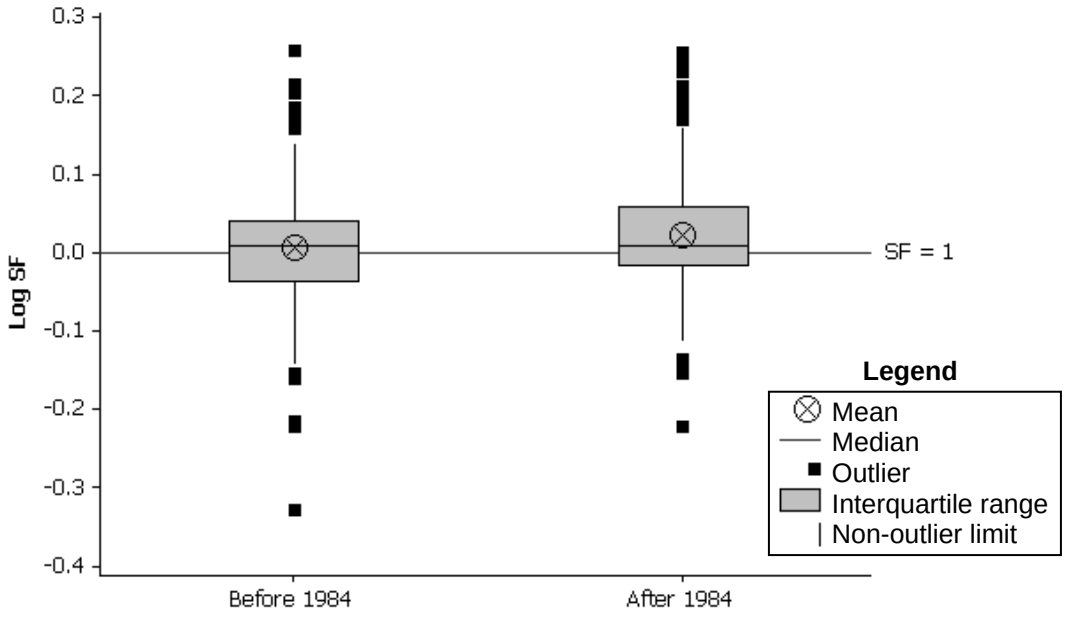

Figure 4. Box plot of Log 10 SF values before and after 1984

Analytical Methods

Thirteen separate methods of stability analysis were reported in the database, and their popularity is shown in Figure 5. The Simplified Bishop's method was the most popular method, accounting for nearly 45% of the database. The $\phi = 0$ method and Ordinary Method of Slices (OMS) each made up about 11% of the total. These two methods coupled with the wedge method, infinite slope, and log spiral make up the direct analytical methods (methods that require only one or two equations to be solved). Direct methods accounted for about 28% of the database. Force equilibrium methods, consisting of Janbu (simplified corrected, simplified uncorrected, and complete), Corp of Engineers Modified Swedish (COE), and Lowe-Karafiath, made up 14%. These methods require iterative solution for the SF and satisfy force equilibrium only. The complete equilibrium methods by Spencer, Morgenstern-Price, Chen-Morgenstern, and Sarma, made up the remaining 14%. The least used analytical method was Chen-Morgenstern, which accounted for only one calculation (0.3%).

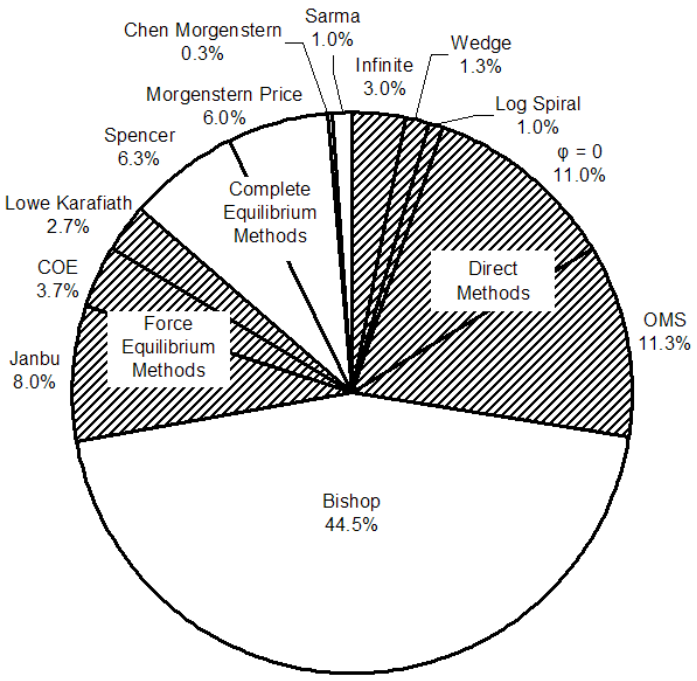

Figure 5. Database partitioned by analytical method

Correction Factors

Correction factors were used in just over half of the minimum safety factors reported (51% of the total number of SF calculations). Often two or more correction factors were applied to a single SF calculation. Six common correction factors were identified that accounted for 97% of the total number of corrections; other factors, usually specific to the region where the slope failure occurred, made up the remaining 3% (see Figure 6). The most common correction was reduced soil strength, which accounted for about 43% of all the corrections, and included residual, critical state, fully softened, and all other reduced strength considerations. Porewater considerations, used to correct for drained, undrained, or rapid drawdown conditions, accounted for 20% of the total; the remaining

corrections were cracks (19%), vane strength (10%), time effects (3%, included consolidation and strain rate), and SHANSEP (3%).

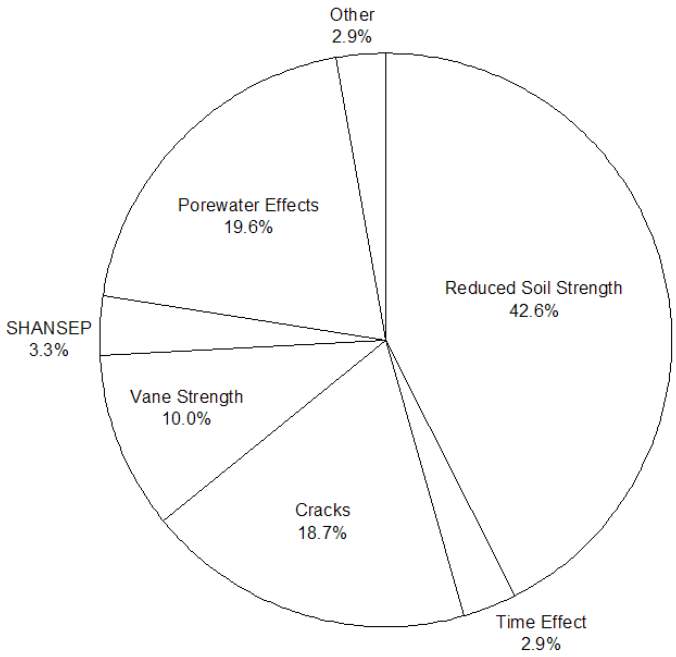

Figure 6. Database partitioned by correction factors

Slope Type

As seen in Figure 7, 73% of slope failures were engineered slopes as opposed to 27% landslides. Of the engineered slopes, fill slopes were the most common (40%). The remaining slopes were cut (10%), test cut (2%), test fill (15%), and experiment (6%). Note that the cut sub-database was generalized to include test cut data in subsequent analyses, since the small number of test cut slopes (4 in total) precluded its use in the higher order statistics and hypothesis testing.

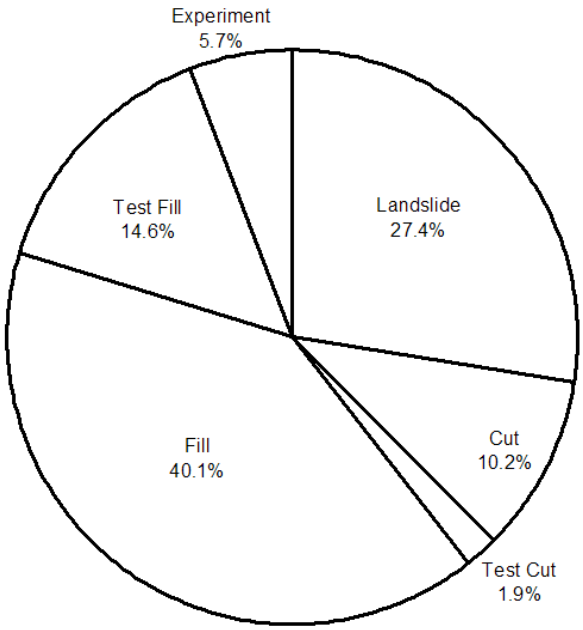

Figure 7. Database partitioned by slope type

Effective vs. Total Stress

The vast majority of calculations assumed effective stress conditions (71% of the total), indicating that implementing porewater pressures directly into the analysis is no longer considered unacceptably difficult, presumably a result of the prevalence of computer aided analysis.

Failure Surface Geometry

The failure surface geometry was primarily driven by the analytical method employed. The configuration of the database consisted primarily of circular failure surfaces (74% of the total) and irregular failure surfaces (22% of the total). Planar failure surfaces (wedge and infinite slope) accounted for the remaining calculations (4%). Because the failure surface typically corresponds with analytical method (Bishop's method requires a circular slip surface, wedge

method requires a planar slip surface, etc.) the differences between calculated SF values for different slip geometries was not further investigated.

Implications

The existing slope failure literature, as reflected in the compiled database here, shows considerable diversity across all model factors. Descriptive analysis by Box-Cox indicated that the database was best fit by a constant log normal statistical distribution, with a corresponding mean of 1.03 and s_d of 0.087. Unfortunately, the pronounced curvature of the residuals indicates the presence of unmodeled contributing factors. Thus, SF calculations are inadequately modeled by descriptive statistics alone; the effects of the slope parameters must be modeled as well. In response to this need, Chapter 3 extends the meta-analysis inferentially, utilizing applied statistical analysis to identify, understand, and quantify the particular contributions of each of the slope parameters.

CHAPTER 3. STOCHASTIC ASPECTS OF SLOPE FAILURES

There are no facts, only interpretations.

– Frederick Nietzsche

Introduction

Chapter 2 introduced a database of 157 slope failures and corresponding 301 safety factor calculations culled from available literature. This database included not only minimum safety factor (SF) calculations for each failure, but also tabulated the analysts' model assumptions, specifically pore water pressure approach (effective versus total stress), slip surface geometry (planar, circular, and irregular), two dimensional limit equilibrium (2DLE) method, and applied correction factor(s), if any. The SF database was approximated by a log normal distribution, but considerable curvature of the residuals indicated significant unmodeled slope factors. The general conclusion was that SF calculation for failed slopes is inherently uncertain, and responsible modeling of the data must include the contributions of the slope factors.

Unfortunately, some of these factors are controllable by the analyst and some are not. Analysis method and slip surface geometry assumptions are elements that the analyst can control. Given enough information, the analyst may be able to adequately model porewater effects. The analyst cannot control soil heterogeneity, which is likely the most significant complicating factor (Christian et al., 1994). Directly affecting that latter are differences between the actual and sampled soils (sample disturbance, strength anisotropy, vane strength bias in clay soils), temporal changes (strain rate, consolidation, creep), hydraulic conductivity

variation, slope integrity (cracking), and strain softening (peak versus mean versus reduced versus residual strength).

The uncertainty and biases of some of the specific factors involved in SF calculation have been investigated in existing literature. Therefore, the first section of this paper utilizes this work to predict how and to what extent these factors are expected to influence the SF database. These predictions are then tested against the data by hypothesis testing. In particular, Analysis of Variance (ANOVA) testing is utilized to identify those factors that have significant main effects on SF calculation and evaluate possible interaction effects. Finally, a reduced ANOVA model of SF calculations is established, and the resulting practical implications for slope stability analysis are explored.

Expected Uncertainties / Biases

General

It is reasonable to assume that uncertainty and bias is introduced to 2DLE analysis from the uncertainty and bias of its inputs. Yet even if the effects of these inputs are disregarded, there may be uncertainty and bias that is fundamental to the 2DLE approach. Kim et al. (1999) note that 2DLE does not satisfy flow, compatibility, pre-failure constitutive requirements, and (at best) satisfies moment and force equilibrium in only a global sense, whereas a rigorous solution must meet equilibrium requirements at every point along a potential slip surface (see also Krahn, 2003).

Another fundamental limitation of 2DLE is that actual slopes are three dimensional, not two-dimensional. In response to this limitation, limit

equilibrium has been generalized to three dimensions (3DLE). Three-dimensional limit equilibrium (3DLE) is reported by Azzouz et al. (1981) to increase predicted SF compared with 2DLE by as much as 30%, a minimum of 7%, and an average of 14%. Ugai (1988) reports an analysis of the Ontake landslide yielded a 3DLE SF of 5% to 30% greater than that predicted by 2DLE. Arellano and Stark (2000) reported a 10% increase between 3DLE and 2DLE SF analysis for the Oceanside Manor landslide. However, Byrne et al. (1992) found only a modest increase of about 5% for 3DLE over 2DLE when analyzing the Kettleman Hills landfill failure, and Sainak (1999; 2004) showed that 3D finite element analysis (3DFEM) can actually produce safety factors 30% lower than predicted by 2DLE, 3DLE, and 2DFEM. This finding was supported by Seed et al. (1990) which showed a reduction of about 9% for a 3DFEM reanalysis of the Kettleman Hills landfill failure. Despite the possibility that 3D slope stability calculations can produce lower SF then 2DLE, the 3D analyses in the literature are usually argued to indicate that 2DLE is inherently conservative (e.g. Arellano and Stark, 2000; Christian et al. 1994).

Failure Surface Model

Christian et al. (1994) point out that there is an inherent non-conservative bias inherent to 2DLE methods since the analyst must find the failure surface that will produce the lowest SF, and estimates this bias to be 5% of the computed SF. For steep slopes, this bias is further compounded by an observed tendency for the critical geometry to lie in close proximity to non-convergent geometries for some analytical methods (Krahn, 2003). It is therefore expected that, for a given

analytical method, modeling of the slip surface with simple geometry assumptions (circle, planar, log spiral) will produce higher SF values then utilizing the more versatile irregular slip surface. However, a number of sources indicate that most failures are circular failures (e.g. Flaate and Preber 1974) and there is some evidence that even non circular failure surface may actually result from rapid progressive circular failures (Burridge 1987).

Analytical Method

Beyond general criticisms of 2DLE, the particular analytical methods of 2DLE have both advocates and detractors. A brief discussion follows of some of the issues specific to particular methods.

Infinite Slope

The infinite slope procedure allows a direct solution for SF by assuming an infinite failure plane parallel to an assumed perfectly linear slope surface. Solution is typically achieved by rotating the Cartesian access to align with the slope, with the *x*'-axis parallel to the slope and the *y*'-axis perpendicular. Implied by the coordinate transformation, but sometimes neglected in practice and the literature, is the requirement that all applied forces are independent of *x*' (Iverson 1990, 1997). When applied correctly, the infinite slope procedure satisfies both force equilibrium and moment equilibrium.

Wedge

The wedge method assumes one, two, or three planar failure surface(s) and thus collapses to the infinite slope procedure if oriented parallel with the

slope. Otherwise, forces and moments are summed about the failure surface to satisfy force and moment equilibrium. Safety factors are usually obtained directly using simple algebra.

LOGARITHMIC SPIRAL

The only direct solution 2DLE method that allows a curved failure surface and satisfies both force and moment equilibrium is the logarithmic spiral (Duncan & Wright, 2005). The restriction of failure surfaces to a logarithmic spiral appears to be its only real limitation. Although no more difficult to apply by computer then some of the higher order methods, it has not been used much for analysis of actual slope failures; the present database contains only three logarithmic spiral calculations.

$\phi = 0$ (SWEDISH CIRCLE)

The $\phi = 0$ method assumes that the Coulomb friction angle ϕ is zero. Also referred to as the Swedish Circle method, the $\phi = 0$ method has historically been a popular total stress analysis procedure, particular for clay slopes where the cohesion is typically much greater than the friction angle effect. The method is equivalent to the logarithmic spiral analysis where a zero friction angle is assumed (Duncan & Wright, 2005). Thus, the resulting failure surface is circular, which simplifies the calculation, and complete equilibrium is satisfied. Unfortunately, the appeal of this simple procedure has led to analysts occasionally ignoring significant friction angles, resulting in inaccurate (but conservative) safety factors. For example, the procedure has been applied to fill slopes on clay which not only neglects the friction angle of the clay, which can be significant,

but also the friction angle of the fill, which is typically much greater than its cohesion. Thus, the $\phi = 0$ method is expected to generate SF values less than the actual value for soils with significant friction angles.

Ordinary Method of Slices (OMS)

The Ordinary Method of Slices (OMS) satisfies moment equilibrium for a circular failure surface and directly calculates SF by assuming the interslice forces are zero. For an infinite radius, OMS thus collapses to the undivided wedge method. Taylor (1948), Whitman and Moore (1963) both argue that OMS is inaccurate. Duncan & Wright (1980) note that OMS typically underestimates SF compared to other methods of slices, particularly for slopes with high pore water pressures modeled by effective stress analysis. The assessment that OMS is significantly conservatively biased appears to be so widely held that some slope failure analysts automatically conclude OMS is less accurate than other methods, even when they have found evidence to the contrary (see Moore, 1970 and Sundaram & Bell, 1972). One complicating factor is that some analysts report SF calculations as based on OMS when in actuality they have assumed a zero friction angle and thus their method of solution is therefore actually the $\phi = 0$ method (e.g. Hanzawa et al., 2000).

Simplified Bishop

The Simplified Bishop method (henceforth described as just the Bishop method) is a method of slices that assumed the interslice forces are horizontal. Bishop's method satisfies moment equilibrium but satisfies force equilibrium in

the vertical direction only. Like OMS, a circular slip surface is assumed. The safety factor is computed by iteration. The Bishop method has been historically very popular, particularly because it is relatively simple to apply yet usually reported to closely agree with the higher order 2DLE methods.

The Bishop method, like all the higher order methods, can sometimes indicate inappropriate stresses along the slice boundaries and at the slip surface toe (Duncan & Wright, 2005).

Janbu

Janbu introduced two methods of 2DLE analysis that satisfy force equilibrium but not moment equilibrium: the Simplified Janbu and Janbu's Generalized Procedure of Slices (GPS). (The latter is sometimes referred to as Janbu's Rigorous method.) The GPS method introduces a line of thrust description to model the interslice force. The Simplified Janbu model is so called because it is the GPS model simplified by assuming the interslice forces are horizontal. Like all of the force equilibrium methods, an irregular failure surface is allowed for both methods and solution must be obtained by iteration. The assumption of horizontal interslice forces used by the Simplified Janbu method was justified by Carter (1971) who found that the SF actually varied according to the vertical coordinate used to sum moments about a slice and therefore concluded that the only consistent vertical coordinate for any force analysis is infinity, corresponding to horizontal force equilibrium. However, Carter's conclusion was contradicted by Boutrup et al. (1979) which found the SF calculated in this manner is actually a maximum when the circular slip surface

intersects the top of the slope at a steep angle. They concluded that Janbu is non-conservative for deep failure surfaces that intersect the ground surface at the top of the slope at angles greater than 60 degrees.

Another persistent issue with Janbu's Simplified method is that, in practice, it is not always reported if the original or corrected Janbu procedure is being applied (Duncan & Wright, 2005). The Janbu correction, as approximated by Abramson et al. (2002), raises the estimated SF up to 13%. Uncorrected Simplified Janbu SF calculations are therefore expected to be biased conservatively.

Another challenge of interpreting the database is that analysts did not always state the Janbu method used. Furthermore, it is difficult to identify the Janbu method used by cited reference, since there appears to be no standard reference for either of Janbu's methods. As a result, analysts were found to sometimes cite difficult to obtain conference papers, titles in other languages, and particular applications of an unspecified Janbu method reported by other authors.

Fortuitously, identifying the particular Janbu method used is not critical for this chapter. The limitations of the meta-analysis as applied here requires all force methods to be grouped as a particular subset, and since both of Janbu's methods are force methods, the specific Janbu method used for the SF analysis is not directly relevant. Therefore, both of Janbu's methods were designated by Janbu's name only, and reported so in the database, although specific information regarding the Janbu method used was sometimes included in the table footnotes (see Table 1 in Chapter 2).

Lowe & Karafiath

The Lowe & Karafiath procedure satisfies force equilibrium by assuming the interslice forces are included at the average angle formed between the ground surface and slip surface. Duncan & Wright (2005) recommend Lowe & Karafiath as the force method that produces the best results. It is presumed, but not typically discussed in the literature, that the issues expressed by Carter (1971) and Boutrop et al. (1979) would also be applicable to the Lowe & Karafiath procedure.

Corp of Engineers Modified Swedish (COE)

The primary limitation of the U.S. Army Corps of Engineer's Modified Swedish (COE) force equilibrium method is an uncertainty as to the procedure's assumption of interslice force inclination, which can be interpreted in several different ways. Unfortunately, force equilibrium safety factors are quite sensitive to the assumed force inclination, with differences up to 25% (Duncan & Wright 2005). Thus, significant differences would be expected between COE safety factors produced by different analysts. Coupled with the Carter (1971) and Boutrop et al. (1979) observations on force equilibrium procedures, some inaccuracy of COE would be expected in practice. It is not clear, however, whether this inaccuracy would be conservative, non-conservative, or unbiased.

Spencer's Method

Spencer's method assumes all interslice forces are inclined at the same angle, the value of which is solved by complete equilibrium. Probably the most popular method of slices that satisfies complete equilibrium and allows irregular

failure surfaces, in practice Spencer's method can be difficult to apply due to convergence problems. Indeed, Boutrup et al. (1979) rejected Spencers method for their STABL program for this reason.

Spencer's method, like all the complete equilibrium methods, is computationally intensive, requiring simultaneous solution of the three static equilibrium equations for each slice.

Morgenstern and Price

The Morgenstern and Price complete equilibrium method extends Spencer's method to allow the interslice resultant force angles to change direction between slices, with the inclination function specified by the analyst. The normal force location is also specified by the analyst. Despite the seemingly arbitrary nature of these inputs, the resulting SF calculation seems to be fairly robust to different assumptions (Duncan and Wright, 2005).

Chen and Morgenstern

The Chen and Morgenstern procedure, which also satisfied complete equilibrium, adds another analyst specified function to the Morgenstern and Price algorithm to align the interslice forces with the slope. The result is reported to restrict the number of solutions for the SF.

Sarma's Method

Sarma's complete equilibrium method was developed to calculate directly the seismic coefficient given a known SF. When applied outside of earthquake modeling (e.g. the seismic coefficient is zero), Sarma's method becomes a

modification of the Morgenstern and Price procedure where the interslice forces are assumed proportional to the shear strength. For frictional materials, this requires the analyst to specify the distribution of normal forces across each slice (Duncan & Wright 2005).

Porewater Pressure

Porewater pressure introduces forces that can be destabilizing or restorative depending on the failure and slope geometry. The two basic approaches for including porewater pressure in the analysis is *effective* or *total* stress analysis. For total stress analysis, the porewater pressures are included implicitly in the strength parameters. For effective stress analysis, the porewater pressures introduced explicitly as contributing forces in the 2DLE formula. Effective stress analysis is generally perceived as more accurate (e.g. Pilot et al. 1982). With the advent of the computer, effective stress analysis has become less computationally difficult and is now often used in practice.

Slope Type

Failed slopes may be divided into five categories depending on available information and control over the slope characteristics. The failed slope with the least known information is clearly a *landslide*, where natural soil conditions are often anisotropic and the slope geometry typically nonlinear and three-dimensional. On the other hand, engineered slopes are better controlled, better understood, and typically more accurately described with simple parameters. In order of increasing information and control, the engineered slopes are c*ut, test cut,*

fill, test fill, and *experiment* slopes. Note that test cut and test fill slopes are full scale experiments done in the field, whereas experiment slopes here refer to typically smaller scale slopes brought to failure under strict laboratory conditions.

Greater information and control should reduce uncertainty and raise model accuracy, suggesting that the failure of engineered slopes should be more predictable than landslides. But engineered slopes often fail over smaller time scales due to consolidation and transient porewater effects not typically as active in most landslides. Given these complications, 2DLE predictions are not expected to be equally accurate over all slope types. In particular, Krahn (2003) argued that those methods satisfying complete equilibrium are the most accurate for natural slopes, and Ferkh and Fell (1994) observed that cut slopes and riverbanks fail at higher SF than other slopes.

Correction Factors

To account for the perceived limitations of 2DLE, correction factors are usually introduced when safety factors have been found to deviate significantly from 1 for a slope at failure. These correction factors may be specific to slope location, soil tests, soil types, anisotropy, etc. The most popular correction factors are:

- **SHANSEP.** Developed by Ladd and Foott (1974) and often referred to by its acronym, the Stress History and Normalized Soil Engineering Properties (SHANSEP) correction attempts to account for sample disturbance and strength anisotropy. The importance of this correction is supported by Wong et al (1982) who estimated that

soil sampling and lab testing uncertainty can result in errors up to 20% in safety factor calculation at slope failure.

- **Reduced strength.** These correction factors correspond to the fully softened, residual, recompressed, or otherwise reduced soil strength as opposed to the mean strength indicated by soil testing. Sometimes the peak strength is used corresponding to a correction factor greater than 1 (non-conservative).
- **Integrity.** The possibility of cracks is often a judgment call by the analyst and may significantly change the computed SF.
- **Strain rate / Consolidation / Creep.** The mismatch between the field loading rates, usually occurring over weeks, and lab loading rates, usually imposed over minutes, can result in inaccurate test estimates of soil strength. While not typically accounted for (Duncan & Wright, 2005), field loading correction factors do exist and are sometimes applied (e.g. Wolski et al., 1989; Hanzawa et al., 2000).
- **Anisotropy**. Duncan & Wright (2005) note that anisotropy arises from both inherent soil properties and stress configuration within the slope. Corrections for anisotropy have historically been lumped into other corrections such as vane strength, etc.
- **Vane strength.** Much work has been contributed to the literature on correction factors for vane strength measurements of plastic soils, established to account for anisotropy and creep strength loss. The original vane strength correction factor is usually attributed to

Bjerrum (1972), later revised by Bjerrum (1973) and Ladd et al. (1977). This correction factor is empirical, typically based on a linear regression of minimum safety factor versus plasticity index (PI).

- **Porewater Pressure.** Some analysts choose to apply correction factors to account for rapid drawdown and other effects of porewater pressure because either a total stress approach is utilized or it is argued that the effective stress utilized under predicts the porewater effect.

Analyst Differences

Different analysts bring their own experience and abilities to slope stability analysis, and can reach much different conclusions from the same data (Christian, 2004). These differences can arise from simple modeling decisions, such as the number and locations of internal slices, interslice force assumptions, slip geometry type and location, and judgment as to when the minimum SF has been reached.

Mostyn and Small (1987) reported on a survey of 20 engineers who solved the same slope problems. They found an average SF standard deviation (s_d) of $s_d = 0.18$ between analysis calculations of the same circular failure problem. For non-circular failure surfaces the difference between analysts was greater, with $s_d = 0.26$. While it is unknown if these results would be consistent for a larger database of analysts, it is likely that analyst differences contribute significantly to the inherent statistical nature of SF analysis.

Summary

Despite the criticisms of specific 2DLE analytical methods, many argue that higher order 2DLE methods (force methods, complete methods, and arguably Bishop's method) produce SF values with no significant difference between them (e.g. Bjerrum, 1972; Christian et al., 1994). Consistent with this assumption, publications sometimes report the result of a limit equilibrium analysis but leave the corresponding 2DLE method unspecified (e.g. Chiasson & Wang, 2007). Indeed, Yu et al. (1998) argue that Janbu, Spencer, Morgenstern and Price, and any other method satisfying complete equilibrium will produce safety factors within 5% of each other, with the caveat that this consistency does not necessarily imply overall accuracy of the limit equilibrium approach.

In terms of the 2DLE approach in general, the position of the engineering community at the present time appears to be that 2DLE safety factors are often biased conservatively compared to its true value (e.g. Babu and Bjoy, 1999; Singh et al., 2008). One geotechnical argument for this position is that slope stability modeling does not always include matric suction in the analysis, the binding effect of which would tend to increase calculated SF (although not always; see Travis et al. 2010a).

Database Testing

The database reports 301 minimum SF calculations for 157 failed slopes. Detailed database information may be found in Chapter 2.

SF Method, Slope Type, and Stress Approach Differences

Limit equilibrium analysis utilizes a number of different factors. Statistical hypothesis testing using Analysis of Variance (ANOVA) was used to investigate potential differences between and within these factors. Differences between SF values were investigated as a function of analytical method (grouped into direct, Bishops, force, and complete methods), stress approach (effective versus total), and slope type (fill, test fill, experimental, and cut slope, where the cut slope factors included the four "test cut" SF calculations to ensure an adequate number of cell values). An unbalanced model was implemented since the number of replicates was not the same in all cells, which is, of course, an inherent (albeit unfortunate) characteristic of a meta-analysis.

An additional complication of the ANOVA analysis was that the number of SF calculations varied per slope. For example, as seen in Table 1 of Chapter 2, the Narbonne fill slope failure) had four published SF calculations whereas the Sieve River landslide had only one. Moreover, many studies analyzed more than one slope, introducing yet another complication.

The appropriate interpretation of multiple responses from the same source, as seen here, is a typical challenge for meta-analyses in general. Bijmolt and Pieters (2001) investigated a number of reasonable approaches to the problem, including simply ignoring the issue (assumes all response are independent), introducing weighted factors, selecting single representative values, and establishing nested relationships between responses. They concluded that the best method was utilizing a nested model. Unfortunately, a nested model would be

difficult to implement in the present work because there are not only multiple analyses of some slopes by different analysts but also multiple slopes analyzed by the same analysts, and even overlap between the two (e.g. some slopes analyzed by multiple analysts were also included in studies of multiple slopes by a single analyst).

As an alternative to a fully nested approach, Bijmolt and Pieters (2001) recommend simply considering all responses as independent, even though this approach may introduce unjustified noise. Therefore, while the present analysis proceeds accordingly, it is possible that some of the main effects and interactions will be significant even if the analysis indicates otherwise. For this reason, while only probability levels ("significance levels") below 5% ($p < 0.05$) will be referred to a statistically significant, probability levels below 10% ($0.05 \leq p < 0.10$) will also be identified and reported as borderline significant. Note that the assumption of independent data is consistent with the apparent homoskedasticity of the database, as shown in Chapter 2.

Preliminary analysis indicated that the database contained enough data points to generate all main effects and first order interactions. Unfortunately, the overall three factor interaction could not be computed with the number of data-points available (that is, the available degrees of freedom were not adequate), but this limitation may not significant since interactions between three or more factors are often negligible from a practical standpoint. Therefore, per standard practice, the overall interaction term was aliased and used as part of the overall model error estimate. A Box-Cox analysis recommended a log (base 10) transform of the

response (SF) in order to meet the ANOVA assumptions of residual normality, independence, and constant variance, consistent with the overall database analysis reported in Chapter 2. Design Expert version 7.1.6 was used to process the ANOVA with the transformed SF values. The residuals of the transformed model were inspected and no obvious violation of the ANOVA assumptions was observed, and no evidence of a lack of fit was indicated ($p = 0.14$).

Source	Sum of squares	Degrees of freedom	Mean square	F	p-value
Overall Model	*0.45*	*27*	*0.017*	*2.44*	*0.0002*
Slope Type	0.015	4	0.00375	0.55	0.6961
Analytical Method	*0.086*	*3*	*0.029*	*4.25*	*0.0059*
Porewater Approach	0.020	1	0.020	2.96	0.0864
Slope Type x Analytical Method	0.14	12	0.012	1.72	0.0621
Slope Type x Porewater Approach	*0.10*	*4*	*0.026*	*3.86*	*0.0045*
Analytical Method x Porewater Approach	0.005727	3	0.001909	0.28	0.8385
Residual	1.85	273	0.006772		
Lack of fit	0.073	7	0.010	1.57	0.1448
Pure Error	1.78	266	0.006675		
Corrected Total	2.29	300			

Table 2. ANOVA analysis results

The ANOVA results (Table 2) indicated that the overall model accurately described the data ($p < 0.0005$). The only clearly significant main effect was analytical method ($p < 0.01$) although the porewater approach was also borderline significant ($p = 0.09$). Slope type was not a significant contributor to the model in terms of main effects ($p = 0.70$) but was part of a significant interaction with porewater approach ($p < 0.005$) and part of a borderline significant interaction

with analytical method ($p = 0.06$). Analytical method and porewater approach did not interact significantly ($p = 0.84$).

These results are consistent with the prevalent opinion that there are differences between safety factor calculation methods and differences between total and effective porewater stress analysis. The lack of evidence for a significant slope type effect is somewhat surprising, however, although it does appear to play a significant role as an interaction term.

The foregoing ANOVA analysis is descriptive but complicated by insignificant terms. A better understanding of the underlying factors as well as the ability to make confident predictions about future events requires a reduced ANOVA model. ANOVA reduction is accomplished by removing insignificant factors and interactions, thus creating a well-defined essential model that minimizes risk of overfitting. The reduction process is also characterized by careful consideration of the residual analysis, ensuring that the final model conforms to normality assumptions and is therefore appropriate for risk analysis.

Model reduction was implemented here by a backward algorithm based on significance. This process first eliminated the Slope Type main effect, then the Analytical Method versus Porewater Approach interaction, and finally the Porewater Approach main effect. The reduced ANOVA model is shown in Table 3.

Source	Sum of squares	Degrees of freedom	Mean square	F	p-value
Overall Model	*0.38*	*19*	*0.020*	*2.90*	*< 0.0001*
Analytical Method	*0.073*	*3*	*0.024*	*3.58*	*0.0143*
Slope Type x Analytical Method	*0.15*	*12*	*0.013*	*1.86*	*0.0387*
Slope Type x Porewater Approach	*0.074*	*4*	*0.019*	*2.72*	*0.0300*
Residual	1.92	281	0.00683		
Lack of fit	0.14	15	0.00956	1.43	0.1316
Pure Error	1.78	266	0.00668		
Corrected Total	2.29	300			

Table 3. Reduced ANOVA Model

The reduced model is non-hierarchical, in the sense that interaction terms are included but their corresponding main effect terms are not. There is some controversy in the literature regarding hierarchy in ANOVA and regression models. Peixoto (1987, 1990) argued that an appropriate model requires that the results of statistical testing be the same under linear transformations of the data, and this can only be achieved if the model includes the main effects of all factors included in higher order interactions, even if these main effects are not statistically significant. However, some more recent publications, such as Montgomery et al. (2005), argue that this requirement is overly restrictive and may result in highly inaccurate predictions as a result of overfitting the data.

The effect of expanding the reduced model to achieve hierarchy was investigated for the reduced model presented here. However, when the Slope Type and Porewater Approach main effects were included, no difference in the

overall analysis conclusions was found, and only a minimal benefit to the model was achieved (adj-R^2 changed from 0.11 to 0.12). Unfortunately, adding these main effects appeared to compromise the normality assumptions, resulting in less well behaved residuals and model sensitivity to a particular data point ($\text{leverage} > 1$). For these reasons, and in order to maximize the predictive accuracy and model parsimony, Slope Type and Porewater Approach were not included as main effects.

The reduced ANOVA model overall fit to the data is quite significant ($p < 0.0001$). Furthermore, unlike the overall analysis, each factor in the reduced model is of similar significance ($0.01 < p < 0.05$), indicating that no one factor dominates. Adequate precision, a measure of signal to noise ratio, was 6.85, indicates that the model is appropriate for prediction. The model R^2 values, however, are quite small, with $R^2 = 0.16$, adj-$R^2 = 0.11$, and pred-$R^2 = 0.04$. These low regression values, even by slope stability standards, suggest that the usual deterministic design methods are wholly inadequate; risk analysis must be utilized for responsible design.

Risk analysis based on the ANOVA model requires that the residuals of the model be normally distributed. The model is consistent with this requirement, as shown by the normal probability plot in Figure 8. The residuals align adequately with the normal probability line, their curvature much reduced from the initial distribution fit shown in Chapter 2. The residual analysis also included residuals versus run order and residuals versus predicted values; like the normal

probability plot, these analyses did not show significant violations. Influence testing did not indicate any significant outliers.

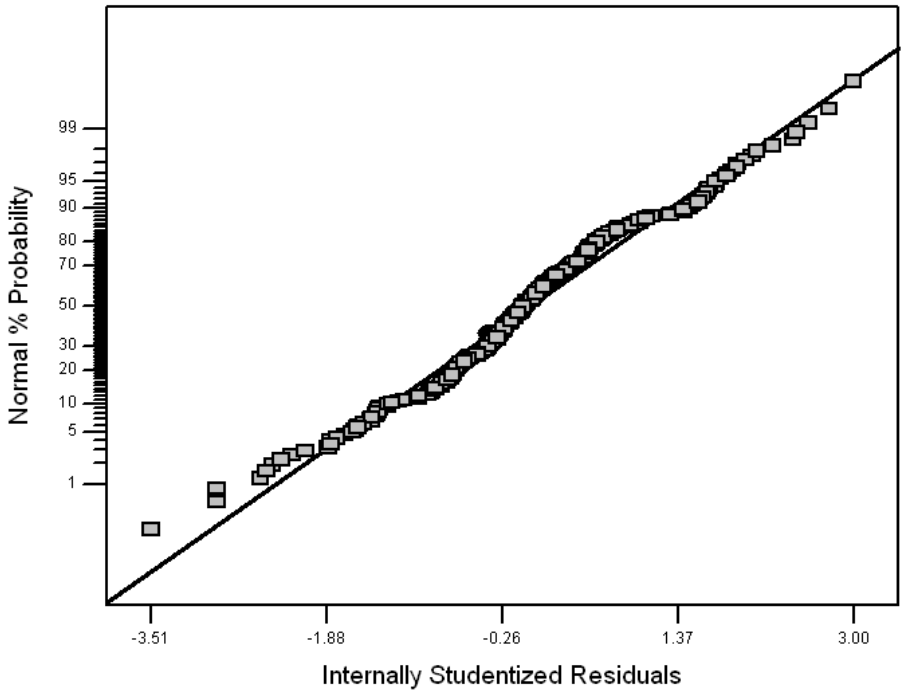

Figure 8. Normal probability plot for the reduced ANOVA model.

The reduced ANOVA model analytical approach main effects are shown in Figure 9. The direct, Bishop, and complete analytical methods all have least significant difference (LSD) bars, a measure of confidence, that overlap SF = 1. The force method calculations, however, are well above SF = 1, evidence that force methods are, on average, significantly non-conservative.

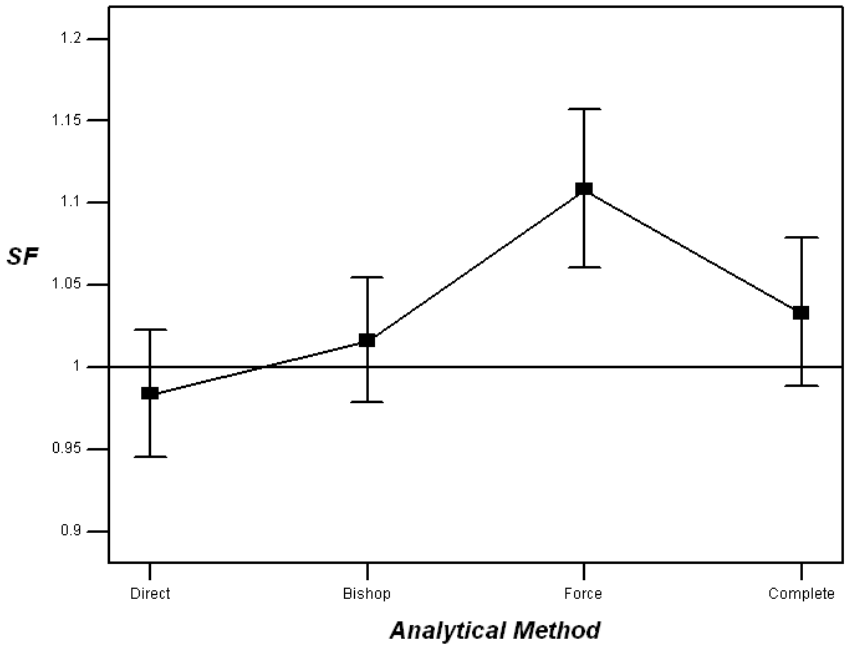

Figure 9. Main Effects Plot: Analytical Method

As shown in Figure 10, Slope Type and Porewater Approach are strongly interactive. While effective stress analysis is fairly consistent near SF = 1 across all slope types, total stress analysis varies considerably for different slope types. It has been theorized that cut slopes and riverbanks fail at a higher SF than engineered slopes (e.g. Ferkh and Fell, 1994), but Figure 10 suggests that this the relationship is more complex, with effective stress analysis predicting a high SF for landslide failures but a low SF for cut failures, and the opposite trend for total stress analysis.

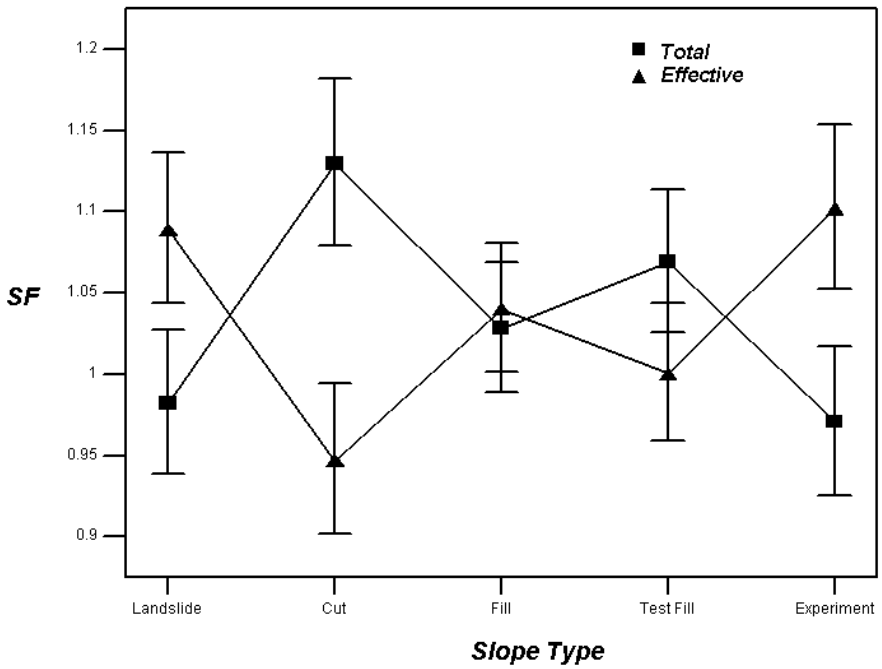

Figure 10. Interaction Effects Plot: Slope Type versus Porewater Approach

Perplexing as well is the strongly correlated nature of the total and effective stress interaction. For each slope type, the predicted SF calculations are more or less reflected about the line defined by $SF = 1.03$, with effective stress greater than total stress SF calculations for landslide, fill, and experiment slopes, and total stress greater than effective stress SF calculations for cut and test fill slopes. The explanation for this interaction is not obvious, but may be related to slip geometry differences. The cut and test fill slope failures tended to be deep and circular, passing through the piezometric surface and several different soil strata, whereas the landslide, fill, and experimental failures tended to be relatively shallow by comparison. A future paper will further consider this relationship.

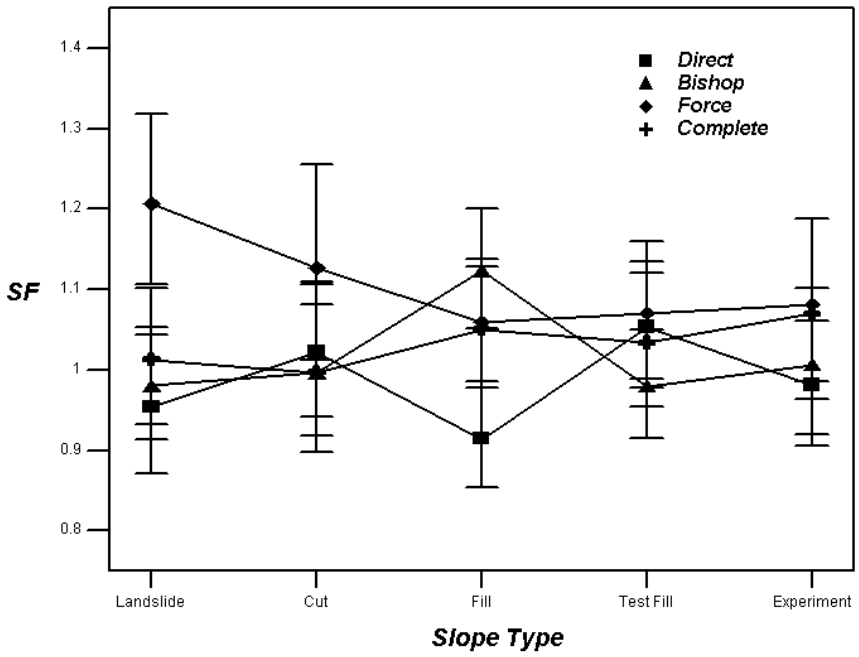

Figure 11. Interaction Effects Plot: Slope Type versus Analytical Method

Figure 11 shows the interaction effects between Slope Type and Analytical Method. This relationship appears quite complicated, but much of the interaction is within error bar range and therefore somewhat inconclusive. The exception is specific to the landslide slope type, where the Force method is seen to have LSD bars well above 1, and also above the LSD bars of all the other analytical methods.

SF Deviations from 1

Overall, the ANOVA model predicted a least squares SF mean of 1.03, or slightly higher than $SF = 1$ as would be expected. This is inconsistent with the prevailing engineering opinion that 2DLE safety factors are conservative, and thus one would suspect that, on average, the minimum safety factors would be significantly less than 1. The SF database was tested against the expected value

of $SF = 1$ with the database partitioned by analytical method (the only main effect contributor found in the ANOVA model.) Independent one-sample t-tests were used for hypothesis testing of the log (base 10) transformed SF values. The results are shown in Table 4.

	Method			
Statistic	**Direct**	**Bishop**	**Force**	**Complete**
Median	1.00	1.02	1.08	1.03
Mean	0.98	1.04	1.10	1.05
s_d (of log SF)	0.093	0.087	0.089	0.064
n	83	134	43	41
T	0.93	2.11	3.19	2.08
p	0.357	***0.036***	***0.003***	***0.044***

Table 4. T-Test results of SF database (based on log SF)

Based on the t-tests of the log SF values, all methods except Direct deviated significantly from $SF = 1$. The Bishop method and the complete method both had mean SF values near 1.04, an effect that was significant at $p = 0.05$. The force method SF values were quite a bit higher, with a mean of 1.10, significant at $p = 0.005$. The direct method SF mean was 0.98 ($p = 0.357$). Assuming a normal distribution for the SF (e.g. not transforming the values) increased the significance of the difference with $SF = 1$ for all methods except Direct (where it actually decreased), and thus did not change any of the hypothesis test conclusions.

Plasticity Index

Although the vane strength correction factor has been in existence for more than three decades, only 24% (10 out of 43) of the SF calculations that were based on vane strength were corrected based on Bjerrum (1972), Bjerrum (1973),

or any other vane strength correction factor formulas. Also, the SF calculated with uncorrected vane strength averaged 1.03 whereas the corresponding corrected SF averaged 1.12, a difference rather the opposite of what would be expected.

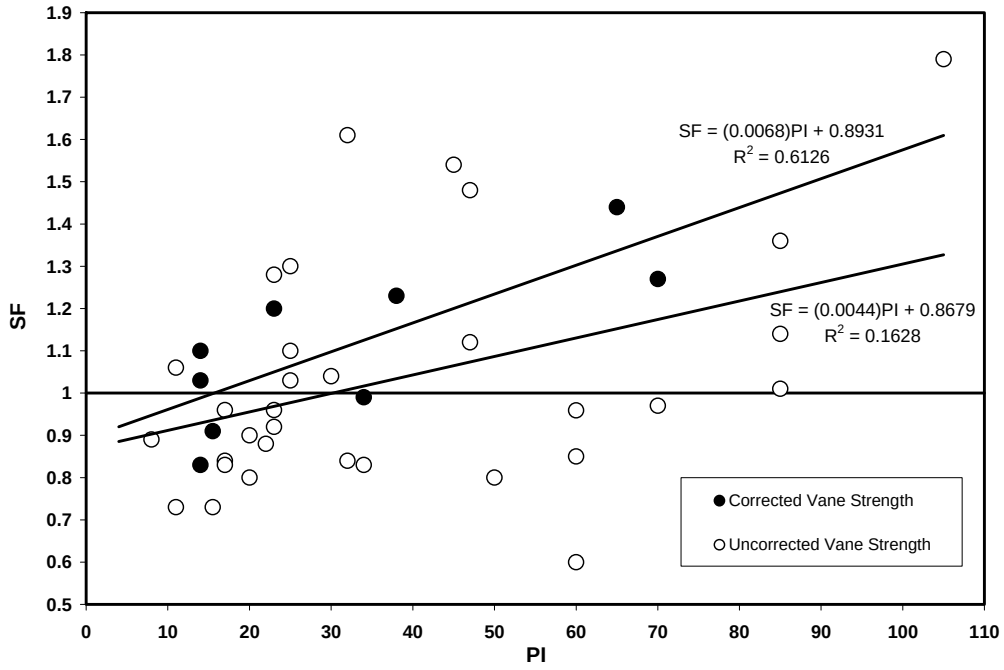

Figure 12. Slope minimum safety factors versus Plasticity Index (PI).

Despite the seeming lack of success regarding the vane strength corrections, the general principle of correction by regression is supported by Figure 12, which shows both the corrected and uncorrected safety factors versus plasticity index (PI) for the vane strength based data (only studies published after Bjerrum's 1972 paper were considered). The corrected values are seen to be closely oriented about its regressed line ($R^2 = 0.61$) whereas the uncorrected values exhibit wide scatter ($R^2 = 0.16$). Surprisingly, the regressed lines onto the corrected and uncorrected SF are nearly coincident. While the implications of

this relationship are not clear, the results inarguably indicate that the vane strength correction alone does not account for SF deviation.

Soils without Clay

The bulk of the literature on failed slopes is specific to clay soils; indeed, almost 90% of the slopes in the current database had soils with significant amounts of clay. The calculated SF (averaged across methods and analysts) for the seventeen slope failures in the database that did not have appreciable clay are shown in Figure 13. A wide range of SF is seen with an average of 1.03 (based on log transformed SF), consistent with the overall results.

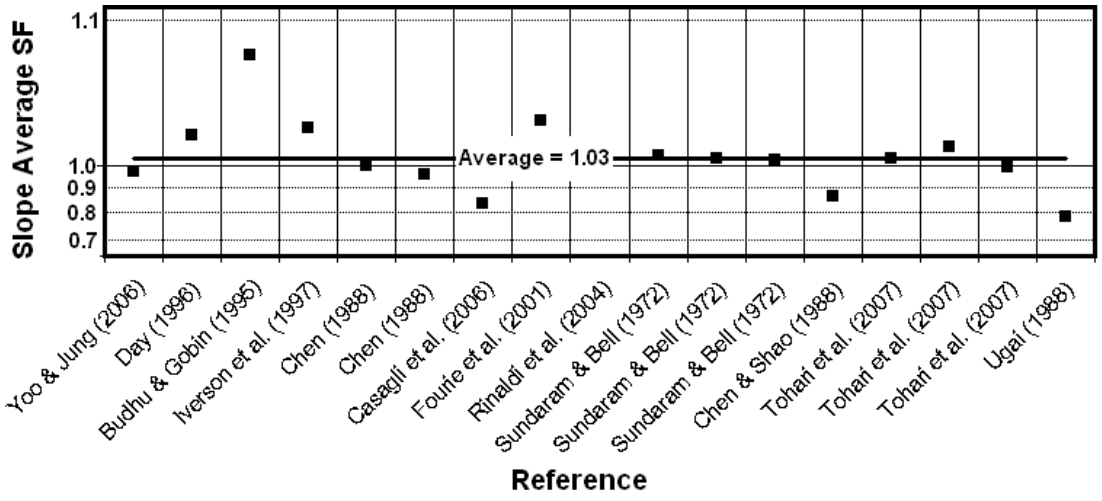

Figure 13. Failed slopes in soils without significant clay.

Discussion

Analytical Method

The ANOVA testing and one-factor t-tests indicate that direct methods of solution averaged closer to the expected value of SF = 1 then alternative methods for calculating SF for unstable slopes. In particular, SF calculation based on the

force method appears to have a non-conservative bias, whereas the average deviation from 1 for the SF calculations from Bishop's method and complete methods of analysis, while statistically significant, tended to be more moderate. Considerable scatter was evident across all methods.

A number of factors likely contribute to these observed differences between methods, including the following:

1. All higher order analytical methods were developed to account for interslice forces. The direct methods, however, are all independent of the interslice forces except OMS, which assumes the interslice forces equal zero. This assumption of zero interslice forces is obviously inaccurate for slopes with a SF significantly greater than one, but may approximate reality as a slope nears failure and the porewater pressure within the slope significantly changes (Moore 1970). Porewater pressure can rapidly increase at failure of a saturated slope, possibly leading to liquefaction of the soil and thus complete loss of the interslice forces, as noted by Iverson (1997). Of course, in the same study, Iverson also found that at failure in unsaturated soils, the porewater pressure dropped and soil dilation occurred, and thus one might expect the corresponding interslice forces to increase. Thus, the only sure conclusion is that, regardless of the saturated condition of the soil, the interslice forces change rapidly near failure and are not likely to be modeled correctly by any limit equilibrium method that

utilizes interslice force modeling but fails to account for force changes near failure.

2. The direct methods have few applicability limits and produce a single solution, whereas higher order methods have associated applicability limitations and multiple solutions, the interpretation of which may require the analyst to apply engineering judgment and/or physical reasoning. For example, the difficulties inherent to determining correct versus incorrect potential solutions are the primary reason that Spencer's method was excluded from the software developed by Boutrup et al. (1979).
3. One of the advantages of higher order methods is the ability to model irregular, and thus arbitrary, failure surfaces, which would seem to allow better modeling of failure and a lower predicted SF. However, unless the analyst already has an idea of the potential critical failure surface geometry, it may take many trials to find the critical failure surface. Moreover, the higher order methods are computationally intensive, requiring numerous iterations to achieve a solution to even a single failure surface. Time and analyst patience are therefore unintended constraints against achieving the critical failure geometry in a higher order model. Thus, it may be that determining the critical slip surface is more important for accurate SF calculation then typically assumed in practice.

4. The apparent accuracy of the direct methods may actually result from inherent compensating errors, perhaps from highly simplified failure geometries, which would tend to increase calculated SF, balanced by the inadequate representation of the interslice forces, which may decrease the calculated SF.

Whatever the reason, the direct methods do appear to predict SF near 1 for failed slopes more successfully than other methods. However, it should not be presumed that this result would also apply to stable slopes. Indeed, as discussed earlier, at high SF values soil response to porewater pressures would be less pronounced and the interslice forces therefore more likely to be consistent with the assumptions of the higher order methods.

Correction Factors

Historically, high SF values for failed slopes have been attributed to the complicating presence of clay; however, it appears that calculated SF values above 1 also occur on average for slopes with soils without significant clay. Moreover, while the vane strength correction factors applied in the database did, indeed, reduce calculated minimum SF, these corrected SF values were still significantly above 1. Thus, while the database supports the ongoing use of SF reducing correction factors, it appears that the correction factors as currently applied are not sufficient, by themselves, to reduce SF calculations to the expected value of SF = 1. The database also does not support the use of correction factors that raise SF, such as those sometimes introduced to account for three-dimensional effects or vane strength at low PI values.

Risk Analysis

Risk analysis as applied to stability analysis requires two critical components. The first is an accurate deterministic model that produces a mean SF prediction of 1.0 for real slope failures. The second is an accurate statistical model to that can be used to produce probabilities of failure.

With regard to the first requirement, the database analysis indicates that direct methods of solution are more successful than other methods for predicting an average SF close to 1 for slope failures. However, while Bishop's method and the complete methods of solution were found to significantly deviate from 1 from a statistical standpoint, the actual extent of this deviation is small enough that it is probably not relevant from a practical standpoint. Force methods of solution, however, must be applied with caution, since there is evidence of significant non-conservative bias to calculated SF.

As for the second requirement, both a Box-Cox analysis and subsequent residual analysis indicates that a lognormal statistical distribution provides an adequate fit.

In terms of the general implications for risk analysis, it is noted that a log (base 10) transform of all of the data results in a mean of log 1.03 and standard deviation of 0.087. Ignoring the effects of the analytical approach, method, or slope type, the SF corresponding to a 99% chance of safety would therefore be the antilog of the total of log 1.03 plus about 2.3 standard deviations, or about 1.65. This is close to several values calculated by Christian et al. (1994), who utilized a direct error analysis approach (propagation of error) and assumed a normal

distribution for SF (as opposed to a log normal distribution). The consistency of the solutions from these two quite different approaches suggests that if comparable values for mean and standard deviation are used, SF risk analysis may be robust with regard to assumed distribution.

Beyond allowing statistical observations and factor reduction, the reduced ANOVA model may be used to predict SF failure values as a function of slope type, analytical method, and porewater approach. In order to discern trends and identify extreme predictions, several charts were generated from the reduced ANOVA model: Figure 14 corresponds to the total stress porewater approach, and Figure 15 to the effective stress porewater approach. Table 5 tabulates the predicted mean SF.

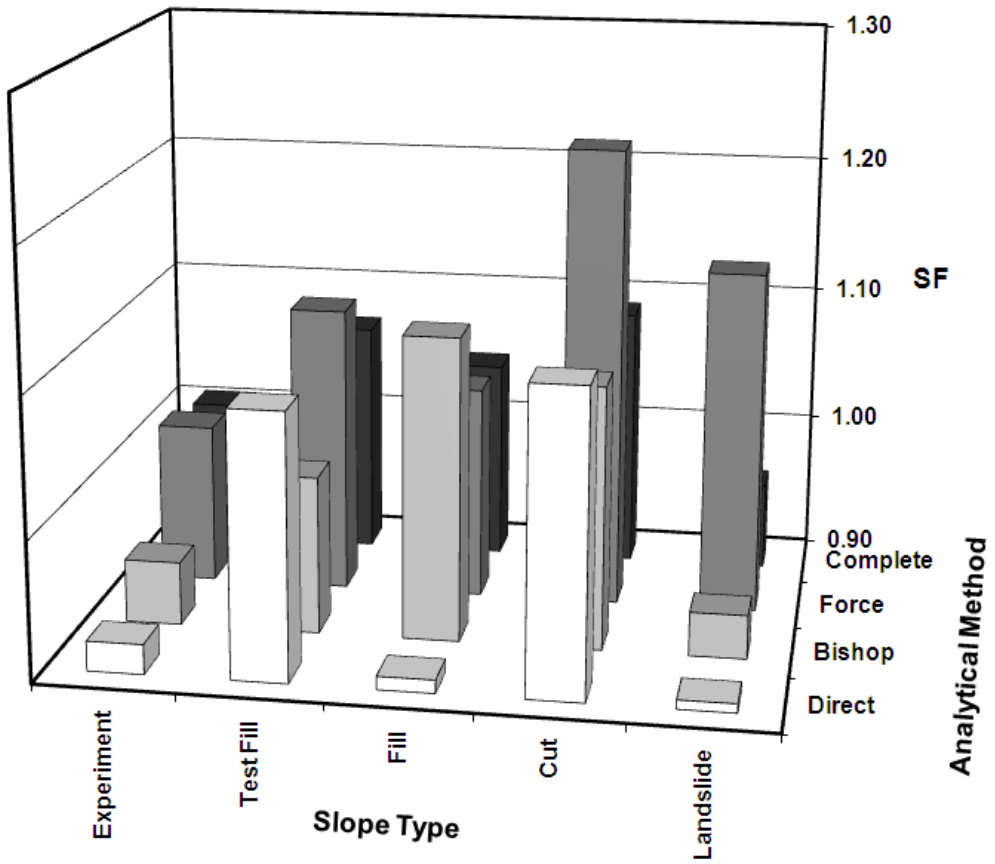

Figure 14. ANOVA predictive model for average failure SF (total stress porewater approach)

The prediction charts show that the total stress analysis tends to predict failure at higher SF values than the effective stress approach. The maximum values of both porewater approaches were similar, however, and specific to the force analytical method, with the total stress approach predicting failure at $SF = 1.23$ for cut slopes and the effective stress method predicting failure at $SF = 1.27$ for landslides. The minimums were less consistent, with the total stress approach showing a minimum SF of 0.91 for fill slopes analyzed by the direct analytical method, whereas the effective stress approach showed a minimum SF

also of 0.91 for cut slopes analyzed by Bishop's method. The direct method predicted failure closer to SF = 1 (across all slope types) better than the other methods, although Bishop's method prediction accuracy was also close to $SF = 1$. The variability was comparable between effective and total stress methods in general. Averaged over all slope types, the direct method was the least variable method for the effective stress approach but the most variable for the total stress approach. The force method was the most variable prediction method for the effective stress approach. The complete method was the least variable prediction method for the total stress approach.

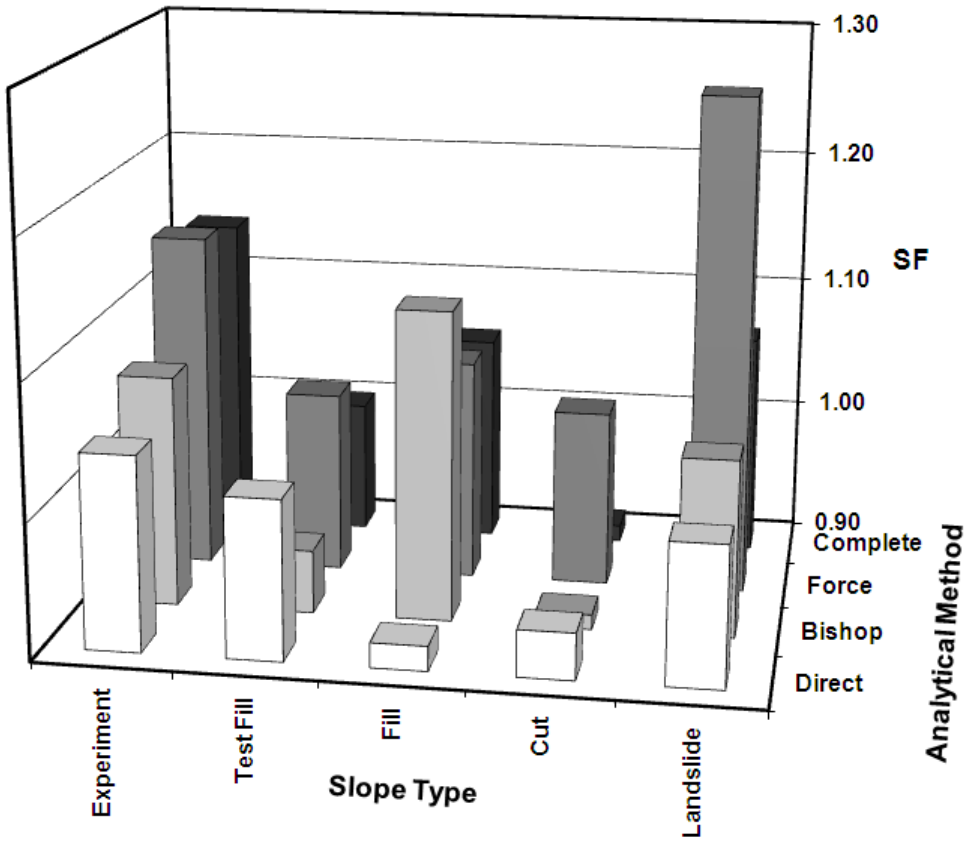

Figure 15. ANOVA model for average failure SF (effective stress porewater approach)

		Slope Type				
		Landslide	**Cut**	**Fill**	**Test Fill**	**Experiment**
Analysis	**Complete**	Eff.: 1.07 Total: 0.96	Eff.: 0.91 Total: 1.09	Eff.: 1.06 Total: 1.05	Eff.: 1.00 Total: 1.07	Eff.: 1.14 Total: 1.01
	Force	Eff.: 1.27 Total: 1.15	Eff.: 1.03 Total: 1.23	Eff.: 1.06 Total: 1.05	Eff.: 1.04 Total: 1.11	Eff.: 1.15 Total: 1.02
	Bishop	Eff.: 1.03 Total: 0.93	Eff.: 0.91 Total: 1.09	Eff.: 1.13 Total: 1.12	Eff.: 0.95 Total: 1.01	Eff.: 1.07 Total: 0.95
	Direct	Eff.: 1.00 Total: 0.91	Eff.: 0.93 Total: 1.12	Eff.: 0.92 Total: 0.91	Eff.: 1.02 Total: 1.09	Eff.: 1.04 Total: 0.92

Table 5. Mean failure SF ANOVA model predictions

For design, it is possible to extend the reduced ANOVA model to predict the SF values corresponding to a given risk of failure. While any desired risk of safety can considered with the model as given, Table 6 lists the minimum predicted SF needed for a 1% failure risk. Note that the wide range of predicted values justifies the need to account for the contributing SF factors. The total and effective stress analyses show little deviation, both averaging to a predicted $SF = 1.75$. In general, the force methods predict the highest SF values, averaging across all slope types SF values of 1.89 and 1.88 for the effective and total stress approaches respectively. The largest single predicted value is $SF = 2.16$ for landslides analyzed by the force method and the effective stress approach. At the low end, fill slopes analyzed by direct methods and the total stress approach predicts $SF = 1.50$. Direct methods using the effective or total stress approach have the lowest average values of any method, with predicted SF values of 1.65 and 1.66 respectively. Direct method prediction utilizing the effective stress approach also shows the least variability across all slope types, whereas complete

methods show the least variability across all slope types for the total stress approach.

Analysis	Slope Type: Landslide	Cut	Fill	Test Fill	Experiment
Complete	Effective: 1.80 Total: 1.62	Effective: 1.59 Total: 1.89	Effective: 1.75 Total: 1.73	Effective: 1.68 Total: 1.79	Effective: 1.99 Total: 1.73
Force	Effective: 2.16 Total: 1.94	Effective: 1.82 Total: 2.12	Effective: 1.77 Total: 1.75	Effective: 1.73 Total: 1.86	Effective: 1.97 Total: 1.74
Bishop	Effective: 1.70 Total: 1.56	Effective: 1.53 Total: 1.85	Effective: 1.86 Total: 1.85	Effective: 1.56 Total: 1.69	Effective: 1.82 Total: 1.61
Direct	Effective: 1.71 Total: 1.54	Effective: 1.57 Total: 1.89	Effective: 1.52 Total: 1.50	Effective: 1.71 Total: 1.81	Effective: 1.74 Total: 1.56

Table 6. 1% failure risk SF ANOVA model predictions

Conclusions

The database compiled here, while broad in terms of time and geography, tells only half of the story. Many slopes with low safety factors do not fail, and a full statistical consideration of SF should consider a random selection of these stable slopes as well. Nonetheless, the following conclusions may be made from the failure data considered here:

1. Different limit equilibrium algorithms produce different safety factors. For failed slopes, the direct methods of SF calculation appear to be the most successful at predicting $SF = 1$ as expected. Bishop's method and the complete methods of solution appeared to have a slight (but statistically significant) non-conservative bias, but the magnitude of this bias is so small it is likely undetectable in field applications. Force methods, however, demonstrated a level of bias that may have a significant, non-conservative effect on SF

calculation. It is not known, however, if the bias and uncertainty shown by the failure database can be generalized to stable slopes.

2. Clay content complicates SF analysis. The database indicated that correction factors for vane strength were not adequate to reduce predicted SF values to average at $SF = 1$ as expected. The relationship between plasticity index and safety factor appears to be more complicated than historically assumed. That said, there was no evidence that soils without clay were different from soils with clay with regard to SF uncertainty or bias.

3. The database overall was best described by a log linear distribution with a mean value of 1.03 and a standard deviation (of the log transformed values) of 0.087. A 1% failure risk for SF of about 1.65 was calculated from the overall database. Moreover, the reduced ANOVA model can be applied in a general way to risk analysis, providing predictions for a given failure risk as a function of analytical method, slope type, and porewater stress approach.

Regardless of interpretation, the results of the meta-analysis of these 301 slope failure calculations shows that while slope stability analysis is unavoidably uncertain it is also well described by statistical modeling. This chapter considered a global approach to understand and model this underlying stochastic formation, and while this is useful, it cannot take the place of site specific risk analysis by error propagation, which directly accounts for project specific observations, such as soil heterogeneity and porewater pressure uncertainty. The primary benefits of this chapter is that it is applicable both at the site level where it can be used as a

check on the slope specific risk analysis, and at the regulatory level to guide responsible and informed policy decisions on slope stability issues in general.

CHAPTER 4. MATRIC SUCTION EFFECTS

In time and with water, everything changes.

– Leonardo da Vinci

Introduction

In this chapter, the role of matric analysis in slope stability is investigated for infinite slopes, defined by a slip surface assumed to be parallel to the slope surface. While infinite slopes do not describe curvilinear slope failures, it is reasonable to assume that the general conclusions of the analysis herein are applicable to all slope failure geometries.

Perhaps the simplest of all slope stability analysis methods, infinite slope stability analysis satisfies complete static equilibrium while requiring only a minimum number of assumptions. Appropriate for shallow failures in slopes with cohesive soils (Duncan & Wright, 2005), it is extensively used in practice, sometimes as the primary analytical method; often as the first method for comparison with more sophisticated procedures.

All forces within an infinite slope can vary only in the direction perpendicular to the slope surface (Iverson, 1997). Accordingly, a typical assumption regarding groundwater in infinite slopes is that the water table lies parallel to the surface at a known depth. Iverson (1990) extended this approach to consider any arbitrary porewater pressure distribution satisfying the infinite slope assumption constraints, but limited his analysis to fully saturated / dry conditions.

The objective of this chapter is thus to derive a mathematical model for an infinite slope subjected to unsaturated flow above a phreatic surface. This

objective is achieved by first establishing rigorous equations for the porewater pressure / matric suction and the degree of saturation profiles. The degree of saturation profile is then used to establish the soil unit weight variation and overburden stress profile consistent with degree of saturation. The derived matric suction and overburden stress profiles are then incorporated into the infinite slope stability equations. A published case study is used to compare the matric suction model safety factor with the traditional approach assuming dry / saturated soil conditions. The results will determine if unsaturated flow significantly influences safety factor calculations in infinite slopes, and if this influence is, in fact, inherently conservative.

Matric Suction Profile

General Formulation

Consider a failure of an infinite slope with angle θ (see Figure 16). The depth perpendicular to the surface is measured by *y*. The soil has a dry unit weight γ_d, and a saturated unit weight γ_s. The phreatic surface is at a depth ℓ measured perpendicularly to the slope. The unit weight of water is γ_w, the pore air pressure is $u_a(y)$, the porewater pressure is $u_w(y)$, and, when unsaturated conditions prevail, the matric suction is $\psi(y) = u_a(y) - u_w(y)$.

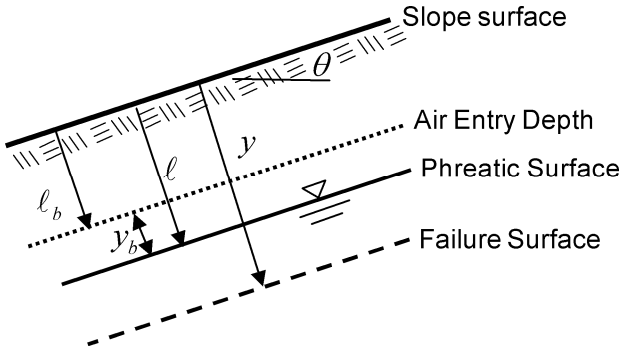

Figure 16. Infinite Unsaturated Slope

The porewater pressure for $y > \ell$ is simply

$$u_w = \gamma_w \ell \left(\frac{y}{\ell} - 1 \right) \cos\theta, \quad y > \ell \tag{1}$$

If $y < \ell$, matric suction occurs. Assuming that the unsaturated hydraulic conductivity is always greater than 0, Fredlund and Rahardjo (1993) showed that the matric suction is related to y, for equilibrium conditions, by

$$\psi = \gamma_w \ell \left(1 - \frac{y}{\ell} \right) \cos\theta, \quad y \le \ell \tag{2}$$

When the matric suction exceeds the air entry value of the soil ψ_b, however, two phase flow may occur and Equation (2) is no longer valid. As shown in Figure 16, this corresponds to the capillary rise (as measured perpendicularly to the slope), denoted by

y_b, where

$$y_b = \frac{\psi_b}{\gamma_w \cos\theta} \tag{3}$$

It is useful to introduce a depth to the capillary fringe, denoted ℓ_b, where $\ell_b = \ell - y_b$. For depths less than ℓ_b, the matric suction may increase, decrease, or remain constant. The distribution is sensitive to climate conditions, soil type, and history. Variation at different depths and locations is likely. Darcy's law extended to include the steady state one-dimensional unsaturated conditions is

$$\frac{d}{dy}\left(k_w(\psi)\frac{dh_w}{dy} \right) = 0 \tag{4}$$

where $k_w(\psi)$ is the unsaturated hydraulic conductivity and h_w the hydraulic head. Recognizing $h_w = u_w / \gamma_w - y\cos\theta$, and expanding Equation (4) results in

$$\frac{d}{dy}\left[k_w(\psi)\left(\frac{1}{\gamma_w}\frac{du_w}{dy} - \cos\theta \right) \right] = 0 \tag{5}$$

Integrating and assuming a constant water flux q_w, defined negative for infiltration and positive for evaporation, Equation (5) may be written as

$$k_w(\psi)\frac{du_w}{dy} = \gamma_w q_w + \gamma_w k_w(\psi)\cos\theta \tag{6}$$

For air, Fick's law describes the flow as

$$\frac{d}{dy}\left(k_a(\psi)\frac{du_a}{dy} \right) = 0 \tag{7}$$

where $k_a(\psi)$ is the permeability of air. An alternative approach to air flow relies on the Air Permeability Index (API), but has been shown to be equivalent to the Fick's law approach (Travis and Mobasher, 2010).

Integrating and introducing a constant air flux q_a, Equation (7) may be expressed as

$$k_a(\psi)\frac{du_a}{dy} = q_a \tag{8}$$

The unsaturated water hydraulic conductivity k_w equals the saturated conductivity k_s, at saturated conditions, and is asymptotic to zero as matric suction becomes infinite. Conversely, the unsaturated air conductivity k_a is zero for saturated conditions, and asymptotic to a constant value for completely unsaturated conditions.

Given the nonzero range of k_w, it is valid to multiply Equation (6) by $k_a(\psi)/k_w(\psi)$ and subtract it from Equation (8) to achieve a differential equation in terms of ψ only,

$$k_a(\psi)\frac{d\psi}{dy} = q_a - \gamma_w q_w \frac{k_a(\psi)}{k_w(\psi)} - \gamma_w k_a(\psi)\cos\theta \tag{9}$$

Equation (9) is valid from the ground surface at $y = 0$ to the air entry depth ℓ_b. At $y = \ell_b$, however, $\psi = \psi_b$, $k_w(\psi_b) = k_s$, $k_a(\psi_b) = 0$, and thus $q_a = 0$.

Equation (8) becomes

$$k_a(\psi)\frac{du_a}{dy} = 0 \tag{10}$$

Equation (10) implies that u_a must be a constant. The boundary condition at the surface indicates that u_a must match atmospheric pressure. Defining pressures as gauge (as opposed to absolute), u_a is thus shown to be 0.

Eliminating q_a and k_a from Equation (9) results in

$$\frac{d\psi}{dy} = -\left(1 + \frac{q_w}{k_w(\psi)\cos\theta}\right)\gamma_w \cos\theta \tag{11}$$

The integral solution to (11) is

$$\int_{\psi_b}^{\psi}\left(1 + \frac{q_w}{k_w(\psi)\cos\theta}\right)^{-1} d\psi = \gamma_w(\ell_b - y)\cos\theta \tag{12}$$

Note that all the variables of the integral term are known if q_w is known.

For solution it is useful to rewrite the integral solution in terms of the non-dimensional variables $Q_w = q_w / k_s$, $\Psi = \psi / \psi_b$, $K(\Psi) = k_w(\psi) / k_s$, $L = \ell / y_b$, $L_b = \ell_b / y_b$, and $Y = y / y_b$. The non-dimensional matric suction profile becomes

$$\int_{1}^{\Psi}\left(1 + \frac{Q_w}{K(\Psi)\cos\theta}\right)^{-1} d\Psi = L_b - Y, \qquad Y \le L_b \tag{13}$$

Equation (13) defines the matric suction profile for depths less than the air entry depth $\left(Y \le L_b\right)$. The matric suction function for $Y > L_b$ is given by Equation (2). Expressed in terms of the non-dimensional variables it is simply

$$\Psi = L - Y, \qquad Y > L_b \tag{14}$$

Unsaturated Hydraulic Conductivity

For nonzero values of Q_w, one formula for K that allows a closed form solution to Equation (13) is Philip (1986):

$$K\left(\Psi\right) = \mathrm{e}^{\alpha(1-\Psi)} \tag{15}$$

where the constant α is a soil specific parameter. Of course, there are many equations that relate permeability with matric suction, and while only the Philip (1986) equation is considered here, other relationships can be used in the subsequent analysis, albeit typically at the cost of obtaining closed-form solutions.

Assuming this form of the hydraulic conductivity, Equation (13) may be written as

$$\int_1^{\Psi} \frac{d\Psi}{1 + \dfrac{Q_w}{\cos\theta}\mathrm{e}^{\alpha(1-\Psi)}} = L_b - Y \tag{16}$$

The closed form solution to Equation (16) follows the same procedure that Lu and Griffiths (2004) applied in their paper for matric suction beneath a

horizontal surface, resulting in

$$\Psi(Y) = 1 + \frac{1}{\alpha}\ln\left[\left(1 + \frac{Q_w}{\cos\theta}\right)e^{\alpha(L_b - Y)} - \frac{Q_w}{\cos\theta}\right], Y \le L_b \qquad (17)$$

Indeed, for $\theta = 0°$ Equation (17) is close in form to the Lu and Griffiths (2004) solution with the important difference that the solution is not bounded in terms of maximum evaporation.

The corresponding permeability as a function of depth is

$$K(Y) = \left[\left(1 + \frac{Q_w}{\cos\theta}\right)e^{\alpha(L_b - Y)} - \frac{Q_w}{\cos\theta}\right]^{-1}, \qquad Y \le L_b \qquad (18)$$

The limits on Q_w are clear from Equation (18). The argument must be greater than 1 in order for the unsaturated permeability not to exceed the saturated permeability. Thus, while positive values of Q_w (evaporation) are not bounded, infiltration, (negative Q_w) is bounded, requiring $Q_w / \cos\theta \ge -1$.

Figure 17 shows an example of the matric suction profile.

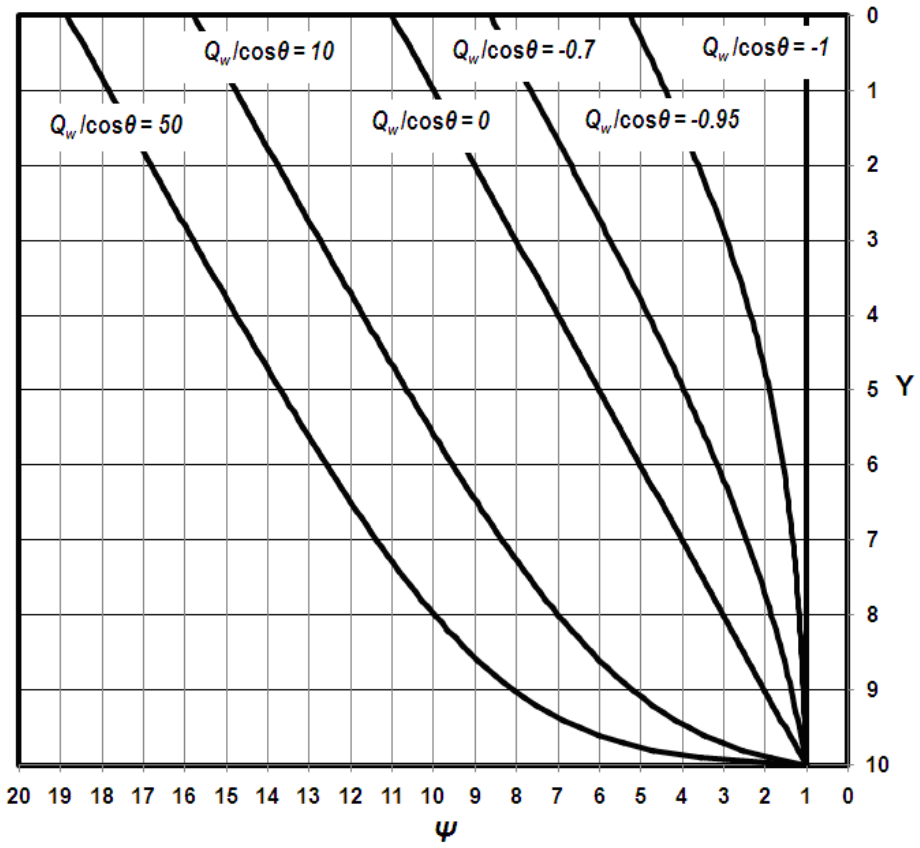

Figure 17. Matric suction profiles with L_b = 10 and α = 0.5

Degree of Saturation

Matric suction is often modeled as a function between Ψ and the normalized (effective) volumetric water content Θ , defined

$$\Theta = \frac{w - w_r}{w_s - w_r} \tag{19}$$

where w is the volumetric water content, w_s is the water content at saturation, and w_r is the residual water content. One particular empirical equation relating Ψ and

Θ is the McKee and Bumb (1984) Boltzmann equation

$$\Theta = e^{\eta - \beta\Psi},\ \Psi > 1 \tag{20}$$

where the constants η and β are specific soil properties. McKee and Bumb also introduced a modified form of this equation that improved fit near saturated conditions, that is, in the region $0 < \Psi < 1$ (McKee and Bumb, 1987), but this modified equation was subsequently found to be numerically unstable (Sillers and Fredlund 2001). The present analysis reduces the error near saturated conditions by restricting the range of applicability to $\Psi > 1$. Full saturation is thus assumed for matric suctions less than the air entry value, and the appropriate boundary condition is $\Theta = 1$ at $\Psi = 1$, and thus $\eta = \beta$. That is,

$$\Theta = e^{\beta(1-\Psi)} \tag{21}$$

While this is a valid application of the Boltzmann equation (Fredlund and Xing, 1994), it should be noted that even at zero suction, unsaturated conditions are still possible (Zhou and Yu, 2005), (from occluded air, for example), so this approach may not be valid for all soils.

A further test of the validity of the assumed unsaturated equations is the implication of the relationship between Θ and K. Leong and Rahardjo (1997) showed that most published empirical and theoretical approaches relating Θ and K tend to converge to

$$K = \Theta^{\delta} \tag{22}$$

where the constant δ tends to range $2 \le \delta \le 52$ as determined experimentally, with many values greater than 4. There exist a number of theoretical predictions for δ as well, including $\delta = 2$ (Yuster, 1951), $\delta = 3$ (Irmay, 1954), $\delta = 3.5$ (Averjanov, 1950) and $\delta = 4$ (Corey, 1954). Sometimes δ is assumed to be 1 which, while unrealistic, linearizes the model and allows more sophisticated applications (e.g. Srivastava and Yeh 1991).

The assumed unsaturated Equations (15) and (21) imply that

$$K = \Theta^{\alpha/\beta} \tag{23}$$

which is consistent with Leong and Rahardjo (1997) only if $\delta = \alpha / \beta$.

Expressing β as α / δ then, Equation (21) becomes

$$\Theta = e^{\alpha(1-\Psi)/\delta} \tag{24}$$

Substituting the matric suction profile Equation (17) into Equation (24) allows expression of the normalized saturation as a function of depth,

$$\Theta = \left[\left(1 + \frac{Q_w}{\cos\theta} \right) e^{\alpha(L_b - Y)} - \frac{Q_w}{\cos\theta} \right]^{-1/\delta} \tag{25}$$

Figure 18 shows the saturation profile for the example used in Figure 17, assuming $\delta = 4$. It is clear that the saturation profiles will tend to show greater non-linearity than the matric suction profiles.

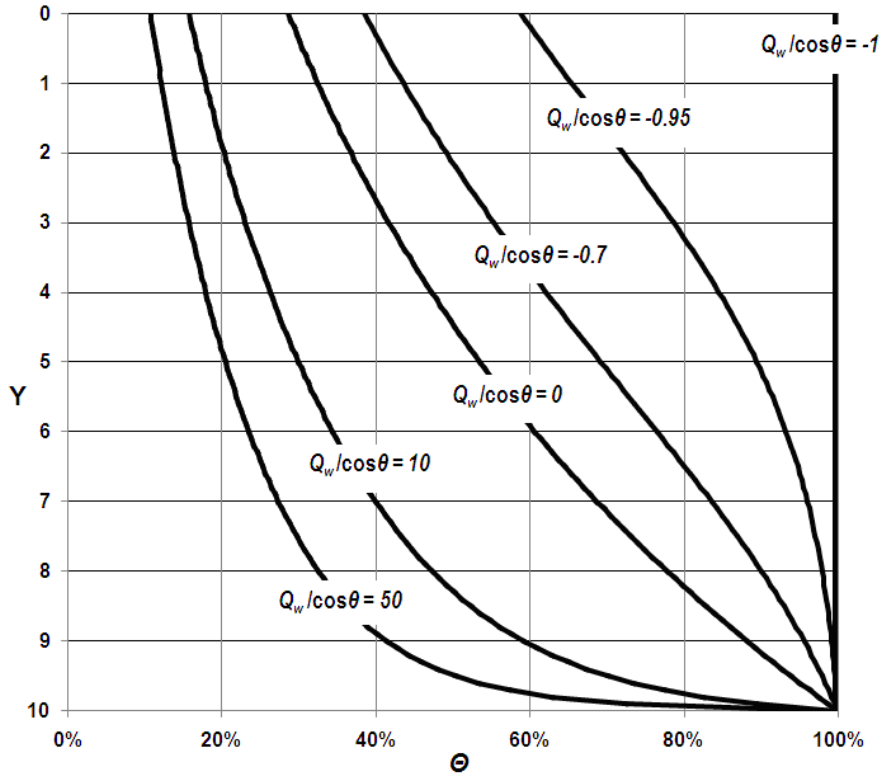

Figure 18. Normalized saturation profiles with $L_b = 10$, $\alpha = 0.5$, and $\delta = 4$

Overburden Stress

Given Θ, the total overburden stress can be calculated which is consistent with the degree of saturation profile, assuming a known dry unit weight that remains unchanged (i.e. neglecting any volume change of the soil). The unit weight γ_{matric} as a function of Θ is given by

$$\gamma_{matric} = \gamma_d + (\gamma_s - \gamma_d)\Theta \tag{26}$$

The overburden stress σ_n is given by integrating the unit weight over y

(utilizing, for mathematical formality, the dummy variable y_*):

$$\sigma_n = \int_0^y \gamma_{matric}\left(y_*\right) dy_* \tag{27}$$

In terms of the non-dimensional depth Y, the overburden stress is determined by substituting Equation (25) into Equation (27). Introducing the dimensionless specific gravities $S_d = \gamma_d / \gamma_w$, $S_s = \gamma_s / \gamma_w$, and the non-dimensional overburden stress $P_{matric} = \sigma_n / \left(\gamma_w y_b\right)$, the overburden equations are

$$P_{matric}(Y) = \begin{cases} S_d Y + \left(S_s - S_d\right) \int_0^Y \Theta\left(Y_*\right) dY_*, & Y \le L_b \\ S_d L_b + \left(S_s - S_d\right) \int_0^{L_b} \Theta\left(Y_*\right) dY_* + S_s\left(Y - L_b\right), & Y > L_b \end{cases} \tag{28}$$

where Y_* is the dummy variable for Y. Unfortunately, $\Theta(Y)$ is highly nonlinear and integration is rather complicated. Integrating over the permeability K, however, reduces the complexity of the integral and allows exact solutions to be obtained. Thus, in order to obtain an exact solutions, the integral function $\Phi(K,\delta)$ is introduced, where

$$\Phi(K,\delta) = \int_0^K \frac{K_*^{(1-\delta)/\delta}}{1 + Q_\theta K_*} dK_* \tag{29}$$

in which $Q_\theta = Q_w / \cos\theta$ and K_* is a dummy variable of K. The saturation

integral is therefore

$$\int_0^Y \Theta(Y_*)\,dY_* = \frac{1}{\alpha}\Big[\Phi\big(K(Y),\delta\big) - \Phi\big(K_0,\delta\big)\Big] \tag{30}$$

where K_0 is the permeability at $Y = 0$: $K_0 = \Big[\big(1+Q_\theta\big)e^{\alpha L_b} - Q_\theta\Big]^{-1}$. Equation (28) becomes

$$P_{matric}(Y) = \begin{cases} S_d Y + \dfrac{S_s - S_d}{\alpha}\big[\Phi(K(Y),\delta) - \Phi(K_0,\delta)\big], & Y \le L_b \\ S_d L_b + \dfrac{S_s - S_d}{\alpha}\big[\Phi(1,\delta) - \Phi(K_0,\delta)\big] + S_s\big(Y - L_b\big), & Y > L_b \end{cases} \tag{31}$$

By the method of partial fractions (Smith 1953), $\Phi(K,\delta)$ is insured closed-form solutions for any rational value of δ. The following closed-form solutions are for the theoretical values cited earlier:

$$\Phi(K,1) = \frac{1}{Q_\theta}\ln\big(1+Q_\theta K\big) \tag{32}$$

$$\Phi(K,2) = \begin{cases} \dfrac{2}{\sqrt{Q_\theta}}\tan^{-1}\Big(\sqrt{Q_\theta K}\Big), & Q_\theta > 0 \\ \dfrac{2}{\sqrt{-Q_\theta}}\tanh^{-1}\Big(\sqrt{-Q_\theta K}\Big), & Q_\theta < 0 \end{cases} \tag{33}$$

$$\Phi(K,3) = \frac{1}{\sqrt[3]{Q_\theta}}\left\{\begin{array}{l} \frac{1}{2}\ln\left(\dfrac{1+2\sqrt[3]{Q_\theta K}+\sqrt[3]{Q_\theta^2 K^2}}{1-\sqrt[3]{Q_\theta K}+\sqrt[3]{Q_\theta^2 K^2}}\right) \\ -\sqrt{3}\left[\tan^{-1}\left(\frac{1}{\sqrt{3}}-\frac{2}{\sqrt{3}}\sqrt[3]{Q_\theta K}\right)-\frac{\pi}{6}\right] \end{array}\right\} \tag{34}$$

$$\Phi(K,4)=\begin{cases}\dfrac{\sqrt{2}}{\sqrt[4]{Q_\theta}}\left[\begin{array}{l}\frac{1}{2}\ln\left(\dfrac{1+\sqrt[4]{4Q_\theta K}+\sqrt{Q_\theta K}}{1-\sqrt[4]{4Q_\theta K}+\sqrt{Q_\theta K}}\right)+\tan^{-1}\left(1+\sqrt[4]{4Q_\theta K}\right)\\ -\tan^{-1}\left(1-\sqrt[4]{4Q_\theta K}\right)\end{array}\right], & Q_\theta>0\\ \dfrac{1}{\sqrt[4]{-Q_\theta}}\left[2\tan^{-1}\left(\sqrt[4]{-Q_\theta K}\right)+\ln\left(\dfrac{1+\sqrt[4]{-Q_\theta K}}{1-\sqrt[4]{-Q_\theta K}}\right)\right], & Q_\theta<0\end{cases} \tag{35}$$

For fractional values of δ and for $\delta > 4$, the complexity of the closed form solution may become prohibitively expensive. For example, if $\delta = 3.5$, a relatively low and simple value corresponding to the Averjanov (1950) model, the closed form solution requires 10 separate terms involving *K*, and many trigonometric functions.

A practical, alternate method of solution is to consider an infinite series approximation. For values of $Q_\theta K \le 1$, the denominator of Equation (29) may be expressed as a geometric series, resulting in

$$\Phi(K,\delta)=\int_0^K\sum_{i=0}^{\infty}(-1)^i\,Q_\theta^i K_*^{(1-\delta)/\delta+i}\,dK_*,\ Q_\theta K\le 1 \tag{36}$$

The solution to Equation (36) may therefore be obtained by term by term integration; the result is

$$\Phi(K,\delta)=-\sum_{i=1}^{\infty}\frac{(-1)^i\,Q_\theta^{i-1}K^{i+(1-\delta)/\delta}}{i+(1-\delta)/\delta},\qquad Q_\theta K\le 1 \tag{37}$$

Unfortunately, for $Q_\theta K > 1$, the series solution shown in Equation (37) will not converge. However, solution may still be obtained by expressing the original integral in the form

$$\Phi(K,\delta) = \int_0^{1/Q_\theta} \frac{K_*^{(1-\delta)/\delta}}{1+Q_\theta K_*} dK + \int_{1/Q_\theta}^{K} \frac{Q_\theta^{-1} K_*^{(1-\delta)/\delta-1}}{1+Q_\theta^{-1} K_*^{-1}} dK, \qquad Q_\theta K > 1 \tag{38}$$

Since the variable term in both denominators of Equation (38) is less than 1, geometric expansions may be used for both integrals. Following the same steps used to derive Equation (37), albeit with a bit more manipulation, the solution to Equation (38) is

$$\Phi(K,\delta) = \frac{\delta Q_\theta^{-1/\delta}}{1-\delta} + \sum_{i=0}^{\infty} \frac{(-1)^i Q_\theta^{-1-i} K^{(1-\delta)/\delta-i}}{(1-\delta)/\delta - i} - Q_\theta^{-1/\delta} \sum_{i=0}^{\infty} \frac{2\left(\delta-\delta^2\right)(-1)^i}{(1-\delta)^2 - \delta^2 i^2}, \; Q_\theta K > 1 \tag{39}$$

The second infinite series in Equation (39) conveniently converges to the closed form function $\delta/(1-\delta) - \pi/\sin(\pi/\delta)$ (Oldham et al., 2008). Thus, Equation (39) may be written as

$$\Phi(K,\delta) = \frac{\pi Q_\theta^{-1/\delta}}{\sin(\pi/\delta)} + \sum_{i=0}^{\infty} \frac{(-1)^i Q_\theta^{-1-i} K^{(1-\delta)/\delta-i}}{(1-\delta)/\delta - i}, \qquad Q_\theta K > 1 \tag{40}$$

For large δ (i.e. $\delta \gg 1$) both limit equations converge to relatively simple formulas:

$$\Phi(K,\delta \gg 1) = \begin{cases} \delta K^{1/\delta} - \ln(1+Q_\theta K), & Q_\theta K \le 1 \\ \delta Q_\theta^{-1/\delta} - \ln\left(1+Q_\theta^{-1}K^{-1}\right), & Q_\theta K > 1 \end{cases} \tag{41}$$

Figures 4.4 through 4.7 show $\Phi(K,\delta)$ for $10^{-10} \le K \le 1$ and $-1 \le Q_\theta \le 2$. Both the exact solutions and the $\delta \gg 1$ approximations are shown. The closed-form solutions were used for $1 \le \delta \le 4$; the series solutions were used for higher δ with a required convergence of 0.1%. The large δ approximations appear to fit the solutions quite well for $\delta > 4$, and particularly well for Q_θ near 0 (Figure 22). For practical purposes, it appears that the closed-form solutions for $\delta \le 4$ and the large δ approximations for $\delta > 4$ are sufficiently accurate for most applications.

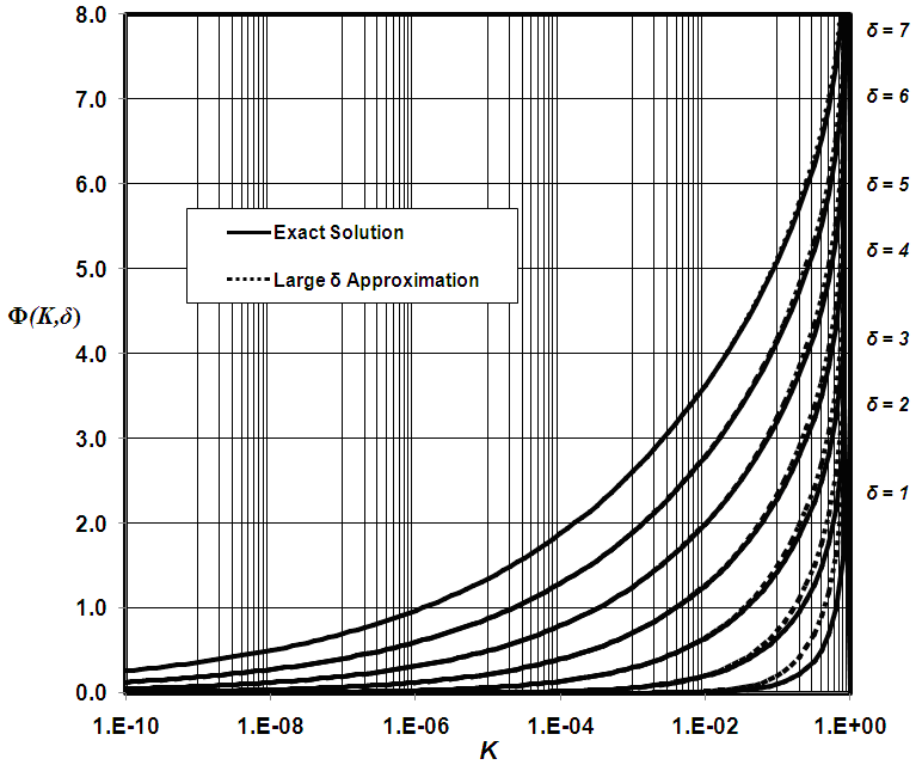

Figure 19. *Φ(K,δ)* function for Q_θ = -1.

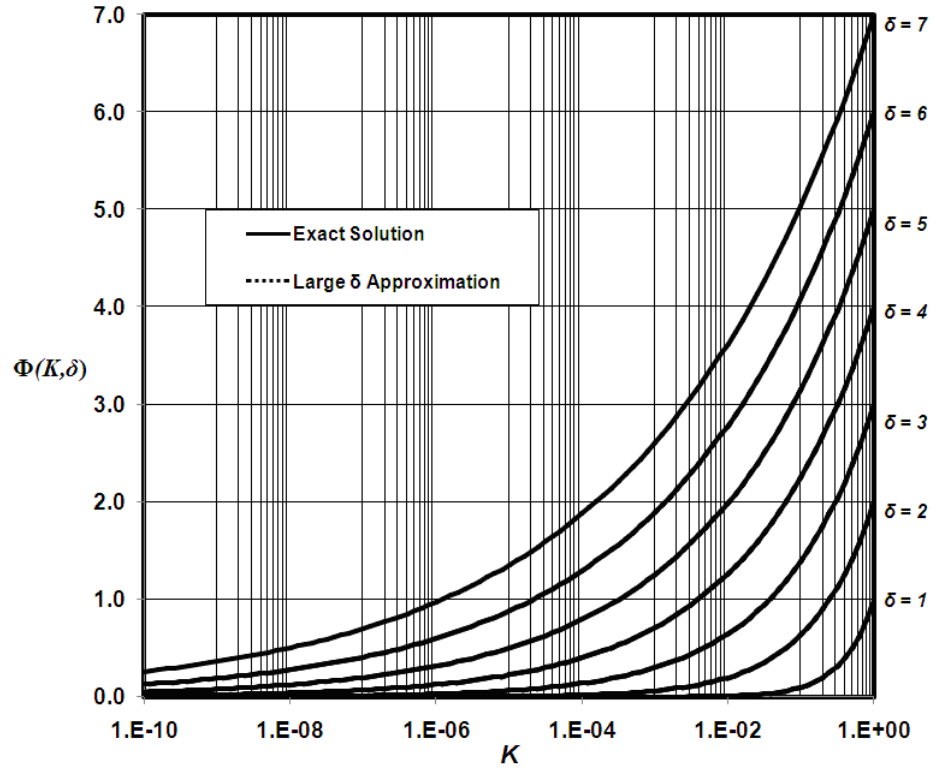

Figure 20. *Φ(K,δ)* function for $Q_\theta = 0$ (Large δ approximations not visible because they lie within exact solution line thickness).

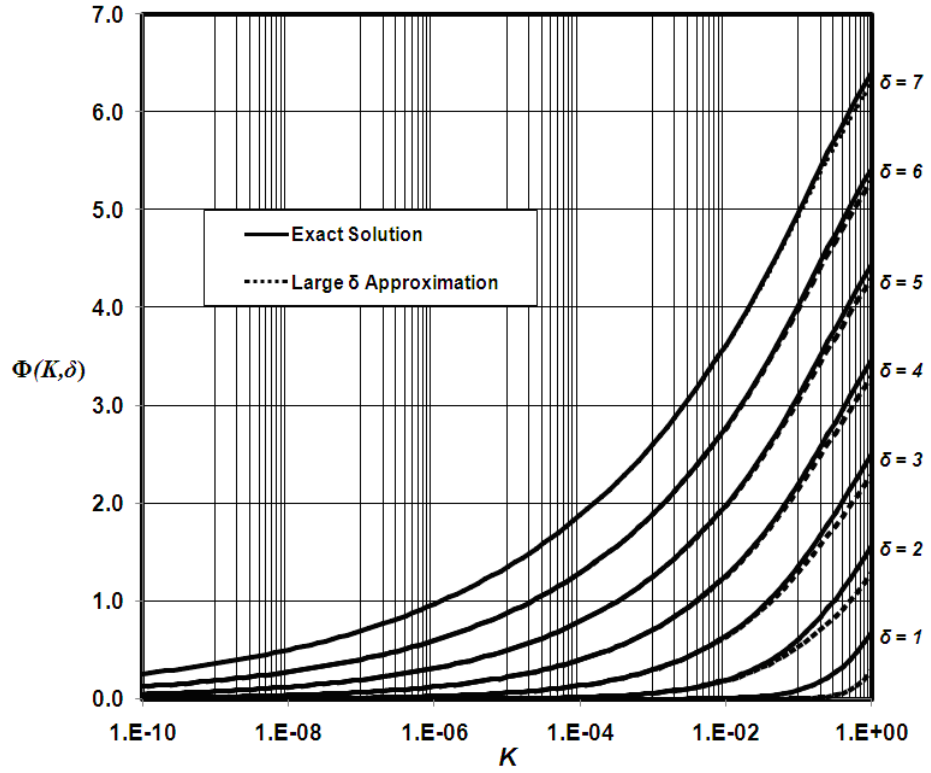

Figure 21. $\Phi(K,\delta)$ function for $Q_\theta = 1$.

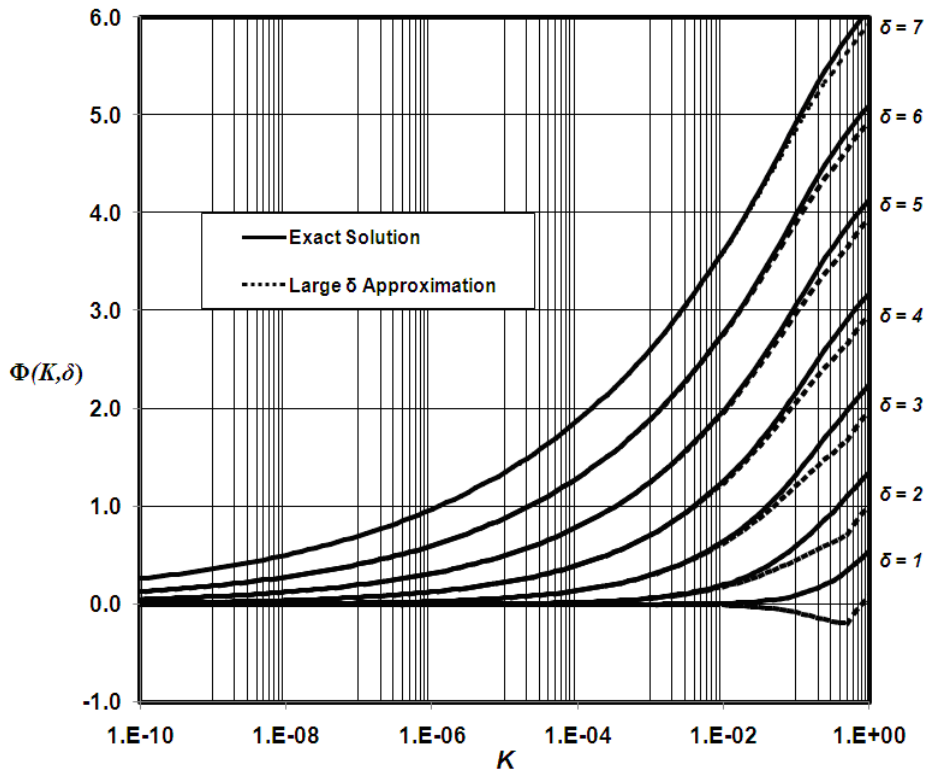

Figure 22. *Φ(K,δ)* function for $Q_\theta = 2$.

Of practical interest is the average unit soil weight $\overline{\gamma}_{matric}(Y)$ over depth Y, given by

$$\overline{\gamma}_{matric}(Y) = Y^{-1}P_{matric}(Y) = \gamma_d + (\gamma_s - \gamma_d)\overline{\Theta}(Y) \tag{42}$$

where $\overline{\Theta}(Y)$ is the average saturation above depth Y, given explicitly by

$$\overline{\Theta}(Y) = \frac{1}{Y}\int_0^Y \Theta(Y_*)\,dY_* = \frac{1}{\alpha Y}\left[\Phi(K(Y),\delta) - \Phi(K_0,\delta)\right] \tag{43}$$

Figures 4.8 through 4.12 show $\overline{\Theta}(Y)$ for different values of Q_θ given $L_b = 10$ and $\alpha = 0.5$.

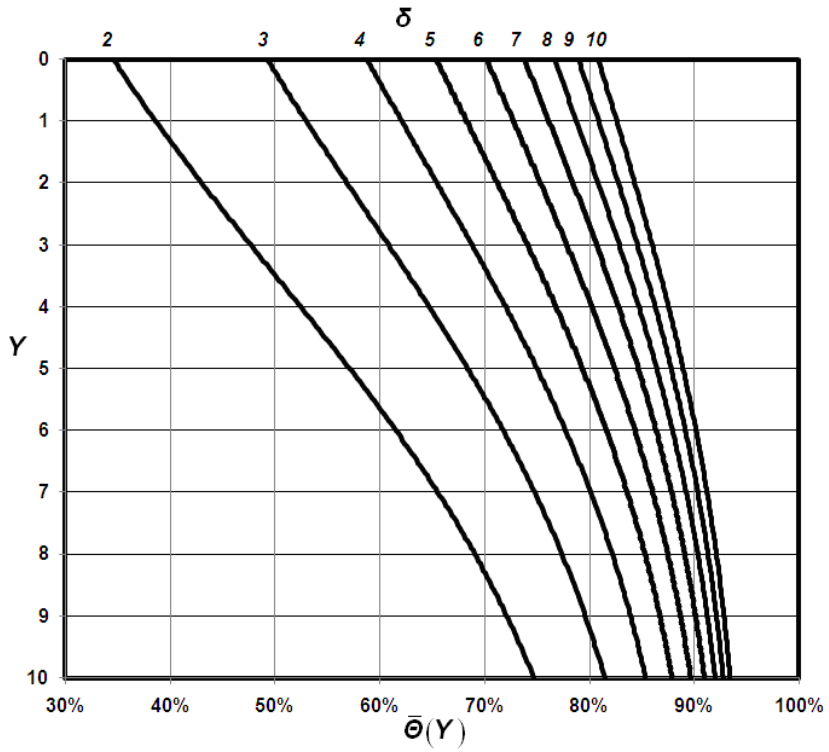

Figure 23. Average saturation over depth Y for L_b = 10, α = 0.5, and Q_θ = -0.95.

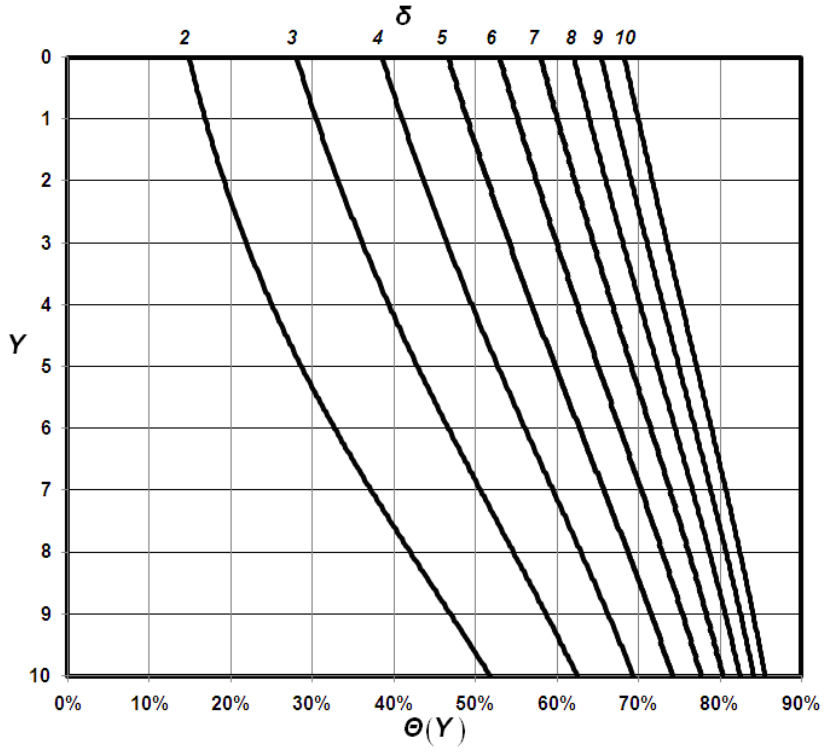

Figure 24. Average saturation at depth Y for L_b = 10, α = 0.5, and Q_θ = -0.70.

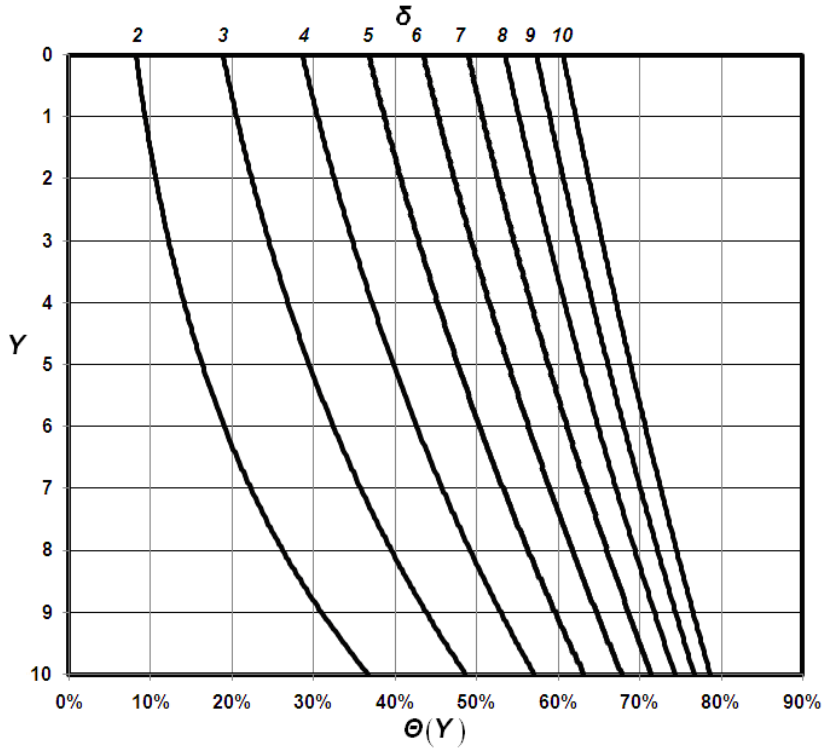

Figure 25. Average saturation at depth Y for L_b = 10, α = 0.5, and Q_θ = 0.

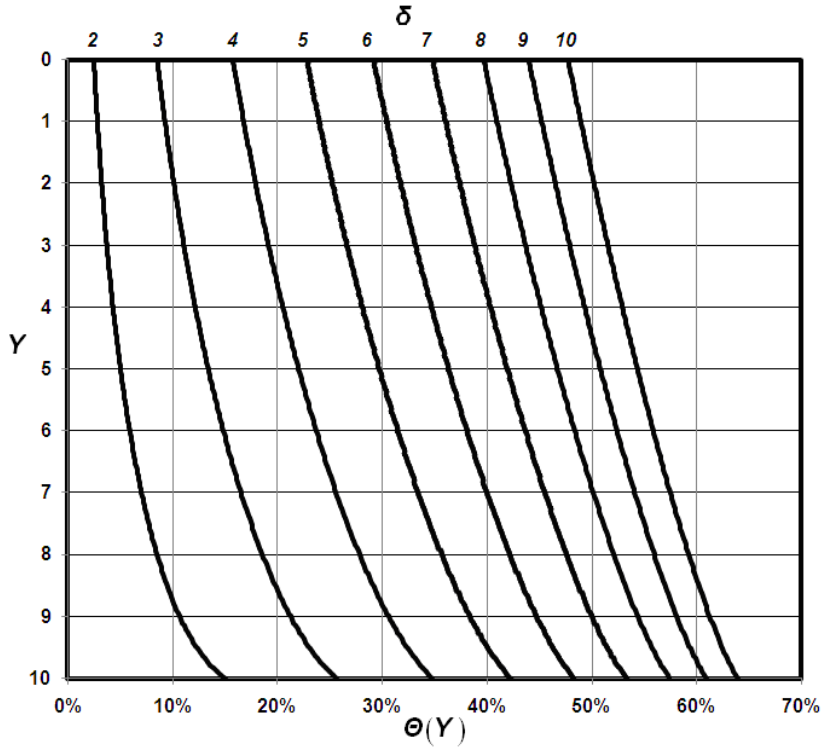

Figure 26. Average saturation at depth Y for L_b = 10, α = 0.5, and Q_θ = 10.

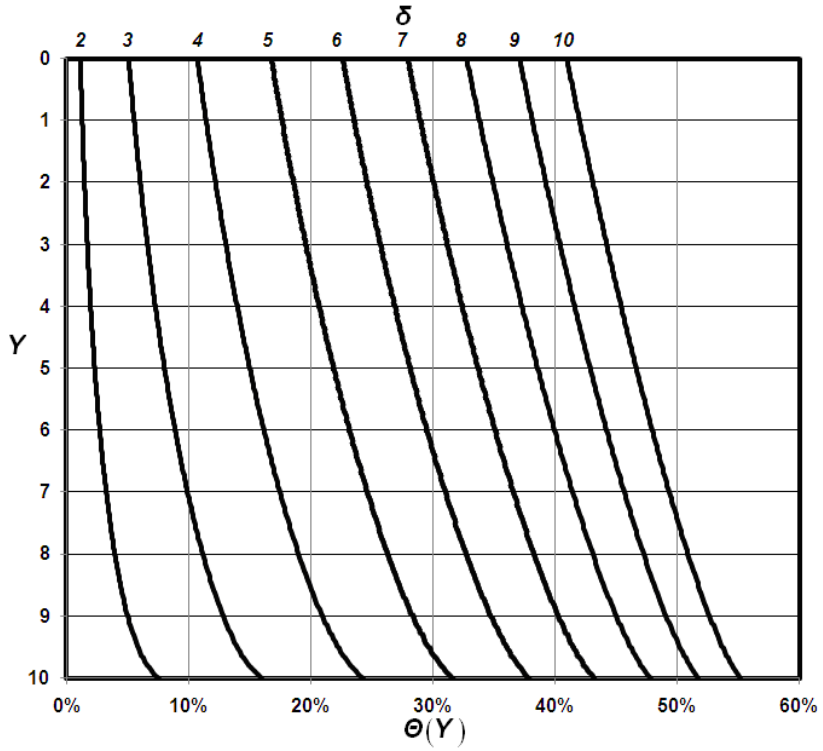

Figure 27. Average saturation at depth Y for L_b = 10, α = 0.5, and Q_θ = 50.

The average saturation is seen in the examples to be quite sensitive to δ, monotonically increasing with δ by as much as 50% for $2 \le \delta \le 10$. The curves themselves tend to be nearly linear near the ground surface but with exhibit strong curvature near the phreatic surface. The dry / saturated unit weight model is thus seen to be difficult to implement with any degree of accuracy, since the correct choice of an average saturation level above the phreatic surface is not obvious. Moreover, nonlinear variation with depth suggests that even extrapolation of near ground saturation measurements to significant depths would result in significant errors.

Shallow Water Tables

For shallow water tables where the matric suction at the ground surface (Ψ_0) is less than 1, or if $Q_w = 0$, then the saturation remains complete throughout the subsurface ($\Theta = 1$), Equation (2) is sufficient to describe the matric suction profile, and the overburden pressure may therefore directly computed from Equation (28) to be

$$P_{matric}(Y) = S_s Y, \quad \Psi_0 < 1 \text{ or } Q_w = 0 \tag{44}$$

Dry/Saturated Model

If matric suction is ignored, and dry / saturated conditions are assumed, the corresponding overburden stress $P_{dry/sat}(Y)$ is simply

$$P_{dry/sat}(Y) = \begin{cases} S_d Y, & \text{for } Y \le L \\ S_d L + S_s (Y - L), & \text{for } Y > L \end{cases} \tag{45}$$

Slope Stability

Overburden Stress

The extended Mohr-Columb equation for unsaturated slopes is (Fredlund and Rahardjo, 1993)

$$\tau = c' + \sigma_n \tan\phi' + \psi \tan\phi^b \tag{46}$$

where τ is the shear stress on the failure plane, c' the effective cohesion, σ_n the total normal stress on the failure plane, ϕ' the effective angle of friction, and $\tan\phi^b$ the rate of change of shear strength with regard to matric suction.

From Equation (46), the general equation for the factor of safety F_{matric} for infinite slopes is easily determined to be

$$F_{matric}(y) = \frac{c' + y\overline{\gamma}_{matric}(y)\cos\theta\tan\phi' + \psi(y)\tan\left(\phi^b(y)\right)}{y\overline{\gamma}_{matric}(y)\sin\theta} \tag{47}$$

Note that φ^b in Equation (47) is shown as a function of y because it is directly related to ψ which is, in turn, a function of y. The average unit weight $\overline{\gamma}_{matric}$ is given by Equation (42).

Matric Suction Angle

While ϕ^b has been found to be nearly constant for some soils (Fredlund and Rahardjo, 1993), ϕ^b is a nonlinear function of Ψ in general. Recent work by Houston et al. (2009) has shown that a good fit to field data may be achieved with a hyperbolic

relation between ϕ^b and Ψ according to

$$\phi^b(\Psi) = \phi' - \frac{\Psi - 1}{a_\phi + b_\phi\left(\Psi - 1\right)} \tag{48}$$

where a_ϕ and b_ϕ are soil specific constants. Thus, since Ψ has been shown to be a factor of *Y*, ϕ^b is a factor of *Y* as well. Note that at high suction or at $a_\phi = 0$, Equation (48) converges to a constant ϕ^b, with

$$b_\phi \approx \frac{1}{\phi' - \phi^b}, \qquad \Psi \gg 1 \tag{49}$$

Matric Suction Factor of Safety

Substituting into Equation (47) the developed functions for the average unit weight and matric suction angle, and defining the non-dimensional cohesion $C' = c'/\psi_b$, the following non-dimensional functions for the matric suction safety factor are developed,

$$F_{matric}(Y) = \begin{cases} \dfrac{C' + P_{matric}(Y)\tan\phi' + \Psi(Y)\tan\left(\phi^b(Y)\right)}{P_{matric}(Y)\tan\theta}, & Y \le L_b \\ \dfrac{C' + (L - Y)\tan\phi'}{P_{matric}(Y)\tan\theta} + \dfrac{\tan\phi'}{\tan\theta}, & Y > L_b \end{cases} \tag{50}$$

Note that all functions in Equation (50) are exact functions of *Y*. It is believed that this is the first time an exact safety factor function has been established with fully realized matric suction model. Moreover, for integer values of $\delta < 5$, the safety factor formula is closed form.

Shallow Water Tables

For $Q_w = 0$, or for shallow failures with high water tables where $\Psi_0 < 1$, then the infinite slope assumption is quite defensible and the overburden stress is described by Equation (44). The matric suction safety factor becomes simply

$$F_{matric}(Y) = \frac{C' + \left[L + (S_s - 1) Y \right] \tan \phi'}{S_s Y \tan \theta}, \quad \Psi_0 < 1 \text{ or } Q_w = 0 \tag{51}$$

Dry / Saturated Factor of Safety

If dry/saturated conditions are assumed, the infinite slope safety factor equations are well known to be

$$F_{dry/sat}(Y) = \begin{cases} \dfrac{C'}{S_d Y \tan \theta} + \dfrac{\tan \phi'}{\tan \theta} & Y \le L \\ \dfrac{C'}{\left[S_d L + S_s (Y - L) \right] \tan \theta} + \dfrac{S_d L + (S_s - 1)(Y - L)}{S_d L + S_s (Y - L)} \dfrac{\tan \phi'}{\tan \theta}, & Y > L \end{cases} \tag{52}$$

Case Study Analysis

Rahardjo et al. (2001) studied matric suction effects on a number of translational and rotational failures following rainfall in February 1995 at the Nanyang Technological University (NTU) campus in Jurong, Western Singapore. Their report included detailed information on the soil parameters of the area and developed an unsaturated groundwater model specific to a particular rotational failure, referred to as Slip Number 3. Within 20 meters of and concurrent with this rotational failure was a translational failure, referred to as Slip Number 4, which is used to verify the slope stability model developed here.

Slip Number 4 occurred near the top of a 45° embankment. The slip surface had a width of 7.8 m, a length of approximately 7 m, and a depth of 1 m, coinciding with the interface between the top layer of sandy clay and a lower layer of hard sandy silt. Assuming applicability of the Rahardjo et al. (2001) groundwater model, the phreatic surface depth changed over the storm from 5 m to less than 1 m (as measured perpendicularly from the slope at the center of the failed surface). The failed soil had a saturated unit weight of 19.6 kN/m^3 and was inferred to have a dry unit weight of 16.1 kN/m^3 and a saturated water content of 35.5%. Strength testing of the sandy clay found $\phi' = 26°$ and $c' = 2$ kPa. The AEV was estimated at 10 kPa from the soil-water characteristic curve (SWCC). The corresponding α value was estimated to be 0.2 by a best fit to between the SWCC and Equation (24) ($R^2 = 0.99$). Both β and w_r were estimated to be 0.06 and 13% based on a best fit to the reported permeability function curve ($R^2 = 0.99$). The b_φ value was estimated at 0.08 using Equation (49) and the reported φ^b value of 13°. The a_φ parameter was estimated at 0.9 from Houston et al. (2009) for a similar soil. The unit weight of water was assumed to be 9.8 kN/m^3 and the specific gravity of soil solids (G_s) was assumed to be 2.6. A best match to the reported matric suction profile before the storm indicated that q_w was approximately -0.07 mm/day. These parameters are summarized in Table 7.

Reported Values			Inferred Values		
Property	**Value**	**Units**	**Property**	**Value**	**Units**
θ	44	degrees	γ_d	16.1	kN/m^3
γ_s	19.6	kN/m^3	α	0.2	
ϕ'	26	degrees	β	0.06	
c'	2	kPa	δ	3.3	
k_s	0.1	mm/day	b_ϕ	0.08	
Assumed Values			ψ_b	10	kPa
a_ϕ	0.9		q_w	-0.07	mm/day
G_s	2.6		w_r	13	%
γ_w	9.8	kN/m^3	w_s	35.5	%

Table 7. Parameters for NTU Failure Number 4

Given these parameters, y_b is 1.42 m. Due to antecedent moisture, matric suction measurements at ground level were estimated by Rahardjo et al. (2001) to be constant and just over the measured air entry value for the sandy clay at the onset of the storm. Thus, even before the storm the soil was nearly saturated throughout the subsurface. Over the course of the storm, their matric suction model indicated very little change to the matric suction at the failure depth, consistent with Zhang et al. (2004).

Since only the phreatic surface depth changed over the course of the storm in the region of the failure, the developed steady state model was applied as a quasi-unsteady model, consistent with similar approaches in the literature including Iverson et al. (1997), Budhu and Gobin (1995a), and Kim et al. (1999). Both the dry / saturated safety factor and matric suction safety factors were

computed as functions of the phreatic surface as it changed over the course of the storm, as shown in Figure 28. The dry / saturated safety factor calculation was done assuming the soil specific unit weight above the phreatic surface was equal to the soil dry unit weight.

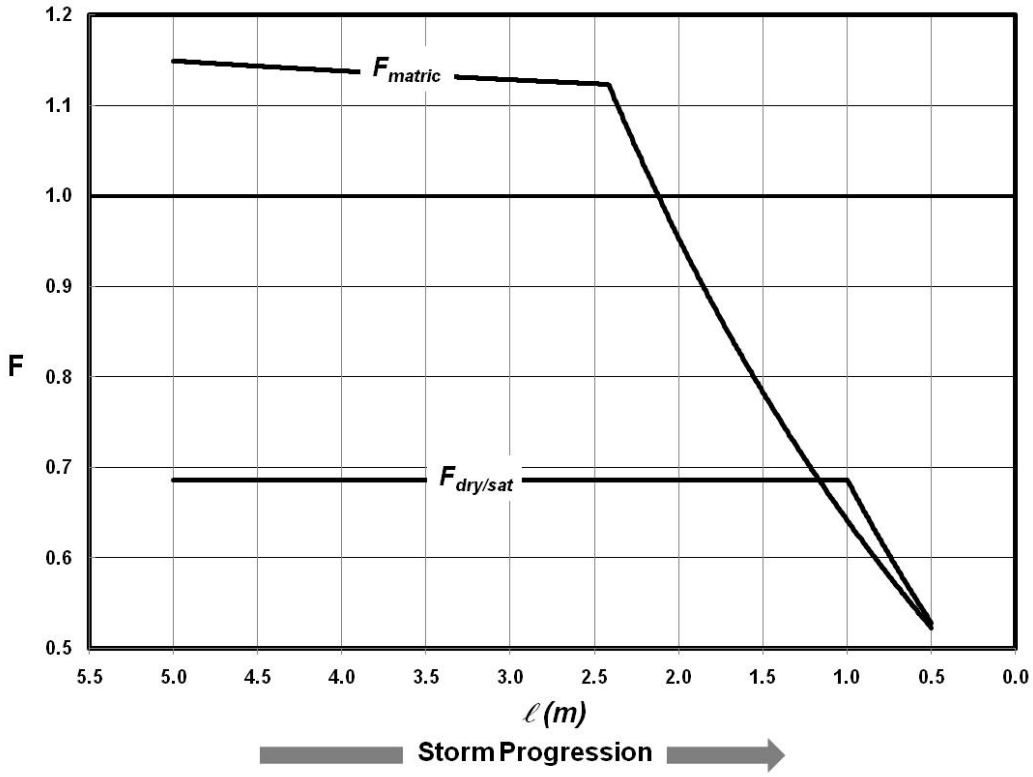

Figure 28. NTU slip number 4 safety factor versus phreatic surface depth

The results show that the dry / saturated model predicts failure ($F_{dry/sat} = 0.68$) even before the storm occurred (e.g., when $\ell = 5$ m), because it does not account for the matric suction stabilizing effect, whereas the matric suction model predicts safety factors well above 1 at the beginning of the storm, indicating a stable slope. As shown in Figure 13, however, F_{matric} decreases over the course of the storm, predicting eminent failure when the phreatic surface rose

to $\ell = 2.2$ m. The $F_{dry/sat}$ model, however, is constant until $\ell = 1$ m, at which point it does begin to decrease, but at a lesser rate than F_{matric}.

One potential criticism of the foregoing interpretation of Figure 28 is that safety factors below 1 are meaningless, presuming failure occurred at $F = 1$. However, research in recent years have shown that predicted safety factors below 1 are necessary for landslide dynamics (e.g. Iverson et al., 1997) and risk analysis (e.g. Duncan and Wright 2005). Thus, while both models predict a high probability of failure here, the matric suction model clearly predicts a higher risk of failure and greater dynamic landslide energy than the dry / saturated model near the end of the storm event. Moreover, only the matric suction model predicts stability prior to the storm event.

Discussion

The safety factor predicted by the infinite slope matric suction model is sensitive to phreatic surface depth. Spatially, the matric suction model tends to predict safety factors higher than the dry/saturated model for depths near the ground surface, but predicts lower safety factors than the dry/saturated approach when failure depths approach the phreatic surface. This finding contradicts the commonly held belief that disregarding matric suction is inherently conservative. It can be explained, however, by noting that for a cohesive soil, the increased unit weight from the loss of matric suction (increase in moisture content) decreases the safety factor. This is usually offset by the net gain in strength from matric suction, but as the depth nears the phreatic surface, matric suction approaches zero while the additional unsaturated water weight, unaccounted for in the

dry/saturated model, reaches a maximum. Specifically, if the specific gravity of the soil above the phreatic surface is assumed by the dry / saturated model to be S_d, then at $Y = L$:

$$P_{matric}(L) = S_d L_b + (S_s - S_d) \int_0^{L_b} \Theta(Y')\, dY' + S_s (L - L_b) \tag{53}$$

$$F_{matric}(L) = \frac{C'}{P_{matric}(L) \tan\theta} + \frac{\tan\phi'}{\tan\theta} \tag{54}$$

$$F_{dry/sat}(L) = \frac{C'}{S_d L \tan\theta} + \frac{\tan\phi'}{\tan\theta} \tag{55}$$

The difference between the unsaturated and dry/saturated safety factors is

$$F_{dry/sat}(L) - F_{matric}(L) = \left(\frac{1}{S_d L} - \frac{1}{P(L)} \right) \frac{C'}{\tan\theta} \tag{56}$$

Equation (56) shows that the unsaturated safety factor will always be less than the dry / saturated safety factor at the phreatic surface, since the actual overburden stress will be greater than the assumed dry / saturated overburden stress. This is because there is a significant difference between dry unit weight and actual average moist (wet) unit weight, particularly for low soil suction conditions. For a failure with a shallow water table, or if $Q_w = 0$, the overburden stress is described by Equation (44), and therefore Equation (56) becomes

$$F_{dry/sat}(L) - F_{matric}(L) = \left(\frac{1}{S_d} - \frac{1}{S_s} \right) \frac{C'}{L \sin\theta}, \quad \Psi_{\max} < 1 \text{ or } Q_w = 0 \tag{57}$$

In terms of the original variables, the safety factor error becomes

$$\Delta F = \left(\frac{1}{S_d} - \frac{1}{S_s} \right) \frac{2c'}{\gamma_w \ell \sin(2\theta)}, \qquad \psi_{\max} < \psi_b \text{ or } q_w = 0 \tag{58}$$

Equation (58) shows that the error introduced by using a dry/saturated model for infinite slope analysis with shallow water tables becomes asymptotically large for both mild and steep slopes. The error is also seen to be inversely proportional to water table depth, becoming infinite as water depth nears the surface.

To illustrate the functional form of Equation (58), Figure 29 shows the error for cohesive optimally compacted soils with characteristics shown in Table 8 (per U.S. Dept. of the Navy, 1982; w_{opt} = optimal water content.) The depth to the phreatic surface was assumed to be $\ell = 10$ m. The resulting safety factor errors are seen to be quite high. Furthermore, only the saturated cohesion values were used here; if the higher unsaturated cohesion values had been used instead the resulting errors would be even more significant. Interestingly, the errors scale directly with increasing clay content and plasticity, consistent with the plasticity correction factors developed by Bjerrum (1973) to explain overestimates of safety factor calculations that continues today (see Travis et al., 2010a).

Optimally compacted soil properties (US Dept Navy, 1982)					Calculated Properties (Assumes 90% saturation at w)	
Soil Type	**Description**	**Average ρ_d (kg/m^3)**	**Average w_{opt} (%)**	**Cohesion (kPa)**	**S_d**	**S_s**
SM	Silty sands, poorly graded sand silt mix	1924	13.5	51	1.93	2.63
SC	Clayey sands, poorly grades sand clay mix	1883	15.0	75	1.88	2.63
ML	Inorganic silts and clayey silts	1760	18.0	68	1.76	2.62
CL	Inorganic clay of low to medium plasticity	1760	18.0	88	1.76	2.62
MH	Inorganic clayey silts, elastic silts	1351	32.0	72	1.35	2.60
CH	Inorganic clays of high plasticity	1474	27.5	105	1.48	2.60

Table 8. Compacted soil properties (per U.S. Dept of the Navy, 1982) and corresponding S_s and S_d calculations.

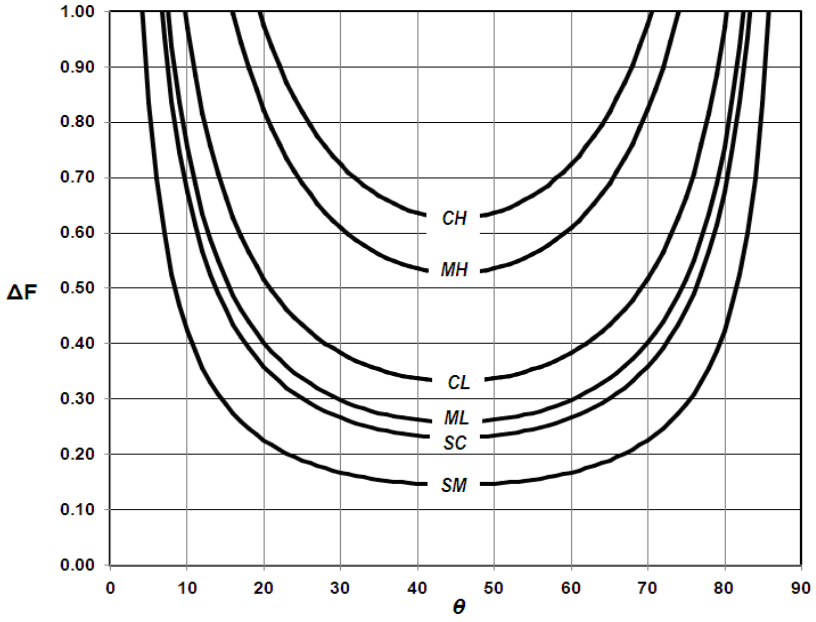

Figure 29. Non-conservative dry / saturated model safety factor error for compacted soils (10 m depth to phreatic surface)

As previously mentioned, one approach to overcome the non-conservative nature of the dry/saturated model is to simply assume soil is everywhere fully saturated (e.g. use only S_s and not S_d). Indeed, if this is done, the dry / saturated safety factors are equal to the matric suction model at the phreatic surface and there is no error. However, the fully saturated assumption is inherently inaccurate and creates an artificial disconnect between the groundwater model and the soil. Moreover, for soils with low δ values full saturation throughout the subsurface cannot be justified.

Implications

The results of this chapter indicate the importance of including matric suction in bank stability models. Matric suction decreases are accompanied by increased soil unit weight due to increased moisture content, which in turn reduces the factor of safety for slip surfaces near the phreatic surface. For shallow water tables, this effect increases as slope angles become less than or greater than 45°. In particular, matric suction must be considered in order to determine appropriate and consistent soil unit weights. It appears that matric suction is an integral and necessary aspect of slope stability that must be accounted for in order to obtain accurate predictions.

CHAPTER 5. BANK FAILURE MODELING BY FINITE ELEMENTS

> Many a hillside do the torrents furrow deeply, and down to the dark sea they rush headlong from the mountains with a mighty roar, and the tilled fields of men are wasted.
>
> – Homer

Introduction

This chapter develops an appropriate model for analyzing dynamic sandbar response to arbitrary river stage changes. The objectives of a comprehensive sandbar model are established which makes the case for the necessity of unsaturated flow analysis within the sandbar. A two-dimensional slope stability model is developed with specific consideration given to matric suction, weight density, and interslice forces. The model is compared to published steady state analyses and temporal predictions are made for an example sandbar.

Of course, two dimensional modeling of bank stability is complicated, particularly because rivers, like all natural features, ignore Cartesian coordinates and well defined boundary conditions. Their sandbars exist in continual contact with their environment; respond immediately to eddy and stage fluctuations, releasing and gaining sediment, all without regard for convenient control volume definitions and simplifying assumptions.

The dynamic dependence of the sandbars upon the other factors of their environment therefore prevents the application of normal "conservative" assumptions in an analytical or computational slope stability model, since a conservative approach to analyzing sandbar response is not self evident. Failure of an upstream sandbar may actually be beneficial to the river as a whole if it

helps to replace sediment lost to critical downstream habitat locations. Moreover, it is not enough to calculate an appropriate long term factor of safety for a given sandbar, as the effect of sandbar release on downstream sediment accumulation may be positive or negative: a lost sandbar may accumulate downstream under low flow conditions, but may be lost completely to the river system during high flow conditions. The factor of safety for sandbars must therefore be calculated as accurately as possible, without the benefit of conservative assumptions.

Field studies have shown that matric suction has been shown to substantially delay or even prevent slope failure since matric suction increases shear strength along a failure surface (Iverson 2000). For this reason, it is usually seen as conservative to neglect unsaturated flow in slope stability analyses (Duncan and Wright 2005). But while matric suction may increase the shear strength of the sandbar it also related to the weight of the material. The weight of moist sand can be twice that of dry sand without being offset by the buoyancy effects incurred by saturation. As shown in Chapter 4, the common assumption that unsaturated sand has a dry weight is inaccurate, particularly if the unsaturated sand has been recently saturated and its pore water distribution index is low and / or its air entry value is high.

Moreover, even when neglecting soil suction is conservative for calculating the safety factor, it is conservative from a sediment transport standpoint only for slopes where failure is not expected. If failure is expected (the safety factor is near 1) then neglecting soil suction may result in a false predicted failure surface, with the actual failure occurring later with more pronounced

effects. Indeed, under drawdown conditions the critical failure surface can change abruptly from surface to deep failure (Baker et al 2005). Predicting the time to failure is thus seen to be a critical objective of a sandbar model.

Besides increasing shear strength and soil saturation, matric suction also affects the interstitial forces critical to analysis of slope stability by the method of slices. The various methods utilizing the method of slices differ primarily in terms of their consideration of these forces. For example, the Ordinary Method of Slices (OMS) assumes the interslice force is zero; Spencer's Method assumes all interslice forces have the same inclination but different magnitudes; the Morgenstern and Price method assumes normal and shear interslice forces related by a specifically bounded but arbitrary function.

Generally speaking, interslice forces are deemed appropriate only if they can be resolved into an equivalent line of thrust that passes through all of the slices. This check on the force validity may not be appropriate for slopes with significant matric suction, however. Consider an arbitrary slice per Figure 30, where ψ indicates an average suction on the slice, u an average porewater pressure, Z the interslice force, S the shear force on the slice, and N the normal force on the slice. For the slice shown, resolving forces into an equivalent line of thrust would neglect the internal moment in the slice caused by a pore pressure gradient near the base and a matric suction gradient above the phreatic surface. The situation is analogous to reinforcement analysis of slopes, where it is usually recommended to separate the reinforcement forces from the interslice forces since

failing to do so may lead to numerical difficulties and unrealistic force considerations (Duncan & Wright 2005).

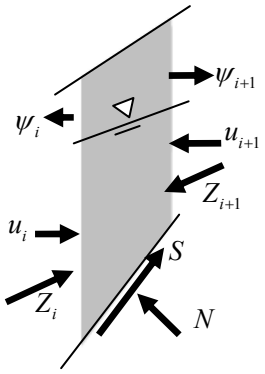

Figure 30. Slice with soil, porewater pressure, and matric suction.

Finally, if failure occurs the true critical slope must be known in order to calculate the mass lost to the sandbar. Significant suction will tend to bind the soil mass together, and likely result in a higher mass released then a failure without suction. Thus, to meet the objective of accurate volume loss prediction, matric suction must be included.

Three objectives have been specified: accurate calculation of minimum factors of safety, time to failure, and failure mass. The following sections describe the full two-dimensional unsaturated sandbar model developed to meet these objectives.

Slope Stability Analysis

The ordinary method of slices (OMS) was utilized for 2DLE analysis. This method was chosen over other methods for the sandbar slope stability modeling because:

a) Studies into riverbank failures indicate that failure surfaces are planar (Simon et al. 2000) or rotational (Budhu & Gobin, 1994), but not typically infinite slope. Moreover, rotational failures are seen to encompass planar failures since a rotational failure with a large enough radius collapses to planar failure.

b) Of the simple methods recommended for the present study from Chapter 2 only OMS provides an explicit equation for safety factor of an arbitrary rotational failure surface.

c) There is some evidence that even irregular surface failures are caused from progressive circular failures (Burridge 1987).

d) Negative stresses within slices are poorly handled by all slice procedures except OMS (Duncan & Wright 2005).

e) Infinite stresses can occur in all slice methods at the toe of the slope except OMS (Duncan & Wright 2005).

f) Liquefaction often occurs with slip surfaces near failure (Iverson 1997) and is often used to determine failure in similar studies (e.g., Budhu & Gobin 1996). Since most sandbars will exhibit safety factors near failure it is likely that the soil forces (equal to the interslice force for the effective stress analysis developed here) will be near 0, consistent with the OMS assumption.

g) The OMS is the only method of slices that allows direct computation of F. Thus, the OMS is many orders of magnitude faster than other

methods, allowing more dependable methods of locating the minimum F and more calculations of F over a given timeframe.

Slip surface location was accomplished by grid search for slip surface center, and golden sector for radius (Mays and Tung, 2002). Other methods were considered, but found to be too computationally expensive. The developed technique was rapid and successful.

Flow Analysis

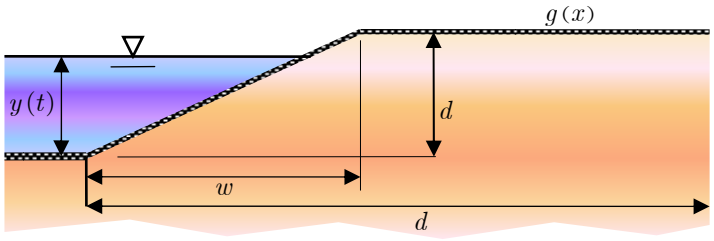

Figure 31. Partially submerged slope.

The flow analysis is conducted considering a sandbar of length *l* and height *d* adjacent to a water surface varying over time with elevation *y(t)*, per Figure 31. The sandbar is initially triangular to a width *w*, and thus has a slope $A = d / w$ and an initial ground surface given by

$$\begin{aligned} g(x) &= Ax, \;\; x < w \\ g(x) &= d, \; x \geq w \end{aligned} \tag{59}$$

Introducing an assumption of zero pore air pressure, then the matric suction of unsaturated flow is simply the negative of the hydraulic head minus the elevation, $h - z$. Thus, flow within all areas of the sandbar can be modeled by

one two dimensional continuity equation:

$$\frac{\partial}{\partial x}\left(k_x \frac{\partial h}{\partial x}\right)+\frac{\partial}{\partial z}\left(k_z \frac{\partial h}{\partial z}\right)=\rho_w g \frac{\partial}{\partial t}\left[m_2^w(h,z)h\right] \tag{60}$$

where ρ_w is the density of water, g the acceleration due to gravity, x, and z are the respective horizontal and vertical Cartesian coordinates, t is time, $k_x(h,z)$ and $k_z(h,z)$ are the respective horizontal and vertical unsaturated hydraulic conductivities, and $m_2^w(h,z)$ is the coefficient of water volume change as defined by Fredlund and Rahardjo (1993). For saturated conditions, $\rho_w g m_2^w(h,z)$ equals s_{s0}, the specific storage.

The boundary conditions require establishing three different flow regions along the sandbar surface, noted here as **I**, **II** and **III**. Region **I** refers simply to that region of the sandbar surface below the depth of the adjacent water: $g(x,t) < y(t)$. In region **I**, the sandbar surface head must equal $y(t)$. Region **II** refers to any region of the sandbar surface not within region **I** and where there is positive flow out of the sandbar. Region **II** requires the head at the surface to be equal to its elevation. Region **III** refers to any region of the sandbar surface not in either **II** or **III**. This region is subject to the no-flow requirement.

Mathematically, Region I is defined by those points $p(x, g, t)$ such that

$$\mathbf{I}:\left\{\mathbf{p}: g < y(t)\right\} \tag{61}$$

Defining $\omega(x,g,t)$ as the angle of $g(x,t)$ with the horizontal, flow out from the sandbar where $g(x,t) > y(t)$ (Region **II**) will occur only if hydraulic head is increasing into the sandbar:

$$\tan\omega\frac{\partial h\left(x,g\left(x,t\right),t\right)}{\partial x}-\frac{\partial h\left(x,g\left(x,t\right),t\right)}{\partial z}>0 \tag{62}$$

Letting $\zeta(x,g,t)$ be defined by the left side of (62), Region **II** is therefore defined as

$$\mathbf{II}:\left\{\mathbf{p}:g\left(x,t\right)>y\left(t\right)\&\,\zeta\left(x,g,t\right)>0\right\} \tag{63}$$

Region **III** is thus formally defined as:

$$\mathbf{III}:\left\{\mathbf{p}:\mathbf{p}\notin\mathbf{I},\mathbf{p}\notin\mathbf{II}\right\} \tag{64}$$

With the regions established, the boundary conditions may be written:

$$\begin{aligned}&\mathbf{p}\in\mathbf{I}: \quad h\left(\mathbf{p}\right)=y\left(t\right)\\&\mathbf{p}\in\mathbf{II}: \quad h\left(\mathbf{p}\right)=g\left(x,t\right)\\&\mathbf{p}\in\mathbf{III}:\zeta\left(\mathbf{p}\right)=0\end{aligned} \tag{65}$$

The no-slip boundary conditions along the base and rear wall are simply

$$\frac{\partial h\left(x,0,t\right)}{\partial z}=0 \tag{66}$$

$$\frac{\partial h\left(l,z,t\right)}{\partial x}=0 \tag{67}$$

The initial condition is defined by an initial head $h_0(x,t)$:

$$h(x,z,0) = h_0(x,z) \tag{68}$$

To generalize the analysis, the non-dimensional lengths X = x/w, $Z = z/d$, $G = g/d$, $Y = y/d$, $L = l/w$, and $H = h/d$ are introduced. Time is non-dimensionalized using any convenient reference time, such as down-ramp or up-ramp loading time. This reference time is denoted t_r and the corresponding non-dimensional time is denoted $T = t/t_r$. The sandbar surface point $\mathbf{p}(x,g,t)$ is denoted $\mathbf{P}(X,G,T)$.

The non-dimensional sandbar surface slope angle is defined as Ω where $\tan\Omega = \tan\omega / W_d$ and $W_d = w / d$. The ζ function may be written in terms of the non-dimensional parameters as

$$\zeta = \tan\Omega \frac{\partial H\left(X, G\left(X,T\right),T\right)}{\partial X} - \frac{\partial H\left(X, G\left(X,T\right),T\right)}{\partial Z} \tag{69}$$

The region members in terms of the non-dimensional parameters are

$$\mathbf{I} : \left\{\mathbf{P} : G < Y\left(T\right)\right\} \tag{70}$$

$$\mathbf{II} : \left\{\mathbf{P} : G\left(X,T\right) > Y\left(T\right) \,\&\, \zeta\left(X,G,T\right) > 0\right\} \tag{71}$$

$$\mathbf{III} : \left\{\mathbf{P} : \mathbf{P} \notin \mathbf{I}, \mathbf{P} \notin \mathbf{II}\right\} \tag{72}$$

The continuity and boundary conditions may be written in terms of these

non-dimensional parameters as

$$\frac{\partial}{\partial X}\left(\frac{k_x t_r d}{w^2}\frac{\partial H}{\partial X}\right)+\frac{\partial}{\partial Z}\left(\frac{k_z t_r}{d}\frac{\partial H}{\partial Z}\right)=s_s d\frac{\partial H}{\partial T} \tag{73}$$

This equation may be simplified by defining the following non-dimensional parameters:

$$K_x\left(X,Z\right)=\frac{k_x\left(x,z\right)t_r}{wW_d};\ K_z\left(X,Z\right)=k_z\left(x,z\right)t_r/d;\ S_s\left(X,Z\right)=s_s\left(x,z\right)d \tag{74}$$

Thus, the governing equation may be written

$$\frac{\partial}{\partial X}\left(K_x\frac{\partial H}{\partial X}\right)+\frac{\partial}{\partial Z}\left(K_z\frac{\partial H}{\partial Z}\right)=S_s\frac{\partial H}{\partial T} \tag{75}$$

The boundary and initial conditions become

$$\begin{aligned}&\mathbf{P}\in\mathbf{I}:\quad H\left(\mathbf{p}\right)=Y\left(t\right)\\&\mathbf{P}\in\mathbf{II}:\quad H\left(\mathbf{p}\right)=G\left(x,t\right)\\&\mathbf{P}\in\mathbf{III}:\ \zeta\left(\mathbf{p}\right)=0\end{aligned} \tag{76}$$

$$\frac{\partial H\left(X,0,T\right)}{\partial Z}=0 \tag{77}$$

$$\frac{\partial H\left(L,Z,T\right)}{\partial X}=0 \tag{78}$$

$$H\left(X,Z,0\right)=H_0\left(X,Z\right) \tag{79}$$

Initially, the ground surface is given by:

$$G(X) = X,\ X < 1;\ G(X) = 1,\ X \geq 1$$

Note that with these parameters defined, the solution is established for a non-dimensionalized slope of 45 degrees, regardless of the actual sandbar slope. This allows the profile to be easily generated and interpreted.

A finite difference grid was established for solution utilizing central differences for both the spatial and temporal derivatives. The temporal average for H is defined as

$$\bar{H} = \tfrac{1}{2}\left(H_{+t} + H_{-t}\right) \tag{80}$$

The governing equation becomes

$$\frac{\partial K_x}{\partial X}\frac{\partial \bar{H}}{\partial X} + K_x\frac{\partial^2 \bar{H}}{\partial X^2} + \frac{\partial K_z}{\partial Z}\frac{\partial \bar{H}}{\partial Z} + K_z\frac{\partial^2 \bar{H}}{\partial Z^2} = S_s\frac{\partial \bar{H}}{\partial T} \tag{81}$$

This equation is solved utilizing a central difference scheme and the following functions:

$$Q_x = \tfrac{1}{2}\left(K_{+x} - K_{-x}\right)\left(\bar{H}_{+x} - \bar{H}_{-x}\right) + K_x\left(\bar{H}_{+x} + \bar{H}_{-x}\right) \tag{82}$$

$$Q_z = \tfrac{1}{2}\left(K_{+z} - K_{-z}\right)\left(\bar{H}_{+z} - \bar{H}_{-z}\right) + K_z\left(\bar{H}_{+z} + \bar{H}_{-z}\right) \tag{83}$$

Here the subscripts $\pm x$ and $\pm z$ refer to adjacent cell values. That is, $+x$ indicates one cell to the right (positive x direction), $-z$ indicates one cell down

(negative z direction) and so forth. The time subscript, $-t$, indicate the previous time step.

With the aforementioned functions defined, the governing partial differential equation may be written

$$\frac{Q_x}{2\Delta X^2}+\frac{Q_z}{2\Delta Z^2}+2S_s\frac{H_{-t}}{\Delta T}=\left(\frac{K_x}{\Delta X^2}+\frac{K_z}{\Delta Z^2}+2\frac{S_s}{\Delta T}\right)\bar{H} \tag{84}$$

Expanding $\bar{H}$ in Equation (84), the following implicit function for H_{+t} is derived:

$$H_{+t}=\frac{\Delta Z^2\Delta TQ_x+\Delta X^2\Delta TQ_z+4\Delta X^2\Delta Z^2S_sH_{-t}}{\Delta Z^2\Delta TK_x+\Delta X^2\Delta TK_z+2\Delta X^2\Delta Z^2S_s}-H_{-t} \tag{85}$$

Thus, a grid of implicit functions is established and may be solved by any number of algorithms, including Newton-Raphson, etc.

The boundary condition for **III** in finite element form is established in towards the sandbar. In terms of the finite element analysis, the boundary condition requires determining the type of adjacent cells. Only those in the sandbar in considered. Any other type, namely a river cell, another boundary cell, or an open air cell, are ignored.

This procedure is quantified by introducing delta functions $\delta_{\pm x}$ and $\delta_{\pm z}$. These functions evaluate the adjacent cells and return either 1 if part of the sandbar, or 0 if not. With these functions defined, the boundary condition for the

sandbar boundary is

$$H = \frac{\left(\delta_{-x} H_{-x} - \delta_{+x} H_{+x}\right)\Delta X \tan\Omega - \left(\delta_{-z} H_{-z} - \delta_{+z} H_{+z}\right)\Delta Z}{\left(\delta_{-x} - \delta_{+x}\right)\Delta X \tan\Omega - \left(\delta_{-z} - \delta_{+z}\right)\Delta Z} \tag{86}$$

Unsaturated functions for the hydraulic conductivity are established per Brooks and Corey (1964). Unlike the hydraulic head, the hydraulic conductivity function was allowed to lag, as doing so vastly improved convergence speed with no discernible decrease in accuracy. The hydraulic conductivity is

$$\frac{K_{BC}}{K_{sat}} = \begin{cases} 1, & 0 \le H_{-T} - Z \\ 1 + \left(2 + 3\lambda\right)\left[\left(\dfrac{H_{-T} - Z}{H_b}\right)^2 - \left(\dfrac{H_{-T} - Z}{H_b}\right)^3\right], & H_b \le H_{-T} - Z < 0 \\ \left(\dfrac{H_b}{H_{-T} - Z}\right)^{2+3\lambda}, & H_{-T} - Z < H_b \end{cases} \tag{87}$$

where K_{sat} the non-dimensional saturated hydraulic conductivity. Likewise, the non-dimensional specific storage function was

$$S_{s,BC}\left(H_{-T}, Z\right) = \begin{cases} S_{s0}, & 0 \le H_{-T} - Z \\ S_{s0} - \dfrac{A_{BC}}{H_b}\left(\dfrac{H_{-T} - Z}{H_b}\right)^2 + \dfrac{B_{BC}}{H_b}\left(\dfrac{H_{-T} - Z}{H_b}\right)^3, & H_b \le H_{-T} - Z < 0 \\ -\dfrac{\lambda}{H_b}\left(\dfrac{H_b}{H_{-T} - Z}\right)^{\lambda+1}, & H_{-T} - Z < H_b \end{cases} \tag{88}$$

where

$$A_{BC} = 3H_b S_{s0} + 4\lambda + \lambda^2 \tag{89}$$

$$B_{BC} = 2H_b S_{s0} + 3\lambda + \lambda^2 \tag{90}$$

Example Application

A recent study by Baker et al (2005) investigated the stability of partially submerged cohesionless 14° slope. Their study assumed steady state conditions and a variety of adjacent water levels. Using Spencer's method for the slope analysis, they found the safety factor decreased from 2.91 for water levels at the slope crest to a minimum of 2.48 for water levels about halfway up the slope, and increased to about 2.73 for water levels at the slope toe. The specific soil and slope parameters for the Baker et al (2005) study are shown in Table 9, along with the additional assumed parameters needed for the unsteady analysis. Note the high value of λ used to replicate the Baker et al. (2005) assumption of strictly wet / dry soil conditions.

From Baker et al (2005)		**Additional assumed parameters**	
Parameter	**Value**	**Parameter**	**Value**
Slope angle	14°	Permeability	0.0001 ft/sec
Slope height	16.4 ft	Specific storativity	0.03 1/ft
Saturated specific gravity	1.8	λ	999
Unsaturated specific gravity	1.54	δ	3.0
Soil porosity	0.35	$(u_a - u_w)_b$	6.24 psf

Table 9. Example Parameters

The Baker et al (2005) study was investigated using the developed model for a range of drawdown rates. The minimum safety factor was evaluated at 20

different drawdown elevations by exhaustive enumeration; more than 10,000 different slip surfaces at each elevation were evaluated. The time steps were chosen as the fraction of the downramp time t_r / 600 for drawdown times up to 100 hours; t_r / 6000 was used for the 500 hour drawdown run, where numerical stability became an issue. Execution time was usually under 1 hour, approximately, on a standard laptop computer. The results are shown in Figure 32, where the water level Y has been normalized by the slope height D.

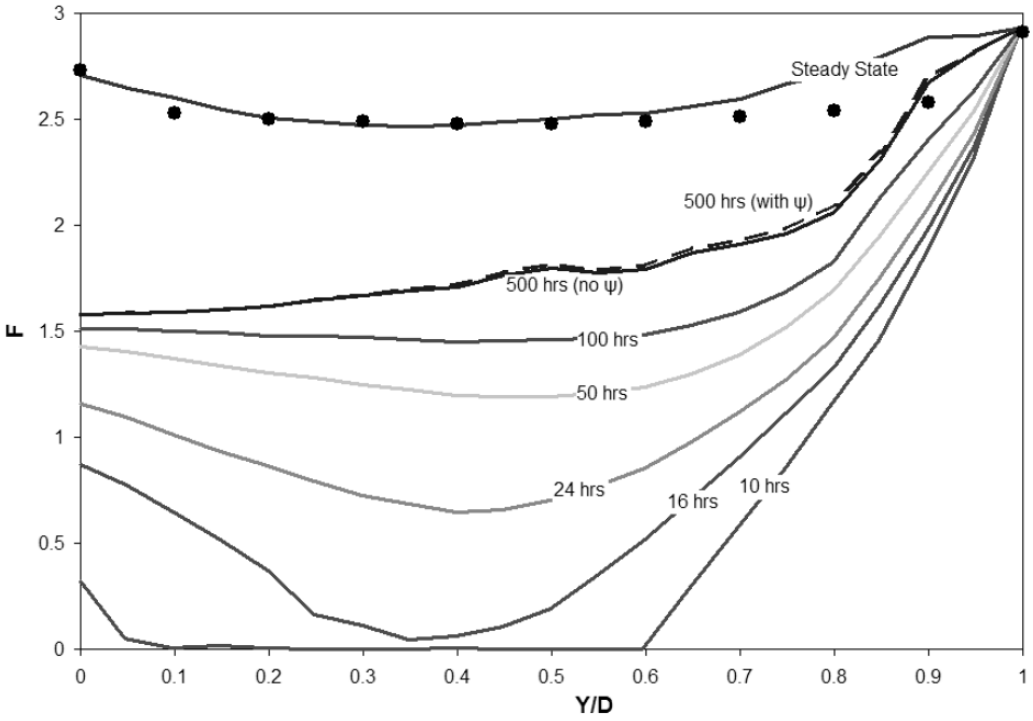

Figure 32. Safety factors versus Y / D for various drawdown rates (points are from Baker et al., 2005)

The safety factors were calculated both considering and not considering the matric suction ψ. Only the 500 hour run generated a perceptible difference between the two computed safety factors and so is the only drawdown rate shown with both safety factors. Thus, even though the simulation required an unsaturated analysis in order to correctly meet the boundary conditions of the

problem, matric suction itself did not play a significant role, or was at least offset by the increased unsaturated soil weight. This would not likely be the case for a finer material, initial unsaturated / saturated conditions (e.g. an initial phreatic surface midway through the slope), and materials with a lower pore size distribution index (deposited sand, for example).

The match of the steady state run to the Baker et al (2005) study was within 1% for Y/D = 0.0, 1.0, and the midrange. A maximum difference of about 10% occurred for Y/D = 0.9. The reason for this mismatch is unknown, but may be related to the unreported depth below the slope used by the Baker et al study; in the present study, the critical failure surface dropped close to the base limit of the grid at several points.

Comparing the steady state result with the other drawdown rates, the safety factor is seen to drop significantly as drawdown rate increases. Complete drawdown over 50 hours reduces the minimum safety factor to about half of the steady state value; failure occurs during the 24 hours drawdown rate at Y/D = 0.65, or about 16 hours into the drawdown. The safety factors for the 16 hour run drop even lower, and the 10 hour drawdown rate shows safety factors below 1.0 for 80% of the drawdown, the majority of which drop to nearly 0.

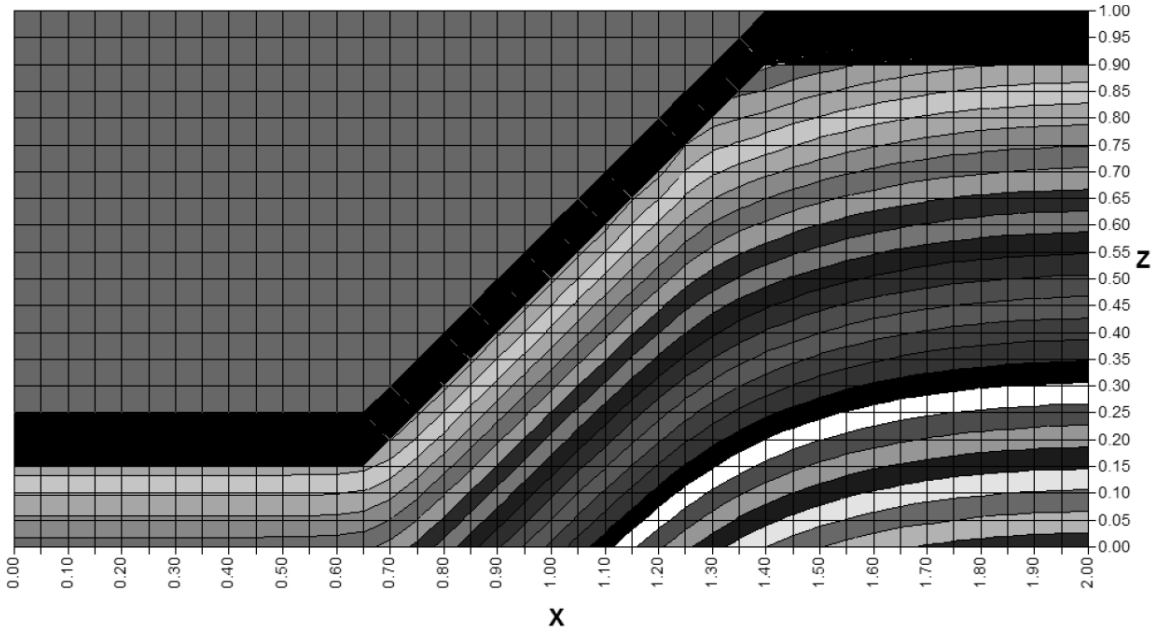

Figure 33. Non-dimensional 0.4 unit pressure contours for the 100 hour drawdown

The pressure contour graphs explain the safety factor changes. Figure 33 shows the non-dimensionalized pressure contours for the 100 hour drawdown; Figure 34 shows the 10 hour drawdown. The pressure contours are at 0.4 intervals. The 100 hour drawdown shows a minimum value of -0.02 (matric suction) at the slope crest, whereas the 10 hour drawdown exhibits a minimum of about 0.04 at the slope crest. The contours are seen to be, in general, higher for the 10-hour run, with high gradients perpendicular to the slope. Failure likely results from high pressures near the toe reducing normal stress along the failure surface under the toe, thereby reducing the shear strength without reducing the overturning moment.

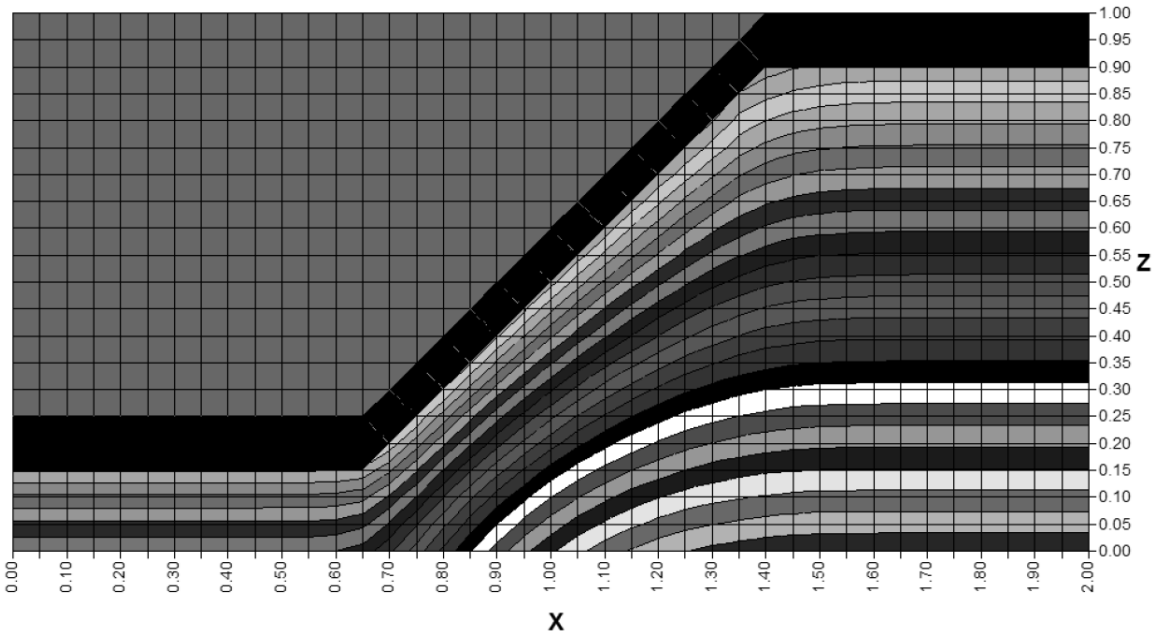

Figure 34. Non-dimensional 0.4 unit pressure contours for the 10 hour drawdown

CHAPTER 6. BANK STABILITY RESPONSE TO PERIODIC STAGES

"I've got a sort of idea," said Pooh at last, "but I don't suppose it's a very good one."
"I don't suppose it is either," said Eeyore.

– from *The House at Pooh Corner*
by A. A. Milne

Introduction

Specific to slope stability risk of sandbars downstream of dams, the following conclusions may be made from the work presented in the previous chapters:

1. For slopes near failure conditions, the slope stability factors of safety must be interpreted statistically (Chapter 2).
2. Of the typical limit equilibrium approaches to slope stability, the direct methods appear to be well behaved for slopes near failure, with the safety factors adhering to a log normal distribution with a mean of about 1.0 (as expected) and a standard deviation of approximately 0.08 (Chapter 3).
3. Matric suction must be included as a component of the analysis. Not only does it increase effective cohesion, it must also be considered for realistic calculation of the unit soil weights (Chapter 4).
4. Finite element analysis indicates that pore water pressures in sandbars can be effectively modeled by Richard's equation, and initial failure can be reasonably predicted for well established boundary conditions. (Chapter 5)

It is evident that a complete model of sandbar failures must include the stability effects of the adjacent river stage, the internal porewater pressure and matric suction dynamic conditions (both dependent on water stage history), and must synthesize these elements into stochastic predictions.

Unfortunately, the stochastic nature of slope failures requires statistical interpretation of a large number of simulations in order to understand slope response to river stage fluctuations. Indeed, the next chapter will show that a Monte Carlo simulation at sufficient power requires many thousands of these calculations. At the speed of the developed finite element model, a thousand simulations would take approximately 750 hours.

There are further challenges as well, specific to periodic, tidal type, loading conditions. For periodic flows the finite element approach is problematic, since both porewater pressure and matric suction distributions have been found to be dependent on their history, and it is not clear what constitutes reasonable initial conditions of periodic river stage fluctuations. One approach to resolving the initial condition problem is to run the finite element model through sufficient cycles that risk response also becomes periodic. The alternative approach is to iteratively adjust the initial conditions until they are in agreement with those at the end of the period. Either method would be expected to significantly increase computing time.

These issues were resolved by taking a new approach. As described herein, the finite element model is replaced with an analytical solution. This

solution, which is apparently new to the field, implements the general results of the previous chapters and allows arbitrary periodic stage functions.

Riverbank Porewater Response

A formal solution of the general problem of modeling the porewater response to n periodic adjacent water stages was obtained by partitioning the slope into saturated and unsaturated regions, as shown in Figure 35. The saturated region is presented first.

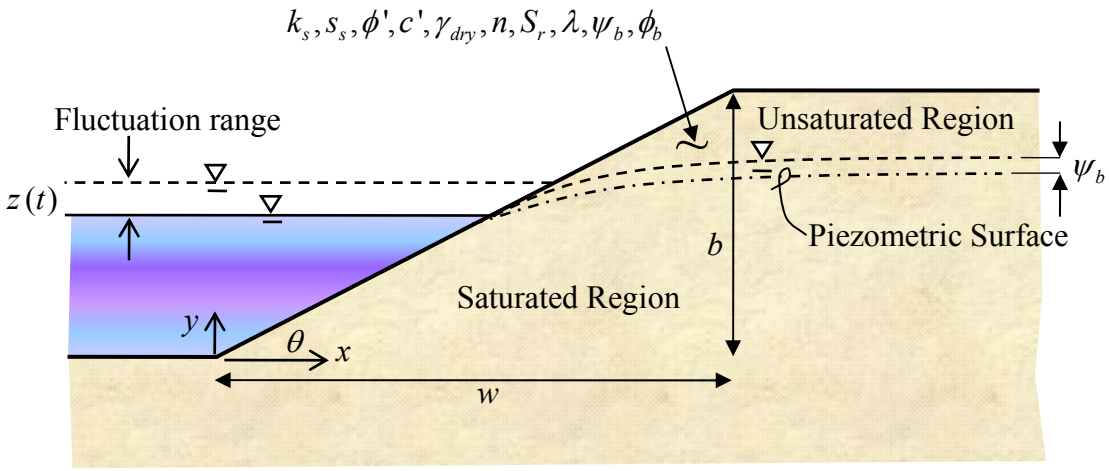

Figure 35. Riverbank Model

Saturated Region

The saturated region in the riverbank is described by the two-dimensional Richards equation for saturated flow (Fredlund and Rahardjo, 1993):

$$\frac{d^2h_s}{dx^2} + \frac{d^2h_s}{dy^2} = \frac{s_s}{k}\frac{dh_s}{dt} \tag{91}$$

where $h_s(x,y,t)$ (m) is the hydraulic head in the saturated region, with x (m) the horizontal coordinate, y (m) the vertical coordinate, and t (sec) denoting time. The origin is located at the interface of the sandbar with the river base. The two

soil properties are s_s (m^{-1}), the specific storage, and k_s (m/sec), the saturated hydraulic conductivity, both assumed constant. The slope, modeled with width w (m), height b (m), and angle θ, is assumed to be homogeneous. The adjacent river stage is denoted $z(t)$ (m). The initial condition for the solution to (91) is assumed to correspond to a constant head h_0 throughout the saturated region. That is,

$$h_s(x, y, 0) = h_0 \tag{92}$$

The four boundary conditions for h_s are

$$h_s(0, y, t) = z(t) \tag{93}$$

$$h_s(\infty, y, t) = h_\infty < \infty \tag{94}$$

$$h_s(x, x\tan\theta, t) = 0 \tag{95}$$

$$h_s(x, -\infty, t) = h_0 < \infty \tag{96}$$

The far field boundary condition is expressed here in terms of an assumed but unknown constant head h_0 which satisfies the initial condition. The implied assumption is that the soil is assumed to extend infinitely homogeneous in both the $-y$ and $+x$ directions. This seems a reasonable assumption for large slopes, such as those of interest along the Colorado River in the Grand Canyon, but may be less accurate for small slopes underlain by impermeable material. It is consistent with the half-space approximation of the Grand Canyon sandbars applied by Carpenter et al. (1995).

Equation (91) is simplified by introducing the composite variable u, where

$$u = x - y / \tan\theta \tag{97}$$

resulting in

$$\frac{d^2 h_s}{du^2} = \frac{s_s \sin^2 \theta}{k_s} \frac{dh_s}{dt} \tag{98}$$

with the initial and spatial boundary conditions for $h_s(u,t)$ reformulated as

$$h_s(u,0) = h_0 \tag{99}$$

$$h_s(0,t) = z(t) \tag{100}$$

$$h_s(\infty, y, t) = h_0 < \infty \tag{101}$$

If $z(t)$ is sinusoidal with period p (sec), the solution to (98) may be expressed

$$h_s(u,t) = h_0 + \exp(-\varepsilon_n u)\left[S_n \sin(\eta_n t - \varepsilon_n u) + C_n \cos(\eta_n t - \varepsilon_n u)\right] \tag{102}$$

where S_n, and C_n are constants with length units in meters, n is an arbitrary integer, and η_n ($\sec^{-1}$) and ε_n (m^{-1}) are

$$\eta_n = \frac{2n\pi}{p} \tag{103}$$

$$\varepsilon_n = \sin\theta \sqrt{\frac{2 s_s n \pi}{k_s p}} \tag{104}$$

For arbitrary, periodic loading, a solution may be obtained by expanding (102) as a Fourier series, in the form

$$h_s(u,t) = h_0 + \sum_{n=1}^{\infty} \exp(-\varepsilon_n u)\left[S_n \sin(\eta_n t - \varepsilon_n u) + C_n \cos(\eta_n t - \varepsilon_n u)\right] \tag{105}$$

In terms of the original variables, Equation (105) is

$$h_s(x,y,t) = h_0 + \sum_{n=1}^{\infty} S_n \sin\left[\eta_n t - \varepsilon_n\left(x - y/\tan\theta\right)\right]\exp\left[-\varepsilon_n\left(x - y/\tan\theta\right)\right] + \sum_{n=1}^{\infty} C_n \cos\left[\eta_n t - \varepsilon_n\left(x - y/\tan\theta\right)\right]\exp\left[-\varepsilon_n\left(x - y/\tan\theta\right)\right] \quad (106)$$

Equation (106) is a general solution, and valid for the groundwater response within any slope experiencing periodic adjacent stage loading. In particular, for sinusoidal *z(t)* and $\theta = 90^{\circ}$, Equation (106) becomes one dimensional and collapses to the well known solution for tidal driven groundwater fluctuations (Furbish, 1997). Expansions of the tidal solution by Fourier series are reported by Nielsen (1990) for sloping beaches, wherein he utilized perturbation to derive similar equations to Equation (106) but expressed in terms of *x* only.

Of course, h_s is valid only when $h_s \geq y + \psi_b$, where ψ_b is the pressure head at the air entry value (a negative value). When this condition is violated (e.g. $h_s < y + \psi_b$), flow is governed by the unsaturated head, the analysis of which is considered next.

Unsaturated Region

The unsaturated hydraulic head h_u (m) must satisfy Richard's equation for unsaturated flow, presented here in the form developed by Fredlund and

Rahardjo, 1993):

$$\frac{d}{dx}\left(k_u \frac{dh_u}{dx}\right)+\frac{d}{dy}\left(k_u \frac{dh_u}{dy}\right)=\gamma m_2^w \frac{dh_u}{dt} \tag{107}$$

where m_2^w (m^2 / N) is the coefficient of water volume change with respect to a change in matric suction, γ (N/m^3) is the specific weight of water, and k_u (m/sec) is the unsaturated hydraulic conductivity. Note that both k_u and m_2^w are functions of h_u, and collapse to the saturated constants k_s and s_s / γ at 100% saturation.

Following Budhu and Gobin (1995b), it is assumed that k_u scales to k_s approximately as $k_u \approx 1000 k_s$ (Bateh and Khoshgoftaar, 1979). Similarly, Fredlund and Rahardjo (2003) reports a value of $\gamma m_2^w \approx 100 s_s$ for a soil with properties akin to the one considered here. Thus, an order of magnitude approximation to Equation (107) is

$$10^{-5}\left(\frac{d^2 h_u}{dx^2}+\frac{d^2 h_u}{dy^2}\right) \approx \frac{s_s}{k_s}\frac{dh_u}{dt} \tag{108}$$

For comparable s_s and k_s values, the left hand side of Equation (108) is much less than the right hand side, resulting in the simplification

$$\frac{s_s}{k_s}\frac{dh_u}{dt} \approx 0 \tag{109}$$

the solution of which is simply

$$h_u \approx a + bx + cy \tag{110}$$

where a, b, and c are constants.

Initially h_u must equal h_0 everywhere in the unsaturated zone. Thus, in accordance with Equation (110), h_u would still equal h_0 when the piezometric

surface rises. However, in areas where the piezometric surface drops below the initial value, the scaling difference between the unsaturated and saturated hydraulic conductivities suggest that the air entry pressure head (ψ_b) is maintained. That is,

$$h_u = \begin{cases} h_0, & \left(y \geq h_0 - \psi_b\right) \\ y + \psi_b, & \left(y < h_0 - \psi_b\right) \end{cases} \tag{111}$$

Note that Equation (111) is a solution in the form required by Equation (110).

Saturated Flow for Arbitrary Fluctuating River Stages

By Taylor's series, *z(t)* can be expressed to any desired precision as a piecewise polynomial (order *K*) with *J* segments in the form $z_j\left(t, t_j, t_{j+1}\right) = z_{o,j} + z'_j t + z''_j t^2 \ldots + z_j^{[k]} t^k + \ldots + z_j^{[K]} t^K$ where *j* corresponds to the *j'th* segment for *z(t)*. The corresponding Fourier coefficients are given by

$$S_n = \sum_{j=1}^{J} \sum_{k=0}^{K} S_{j,k,n}; C_n = \sum_{j=1}^{J} \sum_{k=0}^{K} C_{j,k,n} \tag{112}$$

where $S_{j,k,n}$ and $C_{j,k,n}$ are

$$S_{j,0,n} = z_{o,j} \int_{t_j}^{t_{j+1}} \sin \eta_n t \, dt = z_{o,j} \eta_n^{-1} \left(\cos \eta_n t_j - \cos \eta_n t_{j+1}\right) \tag{113}$$

$$C_{j,0,n} = z_{o,j} \int_{t_j}^{t_{j+1}} \cos \eta_n t \, dt = z_{o,j} \eta_n^{-1} \left(\sin \eta_n t_{j+1} - \sin \eta_n t_j\right) \tag{114}$$

$$S_{j,k,n} = z_j^{[k]} \int_{t_j}^{t_{j+1}} t^k \sin \eta_n t \, dt = z_j^{[k]} \eta_n^{-1} \left[t_j^k \cos \eta_n t_j^k - t_{j+1}^k \cos \eta_n t_{j+1} + C_{j,k-1,n} \right] \tag{115}$$

$$C_{j,k,n} = z_j^{[k]} \int_{t_j}^{t_{j+1}} t^k \cos \eta_n t \, dt = z_j^{[k]} \eta_n^{-1} \left[t_{j+1}^k \sin \eta_n t_{j+1}^k - t_j^k \sin \eta_n t_j - S_{j,k-1,n} \right] \quad (116)$$

In the example application, specific to sandbars downstream of the Glen Canyon dam, the *z(t)* function may be established by considering both the linear water release functions described earlier and the stage relations established by Hazel et al. (2006). In terms of the piecewise notation introduced for *z(t)*, linear flow release functions may be designated $q_{o,j} + q'_j t$, where the constants are functions of the flow variables as defined earlier and have the values shown in Table 10.

j	$q_{o,j}$	$q'_j t$	t_j
1	q_{low}	0	$-\frac{1}{2} p$
2	$q_{low} - q'_{up} t_2$	q'_{up}	$\frac{1}{2}\left(t_{low} - p\right)$
3	q_{peak}	0	$t_2 + \left(q_{peak} - q_{low}\right) / q'_{up}$
4	$q_{peak} - q'_{down} t_4$	$-q'_{down}$	$t_3 + t_{peak}$
5	q_{low}	0	$\frac{1}{2}\left(p - t_{low}\right)$
6	q_{low}	0	$\frac{1}{2} p$

Table 10. Glen Canyon Dam Release Parameters.

For a one day period, as will be henceforth assumed, e.g. $p = 1$ day $\left(86,400 \text{ sec}\right)$.

Hazel et al. (2006) reports stage relationships for sandbars at various locations downstream of the Glen Canyon Dam. Catalogued by river mile (RM),

the relationships are given as

$$z(q) = \varsigma_1 q + \varsigma_2 q^2 \tag{117}$$

where ς_1 [m / (m^3/sec)] and ς_2 [m / (m^3/sec)^2] are regression constants at a particular distance downstream. From Equation (117) and the flow parameters in Table 10, the *z(t)* coefficients are therefore

$$z_{o,j} = \varsigma_1 q_{o,j} + \varsigma_2 q_{o,j}^2 \tag{118}$$

$$z'_j = \left(\varsigma_1 + 2\varsigma_2 q_{o,j}\right) q'_j \tag{119}$$

$$z''_j = \varsigma_2 q'^2_j \tag{120}$$

Overburden Pressure

The overburden pressure, denoted *P*, is given by

$$P(y) = \overline{\gamma}_{soil}(g - y) \tag{121}$$

where $\overline{\gamma}_{soil}$ (kN/m^3) is the average unit weight of the soil from the ground elevation *g* (m) to elevation *y*. Of course, accurate values of $\overline{\gamma}_{soil}$ require the actual unit weight of the soil at elevation *y*, denoted γ_{soil} (kN/m^3), which is, in turn, a function of the saturation *S*, porosity *n*, the dry unit weight of the soil γ_{dry} (kN/m^3) and the unit weight of water γ_{water} (kN/m^3), in the form

$$\gamma_{soil} = \gamma_{dry} + Sn\gamma_{water} \tag{122}$$

From Equation (122), $\overline{\gamma}_{soil}$ is given by

$$\overline{\gamma}_{soil} = \gamma_{dry} + \gamma_{water} \frac{n}{g - y} \int_y^g S\, dy \tag{123}$$

The saturation is a function of matric suction head ψ (m). Many constitutive relationships have been developed to describe this relationship. If the Brooks and Corey (1964) function is assumed, then

$$S = S_r + \left(1 - S_r\right)\left(\psi_b / \psi\right)^{\lambda} \tag{124}$$

where S_r is the residual saturation, ψ_b (m) is the pressure head at the air entry value, and λ is a soil constant.

Given Equation (124), Equation (123) may be written

$$\overline{\gamma}_{soil} = \gamma_{res} + \gamma_{water} \frac{\left(1 - S_r\right) n}{g - y} \int_y^g \left(\psi_b / \psi\right)^{\lambda} \, dy \tag{125}$$

where the residual unit weight γ_{res} (kN/m^3) is

$$\gamma_{res} = \gamma_{dry} + S_r n \gamma_{water} \tag{126}$$

From Equation (111), and noting that $h_u = y + \psi$, the matric suction head as a function of y is

$$\psi = \begin{cases} h_0 - y, & \left(y \geq h_0 - \psi_b\right) \\ \psi_b, & \left(y < h_0 - \psi_b\right) \end{cases} \tag{127}$$

Implementing Equation (127) requires calculating y_b (m), the elevation at which $\psi = \psi_b$. This formula for y_b is the implicit equation

$$h_s\left(x, y_b, t\right) = y_b + \psi_b \tag{128}$$

An approximate solution to Equation (128) is obtained by expanding h_s around $y = z\left(t\right)$:

$$h_s\left(x, y_b, t\right) \approx h_s\left(x, z, t\right) + \frac{dh_s}{dy}\left(y_b - z\right) = y_b + \psi_b \tag{129}$$

Usually the capillary rise is assumed to be a simple vertical projection from the piezometric surface, suggesting that the derivative term in Equation (129) is small. Moreover, assuming a fairly rapid response near the slope surface, the expected difference between y_b and z is also small. An approximate solution for y_b is therefore

$$y_b \approx h_s\left(x,z,t\right)-\psi_b \tag{130}$$

Equation (130) can also be used as the first guess for y_b and Equation (128) then used iteratively to determine y_b. For most applications, however, the approximate solution should be sufficient.

For purposes of determining saturation, it is useful to define an elevation y_{sat} (m), above which the soil becomes unsaturated. Equation (127) requires that $y_b = h_0 - \psi_b$, so y_{sat} is given by

$$y_{sat} = \max\left(y_b, h_0 - \psi_b\right) \tag{131}$$

Therefore, if $y < y_{sat} \le g$, Equation (125) may be expressed

$$\overline{\gamma}_{soil} = \gamma_{res} + \gamma_{water}\frac{\left(1-S_r\right)n}{g-y}\left[\int_{y}^{y_{sat}} dy + \int_{y_{sat}}^{g}\left(\frac{\psi_b}{h_0-y}\right)^{\lambda} dy\right] \tag{132}$$

with solution $\gamma_{res} = \gamma_{dry} + S_r n\gamma_{water}$

$$\overline{\gamma}_{soil} = \frac{y_{sat}-y}{g-y}\gamma_{sat} + \frac{g-y_{sat}}{g-y}\gamma_{res} - \frac{\kappa}{g-y}\left[1-\left(\frac{\psi_b}{y_{sat}+\psi_b-g}\right)^{\lambda-1}\right]\gamma_{water} \tag{133}$$

where γ_{sat} is the saturated soil weight, ($\gamma_{sat} = \gamma_{res} + \gamma_{water} n$), and κ (m) is defined by $\kappa = \left(1-S_r\right)n\psi_b / \left(\lambda - 1\right)$.

If $y_{sat} \le y \le g$, the soil is completely within the unsaturated zone.

Following the same procedure outlined above, the solution for $\overline{\gamma}_{soil}$ is

$$\overline{\gamma}_{soil} = \gamma_{res} - \frac{\kappa}{g-y}\left[\left(\frac{\psi_b}{y_{sat}+\psi_b-y}\right)^{\lambda-1} - \left(\frac{\psi_b}{y_{sat}+\psi_b-g}\right)^{\lambda-1}\right]\gamma_{water} \qquad (134)$$

Of course, if $g \le y_{sat}$, then the soil is completely saturated above *y*, and the average soil weight is simply

$$\overline{\gamma}_{soil} = \gamma_{sat} \qquad (135)$$

Conclusions

The primary advantage of the model developed here is the ability to model the porewater response to tidal type stage loading without stepping through incremental time steps from an assumed initial condition, as required by a finite element analysis. That said, there are other advantages to the model as well. These are:

1. The inherent fluctuations of river stages are directly modeled, eliminating the need to assume potentially inaccurate initial conditions
2. The average piezometric surface can be directly obtained from the constant term in Equation (106).
3. The analytical solution bypasses convergence problems often associated with finite element models of matric suction.

With the porewater model complete, global risk analysis of a river system becomes achievable. A particular approach is presented in the next chapter.

CHAPTER 7. RIPARIAN SCALE BANK FAILURE RISK

> Waves can romp through the earth and sparks fly off to join stars and if you are quiet and listen very carefully you can hear voices in the water.
>
> – from *The Bird in the Waterfall*
> by Glenn Wolff

Introduction

At the riparian scale, periodic stages at a particular sandbar location become functions of the upstream discharge waves. Thus, generalizing porewater response requires a twofold wave model: a discharge wave model must be derived and then coupled with the groundwater wave model that forms in response.

When this is achieved, a full risk model becomes possible by linking the riparian scale groundwater model with a slope stability model and associated stochastic parameters. Here, a Monte Carlo simulation is used to accomplish this generalization, with a simulated experiment applied to account for the inherent uncertainties of the input parameters. Model effectiveness and factor significance are analyzed by Analysis of Variance (ANOVA) hypothesis testing. A reduced ANOVA model is developed to relate slope failure risk with fluctuating stages. Finally, wave attenuation is accounted for by nonlinear regression, thus completing the river reach slope stability model.

Consistent with the earlier work, the ordinary method of slices (OMS) was utilized for the slope stability analysis. River stage loading is developed from the USACE (2003) equation, modified to include matric suction effects per Fredlund

and Rahardjo (1993). The resulting OMS safety factor (SF) equation is

$$SF = \frac{\sum\left\{c'\Delta l + \left[W\cos\chi + F\cos\left(\chi-\theta\right)\right]\tan\phi' - u_p\Delta l\cos^2\chi\tan\phi_b\right\}}{\sum\left\{W\sin\chi - \left[\left(y_0-g\right)\sin\theta + \left(x_0-x\right)\cos\theta\right]F/r\right\}} \quad (136)$$

where Δl (m) is the length of the slice at the slip surface, χ is the angle of the slice at the slip surface, W (N) is the weight of the overburden soil, F (N) is the resultant force of the water pressure (perpendicular to the slope), u_p (Pa) is the fluid pressure (positive for saturated conditions, negative for unsaturated conditions), and ϕ_b is the matric suction friction angle function. The remaining variables are as defined in Chapter 6.

In general, the matric suction function ϕ_b changes from ϕ' at saturated conditions to a function of ψ at unsaturated conditions. Indeed, Houston et al. (2009) found that a good fit of ϕ_b to field data may be achieved with a hyperbolic relation, with an initial value equal to ϕ' for matric suction values less than the air entry value.

However, when only limited data is available, ϕ_b is typically assumed to be constant (Fredlund and Rahardjo, 1993). Thus, since the no information is currently available for ϕ_b for the Colorado River sandbars, and matric suction values are not likely to significantly exceed the air entry value, ϕ_b was assumed to equal ϕ' for the verification process of the present work by simulation of the Glen Canyon Dam system. This assumption is consistent with similar slope stability studies (e.g. Cho and Lee, 2002). Of course, if better estimates of ϕ_b become available, the model can be easily reevaluated.

The soil weight W is obtained from the average soil weight equations (132) through (135). The expressions for F and u_p are easily obtained from the previously defined variables, and are

$$F = \begin{cases} (z-g)\gamma \Delta x / \cos\theta, & g \le z \\ 0, & g > z \end{cases} \tag{137}$$

$$u_p = \begin{cases} \gamma(h_s - y), & y \le y_b \\ \gamma(h_u - y), & y > y_b \end{cases} \tag{138}$$

Verification: Sandbar 172L

The stability risk model was verified by using data from the failure of sandbar 172L on the Colorado River. This sandbar failed on June 18, 1991 following high oscillating flow (Cluer, 1992). Figure 36 shows a sketch of the sandbar (following Fig. 4 in Budhu and Gobin, 1995b).

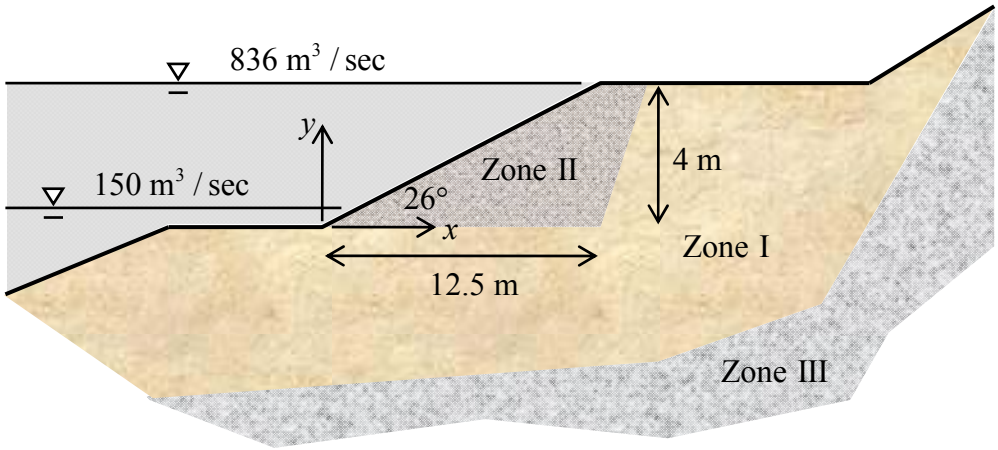

Figure 36. Sketch of Sandbar 172L

Three soil zones were identified in the sandbar and designated Zones I through III. The soil parameters, , including γ_{sat}, k_s, effective soil cohesion (c', kPa) and effective friction angle (φ'), in Zones I and II were determined by field

and laboratory testing. Zone I was categorized as an inactive zone, consisting of fine to medium sand ($\gamma_{sat} = 17.2$ kN/m^3, $c' = 2$ kPa, $\phi' = 32°$, $k_s = 2.3 \times 10^{-4}$ m/sec.) Zone II, the active zone where the failure occurred, consisted of transient sediments of very fine and medium sand ($\gamma_{sat} = 16.0$ kN/m^3, $c' = 4$ kPa, $\phi' = 30°$, $k_s = 4.2 \times 10^{-4}$ m/sec.) Zone III was much less permeable, consisting of rock, Redwall and Muav limestone talus slope.

The lowest and highest stages during the day the failure occurred are also shown in Figure 36, seen to correspond to flows of 150 m^3/sec and 836 m^3/sec.

Budhu and Gobin (1995b) analyzed the slope failure using Biot's (1945) stress-pore pressure theory. Unfortunately, this analysis predicted only a shallow failure in Zone II. Subsequent analyses with four limit equilibrium methods (Spencer's, Janbu, Modified Swedish, and Lowe and Karafiath) all also predicted shallow slope failures, but failed to predict failure near the observed slip surface, where the lowest calculated safety factor was 1.70 (using Lowe and Karafiath method). These limit equilibrium analyses assumed instantaneous drawdown, with the adjacent water stage lowered to 150 m^3/sec but the slope still completely saturated and the pore water pressures maximized at a constant hydraulic head corresponding to the maximum river stage. Given the poor performance of the models, the authors theorized that a fault already existed along the slip surface (within Zone II), and thus had an effective cohesion of zero. When their model was executed with this assumption, failure at the fault was, indeed, predicted.

The method developed here was used to consider three aspects of the

sandbar response of 172L:

1. The observed stability of the transient elements of Zone II during the fluctuating flows;
2. The failure on June 18 at the observed slip surface within Zone II;
3. The original (hypothesized) failure through Zone I that created the fault between Zone I and II. Ideally, failure should be predicted and the failure surface should approximate the observed fault geometry.

Execution of the model required the assumption of several parameters not tested on Sandbar 172L. These values, and the justification for their applicability here, are as follows:

1. The pore size distribution index (λ) was assumed to be 4.0, consistent with a similar soil reported by Fredlund and Rahardjo (1993).
2. The specific storativity (s_s) was implemented as 0.0005 m^{-1}, corresponding to the value reported by Sabol and Springer (2006) in their model of a different sandbar along the Colorado River.
3. The air entry pressure head value (ψ_b) was assumed to be 0.5 m, corresponding to a air entry pressure of 5 kPa reported by Fredlund and Rahardjo, (1993) for a similar soil.
4. The residual saturation (S_r) was assumed to be 15%, also reported by Fredlund and Rahardjo, 1993) for a similar soil.
5. The void ratio (e) was valued at 0.80, an average of the minimum laboratory, maximum laboratory, and field tested respective values of 0.52, 0.95, and 0.85 as reported by Budhu and Gobin (1994).

The flow parameters, estimated from the figures included in Budhu and Gobin (1995a), were: $q'_{down} = 100$ (m^3/sec)/hr, $q'_{up} = 100$ (m^3/sec)/hr, $q_{peak} = 835$ m^3/sec, and $t_{peak} = 10$ hr. The low flow values were different at the beginning from that at the end of the 24 hour period on June 18, initially at $q_{base} = 190$ m^3/sec and ending at $q_{base} = 150$ m^3/sec. The corresponding stages at the sandbar were modeled using the Hazel et al. (2006) reported coefficients at the sandbar of $z_1 = 6.1 \times 10^{-3}$ m / (m^3/sec) and $z_2 = -1.4 \times 10^{-3}$ m / (m^3/sec)^2.

The stage relationship was modeled by the Fourier series, utilizing 100 sine and cosine coefficients. The match between the Fourier model and the inferred stage relationship is shown in Figure 37. The fit is seen to be nearly perfect.

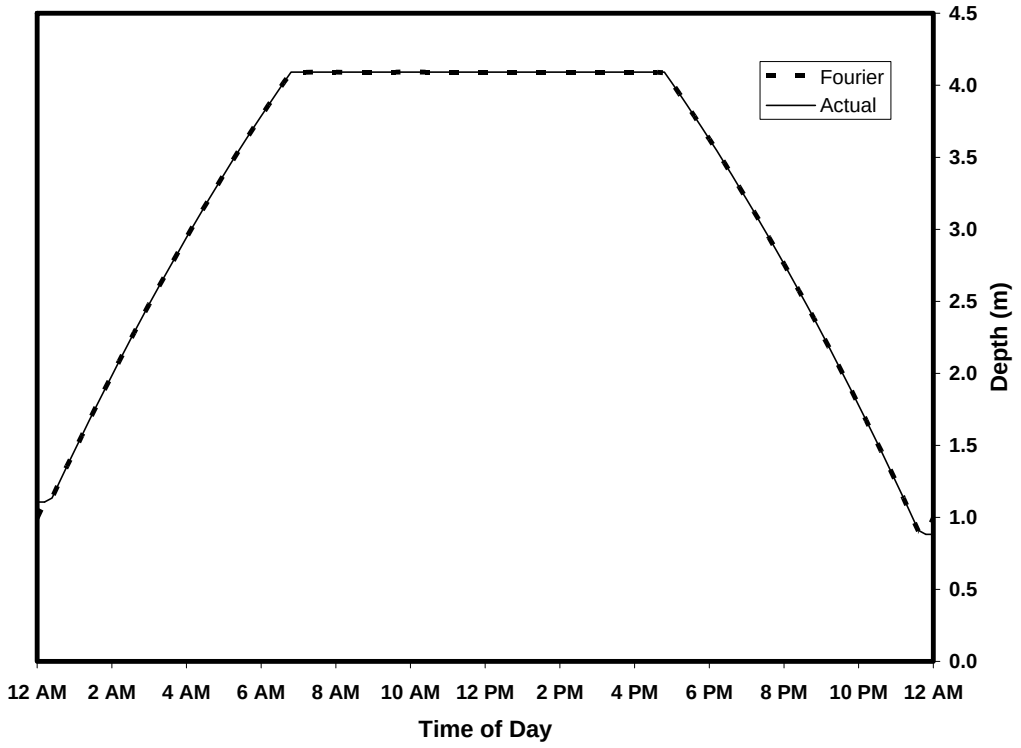

Figure 37. Reported and Fourier Approximated Models of Stage vs. Time Relationship at Sandbar 172L on June 18, 1991.

With the model parameters established, the three cases were evaluated. The resulting minimum safety factors (SF) versus time relationships are shown in Figure 38.

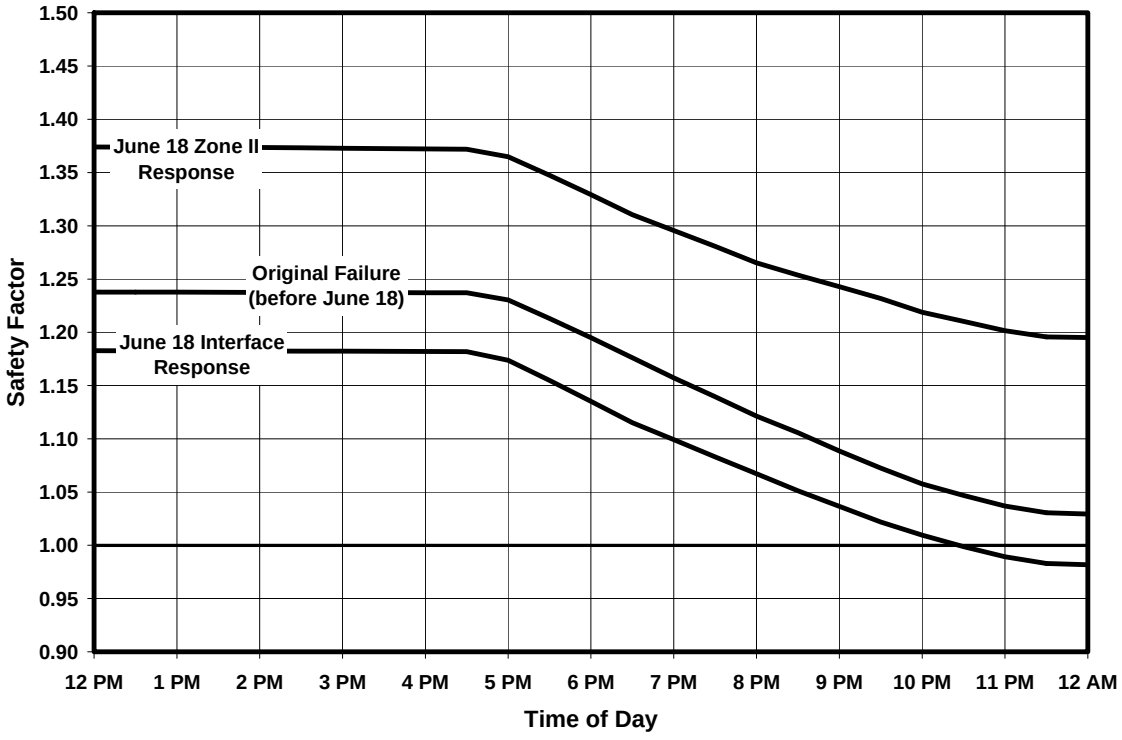

Figure 38. Sandbar 172L Safety Factor calculations for Three Different Simulations.

Figure 38 indicates that failure was not probable within Zone II for the June 18th conditions (minimum SF = 1.20), but was probable assuming the interface reduced cohesion to 2 kPa, this being the minimum of the Zone I and Zone II cohesions (minimum SF = 0.98). Thus, unlike previous efforts, failure is indicated by the present model with an arguably more realistic assumption of cohesion at the slip surface then given in the previous study by Budhu and Gobin (1995b), where the cohesion was assumed to be zero.

Most significantly, perhaps, is the likelihood that the original failure of the sandbar (when it consisted of Zone I material only) took place under similar loading conditions, as suggested by a minimum safety factor near 1 (SF = 1.03). Indeed, Figure 39 shows the slip surface corresponding to the minimum SF

calculated for the Zone I / II fault. Reasonable agreement is also seen between the failure surface and the observed fault geometry, particularly with regard to the endpoints. Of course, the observed fault was not curvilinear at its base, but it is probable that if the slip surface did occur as predicted, the failure block would have leveled the base surface as it progressed.

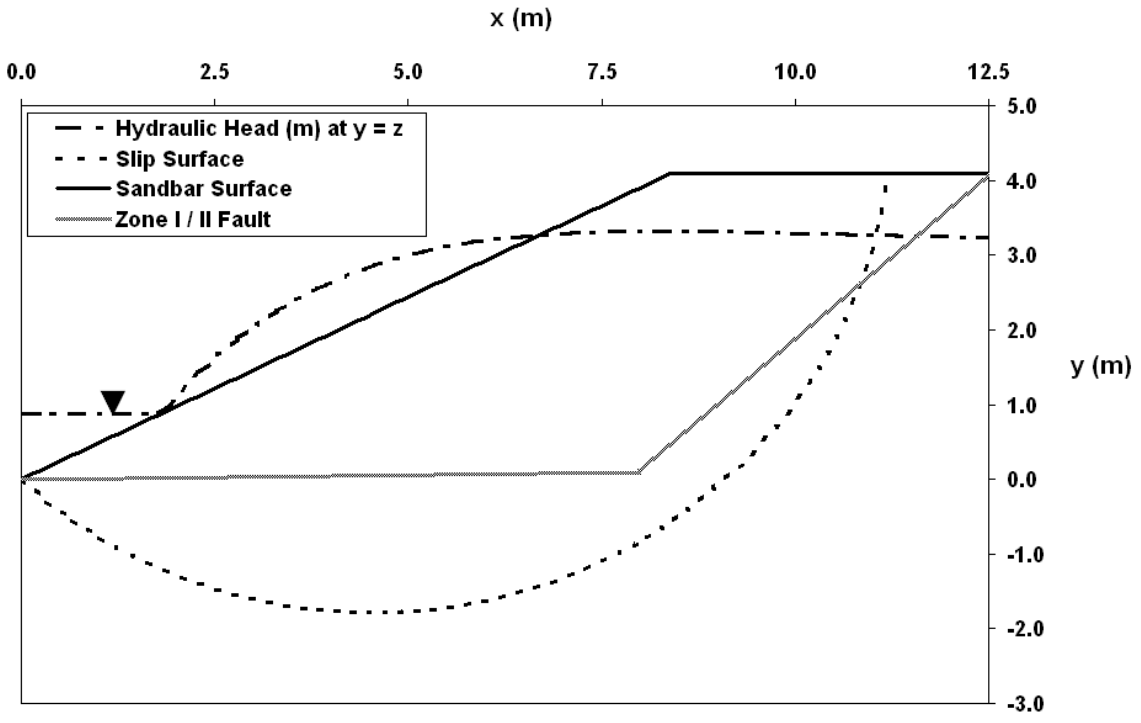

Figure 39. Sandbar 172L Slip Surface and Zone I / II Fault for the Inferred Initial Failure.

Note that the porewater pressures in Figure 39 were quite high, suggested a high probability of liquefaction, more evidence of failure.

The high porewater pressures at the bank surface are consistent with rapid drawdown, which describes the bank stability reaction to rapidly decreasing stages. Analysis by effective stress directly accounts for porewater pressure changes but does not usually account for changes to the effective shear strength due to undrained conditions. Analyses assuming total stress conditions have been

developed to account for undrained shear strength effects. Unfortunately, these analyses are somewhat complex, can only be applied with the Lowe and Karifiath and USACE 2DLE stability calculation methods, require soil parameters that may not be available or easily obtained, and requires three separate safety factor estimates (Duncan and Wright, 2005).

For soils with hydraulic conductivities greater than 10^{-6} m/day, such as those considered here, an effective stress analysis is appropriate and drained shear strengths can be used (Duncan and Wright, 2005). Moreover, it must be noted that soil dilatancy and associated shear strength effects are indirectly included through the empirically based bank stability risk model. However, the analysis procedure here may not be appropriate for soils with smaller hydraulic conductivities; caution is warranted under those circumstances.

Colorado River Simulated Experiment

Independent Variables

Although the model developed here allows any periodic stage function, it is useful to consider the simple flow release schemes typically utilized for hydroelectric dam operations. Five factors describing the water release procedures utilized by dam operations are recognized here. These factors are typically bounded by regulations. Their description, and, as an example, the regulations specific to the Glen Canyon Dam, are as follows:

1. Minimum release flow rate q_{base} (m^3 / sec). This is minimum amount of flow required to be released. For the Glen Canyon Dam, current

regulations (USDI 1996) require nighttime (midnight to 7 a.m.) flow to be greater than 142 m^3 / sec and 227 m^3 / sec during the daytime.

2. The maximum allowable flowrate change over the previous 24 hours, denoted here Δq (m^3 / sec). Current regulations are somewhat complicated regarding this value, resulting in regulations on Δq that can vary daily, weekly, and even monthly, but the highest allowable change is 227 m^3/sec and the ultimate maximum peak flow is strictly less than 566 m^3/sec .
3. Peak hold time t_{peak} (hr). This is the amount of time flow is maintained at the maximum daily flow.
4. Down-ramp rate q'_{down} (m^3 / sec-hr). This is the rate at which the peak flow is reduced. Also regulated, it is not allowed to exceed 42.5 m^3 / sec-hr (USDI 1996).
5. Up-ramp rate q'_{up} (m^3 / sec-hr). The rate at which the flow-rate is increased. Current regulations (USDI 1996) require this rate to be less than 71 m^3 / sec-hr.

Not included in the five factors shown above is the hold time t_{base} (hr) at q_{base}. However, since these parameters are specific to daily operations, t_{base} is seen to be a function of the other five variables in the form

$$t_{base} = 24(\text{hr}) - t_{peak} - \left(1/q'_{down} + 1/q'_{up}\right)\Delta q \tag{139}$$

In addition, it is important to determine if there is a difference in the response of the high elevation sandbars versus the low elevation sandbars. Noting that sandbars are built at a crest elevation close to the adjacent stage, the height of

the sandbars are denoted here as q_{build} (m^3 / sec). This constitutes the sixth independent variable.

Previous investigations are conflicting regarding the relative impact that these variables have on downstream sandbar stability. Darby and Thorne (1995) noted a number of slope failures that had occurred during different stages of rainfall hydrographs, for example. This variability is likely a result of the inherently stochastic nature of the actual slope failures, most likely reflecting the inherent variability of the specific slope characteristics, such as soil strength, unit weights, and groundwater parameters.

Experimental Procedure

A simulated experiment was used in order to

1. quantify the effects of uncertainty inherent to slope failure predictions along the Colorado River;
2. rigorously investigate the effect of the Glen Canyon flow release regulations on downstream slope stability;
3. predict and compare the failure risks of low versus high sandbars;
4. develop a reduced model that may be used for prediction purposes;

The simulated experiment was developed by Monte Carlo simulation. A 2-level factorial experiment (2LFE) was used for analysis of the results. The 2LFE approach varies multiple factors with each run, utilizing well established scientific methods designed to track both main effects and interactions within a rigorous statistical framework.

While the 2LFE approach is well established in other disciplines such as industrial engineering, it is less familiar for the present application, where the "one factor at a time" (OFAT) approach often considered for slope stability research along the Colorado River. Indeed, OFAT was assumed to be the ideal experimental approach by USDI (1996) in their report on the Glen Canyon Dam. The benefits of the OFAT approach are debatable, however. The OFAT approach does not account for interactions of the factors, and requires many more experimental runs then necessary to obtain statistically powerful data. By comparison with 2LFE, OFAT is inaccurate, inefficient, and insufficient. For further discussion of the benefits of 2LFE over OFAT the reader is referred to Mongomery (2009).

For the six independent variables that define the Glen Canyon Dam release guidelines, a complete 2LFE requires 64 separate factors. In order to determine the number of replicates required, statistical power was estimated assuming a probability of failure ($Pr_{failure}$) standard deviation of about 30%, based on some preliminary runs of the model. A signal for $Pr_{failure}$ of 5% was established as the minimum effect of interest. Given these two requirements, 50 replicates for each of the 64 main factors and interactions were selected, corresponding to 3,200 total replicates. The corresponding statistical power was 99.7%.

This rather high number of replications would require a number of simulations several orders of magnitude higher than those typically reported by publications in this field. Indeed, usually only a handful of unsteady slope

stability simulations are reported in most publications. This low number is a result of the long computing times required to solve the porewater pressure finite difference equations. Moreover, for the periodic conditions considered here specific to daily dam operations, the simulation would need to proceed through a number of periods until the porewater pressure response has become accordingly periodic. Given the results of the previous work, a reasonable estimate of the computing time required per simulation would be on the order of several hours at a minimum. However, even if the computing time per simulation could be reduced to 1 hour, 3,200 hours would be necessary to complete the data set, constituting an amount of time probably unobtainable with the resources and timeframe available.

Fortunately, the time constraints on the porewater analysis were greatly reduced by the series solution found for the porewater response (Chapter 6). This solution allowed calculated porewater pressures at a given time directly, foregoing the need for a finite difference analysis, and reduced computation time to about 30 seconds per simulation, an improvement likely more than 2 orders of magnitude.

Stochastic Parameters

The final challenge before the Monte Carlo simulation could be executed was to determine the applicable statistical distributions of the relevant characteristics. Specifically, the variation of the saturated hydraulic conductivity (k_s) , specific storage (s_s), dry soil weight (γ_{dry}), void ratio (e), stage relationships (z_1, z_2) , porewater distribution coefficient (λ), air entry pressure head (ψ_b),

effective soil cohesion (c'), effective soil friction angle (φ'), residual saturation (S_r), and slope angles (θ) needed be modeled as either known constants or appropriately formed statistical distributions.

The following sources were consulted in order to make reasonable inferences about the parameters: Anderson and Woessner (1992), Budhu and Gobin (1994, 1995a, 1995b), Beus et al. (1993), Fredlund and Rahardjo, 1993), Sabol and Springer (2006), Webb et al. (1999). When deemed appropriate, 4-sigma or 6-sigma approximations were used (see Duncan and Wright, 2005). A great deal of variation for these values was found between authors, between different publications of the same authors, and sometimes even between reported values within the same report. These inconsistencies further validate the present use of stochastic methods for analysis.

Property	Assumed Distribution	Mean	Std. Dev.	Comments
φ' (º)	Normal	30	0.7	Does not include a value of 26 º reported by Gobin and Gobin (1994), which appears to be a typographical error.
c' (kPa)	Lognormal (natural log)	0.5	0.3	Accounts for all reported values, including a reported measurement of 4 kPa reported by Budhu and Gobin (1995b) that may be anomalous (Beus et al, 1993 reports an average cohesion of 1 kPa)
k_s (m/sec)	Lognormal (natural log)	-8.5	0.2	
s_s (m^{-1})	Lognormal (natural log)	-8	0.3	This distribution based on a 6-sigma assumption on the range of values for sand reported by Anderson and Woessner (1992).
θ (º)	Normal	26	1.0	
e (%)	Normal	80	7	
γ_{dry} (N/m^3)	Normal	14.5	0.2	
λ	Constant	4.0		No information available on this variable specific to the Colorado River. The value used here is per Fredlund and Rahardjo (1993).
ψ_b (m)	Constant	1.5		No information available on this variable specific to the Colorado River. This value is from a similar soil reported by Fredlund and Rahardjo (1993).

Table 11. Assumed mean values, standard deviations, and statistical distributions for the Colorado River sandbar properties.

The assumed distribution characteristics are shown in Table 11. Not included are the statistics for the z_1 and z_2 parameters, which were found to be negatively correlated. This is to be expected, however, since as z_1 increased, one would expect z_2 to naturally decrease in order to meet the fairly constant average depth typical of the river.

The z_1 versus z_2 correlation was modeled with linear regression. The result is shown in Figure 40. The overall regression fit was significant ($R^2 = 0.82$; R^2-adj = 0.81; $F = 200.0$, $p < 0.0005$) as were the individual factors (constant: $T = 4.62$, $p < 0.0005$; slope: $T = -14.14$, $p < 0.0005$). The residuals conformed well to

the normal distribution. The regression equation was $z_2 = 0.83 - 0.39\, z_1$. The standard error (SE) for the constant was 0.2, and the SE for the slope factor was 0.03. The best distribution found that described z_1 independently was log-normal, with mean 1.8 and standard deviation 0.25. Thus, the stochastic model z_1 and z_2 was assumed in the following form:

$$z_1 = \exp\left[\Phi_{norm}^{-1}\left(e_{rand}, 1.8, 0.25\right)\right] \tag{140}$$

$$z_2 = \Phi_{norm}^{-1}\left(e_{rand}, 0.83, 0.2\right) - \left[\Phi_{norm}^{-1}\left(e_{rand}, 0.39, 0.03\right)\right] z_1 \tag{141}$$

where $\Phi_{norm}^{-1}\left(e_{rand}, \overline{u}, s\right)$ refers to the inverse normal distribution, with $\overline{w}$ the mean, s the standard deviation, and e_{rand} a randomly generated uniform value between 0 and 1.

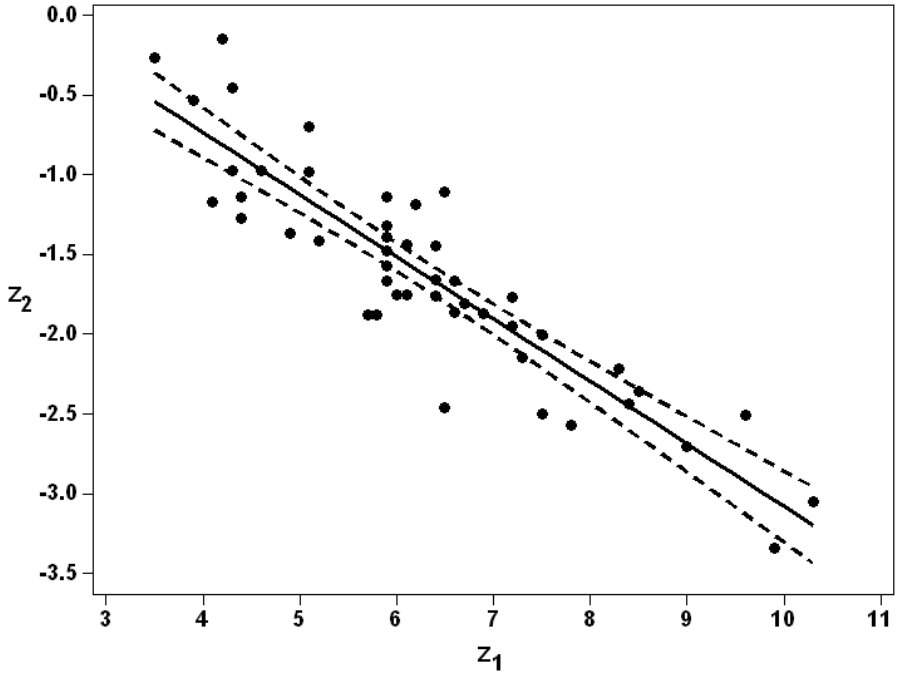

Figure 40. Colorado River Stage Coefficients Regression with 95% Confidence Bands.

Matric Suction and Associated Unit Weight Changes

Model execution would be simplified by ignoring matric suction effects. Chapter 3 demonstrated the importance of including matric suction effects in infinite slope stability models, but these effects may not be significant for curvilinear failure surfaces such as those considered here.

The significance of matric suction (and the associated soil unit weight changes) in the risk model was therefore investigated for a typical Grand Canyon sandbar (see Table 12). Bank stability was evaluated both with matric suction effects included (with $\lambda = 4$ and $\psi_b = 1.5$ m); and for simplified conditions, wherein matric effects were ignored. Only steady state flow conditions were considered.

Figure 41 shows the resulting risk prediction as a function of sandbar height (in terms of building flow) when the river discharge is 100 m^3/sec. It is seen that for small sandbars, the actual risk is higher than the risk computed ignoring matric effects. This is likely a consequence of the increased soil weight above the piezometric surface associated with the matric suction.

For high sandbars, however, the risk prediction is reversed: actual risk is slightly lower than risk computed ignoring matric suction and the associated soil unit weight changes. Thus, it appears that the binding effects of matric suction that stabilize the upper portion of the slope prevail over the destabilizing soil weight.

Property	Value	Property	Value
φ' (°)	30	e (%)	82
c' (kPa)	4	γ_{dry} (N/m^3)	12
k_s (m/sec)	10^{-4}	S_r	0.15
s_s (m^{-1})	10^{-4}	z_1	9
θ (°)	33	z_2	-2

Table 12. Typical Grand Canyon sandbar properties.

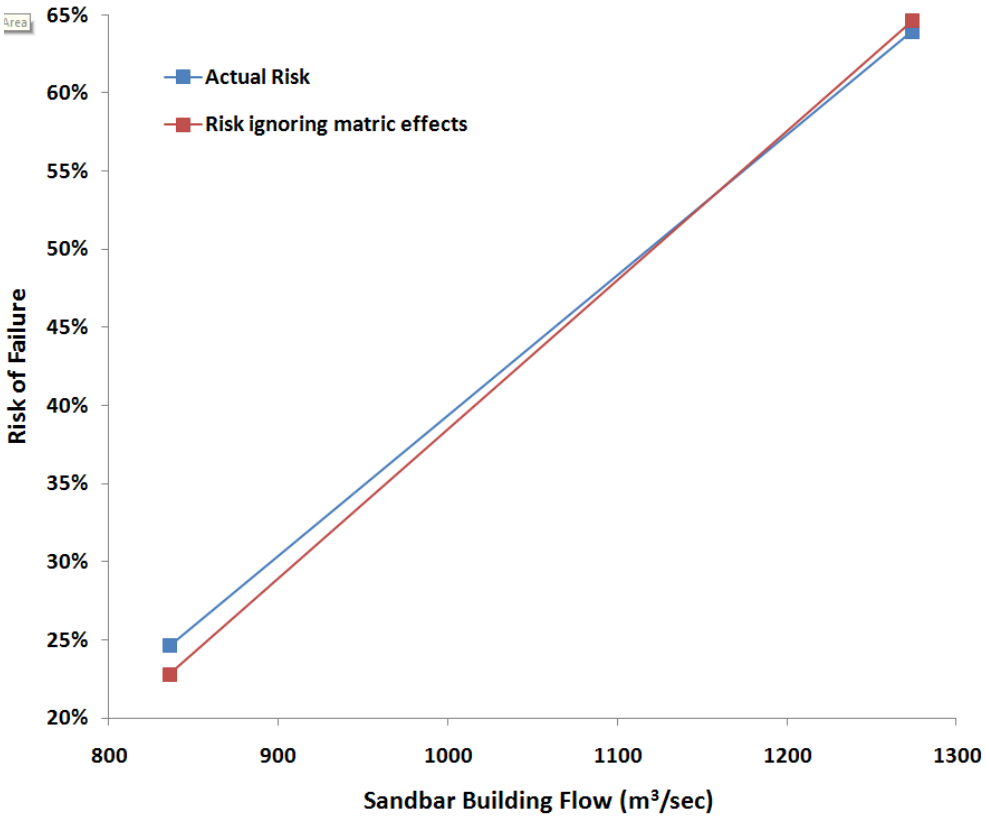

Figure 41. Failure risk as a function of matric suction and associated soil unit weight changes for a typical Grand Canyon sandbar (river discharge = 100 m^3/sec).

For higher flows, however, the effect of the matric suction and the associated soil unit weight changes become more significant. Figure 42 shows bank stability risk for the sandbar at a 500 m^3/sec river stage flow. It is seen that

for smaller sandbars, ignoring the matric suction and associated soil unit weight changes results in a risk underprediction of more than 10%. For larger sandbars, the binding effect of matric suction above the water table reduces this error, although it still remains greater than 6%. Thus, ignoring matric suction and the associated soil unit weight changes can result in significantly non-conservative risk predictions.

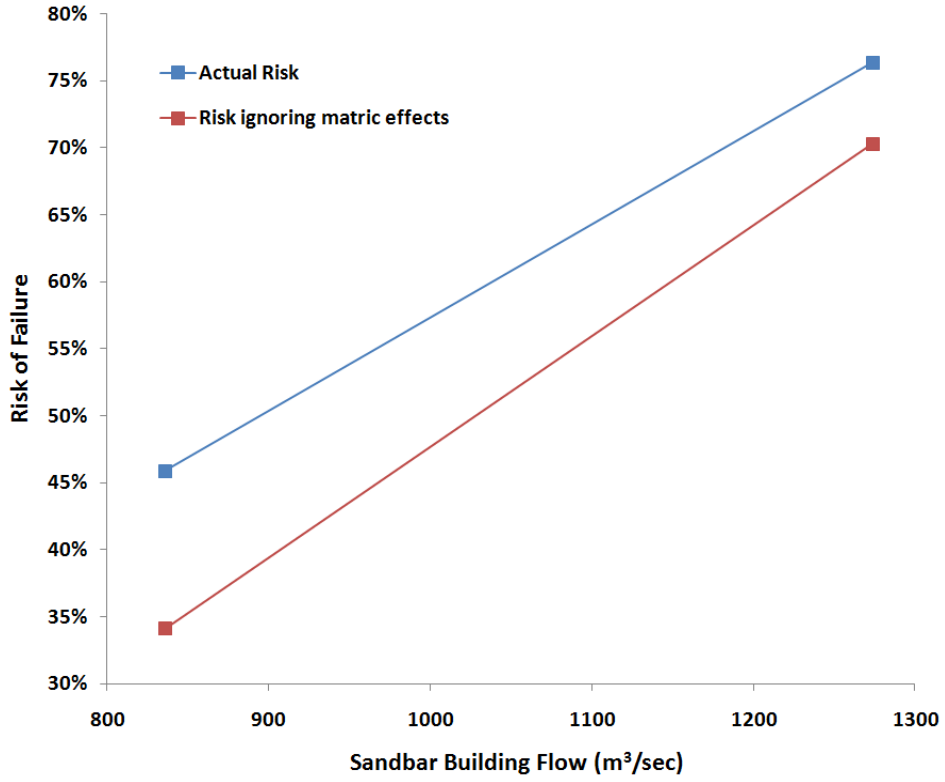

Figure 42. Failure risk as a function of matric suction and associated soil unit weight changes for a typical Grand Canyon sandbar (river discharge = 500 m^3/sec).

Model Execution

As noted earlier, Excel was used to run the simulation. Since Excel's random number generator has been criticized as poorly performing (see

McCullough and Wilson, 2005), Minitab was used to generate all random numbers used in the simulation.

A number of preliminary runs were used to evaluate and validate the simulation. Without exception, the minimum safety factor always occurred at the end of the down ramping stage, a finding consistent with other investigations of the Colorado River sandbars (e.g. Budhu and Gobin, 1998a, 1998b). For the Monte Carlo simulation, then, all minimum safety factors were evaluated at the end of the down ramping stage.

Results and Discussion

Execution of the randomized experiment took approximately 27 hours. The variables describing the slip geometry at the minimum safety factors were always within the established model limits, indicating that a local minimum value had always been reached. All minimum SF values were converted to failure risk assuming a log normal distribution with a mean of $\log_{10} = 0.002$ and a standard deviation of 0.034, consistent with the results of Chapter 3 for a landslide type failure with effective stress analysis and the OMS stability approach

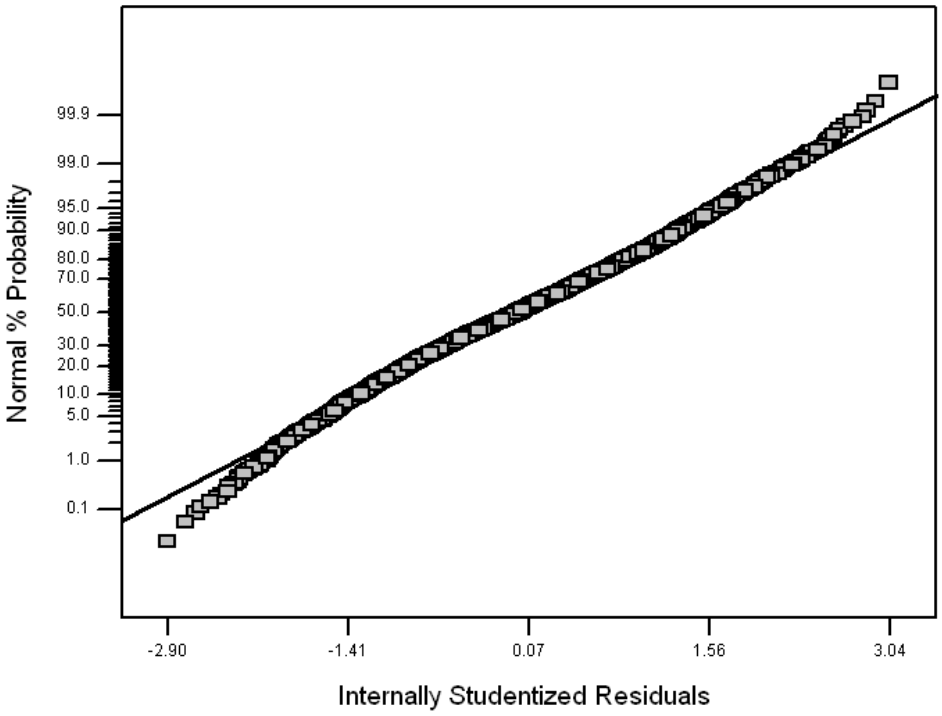

Figure 43. Normal Probability Plot (Full Model).

The ANOVA analysis was conducted in Design Expert with risk response as the dependent variable. The arcsine square root transformation, applicable to response variables bounded by 0 and 1, was utilized. Initially, all 32 possible factors were included for analysis. The overall model was found to be highly significant ($p < 0.0001$), where p is the probability that the observed trends are due to noise only. Overall measures of the model indicated an adequate, if highly variable, fit (adequate precision =f 12.5, $R^2 = 0.12$, adj-$R^2 = 0.11$, pred-$R^2 = 0.09$.) As shown in Figure 43, the residuals were nearly normally distributed with slightly heavy tails, a deviation that is probably not serious, particularly given that ANOVA testing is usually robust with regard to small violations of normality (Lindman, 1974). The specific results are shown in

Table 13.

Source	Sum of Squares	Degrees of Freedom	Mean Square	Fisher-F Value	Prob > Fisher F
Model	***32.64***	***63***	***0.5181***	***6.97***	***< 0.0001***
A-Downramp	***0.3112***	***1***	***0.3112***	***4.19***	***0.0408***
B-Upramp	***1.4083***	***1***	***1.4083***	***18.94***	***< 0.0001***
C-Baseflow	***7.5369***	***1***	***7.5369***	***101.38***	***< 0.0001***
D-Flow Change	***4.8236***	***1***	***4.8236***	***64.88***	***< 0.0001***
E-Peak hold time	***5.9194***	***1***	***5.9194***	***79.62***	***< 0.0001***
F-Building Flow	***5.4928***	***1***	***5.4928***	***73.88***	***< 0.0001***
AB	0.0109	1	0.0109	0.15	0.7021
AC	0.0027	1	0.0027	0.04	0.8491
AD	0.0137	1	0.0137	0.18	0.6673
AE	***0.2209***	***1***	***0.2209***	***2.97***	***0.0848***
AF	0.0613	1	0.0613	0.82	0.3640
BC	0.0002	1	0.0002	0.00	0.9589
BD	0.0623	1	0.0623	0.84	0.3601
BE	0.0072	1	0.0072	0.10	0.7559
BF	0.0554	1	0.0554	0.74	0.3882
CD	0.0119	1	0.0119	0.16	0.6890
CE	0.0074	1	0.0074	0.10	0.7532
CF	0.0082	1	0.0082	0.11	0.7400
DE	***3.2560***	***1***	***3.2560***	***43.80***	***< 0.0001***
DF	0.1010	1	0.1010	1.36	0.2438
EF	0.1770	1	0.1770	2.38	0.1229
ABC	0.0041	1	0.0041	0.05	0.8149
ABD	0.0241	1	0.0241	0.32	0.5695
ABE	0.0175	1	0.0175	0.24	0.6273
ABF	0.0386	1	0.0386	0.52	0.4714
ACD	0.1437	1	0.1437	1.93	0.1645
ACE	0.0012	1	0.0012	0.02	0.9006
ACF	0.0772	1	0.0772	1.04	0.3084
ADE	0.0121	1	0.0121	0.16	0.6866
ADF	0.0761	1	0.0761	1.02	0.3117
AEF	0.0020	1	0.0020	0.03	0.8708
BCD	0.0030	1	0.0030	0.04	0.8399
BCE	0.1184	1	0.1184	1.59	0.2071
BCF	***0.3065***	***1***	***0.3065***	***4.12***	***0.0424***
BDE	0.0283	1	0.0283	0.38	0.5374
BDF	0.0351	1	0.0351	0.47	0.4922
BEF	0.0353	1	0.0353	0.48	0.4907
CDE	0.0154	1	0.0154	0.21	0.6491
CDF	0.0101	1	0.0101	0.14	0.7128
CEF	***0.4229***	***1***	***0.4229***	***5.69***	***0.0171***
DEF	0.1686	1	0.1686	2.27	0.1322
ABCD	0.0611	1	0.0611	0.82	0.3646
ABCE	0.0163	1	0.0163	0.22	0.6399
ABCF	0.0078	1	0.0078	0.10	0.7467
ABDE	***0.4185***	***1***	***0.4185***	***5.63***	***0.0177***
ABDF	0.0008	1	0.0008	0.01	0.9193
ABEF	0.0303	1	0.0303	0.41	0.5235
ACDE	0.1574	1	0.1574	2.12	0.1457
ACDF	0.0292	1	0.0292	0.39	0.5308
ACEF	0.0404	1	0.0404	0.54	0.4611
ADEF	0.0023	1	0.0023	0.03	0.8597
BCDE	0.0787	1	0.0787	1.06	0.3036

Source	Sum of Squares	Degrees of Freedom	Mean Square	Fisher-F Value	Prob > Fisher F
BCDF	0.1431	1	0.1431	1.93	0.1654
BCEF	0.0042	1	0.0042	0.06	0.8118
BDEF	0.0039	1	0.0039	0.05	0.8182
CDEF	0.0435	1	0.0435	0.58	0.4446
ABCDE	0.0313	1	0.0313	0.42	0.5164
ABCDF	0.0118	1	0.0118	0.16	0.6906
ABCEF	0.0066	1	0.0066	0.09	0.7651
ABDEF	***0.2059***	***1***	***0.2059***	***2.77***	***0.0962***
ACDEF	0.1557	1	0.1557	2.09	0.1479
BCDEF	0.0106	1	0.0106	0.14	0.7053
ABCDEF	0.1498	1	0.1498	2.02	0.1558
Pure Error	233.14	3136	0.0743		
Corrected Total	265.78	3199			

Table 13. ANOVA Results (Full Model).

The factor analysis indicates that all main effects are highly significant contributors to failure risk ($p < 0.05$). Four interaction terms were significant ($p < 0.05$) and two others borderline significant ($p < 0.10$).

With the primary contributors identified, the ANOVA model was reduced to maximize predictive ability by reducing the potential for overfitting. Only factors corresponding to $p < 0.10$ were included in the reduced model, with the exception of those required to meet hierarchy (see Peixoto, 1987, 1990.) The probability limit is consistent with typical design of engineering experiments guidelines (Montgomery 2009.) Table 14 shows the results. The reduced model normal probability plot was essentially the same as the overall probability plot. The model fit metrics were as follows: adequate precision = 14.7, $R^2 = 0.12$, adj-$R^2 = 0.11$, and pred-$R^2 = 0.10$. The increase in pred-R^2 and the consistency of the values across all regression coefficients provide evidence that the reduced model is a better predictive tool than the overall model. The rather low value of the regression coefficients are consistent with field research (see Travis et al., 2010b and 2010c) and reflect the highly variable nature of the sandbar slope

stability. The lack of fit probability ($p = 0.88$) for the reduced model indicates a well behaved model with no evidence of a lack of fit. The residual analysis was consistent with the overall ANOVA model results, indicating adequate adherence to the ANOVA assumptions.

Source	Sum of Squares	Degrees of Freedom	Mean Square	Fisher-F Value	Prob > Fisher F
Model	31.30244408	37	0.84601200 2	11.40884 07	< 0.0001
A-Downramp	***0.3112***	***1***	***0.3112***	***4.20***	***0.0406***
B-Upramp	***1.4083***	***1***	***1.4083***	***18.99***	***< 0.0001***
C-Baseflow	***7.5369***	***1***	***7.5369***	***101.64***	***< 0.0001***
D-Flow Change	***4.8236***	***1***	***4.8236***	***65.05***	***< 0.0001***
E-Peak hold time	***5.9194***	***1***	***5.9194***	***79.83***	***< 0.0001***
F-Building Flow	***5.4928***	***1***	***5.4928***	***74.07***	***< 0.0001***
AB	0.0109	1	0.0109	0.15	0.7017
AD	0.0137	1	0.0137	0.19	0.6669
AE	***0.2209***	***1***	***0.2209***	***2.98***	***0.0844***
AF	0.0613	1	0.0613	0.83	0.3634
BC	0.0002	1	0.0002	0.00	0.9588
BD	0.0623	1	0.0623	0.84	0.3595
BE	0.0072	1	0.0072	0.10	0.7556
BF	0.0554	1	0.0554	0.75	0.3876
CE	0.0074	1	0.0074	0.10	0.7529
CF	0.0082	1	0.0082	0.11	0.7397
DE	***3.2560***	***1***	***3.2560***	***43.91***	***< 0.0001***
DF	0.1010	1	0.1010	1.36	0.2432
EF	0.1770	1	0.1770	2.39	0.1224
ABD	0.0241	1	0.0241	0.32	0.5690
ABE	0.0175	1	0.0175	0.24	0.6269
ABF	0.0386	1	0.0386	0.52	0.4708
ADE	0.0121	1	0.0121	0.16	0.6863
ADF	0.0761	1	0.0761	1.03	0.3110
AEF	0.0020	1	0.0020	0.03	0.8707
BCF	***0.3065***	***1***	***0.3065***	***4.13***	***0.0421***
BDE	0.0283	1	0.0283	0.38	0.5368
BDF	0.0351	1	0.0351	0.47	0.4916
BEF	0.0353	1	0.0353	0.48	0.4901
CEF	***0.4229***	***1***	***0.4229***	***5.70***	***0.0170***
DEF	0.1686	1	0.1686	2.27	0.1317
ABDE	***0.4185***	***1***	***0.4185***	***5.64***	***0.0176***
ABDF	0.0008	1	0.0008	0.01	0.9192
ABEF	0.0303	1	0.0303	0.41	0.5230
ADEF	0.0023	1	0.0023	0.03	0.8595
BDEF	0.0039	1	0.0039	0.05	0.8179
ABDEF	***0.2059***	***1***	***0.2059***	***2.78***	***0.0958***
Residual	234.4752	3162	0.0742		
Lack of Fit	1.3352	26	0.0514	0.69	0.8766
Pure Error	233.1400	3136	0.0743		
Corrected Total	265.7776	3199			

Table 14. ANOVA Results (Reduced Model).

The reduced ANOVA model may be expressed in equation form as follows:

$$\Pr_{failure} = \sin^2 \left(\begin{array}{l} 1.23\times10^{-1} + 1.39\times10^{-3} q'_{down} + 1.58\times10^{-4} q'_{up} + 2.23\times10^{-4} q_{base} + \\ 1.41\times10^{-3} \Delta q + 4.18\times10^{-3} t_{peak} + 3.61\times10^{-4} q_{build} - 6.34\times10^{-6} q'_{down} q'_{up} - \\ 8.05\times10^{-6} q'_{down} \Delta q - 2.42\times10^{-4} q'_{down} t_{peak} - 9.85\times10^{-7} q'_{down} q_{build} + \\ 4.08\times10^{-6} q'_{up} q_{base} - 6.02\times10^{-6} q'_{up} \Delta q - 1.64\times10^{-4} q'_{up} t_{peak} - \\ 1.93\times10^{-7} q'_{up} q_{build} - 9.48\times10^{-5} q_{base} t_{peak} + 2.67\times10^{-7} q_{base} q_{build} - \\ 3.71\times10^{-5} \Delta q t_{peak} - 1.05\times10^{-6} \Delta q q_{build} - 3.50\times10^{-5} t_{peak} q_{build} + \\ 3.38\times10^{-8} q'_{down} q'_{up} \Delta q + 1.26\times10^{-6} q'_{down} q'_{up} t_{peak} + \\ 4.48\times10^{-9} q'_{down} q'_{up} q_{build} + 1.01\times10^{-6} q'_{down} \Delta q t_{peak} + \\ 5.67\times10^{-9} q'_{down} \Delta q q_{build} + 1.75\times10^{-7} q'_{down} t_{peak} q_{build} - \\ 3.89\times10^{-9} q'_{up} q_{base} q_{build} + 8.29\times10^{-7} q'_{up} \Delta q t_{peak} + \\ 4.79\times10^{-9} q'_{up} \Delta q q_{build} + 1.29\times10^{-7} q'_{up} t_{peak} q_{build} + \\ 8.75\times10^{-8} q_{base} t_{peak} q_{build} + 5.11\times10^{-8} \Delta q t_{peak} q_{build} - \\ 5.58\times10^{-9} q'_{down} q'_{up} \Delta q t_{peak} - 2.30\times10^{-11} q'_{down} q'_{up} \Delta q q_{build} - \\ 9.73\times10^{-10} q'_{down} q'_{up} t_{peak} q_{build} - 7.05\times10^{-10} q'_{down} \Delta q t_{peak} q_{build} - \\ 6.21\times10^{-10} q'_{up} \Delta q t_{peak} q_{build} + 4.08\times10^{-12} q'_{down} q'_{up} \Delta q t_{peak} q_{build} \end{array} \right) \quad (142)$$

Plots of each significant main effect in the model (evaluated at the mean values of the other factors) are shown in Figure 44 through Figure 49. The two significant two factor interaction terms are shown in Figure 50 and Figure 51. The higher interaction terms become difficult to visualize and are not graphed here.

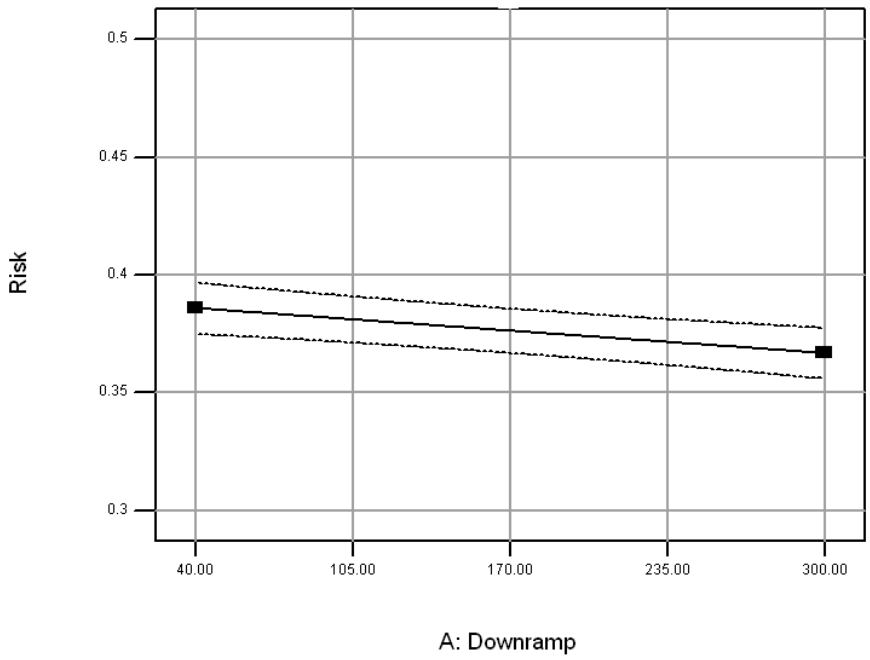

Figure 44. Reduced model A: Downramp (m^3/sec/hr) main effect

As shown in Figure 44 and Figure 45, one surprising result of the experiment is the downramp and upramp main effects. Current standards at the Glen Canyon Dam restrict the ramping rates in the interest of reducing risk of downstream slope failures. The model indicates, however, that increasing both upramp and downramp rates actually slightly reduce failure risk. This is likely a result of the two conflicting contributions of the rate: On the one hand, slow ramping rates provide time for the porewater pressures to equilibrate, thereby reducing instability caused from excessive porewater pressure. But slow ramping also increases the average stage height, raising the overall piezometric surface within the sandbar. The results indicate that it is the second factor that predominates. That is, the dissipation of excess porewater pressure over the relatively short time frame is not sufficient to compensate for the increased overall pressure within the sandbar. As will be shown later, however, it turns out

that the downramping rate adversely affects other flow aspects, resulting in a reverse effect as the released flow wave propagates downstream.

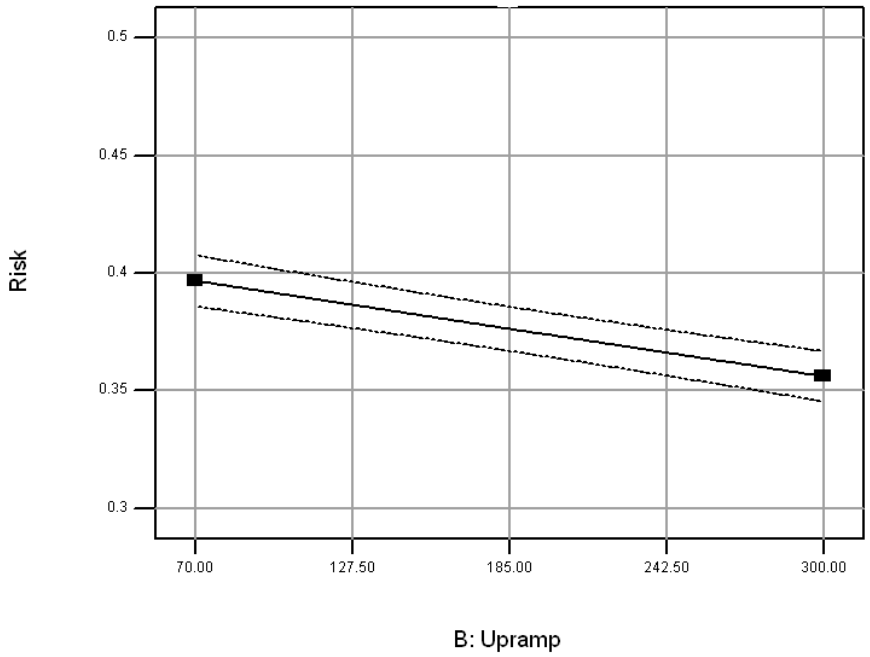

Figure 45. Reduced model B: Upramp (m^3/sec/hr) main effect

As seen in Figure 46, higher baseflows significantly increase slope failure risk, raising risk by approximately 10% when the base rate is increased from 100 to 300 m^3/sec. This is probably due to higher baseflows in turn causing higher pore pressures within the sandbar, as well as increasing adjacent water levels closer to the midpoint of the sandbar, a condition found to increase failure risk for cohesionless slopes (see Baker, 2005). This finding suggests that requiring a minimum baseflow (currently a requirement at Glen Canyon Dam) actually increases risk, rather than decreasing it.

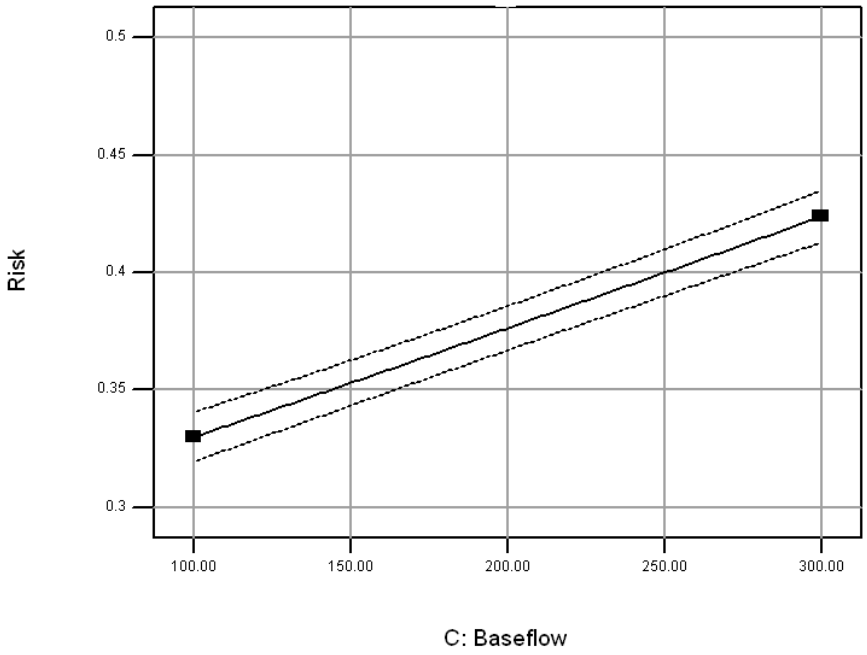

Figure 46. Reduced model C: Baseflow (m^3/sec) main effect

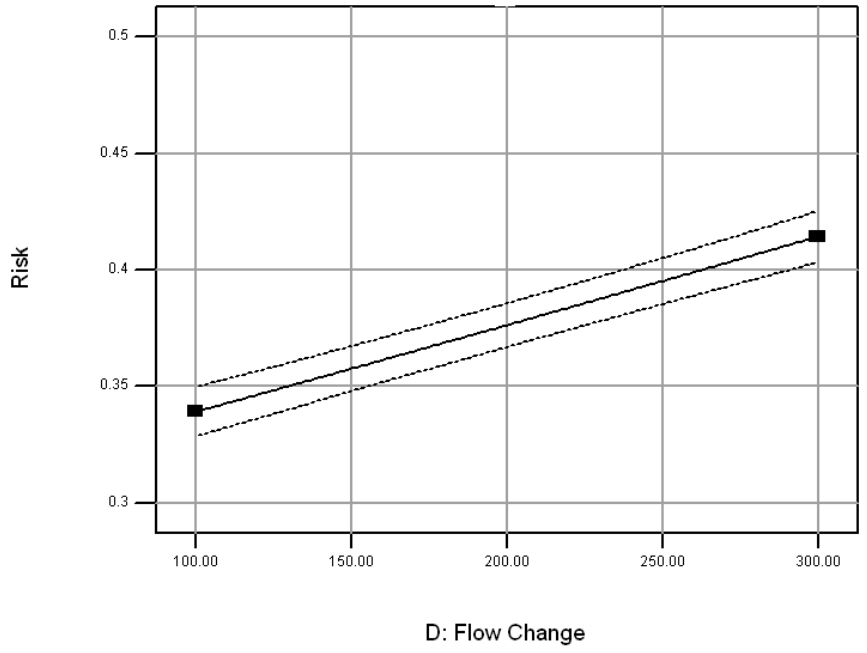

Figure 47. Reduced model D: Flow Change (m^3/sec) main effect

The implication of the downramp and baseflow effects is that it is the average groundwater level within the sandbars that drives failure potential. Thus, reducing the amount of time and extent of high flows would be expected to decrease failure risk. This observation is consistent with empirical observations such as those reported in Goodwin et al. (2000). As seen in Figure 47 and Figure 48, the flow rate change and peak hold times provided further support for this hypothesis.

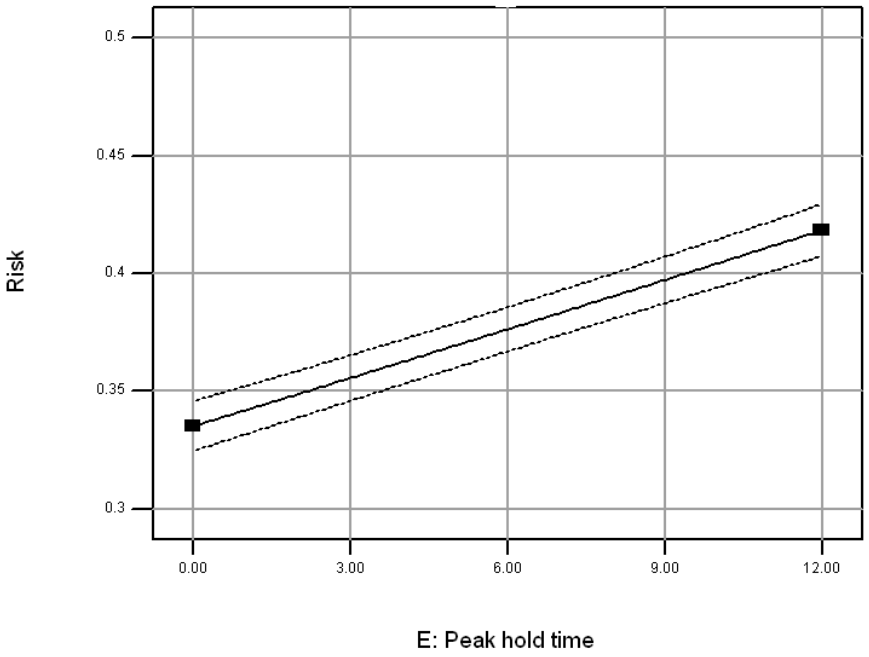

Figure 48. Reduced model E: Peak hold time (hr) main effect

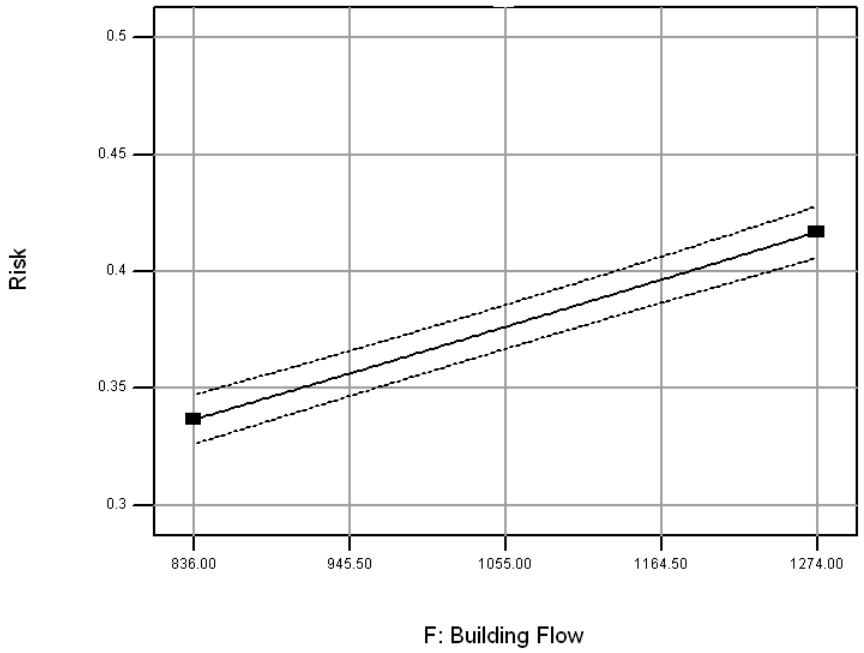

Figure 49. Reduced model F: Building flow (m^3/sec) main effect

Figure 49 shows that larger sandbars are at greater risk for failure than smaller sandbars. This effect is both statistically and numerically significant, with the smaller sandbars likely to experience failure 34% of the time versus a 42% risk of failure for the larger sandbars.

A prediction of 42% failure risk for large sandbars is consistent with field data. Kearley et al. (1994) reported that 33% of campsites had failed between 1965 and 1973. A naturally occurring flood rebuilt the sandbars in 1983, but by 1994, the overall number of sandbars had decreased by 48% (Kearsley et al., 1994). Kearsley et al. (1999) inventoried the rebuilt high elevation sandbars following the 1996 controlled flood and found that 44% of these failed after six months. The average of these three field reports is 42%, the same as predicted.

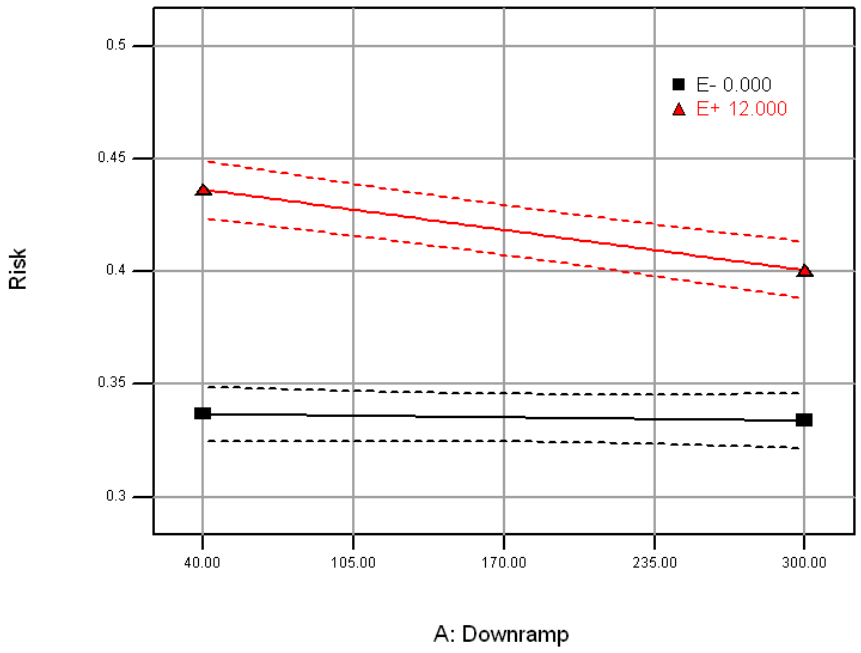

Figure 50. Reduced model A: Downramp (m^3/sec/hr) by E: Peak hold time (hr) interaction

As seen in Figure 50 and Figure 51, the interactions between peak hold time and the downramp rate and flow change are further indicators of the driving failure potential of high average piezometric surfaces. Specifically, a high downramping rate significantly lowers risk potential when the piezometric surface is getting dangerously high (from long peak hold times). Similarly, a large flow change also disproportionately increases risk for long peak hold times.

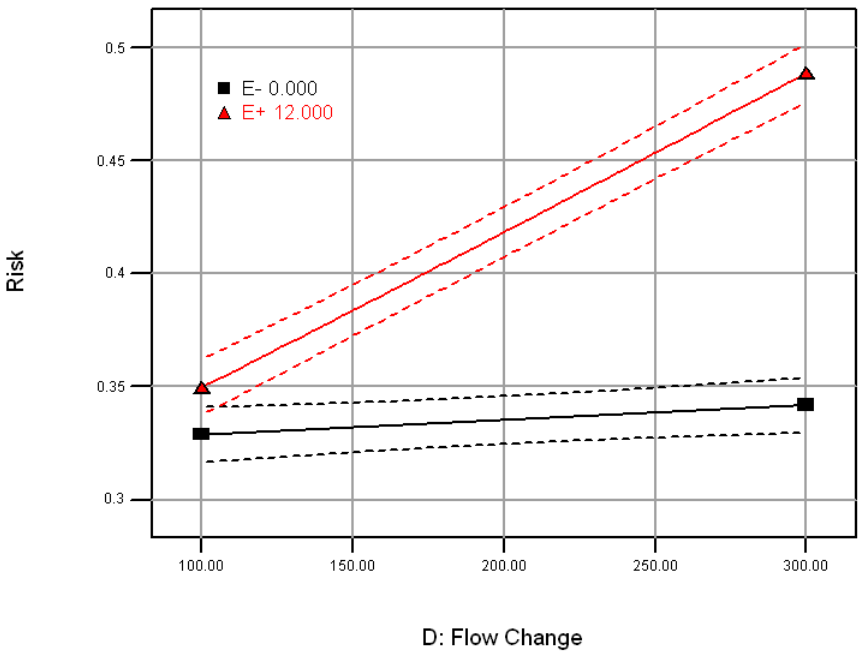

Figure 51. Reduced model D: Flow Change (m^3/sec/hr) by E: Peak hold time (hr) interaction

Attenuation effects

The flow release schedule at Glen Canyon Dam results in deep waves through the Colorado River. Flow attenuation and tributary inflows affect these waves, and thus all of the release parameters at the dam become only the initial condition for dynamically changing wave characteristics. With the overall aim to mitigate sandbar failures over an entire reach, these aspects must be considered.

Modeling unsteady conditions is non-trivial for any size river, and constitutes a large scale effort for the Colorado River. Building on numerous measurements reported in Griffin and Wiele (1996), Wiele and Smith (1996) developed a finite element model that successfully predicted flows within reasonable limits. Unfortunately, both computational and research constraints

prohibit integrating this model into the present effort, although this is suggested as a future application.

A simpler model was developed by direct consideration the latest USGS data (1/10 to 5/10) and the raw data reported in Griffin and Wiele (1996). The USGS data at three different gages were used. Their numbers and designations are: Gage 09380000 (Lees Ferry), 09402500 (Grand Canyon), and 09404200 (Diamond Creek). These gages are located at river kilometer stations (R_K) 0 km, 142 km, and 362 km respectively. 24 km, 166 km, and 386 km downstream of the dam, respectively. Note that because the standard river stationing on the Colorado defines Lees Ferry as zero, which is 24 km downstream of the dam, the actual distances downstream from the Glen Canyon Dam are 24 km, 166 km, and 386 km respectively. The reach of interest was chosen to start at the Glen Canyon Dam and extend all the way to Diamond Creek.

The Lees Ferry gage data was correlated with the Grand Canyon gage data (Figure 52), and the Grand Canyon gage data was correlated with the Diamond Creek data (Figure 53). The best correlation was chosen by successively calculating the R^2 regression factor between datasets for 150 increasing 15 minute intervals. As shown in Figure 54, the best correlation between the Lees Ferry gage and the Grand Canyon gage corresponded to an offset of 1,125 minutes (18 hours, 45 minutes). Likewise, the best correlation between the Grand Canyon gage and the Diamond Creek gage, shown in Figure corresponded to an offset of 1,500 minutes, or 25 hours.

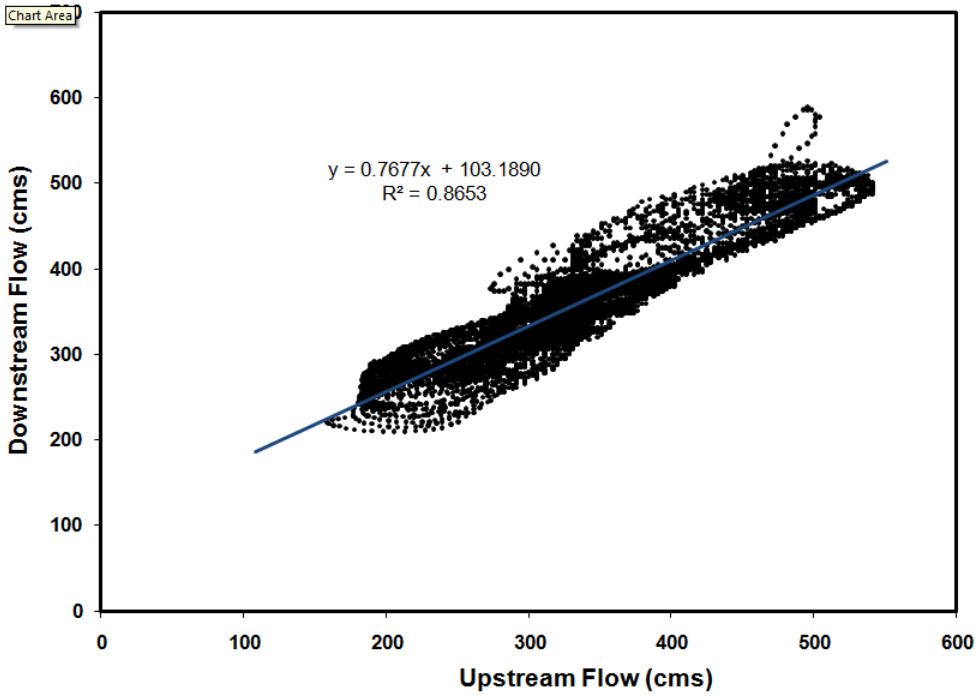

Figure 52. Correlation between upstream flow at Lees Ferry to downstream flow at the Grand Canyon gages (m^3/sec).

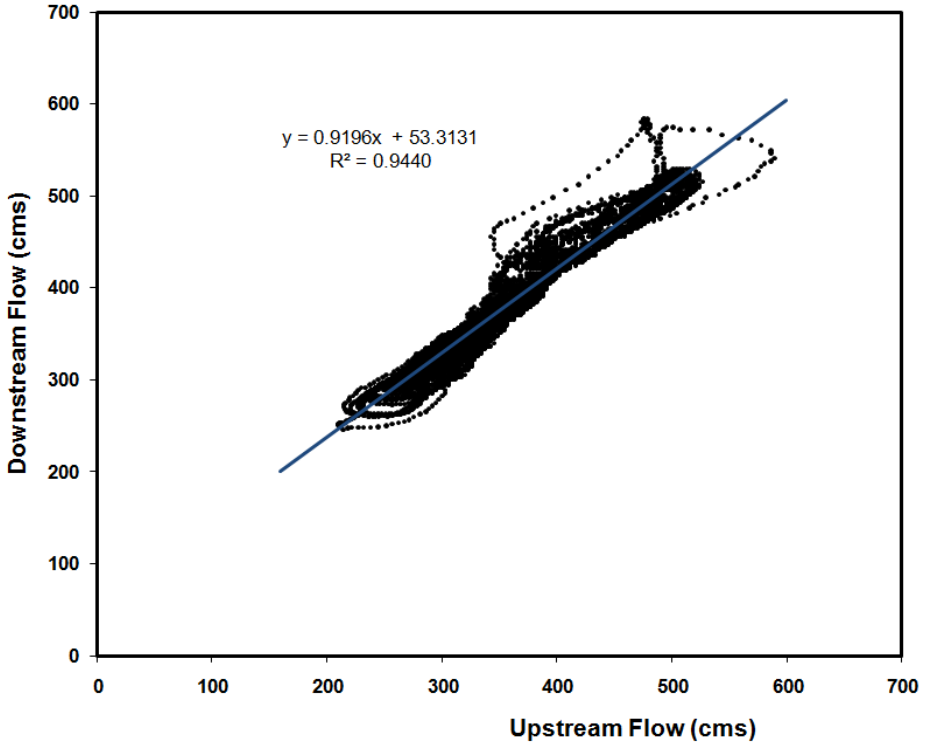

Figure 53. Correlation between upstream flow at the Grand Canyon gage to downstream flow at the Diamond Creek gage (m^3/sec)

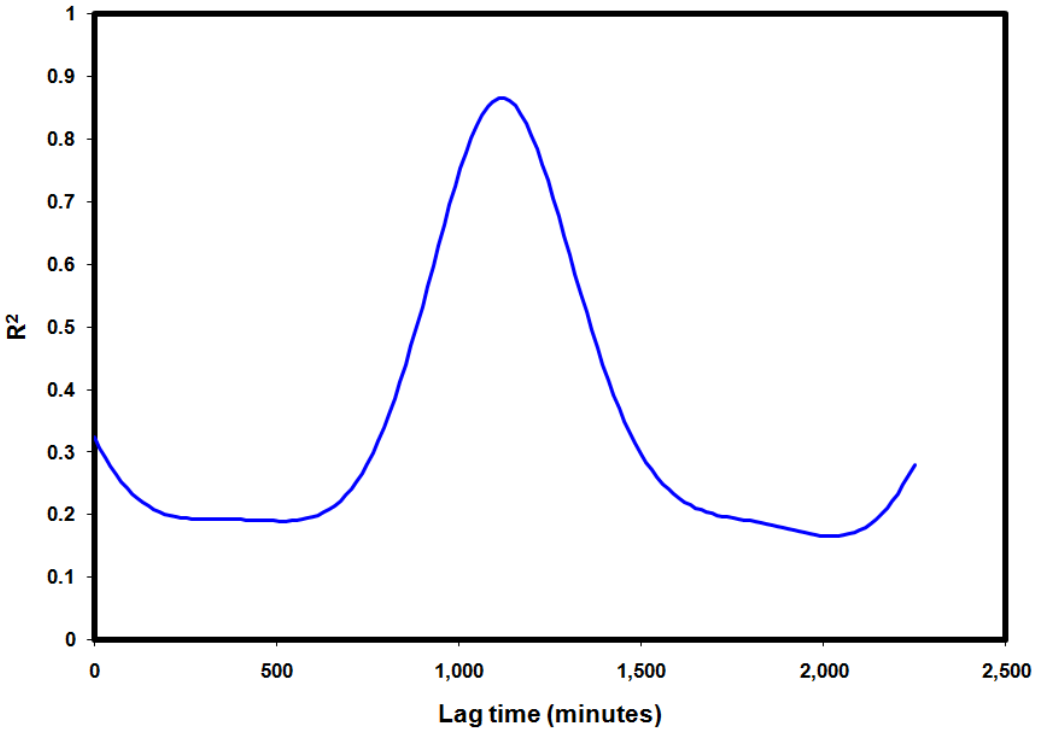

Figure 54. Regression coefficient versus lag time: Lees Ferry gage to Grand Canyon gage

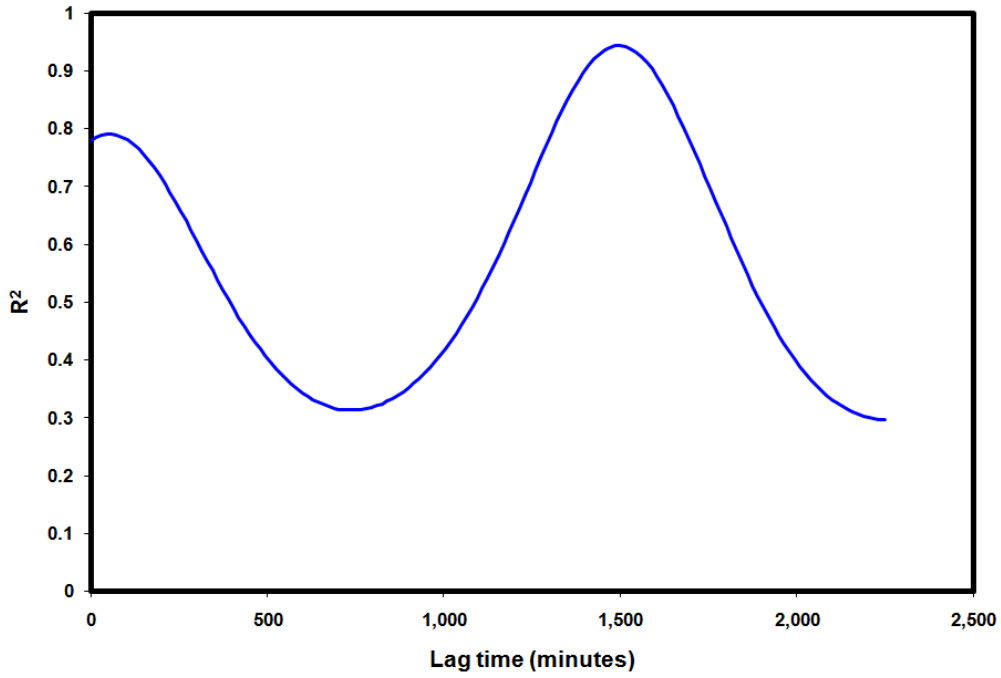

Figure 55. Regression coefficient versus lag time: Grand Canyon gage to Diamond Creek gage

Several important observations are evident from the correlations: 1. The correlations are significant, with R^2 values of 0.87 and 0.94, yet the highly curvilinear nature of the data is indicative of varying wave celebrities, and so this correlation must be considered only approximate; 2. As expected, attenuation is evident from the slope value of 0.77 and 0.92 for the upstream and downstream correlations. 2. On average a tributary inflow of 103 m^3/sec is expected within the upstream area of the reach and an average inflow of 53 m^3/sec within the downstream reach.

With the correlations established, the hydrographs themselves may be compared. Figure 56 and Figure 57 show the respective upstream and downstream reach hydrographs aligned by applying the estimated lag times (the dates shown correspond to the upstream hydrograph). Note the 24 hour and 7 day periodic stage fluctuations.

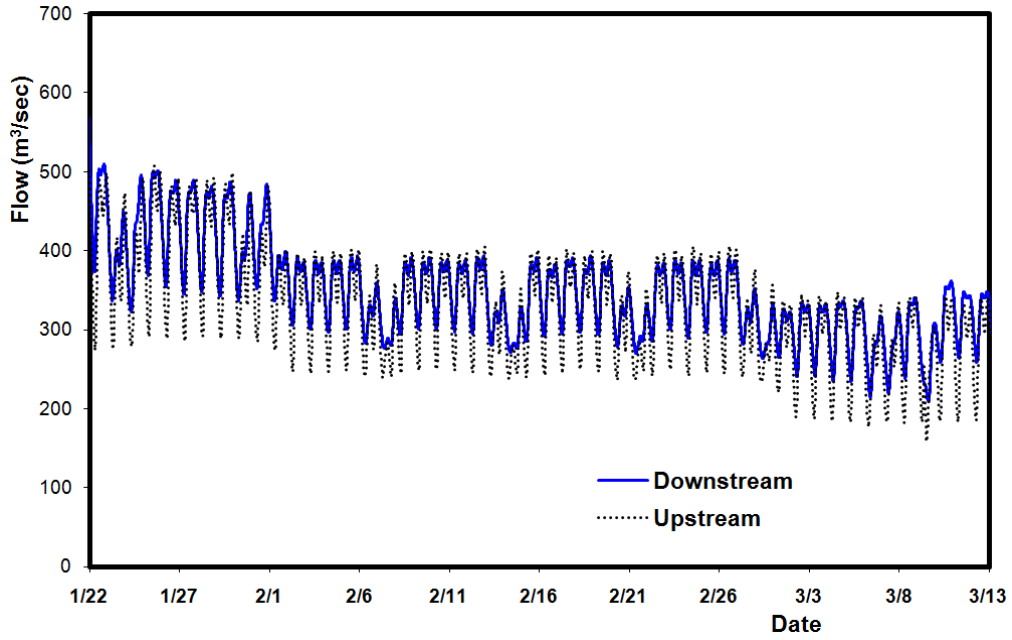

Figure 56. Hydrographs at Lees Ferry (upstream gage location) and at Grand Canyon (downstream gage location, offset by the computed lag time)

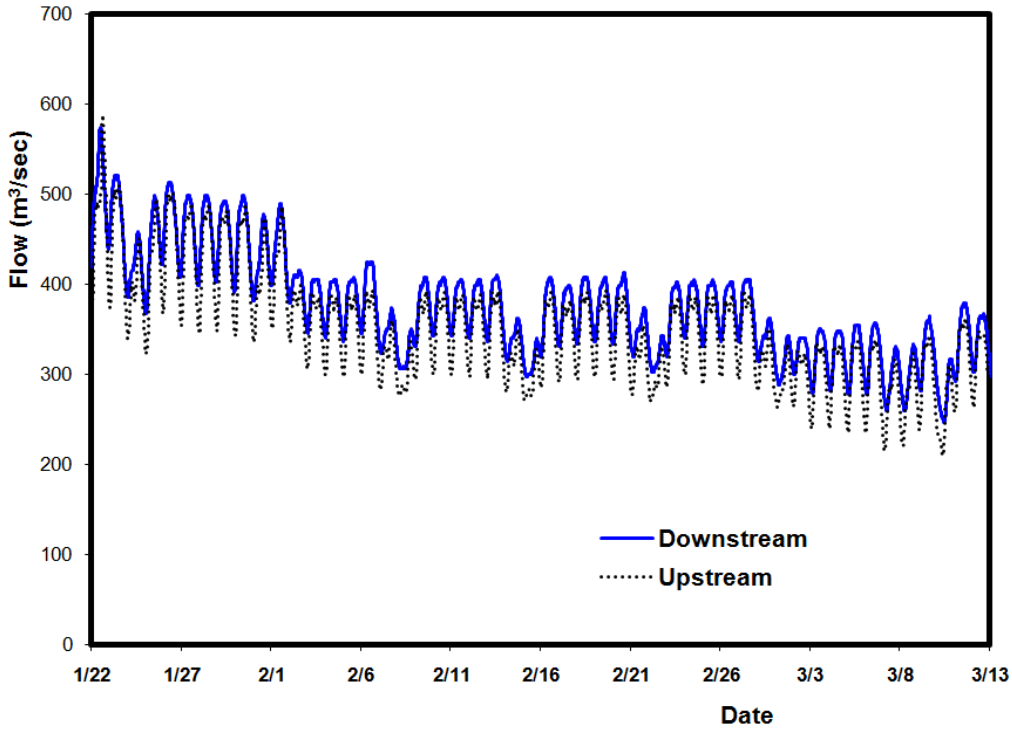

Figure 57. Hydrographs at Grand Canyon (upstream gage location) and at Diamond Creek (downstream gage location, offset by the computed lag time

It is evident from the hydrographs that: a) The general form of the outflows from the dam are preserved; b) The peak flows are nearly perfectly preserved throughout the reach; c) The minimum flow rises significantly throughout the reach, suggesting that the tributary inflows primarily affect the wave troughs; d) The upramp rates are essentially preserved; e) The downramp rates decrease slightly over the reach; and b) The peak flow hold times decrease over the reach.

These results are somewhat surprising. It was expected that both the peak and base flows would decrease downstream, and the tributary inflows would be minimal contributors. Here, the data is taken at face value, but there is a possibility that some of the gage differences might be due to mechanical problems or calibration. Later research will further investigate the observed gage differences.

A more detailed analysis was conducted using the reported data in Griffin and Wiele (1996). This data was particularly useful because it included the actual release parameters of the dam releases. Multiple, nonlinear regression was utilized to fit this data, using the USGS fits to define the outer limits. The regression terms were arranged so that the dam outflows were always returned at river kilometer -24 (e.g. RK = -24), as this corresponds to the dam location in the standard stationing system for the Colorado River, which locates the zero station at Lees Ferry.

The maximum change in flow as a function of river station (Δq_{RK}) was found to be related to the dam operation parameters by the equation

$$\Delta q_{RK} = \max\left\{0, \left[1 - 0.00085\left(q'_{up}\right)\left(q'_{down}\right)^{0.4}\left(R_K + 24\right)/386\right]\Delta q\right\} \qquad (143)$$

The fit between the measured and predicted Δq_{RK} is shown in Figure 58. The fit is good with a corresponding R^2 value of 0.96.

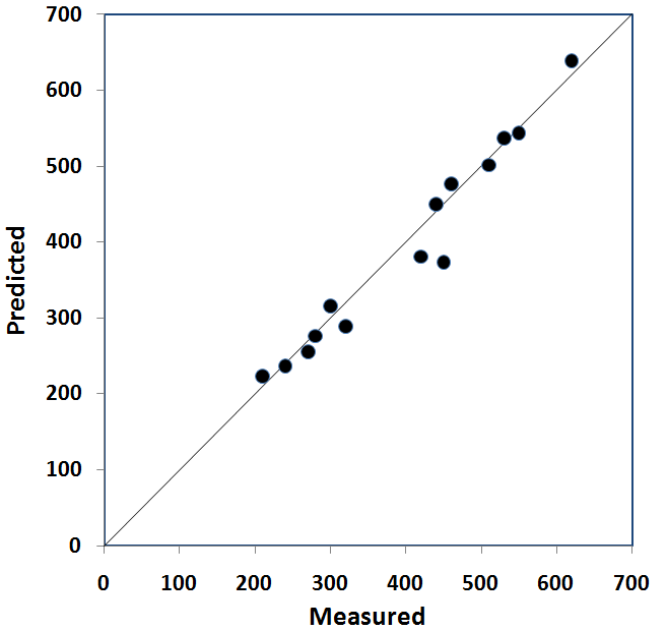

Figure 58. Agreement between predicted and measured maximum river kilometer flow changes (m^3/sec)

The relationship between the local downramp rate $q'_{RK,down}$ and the operations parameters is more complex, but good agreement ($R^2 = 0.87$) was found by regressing downstream downramp changes to the other terms in the form (see Figure).

$$q'_{RK,down} = \max\left\{q'_{down}/10,\ q'_{down} - 0.136 q'_{down} \ln\left[1 + \left(R_K + 24\right) q'_{down} / q_{\min}\right]\right\} \qquad (144)$$

Note that the minimum value of $q'_{RK,down}/10$ is somewhat arbitrary. It was set to insure positive nonzero values of the downramp, but was never needed in the subsequent modeling.

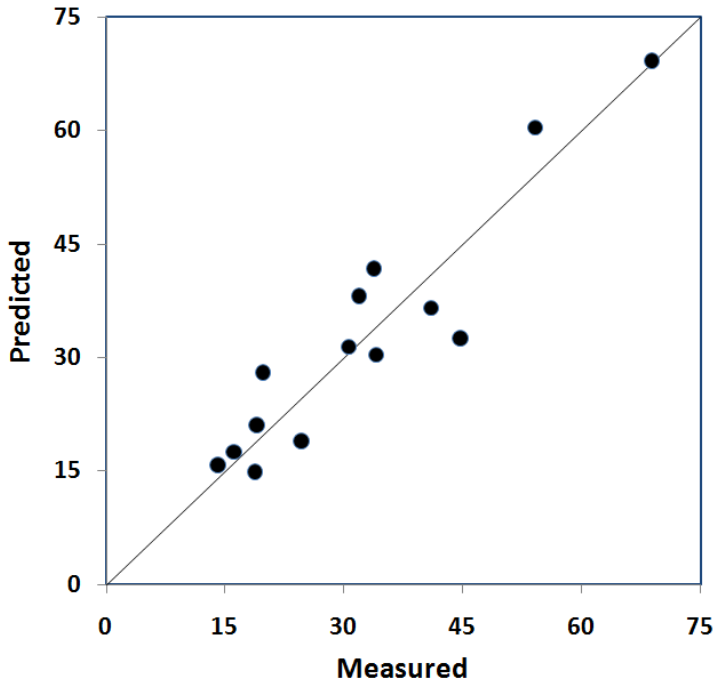

Figure 59. Agreement between predicted and measured maximum river kilometer downramping rates (m^3/sec/hr)

The regression equations developed from the USGS data suggest a strong relationship between $q_{RK,min}$ and the river station R_K. A linear fit between the two was found to be improved by a polynomial term of the downramp. The resulting equation was

$$q_{RK,\min} = \left[1 + (0.0003 q'^{\,2}_{down} - 0.02 q'_{down} + 0.2)(R_K + 24)/386\right] q_{\min} \qquad (145)$$

The fit between predicted and measured is shown in Figure 60. The fit is seen to be quite good, with a corresponding R^2 of 0.95.

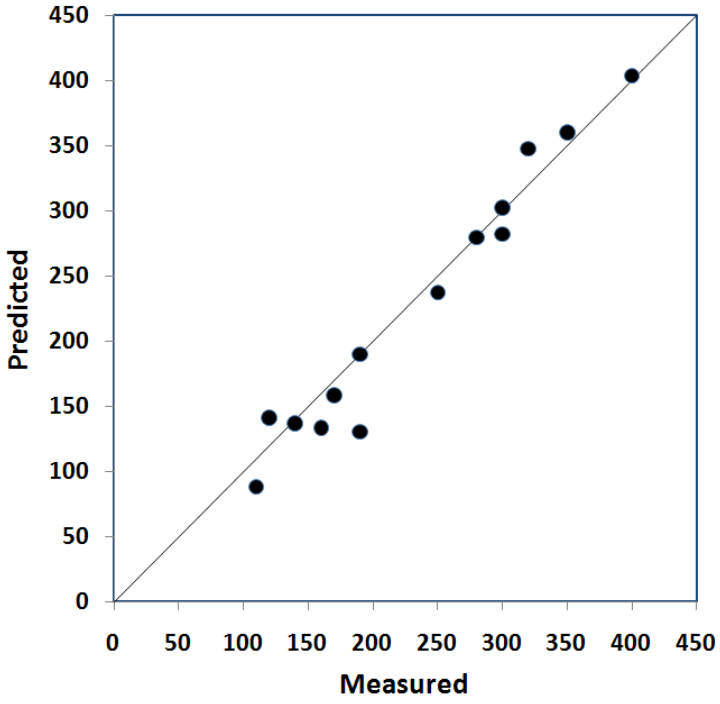

Figure 60. Agreement between predicted and measured maximum river kilometer minimum flows (m^3/sec)

The local peak hold time, $t_{RK,peak}$ was found to be adequate predicted by the following formula:

$$t_{RK,peak} = \left[\left(\frac{R_K + 24}{386} \right)^2 - 1.5 \left(\frac{R_K + 24}{386} \right) + 1 \right] t_{peak} \qquad (146)$$

The fit between measured and predicted values is shown in Figure 61. The corresponding R^2 value is 0.85.

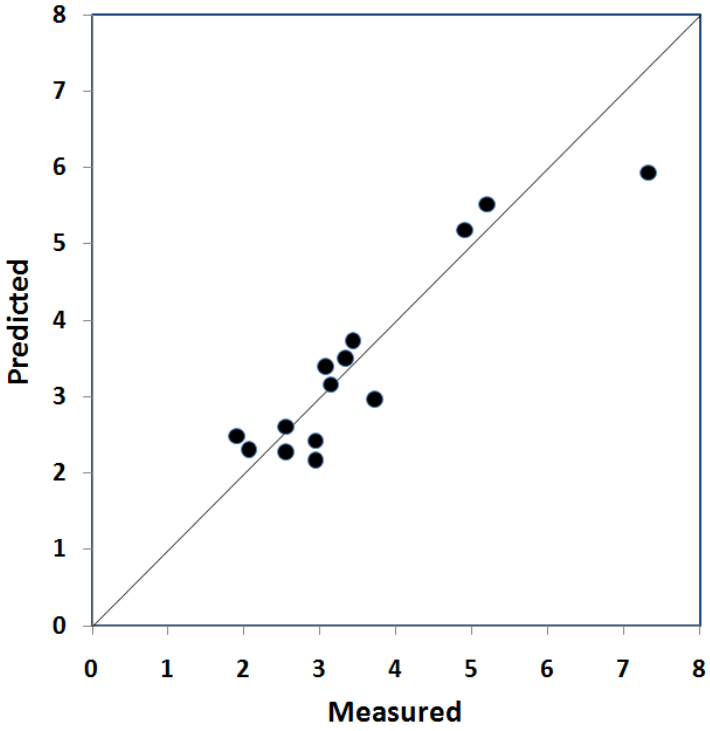

Figure 61. Agreement between predicted and measured maximum river kilometer peak hold time values (hr)

The last variable to be considered was the local upramp, $q'_{RK,upramp}$. Despite numerous attempts to correlate the local upramp to dam operation parameters by linear and nonlinear methods, no significant correlations could be made without introducing so many terms that the risk of overfitting became unacceptable. Thus, the best equation for $q'_{RK,upramp}$ was found to be simply

$$q'_{RK,up} = q'_{up} \tag{147}$$

Equation (147) has the dubious distinction of being the simplest equation in this research.

The attenuation processes have a profound effect on estimated risk. Figure 62 shows the downramp effects on risk for $t_{peak} = 9$ hr,

$q_{build} = 1050\ \text{m}^3/\text{sec}$, $q'_{up} = 71\ \text{m}^3/\text{sec/hr}$, $q_{base} = 227\ \text{m}^3/\text{sec}$, and $\Delta q = 227\ \text{m}^3/\text{sec}$. It is seen that for low downramp rates, the risk throughout the canyon remains nearly constant; whereas for high downramp rates, risk increases throughout the canyon, with bank failures almost assured when downramp rates near 200 m^3/sec/hr. This is consistent with the observed tendency for bank failures to increase downstream of Glen Canyon Dam (Dexter and Cluer, 1999). (It must be noted, however, that the attenuation effects of the downramp rates over 100 m^3/sec/hr are extrapolated from existing data, and therefore must be treated cautiously.)

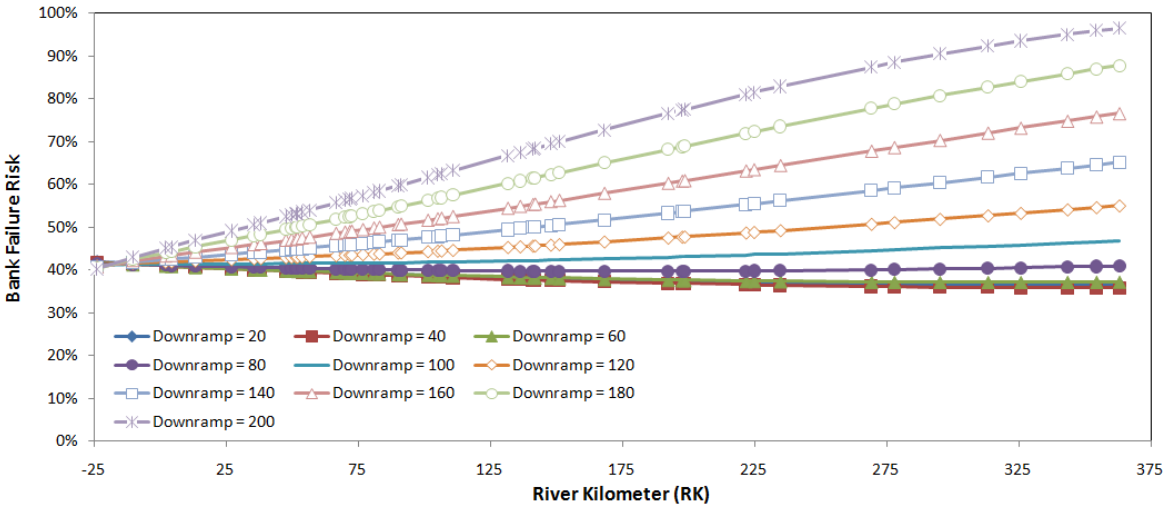

Figure 62. Bank failure risk throughout the Grand Canyon as a function of dam release downramp rates (m^3/sec/hr).

The model was further verified utilizing the Dexter and Cluer (1999) measurements of total sandbar area changes for a number of dynamic sandbars within the Grand Canyon. Interpreting their reported percentage changes as roughly equivalent to failure risk (e.g., a 20% area loss equates to a 20% failure

risk) allowed their measurements to be directly compared with the developed risk model.

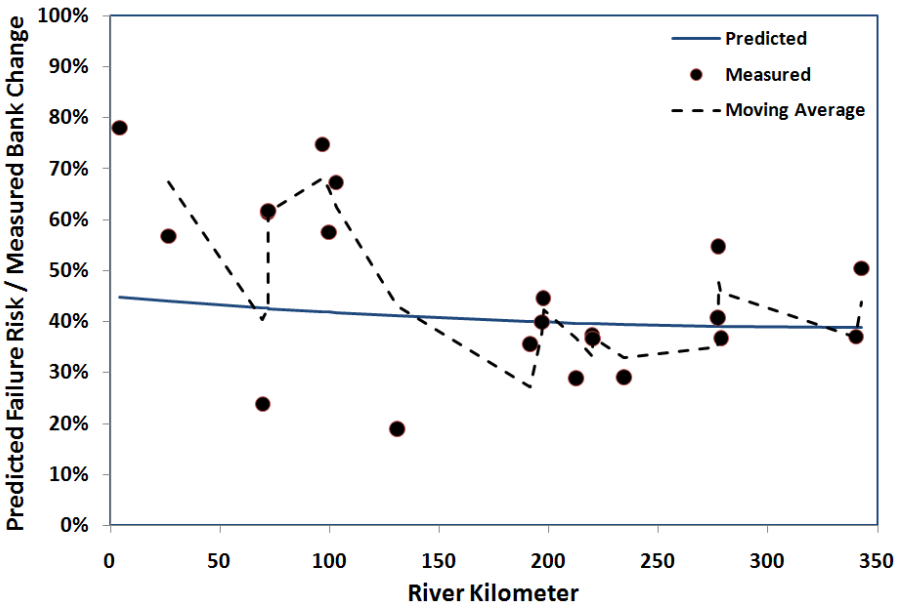

Figure 63. Measured and predicted slope failure risks per river kilometer

Figure 63 shows the results assuming the interim values noted above and a downramp rate of 43 m^3/sec/hr. The following observations may be made:

1. The running average of the data intersects the predicted bank risk curve in a number of places;
2. The theoretical risk curve captures the generally decreasing, convex nature of the data, but is less pronounced.
3. The reach averaged failure risks are the same (rounded to the nearest percent). Both the estimated and the measured overall risk are 41%.

With a riparian scale model developed, optimization of dam operations finally becomes possible. As will be seen, the underlying non-linearity of this model has a key role in determining the optimal flow research strategy.

CHAPTER 8. OPTIMIZING DAM OPERATIONS

> [Numerical] optimization…can be likened to a kangaroo searching for the top of Mount Everest…
>
> In simulated annealing, the kangaroo is drunk and hops around randomly for a long time. However, she gradually sobers up and the more sober she is, the more likely she is to hop up hill.
>
> – from "Neural Network Implementation in SAS Software"
> in *Proc. 19th Annual SAS Users Group Int. Conf. (1994)*
> by Warren S. Sarle

Introduction

Utilizing the general bank stability model developed in the previous chapters, the general optimization problem is seen to be minimizing the cost of mitigating downstream slope failures, subject to the constraints specific to physical limitations, water balance targets, environmental concerns, and others. The objective of this chapter is to develop an algorithm to achieve this optimization.

Harpman (1999) reports that Glen Canyon Dam operations are currently being optimized by a peak shaving algorithm. However, with the introduction of the new nonlinear constraint specific to mitigating downstream failure risk, simpler methods such as peak shaving or simplex are not sufficient.

Moreover, segmentation of the solution space can also prevent optimization by nonlinear methods, such as steepest gradient. For example, Brooke et al. (1996) reported convergence problems for a nonlinear model of hydropower system operations. These segmentation issues appear to complicate the present effort as well.

For example, an early attempt was made to optimize weekly dam operations for the Glen Canyon (the specific optimization parameters and

constraints will be described later in this chapter). Figure 64 shows the returned "optimal" solutions that minimize operations costs, generated by applying steepest gradient technique for different initial conditions generated by a single seed value. As seen in the graph, even the local optima were chaotic, and the global minimum (about 17%) was achieved only for two particular seed values. Simply put, there is not an obvious initial condition guaranteed to lie within the concave region of the global minimum.

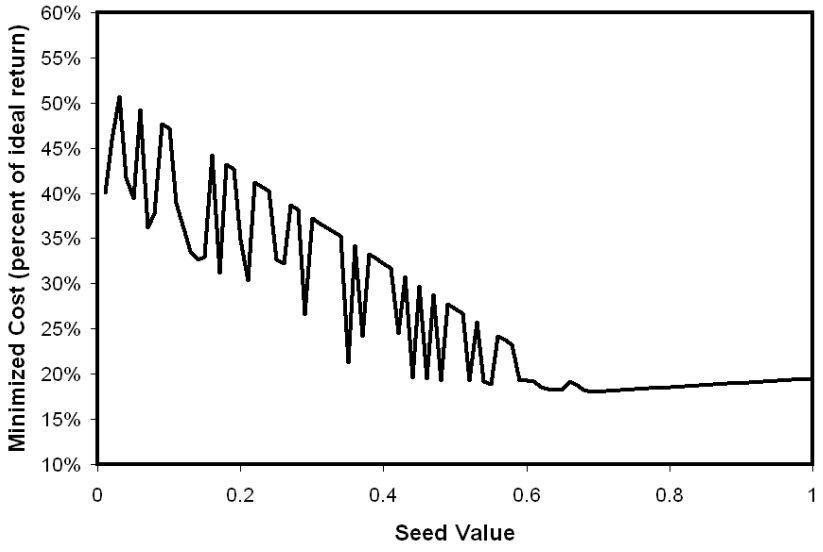

Figure 64. "Optimal" solutions vs. seed values found by gradient technique

With the failure of the standard techniques to achieve dependable results for even the preliminary model, *meta-heuristic* methods of optimization were considered. Meta-heuristics refers to methods that attempt to optimize a problem by iteratively improving candidate solutions based on a predetermined success score. Because this approach is so general, meta-heuristic solvers are simple to apply and easy to adjust for new constraints. The major drawback to the method is that global optimality is not assured (Teegavarapu and Simonovic, 2002).

Given the robust nature of meta-heuristics, the complexities of water systems in general, and the growing need to optimize water resources, it is not surprising that a number of meta-heuristic techniques have been developed for water resource applications. Popular meta-heuristic optimization methods include simulated annealing (Kirkpatrick et al.,1983); genetic algorithms (Goldberg, 1989); swarm intelligence (Beni and Wang,1989; and random search (Zhigljavsky, 1991), which includes ant colony, swarm, bees, and other swarm algorithms.

Simulated annealing (SA), the first published of the well known meta-heuristic optimization techniques, has been shown to be a successful method for optimizing non-linear systems with complex boundary conditions. SA has been applied for to optimize many areas of water resource engineering. Recent applications of SA have focused on water distribution networks (Cunha and Sousa, 1999; Cunha and Sousa, 2001; Geem, 2009); groundwater management (Dougherty and Marryott, 1991; Marryott et al., 1993); irrigation (Georgiou et al., 2006; Kuo et al., 2001); reservoir systems (Teegavarapu and Simonovic, 2002; Vasan and Raju, 2009); rainfall measurements (Pardo-Iguzquiza,1998); waste water systems (Zeferino et al., 2009, 2010); and storm water management (Avellaneda et al., 2009). For a detailed explanation of SA and heuristic methods in general, see Tialbi (2009).

Simulated annealing optimizes by analogy with physical annealing, a metallurgical process wherein a material is repeatedly heated and cooled. The success of annealing comes from heating exciting the energy states of the atoms

within the material, which allows them to settle in different positions resulting in a reduction of the overall material internal energy. The lower internal energy results in a material with greater ductility, fewer defects, and other desirable qualities. For the details of physical annealing, see Verhoeven (1975).

Once the *objective function* of the optimization goal has been defined, and the factors to be optimized have been established (the *state*), SA can be implemented by defining virtual annealing factors, starting with assigning a "temperature" to each state. The temperature gradually cools according to an *annealing schedule*, defined by a temperature function, usually denoted *temp*. Thus, *temp* returns temperatures that decrease with each iteration, but as in metallurgical annealing, these temperatures are always greater than zero.

The simulated annealing process begins with the selection of an initial suboptimal solution, denoted the *initial state*. A new state (the *candidate state*) is generated from the previous state by the *neighbor* function, this being a defined random process. State desirability is measured by a project specific *energy* function, defined in such a way that lower energies correspond to more optimal solutions.

In order to avoid local minima that are suboptimal over the entire search space, a project specific move probability function is established to randomly change the current *neighborhood* to other locations. A move to this new state is described as a *transition*, and the transition criteria are defined by an *acceptance probability function (*Pr_{accept}*)*. This Pr_{accept} function is in turn a function of the

temperature function (*temp*). Like *temp*, Pr_{accept} returns values that decrease with each iteration, but are always greater than zero.

Theoretically, the simulated annealing algorithm is a global optimization technique, but only if an infinite number of iterations are allowed. Unfortunately, infinite iteration tends to require too much computing time, and so the algorithm must be halted through defined *stopping criteria*. These criteria are often (but not always) specific to comparing transition energies and stopping the algorithm once a given change threshold is reached or when the allotted number of iterations or computing time is exhausted.

Thus, while global optimization is not assured, the algorithm's comprehensive treatment of the search space by through the Pr_{accept} and *neighbor* functions, limited only by the analyst defined *stopping criteria*, improves confidence that the returned state at least approaches the global optimum.

Problem *constraints* may be applied through one of two methods. The first and most desirable method is to limit search space through the neighbor function to only those states that meet the constraint requirements. Unfortunately, most problems that utilize simulated annealing are of sufficient complexity that this method is not feasible. The alternative method is to apply a *penalty* to the energy function, the magnitude of which can be selected accordingly.

The general structure of the SA algorithm is shown by pseudocode in Figure 65.

In summary, once the problem *state variable* has been defined, and *objective function* clearly presented, simulated annealing can be utilized for optimization, provided the following parameters and function are established:

- Constraints
- Initial state
- Search space
- Stopping criteria
- *neighbor* (neighbor state generation function)
- *energy* (state desirability function)
- *temp* (temperature function)
- $\mathrm{Pr}_{\mathrm{accept}}$ (acceptance probability function)
- *rand* (random number generator with range from 0 to 1)

select s	/ / initialize current state s
$e \leftarrow \mathbf{energy}(s)$	/ / initialize current energy e
$s_{opt} \leftarrow s; e_{opt} \leftarrow e$	/ / initialize optimal states s_{opt} & e_{opt}
$k \leftarrow 0$	/ / initialize counter k
while $k < k_{\max}$	/ / consider $k_{\max}$ trials...
$s_{test} \leftarrow \mathbf{neighbor}(s)$	/ / choose tested state s_{test} from neighbor function
$e_{test} \leftarrow \mathbf{energy}(s_{test})$	/ / calculate energy of test state
if $e_{test} < e_{opt}$ then	/ / if new state is better...
$s_{opt} \leftarrow s_{test}; e_{opt} \leftarrow e_{test}$	/ / ...then update optimal values
$\tau \leftarrow \mathbf{temp}(k, k_{\max})$	/ / calculate τ from temperature function
$p \leftarrow \mathbf{Pr}_{\mathbf{accept}}(e, e_{test}, \tau)$	/ / assign probability of moving p
if $p >$ **rand()** then	/ / if p is greater than a random value between 0 & 1
$s \leftarrow s_{test}; e \leftarrow e_{test}$	/ / ...then set current state and energy to test values
$i \leftarrow i + 1$	/ / next trial
return s_{opt}	/ / return best state found

Figure 65. General simulated annealing algorithm in pseudo-code

The following sections describe the mathematical definitions of these parameters and functions specific to the present research.

State Variable Definition

The state of the optimization process refers to the current values of the independent variables. Here, the state can be defined in terms of the general linear definition of the outflow function *q(t)*. A linear flow release regime is assumed for *q(t),* in keeping with typical dam operations. If need be, however, the linear flow release model is easily expanded to consider more complicated flow operations. Utilizing the notation introduced in Chapter 6, the linear flow assumption may be expressed

$$q_j(t) = q_{0,j} + q'_j t \tag{148}$$

where each timestep denoted with the integer subscript j. For a flow release schedule with J discrete timesteps, the state variable **S** is therefore a $2 \times J$ vector in the form

$$\mathbf{S} \equiv \begin{bmatrix} q_1 & q'_1 \\ q_2 & q'_2 \\ \vdots & \vdots \\ q_{J-1} & q'_{J-1} \\ q_J & q'_J \end{bmatrix} \tag{149}$$

where the "o" subscript is now eliminated for brevity.

At Glen Canyon Dam, it is policy that flows can be changed only once per hour, and the ramping rate is inferred from the flow change from one hour to the next. That is, the change from the flow at time *j* (q_j) to a higher flow at time *j+1*

(q_{0j+1}), must take place over one hour, or $q'_{up,j} = \left(q_{j+1} - q_j\right)/1\ hour = q_{j+1} - q_j$ where the units of the upramp are therefore in m^3/sec/hr, as previously defined. In general, then

$$q'_{down,j} = \max\left(0, q_j - q_{j+1}\right) \tag{150}$$

$$q'_{up,j} = \max\left(0, q_{j+1} - q_j\right) \tag{151}$$

and thus

$$q'_j = \operatorname{sgn}\left(q_{j+1} - q_j\right)\max\left(q'_{down},\, q'_{up}\right) \tag{152}$$

which is the unfortunately clumsy mathematical way to simply state that $q'_j = q'_{up}$ if flow is increasing, and $q'_j = -q'_{down}$ if flow is decreasing.

Equation (152) allows the state variable to be reduced to

$$\mathbf{S} = \begin{bmatrix} q_1 \\ q_2 \\ \vdots \\ q_{J-1} \\ q_J \end{bmatrix} \tag{153}$$

or simply

$$s_j = q_j \tag{154}$$

The remainder of the chapter expressing flow processes in terms of q_j, and optimization processes in terms of s_j, which should cause no difficulty if the equivalence noted in Equation (154) is always recalled.

The remaining task is to define the number timesteps J and the value of each timestep designated by j, henceforth denoted Δt_j (hr). Typically, discrete timesteps of 1 hour are considered over one week's time, and thus j would span

from 0 (hour 1) to 167 (168 hours in one week). Of course, smaller timeframes, such as one day, could be considered, as could long timeframes, say one month or even an entire year. The corresponding **Δt** vector is

$$\mathbf{\Delta t} \equiv \begin{bmatrix} \Delta t_1 \\ \Delta t_2 \\ \vdots \\ \Delta t_{J-1} \\ \Delta t_J \end{bmatrix} \tag{155}$$

The total volume release over time Δt_j is therefore $\not{V}_j$ (m^3) where

$$\not{V}_j = (3600)\Delta t_j S_j \tag{156}$$

and the total volume over all J is:

$$\not{V}_J = (3600)\sum_{j=1}^{J} \Delta t_j s_j \tag{157}$$

Defining the state variable with one hour timesteps is inefficient for Glen Canyon Dam. Algorithm efficiency can be improved by allowing the timesteps to vary in length. Like most hydroelectric dams, revenue at Glen Canyon dam depends on demand. As will be discussed further in the section on the *energy* function (page 219), for every day except Sunday, onpeak hours of operation (7 am to midnight) have revenue rates at values nearly 40% higher than offpeak hours (midnight to 7 am) (Sunday has only offpeak rates). Also changing over the course of the day is the minimum allowable flow rate, which changes from a low value between 7 pm to 7 am to a higher value from 7 am to 7 pm. Because the revenue rates vary cyclically over each week, the state variable was defined

for one week's time, with each day divided into three time segments: midnight to 7 am, 7 am to 7 pm, and 7 pm to midnight. Thus, for Glen Canyon Dam, J = 21.

With the computing power available, however, 21 state variables were too many for the optimal solution to converge within a reasonable time period. Therefore, the state vector was simplified by symmetry, thus assuming the same flow schedules on Mondays and Saturdays, Tuesdays and Fridays, and Wednesday and Thursdays. This effectively reduced the number of state variable terms to 12.

Objective Function

A number of objective functions could be defined for the present research. Dam operations could be optimized to minimize downstream bank failure risk or to maximize revenue. Here it is recognized that downstream bank failures have an associated cost due to the necessity of rebuilding them with repeated controlled floods, and that this cost can therefore be directly related to the downstream failure risk calculation. Moreover, policy restrictions on dam operations in order to minimize failure risk also incur a cost due to lost hydroelectric power revenue.

Thus, the objective function can be specified in terms of associated costs. Mathematically, the objective function is

$$\min\ C = C_{risk} + C_{flood} \tag{158}$$

where C(\$) is the annual cost resulting from C_{risk}(\$), the annual cost of minimizing downstream bank failure risk; and C_{flood}(\$), the annualized cost of implementing periodic building flows to rebuild failed banks.

Generally speaking, daily dam operations minimize downstream bank failure risk by limiting the flow release parameters on any particular day. As noted earlier, these flow release parameters are q_{min} (m^3/sec) and q_{max} (m^3/sec) (minimum and maximum allowable daily flowrate), $q'_{down,\max}$ (m^3/sec/hr) and $q'_{up,\max}$ (m^3/sec/hr) (maximum allowable daily downramp and upramp rates), and $\Delta q_{24\max}$ (m^3/sec) (maximum allowable flow change over the past 24 hours).

Therefore, C_{risk} is calculated by the lost revenue if operations had been optimized without imposing the above limitations. That is,

$$C_{risk} = R_{ideal} - R_{actual} \tag{159}$$

where R_{ideal}(\$) is the maximum yearly revenue that could be generated without addressing bank failure risk reduction, and R_{actual} (\$) is the actual yearly revenue.

As shown in Chapter 7, bank failure risk can be minimized, but not eliminated. Controlled floods are required to rebuild sandbars. These floods are costly, because they require additional outflow through spillways and intakes beyond the capacity of the turbines. It is useful to relate the cost of the building floods, C_{flood}, with sandbar rebuild target in the form

$$C_{flood} = c_{\$/\%} I_{rebuild} \tag{160}$$

where $c_{\$/\%}$ (\$ / %) is the cost to rebuild 1 percent of the overall sandbars, and $I_{rebuild}$ is the targeted rebuild percentage. For example, the 1996 controlled flood at Glen Canyon Dam rebuilt approximately $I_{rebuild} = 20\%$ of the sandbars. Harpman (1999) predicts that building floods will average approximately \$2

million dollars (in 1996 dollars). Thus, a reasonable estimate for $c_{\$/\%}$ in 1996 dollars is about $100 thousand dollars per percentage rebuild.

Note that it is assumed here and henceforth that the rebuild target can be met with the flooding budget given by Equation (160). For targets larger than 20%, this would probably require more frequent and longer building floods. Modeling these processes and developing these floods is an important and complex process but beyond the scope of this work.

The revenue over time J may be estimated by

$$R_{annual} = (52)(3600)\sum_{j=1}^{21} \tfrac{1}{2}\left(s_j + s_{j+1}\right)\Delta t_j r_j$$

or simply

$$R_{annual} = (93600)\sum_{j=1}^{21} \left(s_j + s_{j+1}\right)\Delta t_j r_j \tag{161}$$

where the r_j (\$ / m^3) vector is the conversion rate from flow volume to revenue over time segment j.

The objective function in the form of the above defined variables is

$$\min\ C = R_{ideal} - (93600)\sum_{j=1}^{21} \left(s_j + s_{j+1}\right)\Delta t_j r_j + c_{\$/\%} I_{rebuild} \tag{162}$$

Other costs include repair, maintenance, and personnel. Harpman (1999) reports that these costs are small compared to the costs already included, and so are not applied here, although they are easily included for other applications.

Finally, it is useful to note that a non-dimensional form of the net revenue R^*_{net} may be defined as

$$R^*_{net} \equiv \left(R_{annual} - c_{\$/\%}\overline{\Pr}_{failure}\right) / R_{ideal} \tag{163}$$

Constraints

The numerous constraints on flow scheduling at Glen Canyon Dam are a result of a wide range of contributing factors, including mechanical, hydrological, human, hydraulic, maintenance, safety, and others. The details and mathematical definition of these constraints are described in the following sub-sections.

Mechanical

Generally speaking, hydroelectric turbines have flow limitations and other mechanical limits that may be expressed in general form as

$$q_{\min,mech} \le q_j \le q_{\max,mech} \tag{164}$$

At Glen Canyon Dam, however, Harpman (1999) reports this is not a governing constraint for daily operations and is not considered further here. Of course, other applications of the algorithm developed here can include these constraints without undue difficulty.

Hydrological

Dam releases are ultimately governed by rainfall and snowmelt, and mature dams must eventually release all of the flows conveyed to it (e.g. "run of the river"). The general form of this hydrological constraint is

$$\sum_{time\ period} \forall_j = \forall_{i,target} \tag{165}$$

where $\forall_{i,target}$ (m^3) refers to a specific volume to be released over the particular time period. The subscript *i* has been included to differentiate requirements, since multiple, even overlapping, hydrological constraints can apply.

When real time targets are established, the volume targets can change very quickly, and control theory applies. While proper treatment of this subject is beyond the scope of the present application, it can be included in the general algorithm presented here without undue difficulty.

The general Glen Canyon Dam policy is to meet annual demands through predetermined monthly outflow targets (Harpman, 1999). Considering an average month, then this constraint is

$$\overline{V}_{21} = \overline{V}_{annual} / 52 \tag{166}$$

In practice, however, since volume is directly related to profit, the optimization process will converge to Equation (166) naturally in order to maximum profit, as long as the following inequality is met:

$$\overline{V}_{21} \leq \overline{V}_{annual} / 52 \tag{167}$$

Equation (167) was utilized as the volume constraint here.

Conveyance

Conveyance over spillways is affected by frictional loss and cavitation potential. Unfortunately, the use of dam spillways is an essential part of a real-time control scheme, and must be used for controlled floods in particular. This can be a particular problem for older dams, because surface roughness increases over time (Williams and Hazen, 1933). Indeed, Glen Canyon Dam suffered nearly catastrophic cavitation damage in 1983 (Frizell, 1985). Since then, methods of predicting and preventing cavitation in older dams have improved (Lee and Hoopes, 1996), as has roughness modeling, with newer methods gradually replacing older methods (Travis and Mays, 2007).

Generally speaking, cavitation occurs when velocities become excessive along the emergency spillways. The corresponding constraint is

$$q_j \leq q_{cav} \tag{168}$$

where q_{cav} refers to the estimated flowrate at which cavitation is expected.

After the 1983 damage, the Glen Canyon Dam hydroelectric components have been updated to prevent further cavitation damage. At present, other operation thresholds prevail over cavitation prevention constraints (Frizell, 1985).

Vortex Formation

Vortices reduce flow efficiency, introduce occluded air, can clog the intake, and constitute a genuine risk to public safety (Rindels & Gulliver, 1983). Preventing vortices can constrain flowrates. Travis and Mays (2010) have developed general risk guidelines.

The vortex constraint depends on a chosen risk of vortex formation r_{vortex}. The vortex constraint then takes the form

$$q_{\min,vortex,i}\left(r_{vortex}\right) \leq q_j \leq q_{\max,vortex,i}\left(r_{vortex}\right) \tag{169}$$

where $q_{min,vortex,i}$ and $q_{max,vortex,i}$ are the low and high thresholds for the flow rates, beyond which the risk of vortex formation exceeds r_{vortex}. The subscript i is included because there are often disparate flowrate regions that are relatively safe from vortex formation.

While once a critical aspect of Glen Canyon operations, vortex problems have since been eliminated by improvements at the intakes, and vortex formation no longer limits operations (Vermeyan, 1999).

Operations

Operational limitations may be a result of available staff, use of automated equipment, maintenance, or others. Some dams are monitored 24 hours a day and operate year round while others may only operate during certain seasons. Automated equipment is becoming more popular, and brings with it specific limitations as a result of its particular design. These limitations can affect all aspects of the operations schedule.

In general form, most operational constraints can be defined by

$$q'_{down,j} \le q'_{down,oper,j} \tag{170}$$

$$q'_{up,j} \le q'_{up,oper,j} \tag{171}$$

$$q_{\min,oper,j} \le q_j \le q_{\max,oper,j} \tag{172}$$

Note that Equation (170) is specific to a positive definition of the allowable downramp rates, consistent with how policy is usually stated (e.g., a downramping maximum rate of 71 m^3/sec/hr is specified, rather than -71 m^3/sec/hr).

Other, less common, operational constraints can also be adopted here as well (maximum peak or minimum flow hold times, etc.) At Glen Canyon Dam, the only operational constraint is the policy that flowrates can be changed only once per hour. For example, an increase of the daily flow to the evening flow on Sunday, q_2 to q_3, must take place over one hour, or $q'_{up,2} = (q_3 - q_2)/1\ hour = q_3 - q_2$ where the units of the upramp are in m^3/sec/hr,

as previously defined. The ramping rates may therefore be defined by

$$q'_{down,j} = \max\left(0, q_j - q_{j+1}\right) \tag{173}$$

$$q'_{up,j} = \max\left(0, q_{j+1} - q_j\right) \tag{174}$$

Of course, if $j = 21$, then $j+1$ actually refers to $j = 1$. That is, the next time period after Saturday from 7 p.m. to 12 a.m is simply Sunday from 12 a.m. to 7 a.m. This could be expressed through multiple versions of the constraints, but this is cumbersome and not necessary from a pragmatic standpoint where the periodic nature of the weekly times is rather obvious. It is henceforth assumed that this incremental structure is understood.

Given the flexible nature of the state variable, it is possible to have two consecutively larger or smaller flows in the same day. When this occurs, it is not obvious which downramp or upramp value to use in the risk calculation. The research in previous chapters indicates that risk is maximized when upramping is minimized and downramping is maximized (the latter a result of the attenuation processes). Therefore, the risk equation used the daily minimum upramp and daily maximum downramps for the calculation (conservative).

Environmental

Supporting existing downstream and upstream habitats can lead to a number of constraints, including minimum and maximum allowable flows and flow changes on different days, weeks, months, and even seasons. Utilizing an "env" subscript to denote that the constraints are environmentally based, the

general form of the constraints are

$$q'_{down,j} \le q'_{down,env,j} \tag{175}$$

$$q'_{up,j} \le q'_{up,env,j} \tag{176}$$

$$q_{\min,env,j} \le q_j \le q_{\max,env,j} \tag{177}$$

Environmental concerns can also result in more complicated operations constraints. For example, it is not uncommon for flowrates and ramping rates to be constrained by recent history. Because of the wide variety of forms these constraints can take, a general formulation of the constraint limits is not possible, although the following discussion of the Glen Canyon Dam operations provides an example of one such constraint.

The environmental constraints at Glen Canyon Dam are shown in Table 15.

Min. Flow (m^3/s)	Max Flow (m^3/s)	Max 24 hr Flow Fluctuation (m^3/s-day)
227 (7am – 7pm) 142 (7pm – 7am)	566	142 – 227 (varies per month)

Table 15. Current Glen Canyon Dam environmental constraints.

The minimum and maximum flow constraints shown in Table 15 are consistent with Equation (177) and may be expressed

$$q_{\min,env,j} \le q_j \le q_{\max,env} \tag{178}$$

$$q_{\min,env,j} \le q_j \le q_{\max,env} \tag{179}$$

The fluctuation constraint is more complicated. Letting the subscript *m* denote the particular month, the maximum 24 hour fluctuation is designated

$\Delta q_{24\max,m}$ and the average requirement per month is defined $\overline{\Delta q}_{24\max}$. The fluctuation constraint at Glen Canyon Dam is therefore

$$\max\left(q_j, q_{j+1}, q_{j+2}\right) - \min\left(q_j, q_{j+1}, q_{j+2}\right) \le \overline{\Delta q}_{24\max} \tag{180}$$

Geomorphologic

Geomorphologic constraints attempt to control sediment transport, limit bank migration, and, as focused on here, minimize bank failure risk. At most dams and at Glen Canyon Dam in particular, these constraints are implemented as limitations on downramping and upramping in the general form

$$q'_{down,j} \le q'_{down,geo,j} \tag{181}$$

$$q'_{up,j} \le q'_{up,geo,j} \tag{182}$$

From Equations (173) and (174), these constraints may be written

$$\max\left(0, q_j - q_{j+1}\right) \le q'_{down,geo,j} \tag{183}$$

$$\max\left(0, q_{j+1} - q_j\right) \le q'_{up,geo,j} \tag{184}$$

Noting that if the maximum value of the parenthetical values is zero, the geomorphologic constraints are automatically met leads to a simpler form of Equations (183) and (184):

$$-q'_{down,geo,j} \le q_{j+1,d} - q_{j,d} \le q'_{up,geo,j} \tag{185}$$

As noted earlier, a critical geomorphologic constraint is mitigating sediment loss and slope failures. This constraint is

$$I_{rebuild} = \overline{\Pr}_{failure}\left(\mathbf{S}\right) \tag{186}$$

where the bar over $Pr_{failure}$ indicates that it is an average over both the river reach of concern and the operations timeframe considered. Equation (186) assumes that the percent rebuild would be equivalent to expected sandbar loss when many sandbars are considered over long periods of time.

Non-negative

Typical for optimization studies, all parameters have been defined in such a way that realistic values must be greater than zero.

Overall

Overall, the general form of the linear operations constraints require

$$q'_{down,j} \le q'_{down,\max} \tag{187}$$

$$q'_{up,j} \le q'_{up,\max} \tag{188}$$

$$q_{\min,j} \le q_j \le q_{\max,j} \tag{189}$$

where

$$q'_{down,\max} = \min\left(q'_{down,oper,j}, q'_{down,env,j}, q'_{down,geo,j}\right) \tag{190}$$

$$q'_{up,\max} = \min\left(q'_{up,oper,j}, q'_{up,env,j}, q'_{up,geo,j}\right) \tag{191}$$

$$q_{\min,j} = \max\left(q_{\min,mech}, q_{\min,env,j}, q_{\min,oper,j}, q_{\min,vortex,i}\right) \tag{192}$$

$$q_{\max,j} = \min\left(q_{\max,mech}, q_{cav}, q_{\max,env,j}, q_{\max,oper,j}, q_{\max,vortex,i}\right) \tag{193}$$

$$\sum_{time\ period} \overline{q}_{i,j}\left(t_{i,j+1} - t_{i,j}\right) = \cancel{V}_{i,target} \tag{194}$$

The particular constraints that govern current Glen Canyon operations are

$$-q'_{down,geo} \le q_{j+1} - q_j \le q'_{up,geo} \tag{195}$$

$$q_{\min,env,j} \le q_j \le q_{\max,env} \tag{196}$$

$$\cancel{V}_{21} \le \cancel{V}_{annual} / 52 \tag{197}$$

$$\max\left(q_j, q_{j+1}, q_{j+2}\right) - \min\left(q_j, q_{j+1}, q_{j+2}\right) \le \overline{\Delta q}_{24\max} \tag{198}$$

$$I_{rebuild} = \overline{\Pr}_{failure}\left(\mathbf{S}\right) \tag{199}$$

Of course, all parameters must also be non-negative.

The goal of the optimization here was to evaluate the potential advantages of eliminating the geomorphology constraints, and so Equation (195), included here for completeness, was not further considered except for comparison of the final results.

Initial state

The initial state was chosen rather arbitrarily as $q_j = 450$ m^3/sec, an average value that initially satisfied all constraints. The failure risk from this value is 48% and the non-dimensional net revenue was $R^*_{net} = 83\%$.

Search Space

The initial search space is defined by Equation (196). As the simulation proceeds, this search space is gradually limited according to the current iteration. This process is best described by the neighbor function (see below).

Stopping Criteria

Figure 66 shows the results of a preliminary optimization run with 100,000 iterations. The moves are seen to be logarithmically related to the iteration number and were still increasing near iteration 100,000. Execution time was still quite reasonable for this run (approximately 4 minutes), and so stopping criteria for the major effort were set to 10,000,000 iterations.

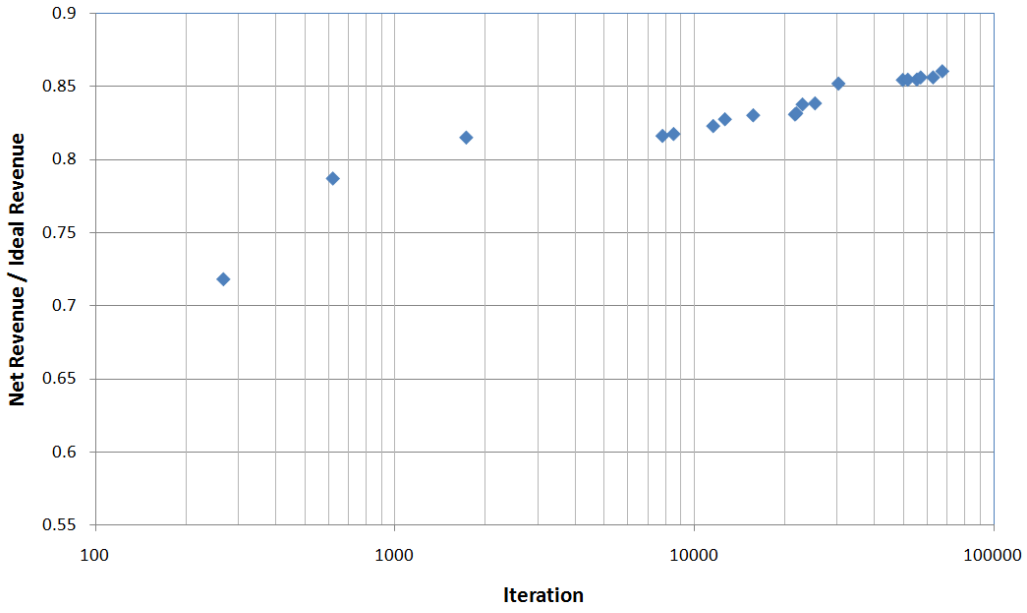

Figure 66. Preliminary SA results showing net revenue vs. iteration number

Neighbor function

The neighbor function returns the next tested state given the current state and search space. Numerous methods can be used for the neighbor function. Here, a simple linear approach was taken, wherein each new state was generated

randomly within a progressively smaller search space. This process is shown in Equation (200)

$$s_{test} = \begin{cases} s_{opt} - \left(s_{opt} - s_{\min}\right)\left(1 - k / k_{\max}\right) \text{ rand}_2(), & \text{rand}_1() \le 1 \\ s_{opt} + \left(s_{\max} - s_{opt}\right)\left(1 - k / k_{\max}\right) \text{ rand}_2(), & \text{rand}_1() > 1 \end{cases} \quad (200)$$

where the subscript on the rand() function is used to indicate that they are separately generated random numbers.

Energy function

The *energy* function was equated to the cost function with the addition of the two penalty terms: $C_{\Delta q}$ and $C_{\not V}$, corresponding to the maximum 24 hour change constraint and the target outflow constraint respectively.

The first constraint was enforced by a penalty function in the form

$$C_{\Delta q} = \Phi\left(\max\left(q_j, q_{j+1}, q_{j+2}\right) - \min\left(q_j, q_{j+1}, q_{j+2}\right) - \overline{\Delta q}_{24\max}\right) C_{\Delta q\, penalty} \quad (201)$$

where Φ is the stepwise function (returns 1 for arguments ≥ 0, otherwise returns 0) and $C_{\Delta q\, penalty} \gg \max\left(C_{risk}, C_{flood}\right)$.

The neighbor function is also restricted by constraint (197). Again, the penalty function may be imposed to meet this constraint, in the form

$$C_{\not V} = \Phi\left(\not V_{21} - \not V_{annual} / 52\right) C_{\not V penalty} \quad (202)$$

where $C_{\not V penalty} \gg \max\left(C_{risk}, C_{flood}\right)$

Designating *e* as the energy return variable, the *energy* function is therefore

$$e = c_{\$/\%}\overline{\Pr}_{failure} + C_{\Delta q} + C_{\not\perp} + R_{ideal} - R_{actual} \tag{203}$$

Temperature function

The *temp* function, which is assigned to variable τ (non-dimensional) in the present work, is analogous to the role of temperature in annealing, is an arbitrary function of iteration step. The only restriction is that $0 < \tau < 1$ and that it decline towards zero as the simulation progresses. Here, the *temp* function was implemented utilizing the selected maximum number of iterations (k_{max}) in the form

$$\tau = 1 - k / k_{\max} \tag{204}$$

Probability acceptance function

The $\Pr_{accept}$ function generates a probability that, if greater than a randomly generated number between 0 and 1, indicates that a new, non-local state (s_{test} with corresponding energy e_{test}) will be tested in the next iteration step. Here, the $\Pr_{accept}$ function was implemented in standard form as

$$\Pr_{accept} = \min\left(1, \exp\left(-\left(e_{test} - e\right)/\tau\right)\right) \tag{205}$$

Rand Function

Excel's random number generator, rand(), was utilized for the rand function. While Excel's random number generator has been criticized as poorly performing (McCullough and Wilson, 2005), the nature of simulated annealing

and the inherent uncertainties of the process did not warrant application of a more sophisticated method.

Input

The constraint values for the optimization run are shown in Table 16. Note that the inherent uncertainty of the variables did not warrant precision greater than about 2 significant digits, and so all variables were adjusted accordingly. Average 1996 values were used for the monthly target volume (1179 million m^3, rounded to 1,200 million m^3) and the corresponding maximum allowable flow change was Δq_{max} = 227 m^3/sec (rounded to 230 m^3/sec). In keeping with the interim criteria, the minimum allowable daily and nightly flows were assumed to be 140 m^3/sec and 230 m^3/sec respectively. The maximum flow assumed to be 570 m^3/sec. An average sandbar building flow of 1050 m^3/sec was assumed.

Harpman (1999) reported an average on-peak energy conversion rate of about $20 per megawatt-hr, equivalent to about $0.60 per m^3 flow. Offpeak rates averaged about $5 dollars less, so the off-peak energy conversion rate was assumed to be $15 per megawatt-hr.

The ideal monthly revenue would be generated if the entire monthly outflow was released during peak hours, or about $7.2 million per month. Harpman (1999) further reported that interim criteria have resulted in a revenue decrease of 6.5% over pre-interim revenue. Assuming the pre-interim revenue was near ideal, and assuming one $2 million building flood every four years, the present monthly revenue is estimated at about $6.2 million.

Table 16 summarizes the input values.

Variable	Value
Building flood success rate:	20%
Building flood unit cost:	$2 million
Maximum allowed 24 hour flow change:	230 m^3/sec
On peak pricing:	$20 / MW-hr
Off peak pricing:	$15 / MW-hr
Building flow:	1050 m^3/sec
Monthly target outflow:	1,200 million m^3
Daily minimum allowable flow:	140 m^3/sec
Nightly minimum allowable flow:	230 m^3/sec
Maximum allowable flow:	570 m^3/sec
Ideal monthly revenue:	$7.20 million
Current average monthly revenue:	$6.20 million
Iterations:	10 million

Table 16. Glen Canyon Dam optimization parameters

Execution

The SA model took just over 6 hours to execute 10 million iterations. Fifteen successively better state vectors were calculated. The relationship between iteration and non-dimensional revenue is shown in Figure 67.

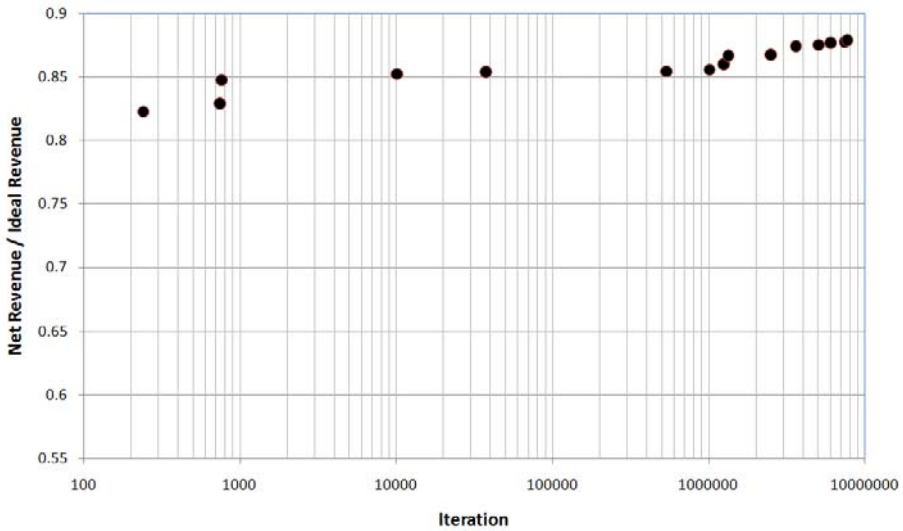

Figure 67. Non-dimensional revenue versus iteration

Results

The resulting optimized schedule is shown in Figure 68. There are several aspects of the optimal returned schedule that are non-intuitive (at least to the author):

1. Neither the maximum allowable flow (570 m^3/sec) or the minimum allowable flows (140 m^3/sec and 230 m^3/sec) were scheduled for any day.
2. The peak flow was not maintained over all of the peak hours, and instead slightly lowered from 7 p.m. to midnight.
3. Sunday's schedule was reversed from normal. That is, the daily flow was scheduled as lower than the nightly flow.
4. The Tuesday and Friday peak flows were lower than the Wednesday and Thursday peak flows.

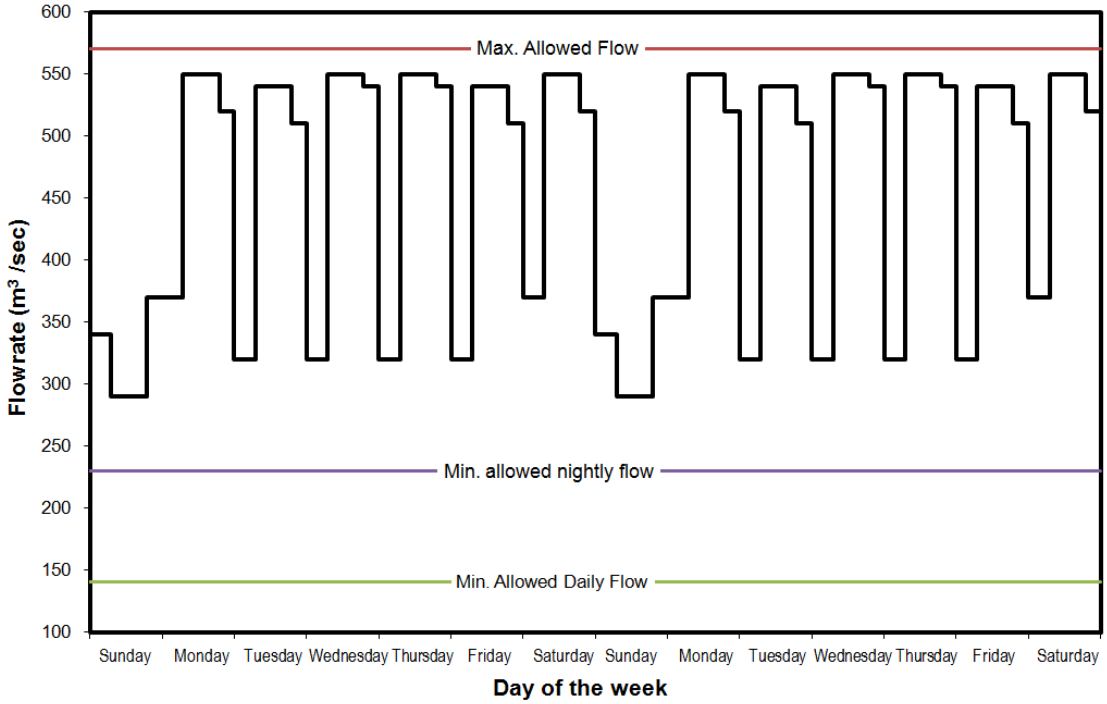

Figure 68. Optimal weekly operations schedule

The centralization of the optimal schedule within the flow constraints suggests the significance of the nonlinear aspects of the problem. In this sense, the results here are consistent with previous work in this field that has found linear methods ineffective (Brooke et al., 1996).

Table 17 compares the estimated consequences of the optimized schedule versus the present conditions under the interim criteria.

Factor	Current Operations	Optimized Operations
Average Bank Failure Risk	41%	42%
Percent rebuilt failed sandbars	20%	100%
Annualized building flood budget	$0.5 million	$4.2 million
Estimated Net Annual Revenue	$74.4 million	$76.0 million

Table 17. Optimized Glen Canyon Dam operations.

The optimized schedule predicts annual revenues of $76.0 million dollars, with annual building floods of sufficient extent to rebuild 100% of the lost sandbars. Using the 1996 revenue as representative, the predicted revenue under interim criteria is $74.4 million (Harpman, 1999) with 20% building flows every four years. Thus, the proposed annual budget for building flows is more than five times the current budget ($4.2 million versus $0.5 million). Average bank failure risk for the optimized schedule is essentially the same as the current risk (41% versus 42%).

Thus, optimizing operations not only mitigates long term sandbar loss and sustains current bank failure risk conditions, it also increases expected revenue by just over 2%.

CHAPTER 9. CONCLUSIONS

> Begin thus from the first act, and proceed; and, in conclusion, at the ill which thou hast done, be troubled, and rejoice for the good.
>
> – Pythagoras

Problem Statement

The success of the research described here must be measured against the overarching problem statement defined in Chapter 1:

How can hydroelectric dam operations be optimized to minimize the cost of successfully mitigating downstream bank failures?"

Answering this problem statement required significant research into slope failure methodology, seepage modeling and matric suction effects, groundwater wave response modeling, generalization of local failure analyses to riparian scales, and optimization by simulated annealing. Thus, the overall conclusions of this research must be built from the conclusions of each of these subsections. For this reason, the remainder of this chapter summarizes and develops conclusions for each of the researched areas and then synthesizes these into both general conclusions. The chapter ends with suggestions for future research and a final assessment of the success of this research in a closing statement.

Quantifying slope failure risk

The existing slope failure literature, as reflected in the compiled database in Chapter 2, shows considerable diversity across all model factors. Interestingly, the easiest modeling choices were not the most popular: the simplified Bishop

2DLE method was used more often than infinite slope or OMS, circular slip surfaces were analyzed more often than planar surfaces, the effective stress approach was applied more often than total stress, and correction factors were applied more often than not.

Despite the indisputable work ethic of the analysts, little improvement in SF calculation is evident: the basic distribution of SF appears to have been essentially constant since the first 2DLE analyses appeared in the literature more than five decades ago. Indeed, analysis by Box-Cox indicated that the database was best fit by a constant log normal statistical distribution, with a corresponding mean of 1.03 and s_d of 0.087. Unfortunately, while this fit may be useful for some applications, caution is advised since the pronounced curvature of the residuals indicates the presence of unmodeled contributing factors.

Thus, it appears that SF calculations are inadequately modeled by descriptive statistics alone; the effects of the slope parameters must be modeled as well.

In response to this need, Chapter 3 extended the meta-analysis inferentially, utilizing applied statistical analysis to identify, understand, and quantify the particular contributions of each of the slope parameters. This analysis revealed the following:

1. Different limit equilibrium algorithms produce different safety factors. For failed slopes, the direct methods of SF calculation appear to be the most successful at predicting $SF = 1$ as expected. Bishop's method and the complete methods of solution appeared to have a slight (but

statistically significant) non-conservative bias, but the magnitude of this bias is so small it is likely undetectable in field applications. Force methods, however, demonstrated a level of bias that may have a significant, non-conservative effect on SF calculation. It is not known, however, if the bias and uncertainty shown by the failure database can be generalized to stable slopes.

2. Clay content complicates SF analysis. The database indicated that correction factors for vane strength were not adequate to reduce predicted SF values to average at $SF = 1$ as expected. The relationship between plasticity index and safety factor appears to be more complicated than historically assumed. That said, there was no evidence that soils without clay were different from soils with clay with regard to SF uncertainty or bias.
3. The database overall was well described by a log linear distribution with a mean value of 1.03 and a standard deviation (of the log transformed values) of 0.087. A 1% failure risk for SF of about 1.65 was calculated from the overall database. A reduced ANOVA model was developed, allowing predictions for a given failure risk as a function of analytical method, slope type, and porewater stress approach.

So while a site specific risk analysis by error propagation is always preferable, since doing so directly accounts for project specific observations such as soil heterogeneity and porewater pressure uncertainty, the reduced ANOVA model allows a global consideration of slope failure risk in general. It therefore

constitutes an adequate resolution of the first task, quantifying slope failure risk, and provided a solid stochastic foundation upon which to build the physical models of seepage pressures and matric suction, described next.

Determining the role of matric suction

Chapter 4 directly and quantitatively evaluated the role of matric suction in bank stability by developing analytical solutions for safety factor calculations of infinite slopes under flux conditions. These solutions utilized published and well established constitutive equations to form steady state closed form equations integrating matric suction, degree of saturation, and overburden stress profiles for typical values of δ, the constant exponent historically used to relate permeability to relative saturation. An infinite series solution for overburden stress was provided for soils with δ values different than standard. The infinite series solution was shown to collapse to a simple form for large values of δ that achieved a reasonable numerical fit for $\delta > 4$.

It was found that matric suction significantly increases the factor of safety when compared with a dry / saturated model. This safety factor increase was shown to be consistent with a field study of an existing stable slope, indicating stability under dry weather conditions whereas the dry / saturated model strongly predicted slope failure under the same conditions.

However, matric suction decreases are accompanied by increased soil unit weight due to increased moisture content, which in turn reduces the factor of safety for slip surfaces near the phreatic surface. For shallow water tables, the

model found that this effect increases when slope angles are significantly less than or greater than 45°.

Thus, infinite slope models that ignore matric suction effects require (for consistency) the engineer to make invalid assumptions about soil saturation that inevitably lead to inaccurate safety factor predictions. Moreover, a case study that verified this approach also showed that accounting for unsaturated soil conditions and matric suction effects in slope stability can result in safety factor predictions that are actually less than those produced by traditional methods. In particular, matric suction must be considered in order to determine appropriate and consistent soil unit weights. It appears that matric suction is an integral and necessary aspect of slope stability that must be accounted for in order to obtain accurate predictions. This result led to an investigation in Chapter 7 that demonstrated that the non-conservative effects of ignoring matric suction effects becomes even more pronounced for curved failure surfaces. Simply put, matric suction effects are a critical component of accurate slope failure prediction.

Seepage effects

Chapter 5 developed a finite difference model of bank failures due to seepage forces by coupling governing flow equations to the model elements developed in Chapters 2 through 4. This model validated the general approach, confirmed the importance of including matric suction effects, and demonstrated the significance of unsteady flow processes on bank stability.

The finite difference model was too slow for comprehensive treatment of an entire river reach, and so an analytical solution was developed instead.

Drawing on the key findings of the finite difference investigation, the analytical model describes saturated flow in a deep streambank and can be interpreted as a generalization of the groundwater tidal response equation. This generalization allows periodic river waves to be considered by means of Fourier series.

The primary advantage of the analytical solution is that the porewater distribution can be modeled for any time without stepping through incremental time steps from an assumed initial condition, as required by a finite element analysis. That said, there are other advantages to the model as well. These are:

1. The inherent fluctuations of river stages are directly modeled, allowing steady state periodic modeling and bypassing the need to assume potentially inaccurate initial conditions
2. The average piezometric surface can be directly obtained from the constant term in Equation (106).
3. The analytical solution bypasses convergence problems often associated with finite element models of matric suction.

With the porewater model complete, global risk analysis of a river system can be achieved by repeatedly executing the porewater model along the river banks at sufficiently small spacing to achieve the desired precision. Alternatively, if the statistical distributions of the contributing bank factors are known in the reach, a general model of bank stability can be derived using Monte Carlos simulation.

Riparian scale translation

The analytical solution allowed the bank stability model to be executed at sufficient speed to perform a large scale Monte Carlo simulation. Utilizing design of experiments (DOE) approach, a simulation of the Colorado River was executed and analyzed using ANOVA hypothesis testing.

The effects of restricting flows and flow ramping were found to be subtle; even extreme values of the release parameters typically corresponded to risk changes of less than 10%. However, attenuation processes can greatly change the downstream flow characteristics and hence magnify the effects of flow release decisions. Indeed, utilizing relatively simple non-linear equations to model the wave progression, the analysis predicts a 50% failure risk large sandbars ($q_{build} = 1274\ \mathrm{m^3/sec}$) operating under current regulations when $q'_{down} = 42\ \mathrm{m^3/sec/hr}$, $q'_{up} = 71\ \mathrm{m^3/sec/hr}$, $q_{base} = 300\ \mathrm{m^3/sec}$, $\Delta q = 266\ \mathrm{m^3/sec}$, and $t_{peak} = 12\ \mathrm{hr}$. At the low end, a 31% failure risk was predicted for large sandbars when $q'_{down} = 43\ \mathrm{m^3/sec/hr}$, $q'_{up} = 300\ \mathrm{m^3/sec/hr}$, $q_{base} = 100\ \mathrm{m^3/sec}$, $\Delta q = 100\ \mathrm{m^3/sec}$, and $t_{peak} = 0\ \mathrm{hr}$. The predictions were verified by field observations. A reduced ANOVA model was then utilized to relate downstream slope stability risk to key dam operation parameters. In this way, a comprehensive model of bank failure risk was developed for the entirety of the Colorado River within the Grand Canyon.

Optimizing dam operations

From the comprehensive reach level bank stability model, an optimal flow release schedule was generated by applied simulated annealing. This solution met the numerous non-linear constraints and, while there is no guarantee that the solution is global, it was found to be 2% more cost effective than current operations while providing five times as much budget for the critical beach building floods.

Synthesis

In order to solve the problem statement, a number of fairly disparate challenges had to be met, ranging from statistical to analytical to algorithmic. Despite these task differences, however, their results are linked by three common conclusions:

1. **Stochastic understanding is critical**. This research found numerous instances where accounting for uncertainty was essential; not only within the bank stability analyses but also within the driving machinery of the simulated annealing optimization algorithm. These uncertainties can be counter-intuitive and must be measured from actual data. Perspective is essential: A single bank stability calculation may account for parameter variations within the bank, but translating this calculation to reach scale requires that one not only account for further variations of these parameters but also recognize that new uncertainties have been introduced as a result.

2. **Large scale problems may be driven by small scale factors**. Past research on the Grand Canyon riverbank stability was usually divided into empirical models based on large scale measurements (number of banks, frequency of failures, etc.) or small scale models assumed applicable to entire region. Neither of these approaches is optimal. Like the failure in the literature to relate bank stability to river kilometer, large scale measurements often represent the end product of multiple processes and may therefore show little correlation to large scale parameters. On the other hand, careless generalization of small scale processes to describe large scale effects, such as assuming a single representative bank can represent an entire riparian region, amounts to unconstrained extrapolation. Translation between scales needs to be modeled as well.
3. **Water complicates physical processes**. Water was one of the key components and one of the key compounding factors at nearly every level of the physical analysis in this research. The stability database meta-analysis showed that analyses that porewater effects are significantly correlated with slope types and this relationship affects stability analysis in ways that are difficult to interpret. Matric suction, another water effect, simultaneously increases soil weight, which decreases the bank safety factor, and increases effective cohesion, which increases the safety factor; only a properly conducted unsaturated analysis can reveal the net effect. For bank slopes, water drives the physical processes in three ways: 1) periodic increases and decreases in water stage significantly affect slope

stability due to applied lateral pressures; 2) seepage from these stages creates a groundwater wave that progresses away from the bank and significantly alters bank stability risk; and 3) porewater within the bank rises through the soil to cause matric suction.

Suggestions for future research

Unregulated rivers

The groundwater wave response function can be used to model any periodic stage changes. Thus, naturally occurring stage hydrographs can be easily modeled. This allows risk assessment of river reaches under natural conditions.

This application can be extended to design storms, wherein the bank stability risk response due to a theoretical, design hydrograph can be modeled. Moreover, the equations themselves are computationally efficient enough to allow the development of a design storm specific to a given return period. For example, the worst case risk response to storms of varying duration can be used to govern bank stabilization efforts.

Other dam applications

The optimization strategies developed in this research can be used at the planning stage of new hydroelectric dam designs. For example, the type, size, and number of turbines can be selected based on cost maximization while dynamically preserving the downstream river reach. It can also be included in a watershed level plan where multiple potential dam sites are being assessed.

At the other end of the spectrum, the methods described herein can be used to guide improvement plans for existing dams. Moreover, since the procedure optimizes expected return on hydroelectric dams, it is a useful assessment tool for the viability of improving existing dams rather than decommissioning them in order to preserve the downstream river resources.

There are many dams that are purely flood control and not hydroelectric. This research can be used to guide operations for these dams as well. That is, outflow regulation can be simply optimized to mitigate adverse downstream riverbank responses without cost considerations.

Scale independence

The physical process modeling developed here is scale independent, and thus can be used for small scale modeling of any size waterway, from rivulets to small tributaries. It can also be applied to large scales, wherein historical, catastrophic floods in engineering or geological timescales.

Regional Sediment Management Plans (RSM)

The United States Army Corps of Engineers (USACE) has developed a Regional Sediment Management methodology for large scale sediment control. Multiple control strategies are considered in these plans, from controlled flooding from existing dams to bank stabilization by differed grading practices to periodic dredging scheduling. The research here can be used as one of the modeling tools for these plans.

Often the goal of RSM plans is to remove excessive downstream sediment. For these applications, the research developed herein can be used to maximize downstream bank failures, releasing sediment from these areas as part of the sediment removal process. The optimization algorithm can then be revised to minimize cost of this operation.

Couple with Infinite Slope Model

Because the application of this research was driven by the circular failures in the Grand Canyon, the infinite slope stability model was used only for purposes of evaluating the significance of matric suction. For other applications where infinite slope type failures appear to govern bank stability risk, the infinite slope model can be coupled with the groundwater response model and optimization algorithm. The result would be a very fast calculation scheme that would allow high resolution riparian scale assessment.

Couple with other objectives

The general approach in this research is flexible enough to include other dam operations objectives, such as downstream sediment control or optimizing real-time response. These objectives can be incorporated by means of additional constraints and / or expanded physical models.

The model can also be expanded to consider other geomorphologic mechanisms, such as surface wave effects, scour from eddies, bed scour, etc.

Field Investigations

The physical model developed here can guide field investigations. The direct application of the inherent uncertainty of measured bank parameters should encourage multiple measurements at various locations through the reach in order to maximize model accuracy. Likewise, the importance of matric suction as discovered herein will hopefully encourage field investigation and laboratory measurements of the governing parameters. The model also makes specific predictions about areas of high bank failure risk, and these areas can be targeted for detailed assessment and / or monitoring.

Closure

This research developed many new techniques in order to meet the overall objective, and these techniques were validated as much as possible through comparison with field measurements and experimental findings. In this sense, the overarching problem statement has been successfully addressed. That is, specific techniques have been developed that should optimize hydroelectric dam operations in order to minimize the cost of mitigating bank failures.

Like the scientific method, the cornerstone of engineering science is reproducibility. Beyond applied science, however, an engineering model must be transferable to other, similar applications. Thus, the true assessment of the research developed here depends wholly on the results of future applications.

The driving motivation behind the research is to benefit both our natural resources and society as a whole. Thus, it is hoped that the success found here will be first of many.

REFERENCES

> If you steal from one author, it's plagiarism; if you steal from many, it's research.
>
> – Wilson Mizner (1876 - 1933)

Abolpour, B., and Javan, M. (2007) "Optimization model for allocating water in a river basin during a drought", *J. Irr. & Drng. Eng.,* 133(6), 559-572.

Abramson, L.W., Lee, T.S., Sharma, S., and Boyce, G.M. (2002). *Slope Stability and Stabilization Methods*, 2nd ed., Wiley, Hoboken, NJ.

Adib, M.E. (2000). "Slope Failure in Weathered Claystone and Siltstone", *J. Geotech. and Geoenv. Eng.* 126(9).

Anderson, M.P., and Woessner, W.W. (1992). *Applied Groundwater Modeling, Simulation of Flow and Advective Transport: San Diego*.

Arellano, D., and Stark, T. (2000). "Importance of three-dimensional slope stability analyses in practice", *Slope Stability 2000: Proc. of Sessions of Geo-Denver 2000*, ed. Griffiths, D., Fenton, G., and Martin, T. 18-32.

Attewell, P., and Farmer, I. (1976). *Princ. of Eng. Geology*, John Wiley and Sons, 645-651.

Avellaneda, P., Ballestero, T., Roseen, R., and Houle, J. (2009). "On parameter estimation of an urban stormwater runoff model." J. Environ. Eng., 135(8), 595–608.

Averjanov, S.F. (1950). "About permeability of subsurface soils in case of incomplete saturation." *Engineering Collection*, 7.

Azzouz, A.S., Baligh, M.M., and Ladd, C.C. (1981). "Three-dimensional stability analyses of four embankment failures", *Proc. of the Tenth Int. Conf. on Soil Mech. and Found. Eng.*, 3, 343-346.

Babu, G.L.S, and Bijoy, A.C. (1999). "Appraisal of Bishop's ethod of slope stability analysis", *Proc. of the Int. Syp. on Slope Stability Eng.*, Yagi, N., Tomagami, T., and Jiang, J-C. eds., 1, 249-252.

Baker, R., Shukha, R., and Leshinsky, D. (2005). "Stability of cohesionless partially submerged slopes." *International Journal for Numerical and Analytical Methods in Geomechanics*, Wiley Interscience, 29, 1157 – 1170.

Balasubramaniam, A., Sivandran, C., and Ho, Y. (1979). "Stability and settlement of embankments on soft Bangkok clay", *Proc. Of the Third Int. Conf. on Num. Methods in Geomech.*, Wittke, W., ed., 4, 1373-1411.

Bathe, K.J., and Khoshgoftaar, M.R. (1979). "Finite element free surface seepage analysis without mesh iteration." *Int. J. Num. Analysis Methods Geomech*., 3, 13 – 22.

Baum, R., and Fleming, R. (1991). "Use of longitudinal strain in identifying driving and resisting elements of landslides", *Geo. Soc. of Am. Bull.*, 103, 1121-1132.

Baum, R.L., and Reid, M.E. (1995). "Geology, hydrology, and mechanics of a slow-moving, clay-rich landslide, Honolulu, Hawaii", in Haneberg, W.C. and Anderson, S.A., eds., *Clay and Shale Slope Instability: Boulder, Colorado, Geo. Soc. of Am. Rev. in Eng. Geology*, 10, 79-105.

Benac, Č., Arbanas, Ž., Jurak, V., Oštrić, M., and Ožanić, N. (2005). "Complex landslide in the Rječina valley (Croatia): origin and sliding mechanism", *Bull. Eng. Geol. Env.*, 64, 361–371.

Beni, G., and Wang, J. (1989). "Swarm Intelligence in Cellular Robotic Systems", *Proceed. NATO Advanced Workshop on Robots and Biological Systems*, Tuscany, Italy, June 26–30.

Beus, S.S., and Avery, C.C. (eds.) (1992). *The influence of variable discharge on Colorado River sandbars below Glen Canyon Dam: final report to the National Park Service*, Flagstaff, AZ.

Bijmolt, T.H.A., and Pieters, R.J.M. (2001). "Meta-Analysis in marketing when studies contain multiple measurements", *Marketing Letters*, 12(2), 157-169.

Biot, M.A. (1941). "Theory of elasticity and three dimensional consolidation." *J. Appl. Physics*, 12, 155 – 164.

Bjerrum, L. (1973). "Problems of soil mechanics and construction of soft clays and structurally unstable soils (collapsible, expansive and others)", State of *the Art Report, Proc. Eighth Int. Conf. Soil Mechanics and Found. Eng.*, 3, 111-160.

Bjerrum, L. (1972). "Embankments on soft ground: State of the Art Report", *ASCE Specialty Conf. on Performance of Earth and Earth Supported Structures*, 2, 1-54.

Boutrup, E., Lovell, C.W., and Siegel, R.A. (1979). "STABL 2 – a computer progra for general slope stability analysis.", *Third Int. Conf. on Num. Methods in Geomech*., Wittke, W. ed., 2, 747 – 757.

Boutt, D. F. (2010). "Poroelastic Loading of an Aquifer Due to Upstream Dam Releases" *Ground Water*, 48: 580–592.

Bowders, J., and Lee, S. (1990). "Guide for selecting an appropriate method to analyze the stability of slopes on reclaimed surface mines", *Proc. 1990 Mining and Reclam. Conf. and Exhibition*, 103-110.

Brand, E.W., and Krasaesin, P. (1970). "Investigation of an embankment failure in soft clay", *Bulletin of the Int. Assoc. Eng. Geology*, 1, 53-64.

Bressani, L., and Ridley, A. (1997). "A slope instability study of a sedimentary formation with swelling clay in Southern Brazil", *Proc. Fourteenth Int. Conf. Soil Mech. and Found. Eng.*, 2, 1215-1216.

Brooke, A., Kendrik, D., and Meeraus, A. (1996). *GAMS: A User's Guide, GAMS Corporation*, Washington, D.C.

Brooks, R.H., Corey, A.T. (1964). *Hydraulic Properties of Porous Media, Hydrology Paper 3*, Colorado State University, Fort Collins, CO.

Budhu, M. (1993). "Mechanisms of erosion and a model to predict seepage-driven erosion due to transient flow" *The influence of variable discharge on Colorado River sandbars below Glen Canyon Dam: final report to the National Park Service*, S.S. Beus and C.C. Avery, eds., Flagstaff, AZ.

Budhu, M., and Gobin, R. (1994). "Instability of sandbars in Grand Canyon." *Journal of Hydraulic Engineering*, ASCE, 120(8), 919 – 932.

Budhu, M., and Gobin, R. (1995a). "Seepage erosion from dam-regulated flow: case of Glen Canyon Dam, Arizona." *Journal of Irrigation Engineering*, ASCE, 121(1), 22 – 23.

Budhu, M., and Gobin, R. (1995b). "Seepage-induced slope failure on sandbars in Grand Canyon." *Journal of Hydraulic Engineering*, ASCE, 121(8), 601 – 609.

Budhu, M., and Gobin, R. (1996). "Slope Instability from Ground-Water Seepage." *Journal of Hydraulic Engineering*, ASCE, 122(7), 415 – 417.

Burns, W. (1999). "Engineering Geology and Relative Stability of the Southern Half of Newell Creek Canyon, Oregon City, Oregon", *M. Geo. Thesis*, Portland State University, Oregon.

Burridge, P.B. (1987). "Failure of Slopes", *Doctoral thesis,* California Institute of Technology, Pasadena, California.

Byrne, R., Kendall, J., and Brown, S. (1992). "Cause and mechanism of failure: Kettleman Hills Landfill B-19, Phase IA", *Proc. Stability and Performance of Slopes and Embankments,* 2, 1188-1215.

Carpenter, M.C., Crosswhite, J.A., and Carruth, R.L. (1995). "Water-level fluctuations, water temperatures and tilts in sandbars -6.5R, 43.1L and 172.3L, Grand Canyon, Arizona", *U.S. Geological Survey Open File Report 94-485*.

Carter, R.K. (1971). "Computer oriented slope stability analysis by method of slices". *Ph.D. thesis*, Purdue University.

Casagli, N., Dapporto S., Ibsen, M.L., Tofani, V., and Vannocci, P. (2006). "Analysis of the landslide triggering mechanism during the storm of 20th–21st November 2000, in Northern Tuscany", *Landslides*, 3, 13-21.

Chen, R. (1988). "A study on some Eng. properties of lateritic soil", *Geomechanics in Tropical Soils*, 1,245-251

Chen, Z., and Shao, C. (1988). "Evaluation of minimum factor of safety in slope stability analysis" *Can. Geotech. J.*, 25(4), 735-748.

Chen, Z., Morgenstern, N., and Chan, D. (1992). "Progressive failure of the Carsington Dam: a numerical study" *Can. Geotech. J.,* 29(6), 971-988.

Chiasson, P., and Wang, Y-J (2007). "Spatial variability of Champlain sea clay and an application of stochastic slope stability of a cut", Characterisation and Engineering Properties of Natural Soils, ed. Tan, Phoon, Hight, and Leroueil, 2707 – 2720.

Cho, S.E. and Lee, S.R. (2002). "Evaluation of Surficial Stability for Homogeneous Slopes Considering Rainfall Characteristics", *J. Geotech. and Geoenv. Eng.,* 128(9), 756 – 763.

Christian, J.T. (2004). "Geotechnical engineering reliability: How well do we know what we are doing?", *J. Geotech. Eng.* 130(10), 985-1003.

Christian, J.T., Ladd, C.C., and Baecher, G.B. (1994). "Reliability applied to slope stability analysis." *Journal of Geotechnical Engineering*, ASCE, 120(12), 2187 – 2207.

Clark, J., DeSion, A., and Stepanek, M. (1971). "Landslides in Urban areas", *Proc. Ninth Annual Eng. Geology and Soils Eng. Symp.*, 289-304.

Cluer, B.L. (1992). "Daily response of Colorado River sandbars to Glen Canyon Dam test flows." *The influence of variable discharge on Colorado River sandbars below Glen Canyon Dam: final report to the National Park Service*, S.S. Beus and C.C. Avery, eds., Flagstaff, AZ.

Corey, A.T. (1954). "The interrelation between gas and oil relative permeabilities", *Producer's Monthly*, 19, 7 – 10.

Cunha, M. C., and Sousa, J. (1999). "Water distribution network design optimization: A simulated annealing approach." *J. Water Resour. Plann. Manage*., 125(4), 215–221.

Cunha, M. C., and Sousa, J. (2001). "Hydraulic infrastructures design using simulated annealing." *J. Infrastruct. Syst*., 7(1), 32–39.

Darcy, H. (1856). *Les fontaines publiques de la ville de Dijon*, V. Dalmont, Paris, 647 pp.

Dascal, O., and Rournier, JP. (1975). "Embankment on soft and sensitive clay foundation", *J. Geotech. Eng.*, 101(GT3), 297-314.

Dascal, O., Tournier, J.P., Tavenas, F., and La Rochelle, P. (1972). "Failure of a test embankment on sensitive clay", *ASCE Specialty Conf. on Performance of Earth and Earth Supported Structures*, 1(1), 129-158.

Day, R.W. (1996). "Failure of Desert View Drive embankment", *J. Perf. Const. Fac.* 10(1).

Dougherty, D. E., and Marryott, R. A. (1991). "Optimal groundwater management. 1: Simulated annealing." *Water Resour. Res*., 27(10), 2493–2508.

Drower, MS. (1954). "Water supply, irrigation, and agriculture", in *The History of Technology*, Singer, C. et al. (ed.), Vol 1, Oxford University Press, NY, 520–57.

Duncan, J. M. and Wright, S. G. (2005), *Soil Strength and Slope Stability*. John Wiley &. Sons, Hoboken, N.J..

Duncan, J. M., Wright, S. G., and Wong, K. S. (1990). "Slope stability during rapid drawdown", H. *Bolton Seed Memorial Symp. Proc.*, 2, 253-272.

Duncan, J.M. and Wright, S.G., (1980). "The accuracy of equilibrium methods of slope stability analysis", *Eng. Geol.,* 16, 5 – 17.

Duncan, J.M., and Buchignani, A.L. (1973). "Failure of underwater slope in San Francisco bay." *Journal of the Soil Mechanics and Foundation Division*, ASCE, 99(9), 687 – 703

Eden, W., and Mitchell, R. (1973). "Landslides in sensitive marine clay in eastern Canada", *Highway Research Record*, 463, 18-27.

Edil, T.B., and Vallejo, L.E. (1977). "Shoreline erosion and landslides in the Great Lakes", *Proc. Ninth Int. Conf. on Soil Mech. and Found. Eng.,* 2, 51-57.

Eide, O., and Holmberg, S. (1972). "Test fills to failure on soft Bangkok clay", *ASCE Spec. Conf. Perf. Earth and Earth Supported Structures*, 1, 159-160.

Ferkh, Z., and Fell, R. (1994). "Design of embarkments on soft clay", *Proc. Thirteenth Int. Conf. on Soil Mech. and Found. Eng.*, 2, 733-738.

Flaate, K., and Preber, T. (1974). "Stability of road embankments in soft clay", *Can. Geotech. J.,* 2(1), 72-88.

Fourie, A.B., Blight, G.E., and Papageorgiou, G. (2001). "Static liquefaction as a possible explanation for the Merriespruit tailings dam failure", *Can. Geotech. J*., 38, 707–719.

Fredlund, D.G. and Rahardjo, H. (1993). *Soil Mechanics for Unsaturated Soils*, John Wiley & Sons, Hoboken, N.J.

Fredlund, D.G., and Xing, A. (1994). "Equations for the soil-water characteristic curve." *Can. Geotech. J*., 31, 521 – 532.

Friznell, K.W. (1985). *Spillway tests at the Glen Canyon Dam*, Engineering and Research Center, U.S. Dept. of the the Interior, Bureau of Reclamation.

Furbish, D.J. (1997). *Fluid Physics in Geology*, Oxford University Press.

Garga, V.K., and de la Torre, M. (2002). "Emergency remediation of instability at Caudalosa tailings dam, Peru: a case history", *Can. Geotech. J*. 39, 1193 – 1200

Geem, Z. (2009). Particle-swarm harmony search for water network design. *Engineering Optimization*, *41*(4), 297-311. doi:10.1080/03052150802449227

Georgiou, P. E., Papamichail, D. M., and Vougioukas, S. G. (2006). "Optimal irrigation reservoir operation and simultaneous multi-crop cultivation area selection using simulated annealing." *Irrig. Drain*., 55, 129–144.

Goldberg, D. E. (1989). *Genetic Algorithms in Search, Optimization, and Machine Learning*. Addison-Wesley.

Goodwin, P., Falte, M., and Betss, A.D.K. (2000). "Managing for unforeseen consequences of large dam operations", contributing paper to Howard, C.D.D. (2000), *Operations, Monitoring, and Decomissioning of Dams, Thematic Review V IV.5*, prepared as an input to the World Commission on Dams, Cape Town, www.dams.org.

Griffin, E. R., and Wiele, S. M. (1996). Calculated hydrographs for unsteady research flows at selected sites along the Colorado River downstream from Glen Canyon Dam, Arizona, 1990 and 1991. Boulder, Colo.: U.S. Dept. of the Interior, U.S. Geological Survey.

Haitjema, H., Feinstein, D., Hunt, R. and Gusyev, M. (2010). "A Hybrid Finite-Difference and Analytic Element Groundwater Model", *Ground Water*, 48: 538–548.

Hanzawa, H., Kishida, T., Fukasawa, T., and Suzuki, K. (2000). "Case studies on six earth structures constructed on soft clay deposits", *Proc. Of the Int. Symp. Costal Geotech. Eng. In Practice*, Nakase, A., and Tsuchida, T., eds., 1, 287-290.

Harpman, D.A. (1999). "The economic cost of the 1996 controlled flood", in Webb, R.H., Schmidt, J.C., Marzolf, G.R., and Valdez, R.A. (Ed.) *The Controlled Flood in Grand Canyon,* Geophysical Monograph 110, American Geophysical Union.

Haupt, R., and Olsen, J. (1972). "Case history – Embankment failure on soft varved silt", *Proc. Spec. Conf. Perf. of Earth and Earth Supported Structures*, 1(1), 1-28.

Hazel, J.E. Jr., Kaplinski, M., Parnell, R., Kohl, K, and Topping, D.J. (2006). *Stage-Discharge Relations for the Colorado River in Glen, Marble, and Grand Canyons, Arizona: U.S. Geological Survey Open-File Report 2006-1243*.

Hazel, J.E. Jr., Kaplinski, M., Parnell, R., Kohl, K, Manone, M., and Dale, A. (1999). "Topological and bathymetric changes at thirty-three long-term study sites", in Webb, R.H., Schmidt, J.C., Marzolf, G.R., and Valdez, R.A. (Ed.) *The Controlled Flood in Grand Canyon,* Geophysical Monograph 110, American Geophysical Union.

Hill, M. E., Stewart, M. T. and Martin, A. (2010). "Evaluation of the MODFLOW-2005 Conduit Flow Process", *Ground Water*, 48: 549–559.

Ho, C., Rodriguez-Marek, A., and Muhunthan,B. (1997). "Slope stability analysis application of a static discrete element method", *Proc. Fourteenth Int. Conf. Soil Mech. and Found. Eng.*, 2, 1219-1222.

Horman, M.J., and Kenley, R. (2005). "Quantifying levels of wasted time in construction with meta-analysis*", J. Cons. Eng. and Mgt*., 131(1), 52 – 61.

Houston, S., Perez-Garcia, N., Houston, W. (2009) "Shear Strength and Shear-Induced Volume Change Behavior of Unsaturated Soils from a Triaxial Test Program", *J. Geotech. and Geoenv. Eng.,* ASCE, In Press.

Huang, S.L., and Yamasaki, K. (1993). "Slope Failure Analysis Using Local Minimum Factor-of-Safety Approach", *J. Geotech. Eng.*, 119 (12), 1974-1989

Hughes, D.B., and Clarke, B.G. (2001). "The River Aire slope failure at the St. Aidans extension opencast coal site, West Yorkshire, United Kingdom", *Can. Geotech. J.,* 38, 239–259.

Irmay, S. (1954). "On the hydraulic conductivity of unsaturated soils", *Proc., Soil Sci. Soc. Of Am.*, 36, 380 – 382.

Iverson, R. M. (1990). "Groundwater flow fields in infinite slopes." *Géotechnique*, 40(1), 139 – 143.

Iverson, R. M. (1997). "Discussion: Slope Instability from Ground-Water Seepage." *J. Hyd. Eng.*, ASCE, 123(10), 929 – 930.

Iverson, R. M. (1997). "The physics of debris flows." *Reviews of Geophysics*, 35(3), 245 – 296.

Iverson, R. M. (2000). "Landslide triggering by rain infiltration." *Water Resources Research*, 36(7), 1897 – 1910.

Iverson, R.M., Reid, M.E., and LaHusen, R.G. (1997). "Debris-Flow Mobilization from Landslides", *Annu. Rev. Earth Planet Sci*, 25, 85-138.

Jakob, M., and Hungr, O. (2005), *Debris-flow Hazards and Related Phenomena*, Praxis Publishing Ltd, Chichester, UK.

Jacquot, J. (2009). "Dams, From Hoover to Three Gorges to the Crumbling Ones", *Discover Magazine*, March.

Kawamura, K., and Ogawa, R. (1997). "Slope failure in major tertiary mudstone zone", *Deformation and Progressive Failure in Geomechanics*, 701-706.

Kearsley, L.H., Quartaroli, R.D., and Kearsley, M.J.C. (1999). "Changes in the number and size fo campsites as determined by inventories and measurement", in Webb, R.H., Schmidt, J.C., Marzolf, G.R., and Valdez, R.A. (Ed.) *The Controlled Flood in Grand Canyon,* Geophysical Monograph 110, American Geophysical Union.

Kenney, T., and Drury, P. (1973). "Case record of the slope failure that initiated the retrogressive quick-clay landslide at Ullensaker, Norway", *Géotechnique*, 23(1) 33-47.

Kim, J., Salgado, R., and Yu, H.S. (1999). "Limit analysis of soil slopes subjected to pore-water pressures", *J. Geo. and Geoenv. Eng.,* 125(1), 49 – 58.

Kirkpatrick, S., Gelatt, C. D., and Vecchi, M.P. (1983). "Optimization by Simulated Annealing". *Science* 220 (4598): 671–680.

Kjaernsli, B., and Simons, N (1962). "Stability investigations of the north bank of the Drammen River", *Geotchnique*, (12), 147-167.

Krahn, J. (2003). "The 2001 R.M. Hardy Lecture: The limits of limit equilibrium analyses" ", *Can. Geotech. J.*, 40(2), 643-660.

Kuo, S. F., Liu, C. W., and Merkley, G. P. 2001 . "Application of the simulated annealing method to agricultural water resource management." J. Agric. Eng. Res., 80 1 , 109–124.

Kwan, D. (1971). "Observations of the failure of a vertical cut in clay at Welland, Ontario", *Can. Geotech. J.*, 8(2), 283-298.

La Rochelle et al. (1974). "Failure of a test embankment on a sensitive Champlain clay deposit", *Can. Geotech. J.*, 11(1), 142-164.

Lacasse, S., Ladd, C., and Barsvary, A. (1977). "Undrained behaviour of emankments on New Liskeard varved clay", *Can. Geotech. J.*, 14(3), 367-388.

Ladd, C.C. (1972). "Test embankment on sensitive clay", *Proceedings of the Specialty Conference on Performance of Earth and Earth Supported Structures*, Purdue University, Lafayette, IN, June 11 – 14, 101 – 128.

Ladd, C.C., and Foott, R. (1974). "New design procedure for stability of soft clays.", *J. Geo. Eng. Div.*, 100(7), 763 – 786.

Ladd, C.C., Foott, R., Ishihara, K., Schlosser, F., and Poulos, H.G. (1977). "Stress-deformation and strength characteristics" , *Proc. Ninth Int. Conf. Soil Mech. and Found. Eng.*, 421-494.

Lade, P. (1993). "Initiation of static instability in the submarine Nerlerk berm" *Can. Geotech. J.*, 30(6), 895-904.

Lafleur, J., Silvestri, V., Asselin, R., and Soulie, M. (1988). "Behaviour of a test excavation in soft Champlain Sea clay", *Can. Geotech, J.*, 23(4), 705-715.

Leadbeater, A.D. (1985). "Snake Pass, remedial work to slip near Alport Bridge", *Failures in Earthworks*, 29 – 38.

Lee, W. and Hoopes, J.A. (1999). "Prediction of cavitation damage for spillways", *J. Hyd. Eng.,* ASCE, 122(9), 481 – 488.

Lee, S.-H., and Kim, H.-B. (2000). "A study to incorporate engineering probability techniques into deterministic slope stability methods", *KSCE J. Civil Eng.*, 4(3), 153-160.

Lefebvre, G. (1981). "Fourth Canadian geotechnical colloquium: Strength and slope stability in Canadian soft clay deposits" *Can. Geotech. J.*, 18(3), 420-442.

Leong, E.C., and Rahardjo, H. (1997). "Permeability functions for unsaturated soils", *J. Geotech. and Geoenv. Eng.,* ASCE, 123(12), 1118 – 1126.

Lindman, H.R. (1974). *Analysis of Variance in Complex Experimental Designs*, W.H. Freeman and Company.

Lo, K., and Stermac, A. (1965). "Failure of an embankment founded on varved clay." *Can. Geotech. J.*, 2(3), 234-253.

Lu, N., Griffiths, D.V. (2004). "Profiles of Steady-State Suction Stress in Unsaturated Soils." *J. Geotech. and Geoenv. Eng.,* ASCE, 130(10), 1063 – 1076.

Lydon, I., and Long, M. (2001). "Analysis of slope stability of an earth dam due to rapid drawdown effects", *Proc. Fifteenth Int. Conf. Soil Mech. and Found. Eng.*, 3, 2139-2142.

Marryott, R. A., Dougherty, D. E., and Stollar, R. L. 1993¬ . "Optimal groundwater management. 2: Application of simulated annealing to a field-scale contamination." Water Resour. Res., 29 4¬ , 847–860.

Marsland, A., and Powell, J. (1977). "The behaviour of a trial bank constructed to failure on soft alluvium of the River Thames", *Int. Symp. on Soft Clay*., 505-526**.**

Mays, L. W., and Tung, Y-K. (2002). *Hydrosystems Engineering and Management*. Water Resources Publications, Highlands Ranch, Colorado.

Mays, L. W. (2010). *Ancient Water Technologies*. Springer Publishing, New York, NY.

Mays, L.W., and Bedient, P.B. (1982). "Model for optimal size and location of detention." *J. Water Resources Planning and Management*, ASCE, 108(3), 270-285.

Mays, L.W., and Todd, D.K. (2005). *Groundwater Hydrology*. John Wiley & Sons, Inc. McGraw-Hill, New York.

McKee, C.R, and Bumb, A.C., (1987). "Flow-testing coalbed methane production wells in the presence of water and gas." *SPE Formation Evaluation*, (10), 599 – 608.

McKee, C.R., and Bumb, A.C. (1984). "The importance of unsaturated flow parameters in designing a hazardous waste site." In *Hazardous Waste and Environmental Emergencies (Hazardous Materials Control Research Institute National Conference),* Houston, TX, 12-14 March 1984, Silver Spring, Md., 50 – 58.

Merifield, P.M. (1992). "Surficial slope failures in southern California hillside residential areas: Lessons from the 1978 and 1980 rainstorms" *Landslides/Landslide Mitigation: Boulder, Colorado, Geol. Society of Am. Rev. in Eng. Geol.*, Slosson, J.E., Keene, A.G., and Johnson, J.A. eds., 9, 11 - 22.

Mesri, G., and Abdel-Ghaffar, M. E. M. (1993). ''Cohesion intercept in effective stress-stability analysis.'' *J. Geotech. Engrg.*, 119(8), 1229–1249.

Mitchell, R, and Williams, D. (1981). "Induced failure of an instrumented clay slope", *Proc. Tenth Int. Conf. on Soil Mech. and Found. Eng.*, 3, 479-484.

Montgomery, D.C. (2009). *Design and Analysis of Experiments*, 7th edition, John Wiley & Sons, New York.

Montgomery, D.C., Myers, R.H, Carter, W.H., and Vining, G.G. (2005) "The hierarchy principle in designed industrial experiments", *Qual. Reliab. Engng*. Int., 21, 197–201.

Moore, P.J. (1970). "The factor of safety against undrained failure of slopes." *Soils and Found.*, 10(3), 81-91.

Mostyn, G.R., and Small, J.C. (1987). "Methods of stability analysis", *Soil Slope Instability and Stabilisation*, Walker, B.F., and Fell, R. eds., 71 – 120.

Nagarkar, P., Kulkarni, R., Kulkarni M, and Kulkarni, D. (1981). "Failures of a monozone earth dam of expansive clay", *Proc. Tenth Int. Conf. Soil Mech. and Found. Eng.*, 3, 491-494.

Neuffer, D.P., and Schultz, R.A. (2006). "Mechanisms of slope failure on Valles Marineris, Mars", *Quarterly Journal of Engineering Geology and Hydrogeology*, 39, 227 – 240.

Nielsen, P. (1990). "Tidal Dynamics of the Water Table in Beaches", Water Resources Research, 26(9), 2127 – 2134.

Oldham, K., Myland, J., and Spanier, J. (2008) *An Atlas of Functions: with Equator, the Atlas Function Calculator*, 2nd Ed.,Springer.

Otoko, G. (1987). "A study of five embankment slope failures", *Proc. Of the Ninth Regional Conf. for Africa on Soil Mech. and Found. Eng.*, Akinmusuru, J., Malomo, S., and Mesida, E., eds., 1, 363-370.

Pardo-Iguzquiza, E. (1998). "Optimal selection of number and location of rainfall gages for areal rainfall estimation using geostatistics and simulated annealing." *J. Hydrol*., 210 1–4, 206–220.

Parry, R. (1968). "Field and laboratory behaviour of a lightly overconsolidated clay." *Géotechnique*, 18, 151-171.

Peixoto, J.L. (1987). "Hierarchical variable selection in polynomial regression models." *The American Statistician*, 41, 311–313.

Peixoto, J.L. (1990). "A property of well-formulated polynomial regression models." *The American Statistician*, 44(1), 26–30.

Philip, J.R. (1986). "Linearized unsteady multidimensional infiltration", *Water Resources Research*, 22, 1717 – 1727.

Pilot, G. (1972). "Study of five embankments on soft soils." *ASCE Specialty Conf. on Performance of Earth and Earth Supported Structures*, 1(1), 81-99.

Pilot, G., Trak, B., and La Rochelle, P. (1982). "Effective stress analysis of the stablity of embankments on soft soils" *Can. Geotech. J.*, 19(4), 433-450.

Rahardjo, H., Li, X.W., Toll, D.G., and Leong, E.C. (2001) "The effect of antecedent rainfall on slope stability.", *Geotechnical and Geological Engineering*, 19, 371-399, as reprinted in *Unsaturated Soil Concepts and Their Application in Geotechnical Practice*, 2001, ed. Toll, D.G., 371-399.

Ramalho-Ortigao, J., Werneck, L., and Lacerda, W. (1983). "Embankment failure on clay near Rio de Janeiro.", *J. Geotech. Eng.*, 109(11), 1460 – 1479.

Rinaldi, M., Casagli, N., Dapporto, S., and Gargini, A. (2004). "Monitoring and modeling of pore water pressure changes and riverbank stability during flow events." *Earth surface processes and landforms,* 29, 237 – 254.

Rivard, P., and Lu, Y. (1978). "Shear strength of soft fissured clays.", *Can. Geotech. J.*, 15(3), 382-390.

Rivard, P.J., and Kohuska, A. (1965). "Shellmouth dam test fill" *Can. Geotech. J.*, 2, 198-211.

Rojas, R., L. Feyen, O. Batelaan, and A. Dassargues (2010). "On the value of conditioning data to reduce conceptual model uncertainty in groundwater modeling", *Water Resour. Res.*, 46, W08520.

Sabol, T., and Springer, A. (2006). "Simulating the phreatic surface with new sediments deposited during the November 2004 high flow test along the Colorad River, Grand Canyon, Arizona." *Draft Report Prepared for the Grand Canyon Monitoring and Research Center*, Flagstaff, AZ.

Sainak, A. (1999). "Three-dimensional finite element analysis of slope stability, geometric and parametric studies", *Proc. Of the Seventh Int. Symp. On Numerical Models in Geomechanics*, Pande, G., Pietruszczak, S., and Schweiger, H., eds., 547-552.

Sainak, A. (2004). "Application of three-dimensional finite element method in parametric and geometric studies of slope stability analysis", *Advances in Geotechnical Engineering: The Skempton Conference*, 933-942.

Sarle, W. (1994). "Neural Network Implementation in SAS Software", *Proc. 19th Annual SAS Users Group Int. Conf.,* 1 – 24.

Schueler, T.R., Fraley-McNeal, L., and Cappiella, K. (2009). "Is impervious cover still important? Review of recent research", *J. Hydrologic Eng.*, 14(2), 309 – 315.

Seed, H., Seed, R., Schlosser, F., Blondeau, F., and Juran, I. (1988). "The Landslide at the port of Nice on October 16, 1979*" Report UCB/EERC-88/10*.

Seed, R.B., Mitchell, J.K., and Seed, H.B. (1990). "Kettleman Hills waste landfill slope failure. II: Stability analyses", *J. Geotech. Eng.*, 116 (4), 669-690.

Seneviratne, H., and Ilmudeen, M. (1994). "Geotechnical investigation of a landslide in Sri Lanka", *Proc. Thirteenth Int. Conf. Soil Mech. and Found. Eng.*, 3, 1083-1086.

Sevaldson, R.A. (1956). "The slide in Lodalen, October 6, 1954", *Geotechnique*, 6, 167-182.

Siade, A. J., M. Putti, and W. W.-G. Yeh (2010). "Snapshot selection for groundwater model reduction using proper orthogonal decomposition", *Water Resour. Res.*, 46, W08539.

Sillers, W.S., and Fredlund, D.G. (2001). "Statistical assessment of soil-water characteristic curve models for geotechnical engineering." *Can. Geotech. J.*, 38, 1297 – 1313.

Simon, A., Curini, A., Darby, S.E., and Langendoen, E.J. (2000). "Bank and near-bank processes in an incised channel." *Geomorphology*, 35, 193 – 217.

Simon, A., Thomas, R.E., Curini, A., and Shields, F.D. (2002). "Case study: Channel stability of the Missouri River." *J. Hydr. Eng.*, 128(10), 880 – 890.

Singh, T.N., Gulati, A., Dontha, L., and Bhardwaj, V. (2008). "Evaluating cut slope failure by numerical analysis—a case study", *Nat Hazards*, 47, 263–279.

Skempton, A.W. (1964). "Long term stability of clay slopes", *Geotechnique*, 14, 77-101.

Skempton, A.W., and Coats, D.J. (1985). "Carsington dam failure", *Failures in Earthworks*, 203 – 220.

Skempton, A.W., and Hutchinson, J.N. (1969). "Stability of natural slopes and embankment foundations", *Proc. Seventh Int. Conf. Soil Mech. and Found. Eng.*, State of the Art volume, 291 – 340.

Smith, L.P. (1953). *Mathematical Methods for Scientists and Engineers*, Prentice-Hall, Inc., New York, N.Y.

Srivastava, R., and Yeh, T. -C. J., (1991). "Analytical solutions for one-dimensional, transient infiltration toward the water table in homogeneous and layered soils", *Water Resources Research*, 27, 753-762.

Stark, T.D., and Eid, H.T. (1992). "Comparison of field and laboratory residual strengths", *Stability and Performance of Slopes and Embankments II*, Seed, R.B., and Boulanger, R.W. eds., 1, 876 – 889.

Sundaram, A.V., and Bell, J.M. (1972). "Modeling failure of cohesive slopes", *Proc. Tenth Annual Eng. Geology and Soils Eng. Symp.*, 263-286.

Talbi, E-G (2009). *Metaheuristics: From Design to Implementation*, Wiley Series on Parallel and Distributed Computing.

Talesnick, M., and Baker, R. (1984). "Comparison of observed and calculated slip surface in slope stability calculations." *Can. Geotech. J.*, 21(4), 713-719.

Taylor, D.W. (1948). *Fundamentals of Soil Mechanics*, Wiley, New York, N.Y.

Teegavarapu, R. S. V., and Simonovic, S. P. 2002┐. "Optimal operation of reservoir systems using simulated annealing." Water Resour. Manage., 16, 401–428.

Teoman, M.B., Topal, T., and Işık, N.S. (2004). "Assessment of slope stability in Ankara clay: a case study along E90 highway", *Environmental Geology*, 45(7), 963-977.

Tohari, A., Nishigaki, M., and Komatsu, M. (2007). "Laboratory rainfall-induced slope failure with moisture content measurement", *J. Geotech. and Geoenv. Eng.*, 133(5), 575–587.

Travis, Q. B., and Mays, L.W. (2007). "Relationship between Hazen-Williams and Colebrook-White roughness values", *J. Hyd. Eng.*, 133(11), 1270 – 1273.

Travis, Q. B., and Mays, L.W. (2008). "Optimization of retention basin networks", *J. Water Res. Plng. and Mgmt*., 134(5), 432 – 439.

Travis, Q. B., and Mays, L.W. (2010). "Prediction of intake vortex risk by nearest neighbors modeling", *J. Hyd. Eng.*, in production.

Travis, Q. B., and Mobasher, B. (2010). "Correlation of elastic modulus and permeability in concrete subjected to elevated temperatures", *J. Mat. Civil Eng.*, 22(7), 735–740.

Travis, Q.B., and Schmeeckle, M. (2007) "Sandbar response to stage changes", *Sediment Transport Modeling Review Workshop*, Santa Cruz, CA

Travis, Q.B., Houston, S.L., Marinho, F.A.M., and Schmeeckle, M. (2010a). "Unsaturated Infinite Slope Stability Considering Surface Flux Conditions", *J. Geotech. and Geoenv. Eng.*, 136(7), 963 – 974.

Travis, Q.B., Schmeeckle, M., and Serbert, D. (2010b) "Meta-analysis of 301 slope failure calculations. I: Database description", *J. Geotech. and Geoenv. Eng.,* ASCE, in review.

Travis, Q.B., Schmeeckle, M., and Serbert, D. (2010c) "Meta-analysis of 301 slope failure calculations. II: Database analysis", *J. Geotech. and Geoenv. Eng.,* ASCE, in review.

U.S. Dept. of the Navy (1982). *Foundations and Earth Structures* NAVFAC DM-7.2., Alexandria, VA: Naval Facilities Engineering Command.

Ugai, K. (1988). "Three-dimensional slope stability analysis by slice methods", *Proc. Of the Sixth Int. Conf. on Num. Methods in Geomech.*, Swoboda, G., ed., 2, 1369-1374.

United States Army Corp of Engineers (USACE) (2003). *Slope Stability* EM-1110-2-1902, Washington D.C.

United States Department of Agriculture (USDA) (1994). *Slope Stability Reference Guide for National Forests in the United States*, EM-7170-13, Volume II, Washington D.C., Forest Service Engineering Staff.

United States Department of the Interior (USDI) (1996). "Final Environmental Impact Statement", *Record of Decision: Operation of Glen Canyon Dam*, Bureau of Reclamation, Appendix G.

Vasan, A., and Raju., K.S. (2009). "Comparative analysis of Simulated Annealing, Simulated Quenching and Genetic Algorithms for optimal reservoir operation", *Applied Soft Computing*, 9(1), 274-281.

Verhoeven, J.D. (1975). *Fundamentals of Physical Metallurgy*, Wiley, New York, 1975.

Webb, R.H., Schmidt, J.C., Marzolf, G.R., Valdez, R.A. (eds) (1999). *The Controlled Flood in Grand Canyon*, Geophysical Monograph 110, American Geophysical Union, Washington D.C.

White, H. (1980). "A heteroskedasticity-consistent covariance matrix estimator and a direct test for heteroskedasticity", *Econometrica*, 48(4), 817 – 838.

Whitman, R. V. and Moore, P.J. (1963). "Thoughts Concerning the Mechanics of Slope Stability Analysis," *Proceedings, Second Pan-American Conference on Soil Mechanics and Foundation Engineering*, (1).

Wiele, S. M., and J. D. Smith (1996). "A Reach-Averaged Model of Diurnal Discharge Wave Propagation Down the Colorado River Through the Grand Canyon", Water Resour. Res., 32(5), 1375–1386,

Wilkes, P. (1972). "An induced failure at a trial embankment at Kings Lynn, Norfolk, England", *Proc. Spec. Conf. Perf. of Earth and Earth Supported Structures*, 1(1), 29-63.

Wolfskill, L.A. and Lambe, T.W. (1967) "Slide in the Siburua Dam," *Journal of the Soil Mechanics and Foundations Division*, 93(SM4), 107 – 133.

Wolski, W., Szymanski, A., Lechowicz, Z., Larsson, R., Hartlén, J., Bergdahl, U. (1989). *Full-scale failure test on a stage-constructed test fill on organic soil, Report No 36*, Swedish Geotechnical Institute.

Wong, K., Duncan, J., and Seed, H. (1982). "Comparisons of methods of rapid drawdown stability analysis", *Report UCB/GT/82-05*, Dept. of Civil Eng., U. of Cal., Berkeley.

Wu, T.H., Thayer, W.B., and Lin, S.S. (1975). "Stability of embankment on clay." *J. Geotech. Eng. Div.*, 101(GT9), 913-932.

Yoo, C., and Jung, H.Y. (2006). "Case History of Geosynthetic Reinforced Segmental Retaining Wall Failure", *J. Geotech. and Geoenv. Eng.*, 132(12).

Younes, A. and P. Ackerer (2010). "Empirical versus time stepping with embedded error control for density-driven flow in porous media", *Water Resour. Res*., 46, W08523.

Yu, H.S., Salgado, R., Sloan, S.W., and Kim, J.M. (1998). "Limit analysis versus limit equilibrium for slope stability", *J. Geotech. and Geoenv. Eng.*, 124(1), 1 – 11.

Yuster, S.T. (1951). "Theoretical consideration of multiphase flow in idealized capillary systems", *Proc., Third World Pet. Congr*., 2, 437 – 445.

Zeferino, J. A., Antunes, A. P. and Cunha, M. C. (2009), "An Efficient Simulated Annealing Algorithm for Regional Wastewater System Planning". *Computer-Aided Civil and Infrastructure Engineering*, 24: 359–370.

Zeferino, J. A., Antunes, A. P. & Cunha, M. C. (2010). "Multi-objective model for regional wastewater systems planning." *Civil Engineering and Environmental Systems*, *27*(2), 95-106.

Zhang, L.L., Fredlund, D.G., Zhang, L.M, and Tang, W.H. (2004). "Numerical study of soil conditions under which matric suction can be maintained", *Can. Geotech. J.*, 41(4), 569 – 582.

Zhang, Z., Tao, M., and Movant, M. (2005). "Cohesive slope surface failure and evaluation", *J. Geotech. and Geoenv. Eng.,* 131(7), 898 – 906.

Zhigljavsky, A. A. (1991). *Theory of Global Random Search*. Kluwer Academic.

Zhou, J., and Yu, J. (2005) "Influences affecting the soil-water characteristic curve." *Journal of Zhejiang University SCIENCE*, 6A(8):797 – 804. Al Ahram (16 September 2004), Archaeo News, "The world's oldest dam", 16 September 2004.